UNIVERSITÀ DELLA CALABRIA

UNIVERSITA' DELLA CALABRIA

Dipartimento di Fisica

Dottorato di Ricerca in

Scienze e Tecnologie Fisiche, Chimiche e dei Materiali
in convenzione con il Consiglio Nazionale delle Ricerche (CNR)

CICLO

XXXIII

Conventional and innovative technological systems for measuring mercury (Hg) in ambient air: inter-comparison and case-studies to assess variability and Hg seasonal trends within regional and global monitoring networks

Settore Scientifico Disciplinare

CHIM/12 Chimica dell'ambiente e dei beni culturali

Coordinatore: Ch.mo Prof.ssa Gabriella Cipparrone

Firma _ Firma oscurata in base alle linee guida del Garante della privacy

Supervisore: Dott.ssa Francesca Sprovieri

Firma___ Firma oscurata in base alle linee guida del Garante della privacy

Tutor: Dott.ssa [redacted]

Firma [redacted] Firma oscurata in base alle linee guida del Garante della privacy

Dottoranda: Dott.ssa Maria Martino

Firma Firma oscurata in base alle linee guida del Garante della privacy

Contents

Abstract in Italian

Uno dei maggiori rischi ambientali per la salute umana è l'inquinamento atmosferico, un tema che ha acquisito notevole importanza negli ultimi anni a causa degli effetti tossici causati dagli inquinanti sulla salute umana e sui vari ecosistemi. In questo contesto, un ruolo chiave è occupato dal mercurio (Hg) che è un inquinante in grado di causare gravi effetti negativi sulla salute degli ecosistemi e degli esseri viventi in tutto il mondo come evidenziato da noti episodi storici di avvelenamento da mercurio riconosciuti dalla comunità globale come il disastro di Minamata. Gli effetti tossici causati dal Hg costituiscono una grande minaccia ed è questo il motivo principale che identifica il mercurio come inquinante globale da sottoporre a monitoraggio continuo, all'attenzione della comunità scientifica e dell'agenda politica a livello nazionale, regionale e globale. L'impegno da parte della comunità scientifica e politica nell'attivazione di nuovi piani di monitoraggio e miglioramento di quelli esistenti, volti al controllo delle concentrazioni di Hg e delle sue specie ha l'obiettivo di garantire un controllo rigoroso della presenza di questo inquinante nell'ambiente. Oltre all'atmosfera, le attività di monitoraggio del mercurio interessano anche altre matrici ambientali come acqua, suolo e sistemi biologici viventi. A causa del suo ciclo biogeochimico che ne permette un'ampia distribuzione nei diversi comparti ambientali una volta rilasciato in atmosfera da sorgenti naturali e antropiche. La capacità del mercurio di essere trasportato su lunghe distanze, lontano dalla fonte di emissione prima di essere trasformato nelle sue varie forme e raggiungere diversi comparti ambientali, la sua persistenza, la sua capacità di bioaccumulo negli ecosistemi e i suoi impatti considerevolmente negativi, sono le ragioni chiave che hanno evidenziato il mercurio come un problema ambientale rilevante di interesse globale che richiede azioni concertate per una protezione efficace della salute umana e dell'ambiente. Sulla base di tali motivazioni è stata sottolineata la necessità di avere una prospettiva globale nell'affrontare il problema dell'inquinamento da mercurio nell'ambiente guidata da uno strumento legalmente vincolante quale la Convenzione di Minamata sul Mercurio che ha come obiettivo la protezione della salute e dell'ambiente dalle emissioni di mercurio e dei suoi composti, considerando l'intero ciclo di vita del mercurio, dall'estrazione primaria dell'elemento sino alla gestione dei rifiuti che lo contengono. A tal fine, le disposizioni della Convenzione di Minamata evidenziano una crescente

richiesta di attività di monitoraggio e il continuo miglioramento delle stesse al fine di arricchire la comprensione dell'impatto dell'inquinamento da mercurio sull'ambiente grazie alla fornitura di dati coerenti ai responsabili politici, oltre che a ricercatori e al pubblico in generale. Inoltre, i requisiti della Convenzione di Minamata identificano l'osservazione e il monitoraggio dei cambiamenti dei livelli di mercurio nell'atmosfera su scala globale come un modo per poter valutare l'efficacia delle azioni volte alla riduzione dei livelli globali del mercurio stesso. È quindi importante essere in grado di definire gli aspetti chiave come la comparabilità dei dati, l'affidabilità e l'accessibilità dei dati e la garanzia della qualità. In questo contesto, all'interno del network GMOS (Global Mercury Observation System), coordinato dall'Istituto di Ricerca sull'Inquinamento Atmosferico del Consiglio Nazionale delle Ricerche (CNR-IIA) di Rende sono stati sviluppati e implementati diversi strumenti quali le SOP (Standard Operational Procedures). Le SOP sono protocolli comuni standardizzati specifici che forniscono sia informazioni sul metodo per valutare le concentrazioni di mercurio in una matrice ambientale specifica, sia le procedure per l'uso e la manutenzione tecnica su campo degli strumenti automatizzati utilizzati nei siti della rete, e il G-DQM (GMOS-Data Quality Management) sistema utile per l'acquisizione e l'elaborazione dei dati raccolti dai vari siti appartenenti alla rete. Lo scopo di tali strumenti è quello di armonizzare le misure ottenute nella rete e garantire un alto grado di comparabilità tra i dati ottenuti da tutti i siti di monitoraggio e la possibilità di scambio e valutazione congiunta dei dati. A supporto di una più efficace azione di monitoraggio negli anni, è emersa la necessità di metodi innovativi di monitoraggio e analisi a basso costo e di facile utilizzo in grado di integrare l'uso ed i limiti dei metodi analitici convenzionali in aree geografiche ampie o remote.

Il lavoro di ricerca presentato in questa tesi è stato rivolto al monitoraggio delle concentrazioni di mercurio atmosferico, sfruttando approcci sia convenzionali che innovativi. Riguardo il campionamento con strumentazione tradizionale, sono stati analizzati i dati di misura derivanti dal campionamento di mercurio atmosferico presso tre diverse stazioni di monitoraggio, dislocate su territorio italiano, quali Monte Sant'Angelo, Monte Curcio, Montelibretti. Tutti i dati, a seguito di opportuna trattazione statistica, e con il supporto di mappe satellitari e di simulazioni modellistiche sulle retro-traiettorie delle masse d'aria, sono stati interpretati alla luce della loro variabilità temporale, delle dinamiche meteorologiche e dell'influenza di specifiche sorgenti, di tipo

sia naturale che antropico. Il lavoro di ricerca presentato in questa tesi è rivolto al monitoraggio del mercurio anche mediante approcci innovativi. In questo contesto, il campionamento attivo, su cui si basano i comuni analizzatori di mercurio, è stato confrontato con le prestazioni di dispositivi passivi (PASs) di nuova concezione, la cui struttura è stata migliorata durante il mio dottorato di ricerca e testati sul campo attraverso una campagna di intercomparazione. Nell'ambito dell'indagine comparativa, è stato evidenziato come il campionamento passivo possa essere proposto come alternativa praticabile o sistema complementare utile per colmare le lacune del monitoraggio mondiale del mercurio visti i suoi numerosi vantaggi che aumentano la possibilità concreta di una rete globale sostenibile e la disponibilità di misurazioni del mercurio atmosferico a lungo termine che includa aree geografiche attualmente non coperte da sistemi di monitoraggio esistenti.

Abstract in English

One of the greatest environmental risks to human health is atmospheric pollution, an issue that has acquired considerable importance in recent years due to the toxic effects caused by pollutants on human health and various ecosystems. In this context, a key role is played by mercury (Hg) which is a pollutant capable of causing serious negative effects on health ecosystems and living beings around the world as evidenced by known historical episodes of mercury poisoning recognized by the global community like the Minamata disaster. The toxic effects caused by Hg constitute a great threat and this is the main reason that identifies mercury as a global pollutant to be subjected to continuous monitoring, to the attention of the scientific community and of the political agenda at national, regional, and global level. The commitment by the scientific and political community in the activation of new monitoring plans and improvement for the existing ones, aimed at controlling the concentrations of Hg and its species, has the aim of guaranteeing rigorous control of the presence of this pollutant in the environment. In addition to the atmosphere, mercury monitoring activities also affect other environmental matrices such as water, soil, and biological living systems. Due to its biogeochemical cycle mercury can be widely distributed in different environmental compartments once released into the atmosphere from natural and anthropogenic sources. The ability of mercury to be transported over long distances, away from the emission sources before being transformed into its different forms and reaching the various environmental compartments, its persistence its ability to bioaccumulate in ecosystems, and its considerably negative impacts, are the key reasons that have highlighted mercury as a significant environmental problem of global concern that requires concerted action for effective protection of human health and the environment. Based on these reasons, the need to have a global perspective in addressing the problem of mercury pollution in the environment was underlined, guided by a legally binding instrument such as the Minamata Convention on Mercury aims to protect health and the environment from mercury emissions and its compounds, considering the entire life cycle of mercury, from the primary extraction of the element to the management of the waste containing it. For this purpose, the provisions of the Minamata Convention highlight a growing demand for monitoring activities and their continuous improvement in order to enhance the understanding the impact environmental mercury pollution thanks

to the provision of consistent data to policy makers as well as researchers and the general public. Furthermore, the requirements of the Minamata Convention identify the observation and monitoring of changes in mercury levels in the atmosphere on global scale to evaluate the effectiveness of actions aimed at reducing global mercury levels. It is therefore important to be able to define key aspects such as data comparability, data reliability and accessibility and quality assurance. In this context, within the GMOS network (Global Mercury Observation System), coordinated by the Institute of Atmospheric Pollution Research of the National Research Council (CNR-IIA) of Rende various tools have been developed and implemented such as SOPs (Standard Operational Procedures). The SOPs are specific standardized common protocols that provide both information on the method for assessing mercury concentrations in a specific environmental matrix, and the procedures for use and technical maintenance in the field of automated tools used across the network sites, and the G-DQM (GMOS-Data Quality Management) system useful for the acquisition and processing of data collected from the various sites belonging to the network. The aim of these tools is to harmonize the measurements obtained within the network and to ensure a high degree of comparability between the data obtained from all the monitoring sites and the possibility of exchanging and jointly evaluating the data. In support of a more efficacy monitoring action over the years, has been emerged the need for innovative monitoring and analytical methods at low cost and easy to use able to integrate the use and limitations of conventional analytical methods in large or remote geographical areas.

The research work presented in this thesis was aimed at monitoring atmospheric mercury concentrations, using both conventional and innovative approaches. With regards to the field campaigns carried out through conventional instruments, a specific investigation has been performed over the Hg atmospheric measurements recorded at three monitoring stations, located across the Italian territory, and corresponding to Monte Sant'Angelo, Monte Curcio, Montelibretti sampling sites. All data, after an appropriate statistical treatment, and with the support of satellite maps, as well as modelling simulations providing air mass backward trajectory, have been interpreted in light of their temporal variability, meteorological dynamics and the influence of specific sources, both natural and anthropogenic.

The research work presented in this thesis is addressed to the monitoring of mercury also by innovative approaches. In this context, the active sampling, which the common Hg analyzers are based on, was compared with the performances of newly developed passive devices (PASs), whose structure has been improved during my Ph.D. studies and tested in the field through an inter-comparison campaign. Within the intensive comparative investigation has been highlighted how passive sampling can be proposed as a viable alternative or additional-integrating system useful for filling the gaps in global mercury monitoring, given its many advantages that increase the concrete possibility of a sustainable network, the availability of long-term global atmospheric mercury measurements, which includes geographic areas not currently covered by existing monitoring systems.

Acknowledgements

I would like to express my deep gratitude to Dr. Gabriella Cipparrone, Coordinator of the Ph.D. course, to Dr. Nicola Pirrone and to Dr. Francesca Sprovieri to have given me the opportunity to pursue the Ph.D. studies, a fundamental experience of formation that enriched my education from both a scientific and personal point of view. A great thank is for my supervisor Dr. Francesca Sprovieri, which has really helped me in these years of study to broaden my scientific knowledge, allowing me to participate in various research activities. Furthermore, I would like to express my sincere gratitude to my tutor Dr. Mariantonia Bencardino, who together with Dr. Francesca Sprovieri, guided and managed my research path with motivation, patience and availability, for having continuously offered me new ideas of work, enriching my professional and human growth. I thank researchers of ARPA Puglia, in particular Dr. Lorenzo Angiuli, and Dr. Giulio Esposito from CNR-IIA in Rome who, collaborating with the researchers of the CNR-IIA in Rende, providing the data that were validated by Dr. Mariantonia Bencardino and Dr. Francesco D'Amore and then analyzed and discussed in my thesis. Furthermore, I thank all the personnel of the CNR-IIA of Rende whom I have met in recent years and who have greatly enriched my professional daily life both humanly and intellectually. Thanks to Dr. Attilio Naccarato for supporting me during laboratory activities and in the realization of scientific results. I thank my labmates Antonella, Sacha and Giovanni for the precious time shared and spent working together and for laughing with me.

I thank my wonderful family, a certainty in everything, which I always enclose in a single term: Mom. Thanks to my fantastic parents, Salvatore and Ermelinda, a certainty always ready to support me in every step of my life. To my sister Michela Ilenia, my hurricane of strength, always present and ready to smile at me: my goal is for you. To my boyfriend Francesco, a special person always by my side.

Thanks you to the pillars of my life who from up there are always ready to toast in my honour.

Finally, special thanks is for you. You asked me not to stop and I did not do it.

I hope that this is the starting point for new goals to achieve.

List of Figures

List of Tables

Preface

In the last decades, a great concern about the linkage between mercury pollution and its harmful impacts on the environment and on living species has increased leading policymakers to create several monitoring programs for mercury on a global scale that also extends to areas where data are limited or do not exist, and the scientific community to develop innovative techniques for determining the levels of this pollutant. Mercury (Hg) is a major environmental pollutant and poses a global threat to both human health and the environment, due to its persistence in the environment, its long-range atmospheric transport, its ability to bioaccumulate in ecosystems, and its significant negative effects. In this context, the information on the relationships between mercury in the atmosphere, in the deposition and contamination of ecosystems represents a fundamental challenge for the scientific community. It is important to acquiring useful knowledge to evaluate the processes of emission from natural and anthropogenic sources, transport and deposition of mercury and to understand the impact of mercury pollution on the environment and health. The aim of this commitment is to identify and apply appropriate control strategies to prevent and reduce the negative effects of mercury on ecosystems and health, supporting the Minamata Convention on Mercury.

The work carried out during my Ph.D. studies deals with the analytical monitoring of mercury in atmosphere which is the most important source of Hg to ecosystems in addition to being a dominant cycling pathway for the global mercury dispersion. This thesis consists of 7 chapters and includes studies based on mercury monitoring in atmosphere obtained by both conventional and innovative approaches. Therefore, both active and passive sampling methods of Hg species were explored and consequently the principles behind these approaches were displayed. Chapter 1 consist of an introduction to mercury, its natural and anthropogenic sources, its presence in the various environmental compartments. Moreover, it also deals with the problem of mercury pollution in its various forms, as a threat to human health and ecosystems. Chapter 2 describes mercury as a global pollutant and its potential impacts on human health highlights the importance of continually improving monitoring programs in terms of effectiveness and reliability, as required by the Minamata Convention on Mercury. In this context, the importance of monitoring network programs such as GMOS and Reti Speciali

networks in support of the Minamata Convention and the requirements of EU legislation were highlighted. Chapter 3 summarizes conventional and new monitoring and analytical methods employed for the measurement of Hg in atmosphere and water. In addition, this chapter also includes the Standard Operational Procedures (SOPs), the quality assurance and quality control procedures (QA/QC) and the GMOS-Data Quality Management (G-DQM) system developed within the GMOS network and used for quality screening data from Tekran investigated in Chapter 4. The centralized G-DQM system by acquiring mercury atmospheric data in real time from Tekran instruments, processes them automatically, checking whether the monitoring process adheres to standard procedures, in order to minimize the risk of a possible loss of data and to have inaccuracies in data production. By doing this, the G-DQM system ensures the data comparability between the atmospheric mercury datasets collected in the various sites of the network. Regard, the Hg levels analysis of aqueous samples, this Chapter reports a new modified version of the United States Environmental Protection Agency (EPA) method 1631E ("Mercury in water by oxidation, purge, and trap, and cold vapor atomic fluorescence spectrometry") developed and implemented during the Ph.D. thesis's work, and that provides, in particular, new procedures and strategies to minimize of Hg contamination during sampling and analysis of aqueous matrices, which could affect the results of the analysis. Chapter 4 presents three case-studies that describe the field application of conventional instrumental techniques for monitoring the atmospheric gaseous mercury concentrations and the results obtained from carrying out field air sampling campaigns in three different Italian monitoring sites. The first case study reports the results of Total Gaseous Mercury (TGM) performed during a measurement campaign carried out at the Monte Sant'Angelo (MSA, Apulia, Southern Italy) monitoring station during the period from April 2018 to August 2020. The second case study shows the results of measurements of TGM performed during a measurement campaign at the Monte Curcio (MCU) Environmental – Climate Observatory (Calabria, Southern Italy), which is a monitoring station managed by the Institute of Atmospheric Pollution Research of the National Research Council (CNR-IIA). The measurement campaign was carried out from May 2019 at August 2020. The third case study reports the results of atmospheric mercury species (Gaseous Elemental Mercury (GEM), Gaseous Oxidize Mercury (GOM) and Particulate Bound (PBM)) performed during a measurement campaign at the Montelibretti (MLI, Lazio,

Central Italy) monitoring station, during the period from October 2018 to February 2019. In each of these three case-studies, a discussion was conducted on the levels of atmospheric mercury detected and the Hg temporal trends were observed on an hourly, daily, monthly, seasonal, annual and inter-annual basis. Furthermore, meteorological parameters were also monitored at these investigated sites in order to better characterize the sites and the observed mercury variations. The support of meteorological variables and others information gained by available free tools allowed to identify the most likely influencing sources.

In Chapter 5, passive sampling was described as an innovative and promising method for monitoring atmospheric mercury, as well as being able to integrate the use of the active sampling method, increasing the spatial resolution of Hg data and fostering a sustainable long-term global network. This chapter describes the operation and the advantages of passive air samplers (PASs) that allow the monitoring of atmospheric mercury levels even in areas where the characteristics of use of conventional instrumentation such as purchase and maintenance costs, electricity demand for operation, could represent limitations and make it difficult. This chapter provides a detailed description, including information on PASs design, used in the field as well as the storage and the analysis of three passive devices. The CNR-PAS with gold nanoparticles as a sorbent, developed by the Italian National Research Council, the IVL-PAS using an activated carbon-coated disk, developed by the Swedish Environmental Research Institute, and the *Mer*PAS® using a sulfur-impregnated activated carbon sorbent, developed at the University of Toronto and commercialized by Tekran.

Chapter 6 provides an overview of the results of a comparison study carried out through an intensive field measurement campaign aimed at monitoring background atmospheric concentrations of gaseous mercury at two monitoring sites located in Italy (Southern Italy) and Canada (Southern Ontario) by using conventional samplers and passive air samplers for gaseous mercury. The measurement campaign was carried out from February 2019 at April 2019, for a period of three months, between late winter and early spring of 2019. The analytical performance of these passive devices was evaluated in terms of accuracy through a comparison with active sampling data, precision, sensitivity and linearity of uptake over extended deployment periods. During the investigation the three types of passive devices for mercury described in Chapter 5 (CNR-PAS, IVL-PAS

and *Mer*PAS®) were used, all of them based on unassisted molecular diffusion of the target species from ambient air over an absorbent membrane. Finally, in Chapter 7 the principal key findings obtained during the research work were discussed.

Chapter 1

Mercury: an environmental pollutant of global concern

1.1 Introduction

Mercury (Hg) is a highly toxic pollutant for environmental ecosystems and human health of a global interest due to its unique chemical and physical properties. Its long-range mobility through the atmosphere is indeed favoured by the volatility and relative stability of its elemental form (Hg^0), and through the hydrosphere by the solubility of its various species. Mercury is therefore of global environmental concern, because of the major perturbation of its natural cycle by human activities, its long-distance transport via the atmosphere resulting in its ubiquity in terrestrial and marine ecosystems, and finally because of its long persistence in biologically-crucial zones of the aquatic environment due to intense biogeochemical recycling between the atmosphere and surface waters [1,2,3,4].

Mercury exists in three oxidation states: Hg^0 (elemental or metallic mercury), Hg^+ (monovalent or mercurous mercury), and Hg^{2+} (divalent or mercuric mercury). However, of this three forms, only elemental mercury and divalent mercury contribute to the global mass balance, while the compounds containing Hg^+ are rare because the instability of Hg-Hg bonds [5,6]. Mercury is known as liquid silver or quicksilver, compared to other metals it appears as liquid and can vaporize easily at ambient temperature and pressure. Given its high volatility, Hg can be found in the gaseous phase at the elemental state. Moreover, Hg has a boiling point below 650°C and it is a chemically quite inert metal with a high ionization potential [7]. The high mobility and long life in nature allow Hg to be widely distributed in the environment and in living organisms in various chemical forms. These latter, together with the characteristics of the environmental and biological matrices, with which they come into contact, influence the Hg reactivity, mobility, bioavailability, persistence and impact on the environment and biological systems. Generally, all the Hg chemical forms show negative effects but the most toxic species for human health and ecosystems is the cation methylmercury (CH_3Hg^+ or $MeHg^+$), which is an organometallic (or organomercury) compound obtained from the combination of Hg with carbon. Due to its lipophilic properties, methylmercury is able to cross biological

membranes, bioaccumulate, and biomagnify in the living organisms throughout trophic chain thus reaching humans through diet [3,8]. The devastating effects of environmental mercury contamination have been highlighted by historical episodes of Hg poisoning such as the well-known Minamata disaster (1956, Japan). Over the years, the attention of scientific and political communities on the serious problem of Hg pollution and on the need to develop adequate monitoring actions, aimed at controlling and reducing Hg emissions into the atmosphere to protect human health and the environment. The global issue of Hg has been therefore addressed, in part by the UNEP through the implementation of the Minamata Convention, which entered into force in 2017, and has now been ratified by over 100 countries. The Minamata Convention bans Hg in many products and processes and regulates emissions to reduce human exposure.

1.2 Sources and release of mercury into the environment

Mercury is a natural element present in the Earth's crust mainly in the form of cinnabar (mercuric sulfide, HgS), which represents the most common mineral form and from which most of Hg is extracted [8,9]. In addition to sulfur, Hg also easily reacts with other non-metal elements such as oxygen and halogens to form salts, which are inorganic mercuric compounds appearing, unlike the red-coloured HgS, in the form of crystals or white powder. Mercury can also react with other metals such as silver, copper and especially with gold to form alloys, known as amalgams. Given its characteristics, Hg has been widely used in various ways to produce thermometers, pharmaceuticals, cosmetics, skin creams, dental amalgams, insecticides, fluorescent lamps, and batteries. However, in the last decades, the increased scientific awareness regarding the significant Hg toxicity, the contamination of the food chain and the consequent government restrictions on the emissions of this pollutant, have significantly or completely reduced most of its industrial uses, such as those in agriculture or to produce batteries, electrical equipment, and dental amalgam [9,10].

In addition to the weathering processes of the Earth crust (weathering of mercury-containing rocks), there are additional natural sources of Hg, which, together with anthropogenic sources, can release this element in the various natural ecosystems and govern the cycling of Hg in the environment [8,11]. Natural sources of Hg include volcanoes, forest wildfires, evasion from soil and water surfaces which contribute

significantly to the overall pool of atmospheric Hg. Their contributions can vary in time and space depending on a number of factors as geological formations with high Hg concentration like cinnabar deposits, presence of volcanic or geothermal activities, exchange processes between water and atmosphere, re-emission of previously deposited Hg from top-soils, plants, and forest fires [8,12,13]. A large amount of Hg^0, also known as gaseous elemental mercury (GEM), is released into the atmosphere from the geothermal activity of volcanoes [8]. The release of Hg emissions from volcanoes and other geothermal activities, as calderas, is approximately 90 Mg yr^{-1}, and represent the 2% of the total contribution from natural processes to the global Hg atmospheric balance [8]. Anthropogenic sources of Hg mainly include coal-fired power plants, processing of mineral resources, as artisanal and small scale gold mining activities where mercury is used to extract gold from ore, incineration of many types of waste, industrial production of cement, chlor-alkali (chlorine and sodium hydroxide), vinyl-chloride, and other metallurgic activities such as mining and smelting of iron and non-ferrous metals [3,12,13]. Mercury emissions due to human activities represent a large factor of imbalance in the global Hg natural cycle. It was estimated that human activities caused an increased by 300–500% of atmospheric Hg concentrations over the past 100 years [14,15]. Nowadays, the major anthropogenic source of mercury is represented by coal combustion in power plants and residential heating, followed by cement production, artisanal and small-scale gold mining activities, and waste incineration [16]. Due to industrial activities, mainly based on combustion of fossil fuels (especially coal), and to incineration of waste material, East and Southeast Asian (China) together with South Asian (India) are the region that contribute to most of anthropogenic Hg emissions. Indeed, in 2015 these countries produced together about 50% of the total global anthropogenic Hg emissions while Europe Union with its 28 member states (EU28) contributed for only 3.5% [15], see Table 1.1 and Figure 1.1 for a complete overview).

	Sector group (emissions, tonnes)				Regional total (range), tonnes	% of global total
	Fuel combustion	Industry sectors	Intentional-use (including product waste)	Artisanal and small-scale gold mining		
Australia, New Zealand & Oceania	3.57	4.07	1.15	0	8.79 (6.93-13.7)	**0.4**
Central America and the Caribbean	5.69	19.1	6.71	14.3	45.8 (37.2-61.4)	**2.1**
CIS & other European countries	26.4	64.7	20.7	12.7	124 (105-170)	**5.6**
East and Southeast Asia	229	307	109	214	589 (685-1430)	**38.6**
EU28	46.5	22	8.64	0	77.2 (67.2-107)	**3.5**
Middle Eastern States	11.4	29	12.1	0.225	52.8 (40.7-93.8)	**2.4**
North Africa	1.36	12.6	6.89	0	20.9 (13.5-45.8)	**0.9**
North America	27	7.63	5.77	0	40.4 (33.8-59.6)	**1.8**
South America	8.25	47.3	13.5	340	409 (308-522)	**18.4**
South Asia	125	59.1	37.2	4.5	225 (190-296)	**10.1**
Sub-Saharan Africa	48.9	41.9	17.1	252	360 (276-445)	**16.2**
Global inventory	533	614	239	838	2220 (2000-2820)	**100**

Table 1.1 Quantities of mercury emitted to air from anthropogenic sources in 2015, by different sectors in different regions (adapted from [15]).

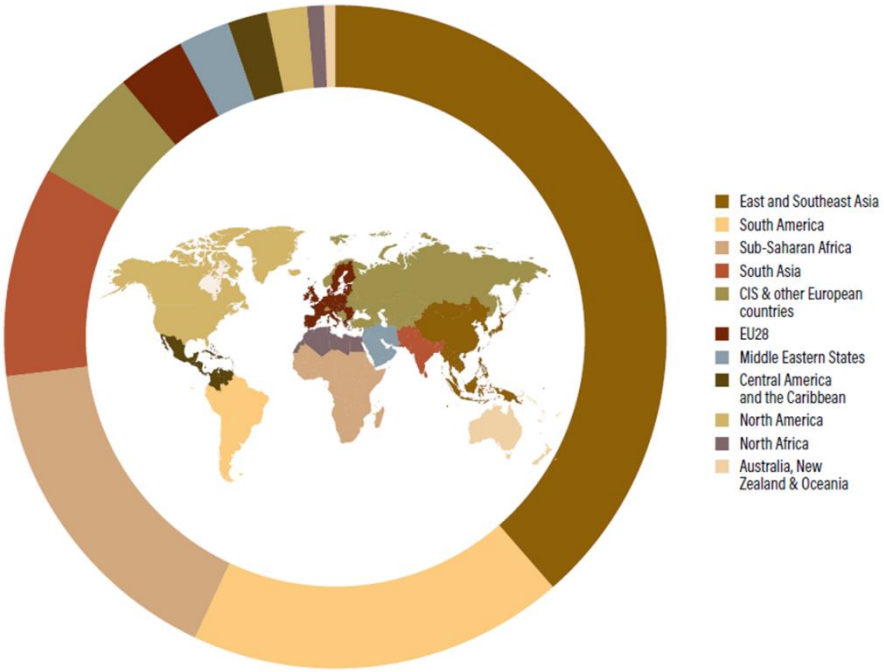

Figure 1.1 Regional breakdown of global emissions of mercury to air from anthropogenic sources in 2015 (adapted from [15]).

The contributions of anthropogenic and natural sources to the total atmospheric Hg pool are different and both significant. In 2015, anthropogenic emissions were estimated at around 2500 t y^{-1} representing the 30% of Hg emitted annually to the atmosphere, meanwhile natural geogenic emissions represents only the 10%. The greatest amount (60%) of Hg released to atmosphere is represented by environmental processes resulting

in re-emission and re-mobilization of Hg previously deposited to soils and water ([15], see Figure 1.2 for reference).

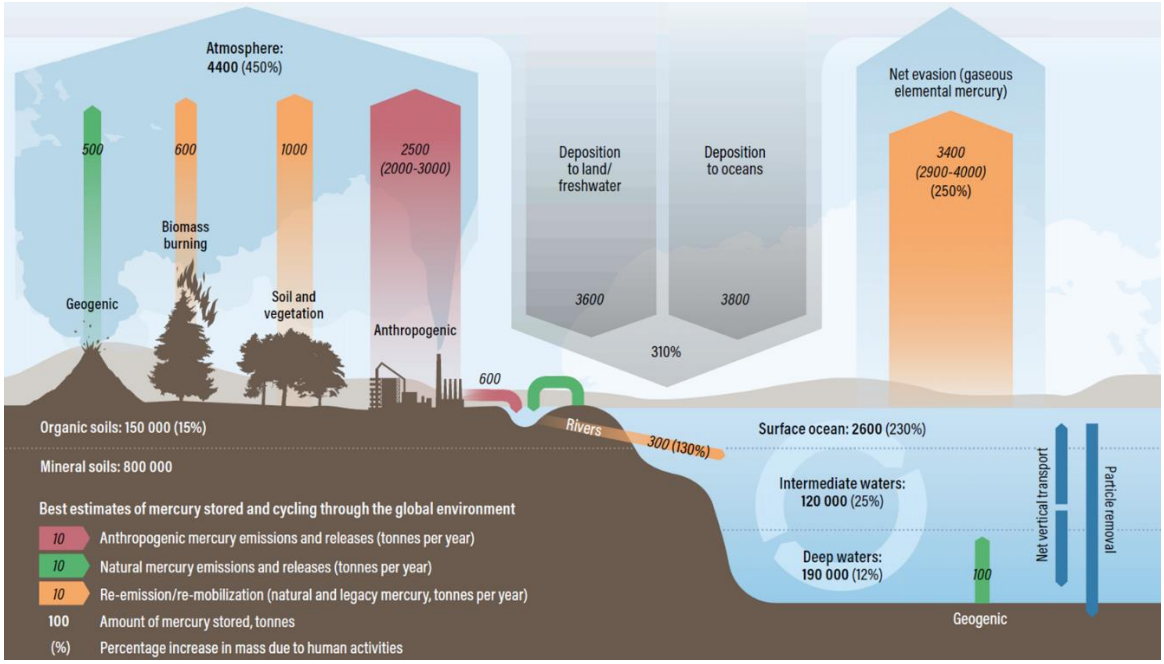

Figure 1.2 The updated global Hg budget shows the impact of human activities on the Hg cycle and the resulting increase in Hg accumulated in soils and oceans (adapted from [15]).

The atmosphere is the major transport pathway for distribution of Hg globally. The release of Hg into the atmosphere can occur in both elementary and oxidized forms. The predominant specie of Hg, emitted by natural sources, is the Gaseous Elemental Mercury (GEM, that is Hg^0 vapor), while anthropogenic sources can emit mercury in both the elemental (GEM) and oxidized forms of mercury, the latter being able to be in gaseous phase (Gaseous Oxidized Mercury, GOM) or bound to particulate matter (Particulate Bound Mercury, PBM) [2,17]. The properties of these different forms of mercury determine the fate and transport of Hg in the environment and the consequent interactions with the different matrices and with other atmospheric contaminants.

1.3 Main processes overview of the mercury cycling

Hg transfer between different reservoirs of the Earth occurs as a result of a complex combination of transport and transformation processes that, by operating on different temporal and spatial scales, guides the dynamic distribution, the exchange, and continuous recycling and partitioning of Hg and its species between and inside

atmosphere, soil and water, thus influencing environmental ecosystems and human health (Figure 1.3) [12].

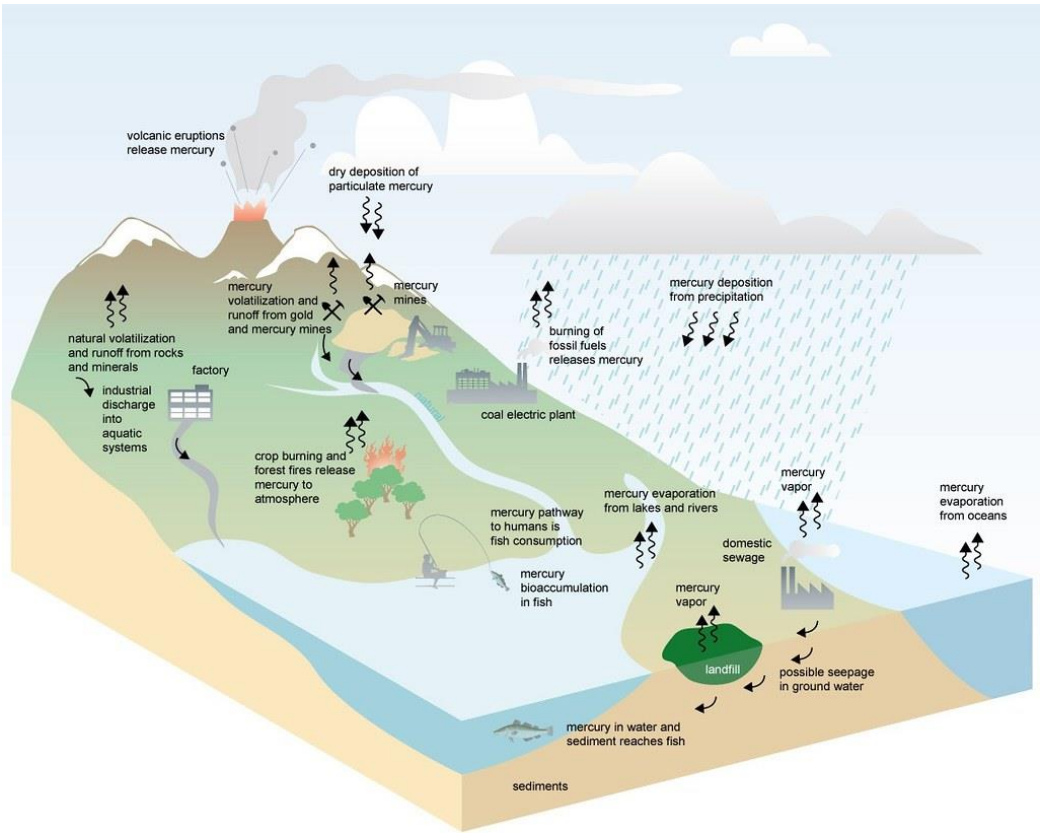

Figure 1.3 Mercury biogeochemical cycle [18]**.**

The properties of each Hg chemical form present in a specific environmental matrix, together with the characteristics of the matrix itself, affect the cyclical distribution and the pattern of deposition of Hg on a local, regional, and global scale. In the global Hg cycle, the various Hg forms play different roles and have different fate [19]. The main chemical reactions of the Hg cycle in the environment may be roughly summarized thus: interconversions between elemental Hg (Hg (0)), inorganic divalent Hg (Hg (II)), and organic divalent, including dimethylated species (CH_3Hg^+/MMHg and CH_3HgCH_3/DMHg, hereafter abbreviated as MeHg) [20].

GEM (or Hg^0) is the most abundant form of Hg in the atmosphere and is important in the exchange of mercury between the atmosphere, aquatic, and terrestrial surfaces. Given the Hg^0 long atmospheric residence time it is transported for long distances and then deposited elsewhere, even in remote areas [1,3,5,12,13]. The divalent (Hg^{2+}) form is

obtained from the photochemical oxidation of GEM during atmospheric transport and it is deposited in terrestrial and aquatic systems mainly by wet and dry deposition processes [21]. A portion of the divalent mercury, deposited and accumulated in aquatic and terrestrial ecosystems, may be reduced to Hg^0 and subsequently re-emitted in the free troposphere where it is diluted in the global Hg^0 pool. The reduction process of inorganic divalent mercury (Hg^{2+}) to its elemental form (Hg^0) is responsible for its from terrestrial and aquatic ecosystems. This process contributes to Hg loss from terrestrial and aquatic ecosystems since it competes with the mechanisms of Hg adsorption and sedimentation [21,22]. As an example, after accumulating in terrestrial soil, Hg can re-volatilize from this environmental matrix to the atmosphere following events such as forest fires. Similarly, in aquatic systems, inorganic Hg can be photo-reduced again to its volatile form which is concentrated in surface waters thus, being supersaturated by this form promoting the exchange processes with the atmosphere [24].

The strong affinity that Hg has with organic matter and especially with organic thiol [9], in aquatic matrix Hg can bind to organic matter or forms complexes, such as insoluble Hg sulfide that are deposited into sediments. Alternatively, through biotic and abiotic processes Hg can be transformed into methylmercury that once formed and released by bacteria can be adsorbed by plankton, and thus enters in the food chain where it can bioaccumulate and biomagnificate. Through invertebrates and fishes located in the lowest levels of the food chain, methylmercury passes to the large predatory fishes located in the upper part of the food chain, which will result to have the highest concentrations of methylmercury. The bioaccumulation and biomagnification processes of methylmercury up to the higher trophic levels occurs since organisms require a long time to eliminate methylmercury from their tissues. Subsequently, the contaminated large predatory fishes are eaten by humans and this relation explains why diet is the main pathway through which people come into contact with this highly toxic form of Hg representing a threat for human health and ecosystems (Figure 1.4) [10,24].

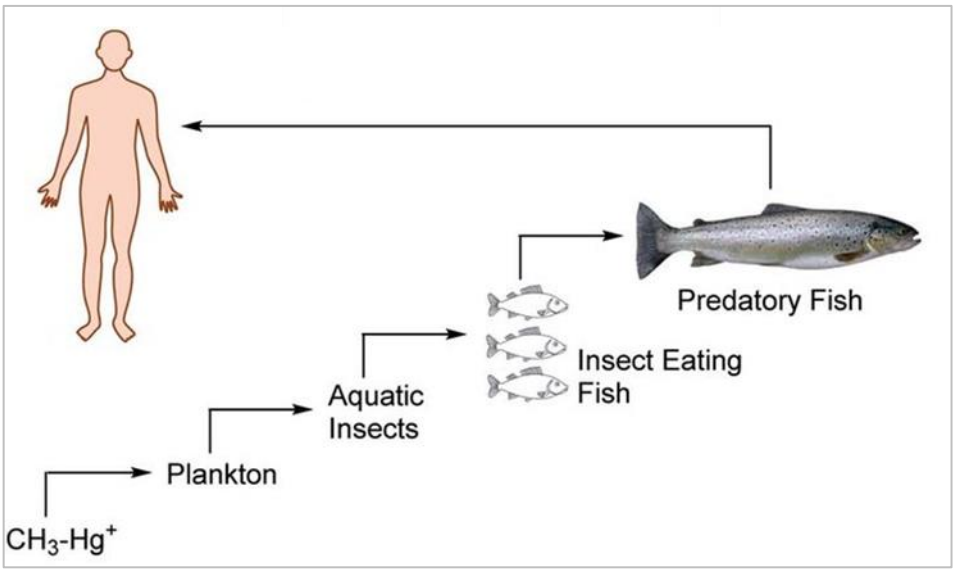

Figure 1.4 Bioaccumulation of mercury along the food chain (adapted [26]).

1.3.1 Mercury in atmosphere

The atmosphere is the most important source of Hg to ecosystems and is a dominant cycling pathway for the global dispersion of mercury. The three forms of atmospheric mercury are Gaseous Elemental Mercury (Hg^0 or GEM), Gaseous Oxidised Mercury (GOM) also known as Reactive Gaseous Mercury (RGM), which includes species of oxidized mercury soluble in water but with a relatively high vapor pressure that allows its existence in the gas phase, and Particulate Bound Mercury (PBM or $Hg_{(p)}$), which include species of Hg bound or adsorbed to airborne particulate matter, such as soot, dust and sea salt aerosol [27]. Therefore, Hg in the atmospheric environment is present as gaseous, aqueous (cloud, fog, and rain waters) and solid (particulate matter) phases. The sum of GEM and GOM is defined as Total Gaseous Mercury (TGM); GEM is the dominant form [28] and GOM represents a fraction of 1-3% of TGM in clean background air [29]. These mercury species have different physicochemical properties as the solubility, residence time and transport mechanisms. The most common form of mercury in the atmosphere is the elemental one, Hg^0, which is relatively insoluble in water, has a low deposition velocity, and has a long atmospheric residence time that can be vary from few months to a year and a half [2,13]. Its atmospheric lifetime throughout the troposphere is sufficient to enable Hg^0, once released by emission sources, to be transported for long distances and distributed on a global scale. The persistence in the

atmosphere and its long-range atmospheric transport allows to define Hg as a global pollutant able to reach remote regions [3].

The long-term atmospheric circulation allows a widespread increase of Hg concentrations and a mixing of mercury from different sources, with the formation of a global pool of atmospheric Hg^0, whose average background concentrations are distributed in a spatially homogeneous way, and result to be different in the two hemispheres. In fact, mean background Hg^0 concentrations are different between Northern and Southern Hemispheres, ranging between 1.5-1.7 ng m^{-3} and 0.9-1.5 ng m^{-3}, respectively. This difference is influenced by the greater contribution of anthropogenic emissions in the Northern Hemisphere [13,28,29]. Otherwise, the forms of GOM and PBM have lower concentration than GEM because they have an atmospheric residence time of about 1-7 days, since these species are much more reactive and less volatile thus settling more quickly than GEM [8]. Once emitted from anthropogenic and natural sources, oxidized species of Hg tend to condense onto particulate matter or to be readily removed and transferred to aquatic and terrestrial receptors by dry and wet deposition processes or scavenged by clouds or rain, due to their solubility in atmospheric droplets. For this reason, both GOM and PBM species, generally settle down locally or regionally, near emission sources, such as power plants, incinerators, and non-metal smelters [3,13]. As previously reported, GOM is also known as RGM due to the reactivity towards stannous chloride, which act as a reducing agent and can convert it into GEM. The main divalent species of mercury that make up the RGM are $HgCl_2$, $HgBr_2$, HgBrOH and HgO [27,30,31]. The oxidation processes represent an important step for the removal of mercury from the atmosphere because they determine and, in turn, control, the mean residence time of atmospheric mercury [34]. The oxidation processes are also influenced by environmental conditions as well as the presence of oxidizing species, such as hydroxyl radical ($^{\cdot}OH$), ozone (O_3), reactive halogen species including atomic and various molecular and radical forms of bromine, chlorine, and iodine, hydrogen peroxide (H_2O_2), and nitrate radical, [35]. Rapid oxidation events of elemental mercury to divalent mercury, with consequent decrease in the residence time of GEM in the atmosphere, occurs for example throughout spring in the Polar Regions (Arctic) at the occurrence of the Atmospheric Mercury Depletion Events (AMDEs). During these AMDE events GEM can be easily oxidized, due to the high concentration of Br radicals, subsequently

deposited as GOM in a short time that varies from days to hours, and then re-released into the atmosphere [34,35]. Similar situations of rapid oxidation of elemental mercury and consequent formation and deposition of oxidized mercury species occur in the marine boundary layer (MBL) [36,37].

1.3.2 Mercury in aquatic ecosystems

The environmental fate of mercury in aquatic ecosystems is quite complex, since its toxicity, mobility and bioaccumulation depend on its chemical form [40]. Therefore, the study of Hg speciation in seawater is of key importance to understanding the Hg cycle in the global environment, and more specifically, its fate in the biotic and abiotic components of marine ecosystems, improving our understanding of patterns that may impact human health [40]. Aquatic ecosystems are the main environmental matrices through which methylmercury exerts its primary environmental and human health impacts using the aquatic organisms that will subsequently be consumed by humans through diet [12]. During its global cycle, the atmospheric mercury reaches aquatic environments mainly through different processes of atmospheric deposition [41]. Hg can be found in rainfall, snow or it can be absorbed by fog droplets and clouds or adsorbed on atmospheric particulate matter and then deposited in the aquatic environment. The inorganic mercury is the main form present in rainfall and snow that deposit in the aquatic environments [42]. The Hg^0 long-range transport favours the atmospheric deposition processes in achieving other aquatic ecosystems far from the emission sources [12,38]. The aquatic environment (freshwater, marine and ocean) includes water, sediment, aquatic fauna, and flora, where Hg can be present in different physical forms (dissolved or particulate), and in different oxidation states. The presence of some species rather than others, their transformation, mobility, distribution between solid and aqueous phases, their toxicity and uptake by living organisms, are determined by the propriety of each of them [21]. Once in the water, mercury can be present in different forms. The main Hg forms are elemental mercury (Hg (0)), complexes of Hg (II) with various organic and inorganic ligands, and organic Hg forms, mainly as monomethylmercury cation and dimethylmercury (DMHg) [40]. A crucial part of the global mercury cycle lies in oceanic production of volatile dissolved forms of mercury, called dissolved gaseous mercury (DGM). DGM is present as Hg (0) and DMHg [40], but Hg (0) is the dominant form in

the upper ocean, while dimethylmercury may be present at greater depths [40]. The most important sources of Hg (0) are reduction of Hg (II) by aquatic microorganisms and photoreduction of Hg (II). The presence of dissolved organic matter (DOM) may play a role in the rate of DGM formation; in particular, a photo-sensitizing role of humic substances in marine photochemical reactions has been identified [40].

Inorganic mercury Hg^{2+} in dissolved or particulate form is the main form of Hg in freshwater and marine water systems. It can be sorbed onto suspended particulate matter (SPM), which includes inorganic particles, organic matter, and living species such as phytoplankton and zooplankton [6]. Moreover, the inorganic mercury can undergo methylation mainly through biological mechanisms or abiotic processes. The formed methylmercury can bioaccumulate and biomagnify through the food web or can be photo-reduced to Hg^0 and re-emitted to atmosphere, alternatively it, can be demethylated. The methylation of inorganic Hg^{2+} to methylmercury is the key step in the Hg cycle leading to wildlife and human exposure. This organic compound is the only that can biomagnify. In fishes' muscular tissues, most of mercury is present in the methylated form and it is bioavailable for transfer to upper trophic levels, increasing in concentration as it moves up the food web. The top predators in the food web may have higher concentrations of methylmercury in their tissues than the concentrations found in the surrounding aquatic area (Figure 1.5).

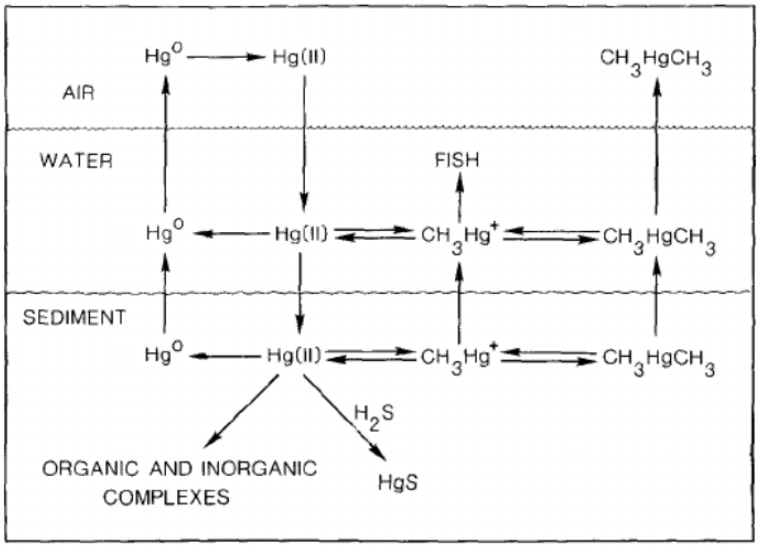

Figure 1.5 Schematic representation of mercury cycle [43].

1.3.3 Air-sea exchange processes

A critical aspect of the mercury biogeochemical cycle is represented by the exchange processes and mercury flows that occur at the air-water interface, between the atmosphere and aquatic systems, which are environmental ecosystems particularly important for the global cyclical distribution. The atmosphere is the main environmental matrix for the global mercury distribution and aquatic systems are important environmental tanks of mercury where it is deposited by atmospheric deposition (wet and dry) and from which it is subsequently re-emitted into air through evasion processes. At the basis of the mercury exchanges between the two ecosystems, different reaction mechanisms take place, involving oxidation and reduction processes among the mercury forms present in the various environmental compartments and influencing it biogeochemical cycle. Over the years, the understanding of the dynamics of mercury exchange between atmosphere and ocean in the marine boundary layer (MBL) has been the subject of growing scientific interest, given its important role in cycling and transport of mercury. In the MBL, photochemical processes positively influence the oxidation of elemental mercury and consequently increase the levels of oxidized mercury species [44]. The flow between atmosphere and water occurs when the Hg^{2+} dissolves or when the Hg^{0} evaporates from the surface water layer and the saturation state of each matrix involved will determine the direction of mercury flow. However, the concentration gradient of the Hg flow at the air-water interface, the solar radiation that determines the photo-reduction of Hg^{2+} in the surface water, the temperature of water, and air surfaces, affect mercury evasion flow into the atmosphere, which seems to be predominant over deposition [8,43,44].

1.4 Mercury and human health

Mercury is a highly toxic metal that represents a global threat to human health and the environment since all its forms present in the various environmental media may have adverse effects on environmental ecosystems and human health. The toxic effects and the severity of the damages strongly depend on the mercury chemical form, and on additional factors, such as the exposure dose, the combination of its toxicokinetic mechanisms like absorption, distribution, metabolism, and excretion. As previously reported, the most toxic and dangerous form of Hg is the organic one, the methylmercury [47], the main source for human exposure is the dietary consumption of methylmercury-contaminated

fish and seafood [45,46]. The high methylmercury concentration in fishes are extremely hazardous to consumers and, in this regard, a limited human consumption of marine fish has been recommended. The toxic effects of methylmercury have been highlighted by dramatic episodes of poisoning in the past where human population have been exposed to mercury through the trophic chain. Among these events the most important case was that occurred within the Minamata Bay (Shiranui Sea, Japan, 1932-1968). There was a release of wastewater containing inorganic mercury from the Japanese chemical industry Chisso Corporation, which caused high mercury concentration in water, significantly influencing methylmercury accumulation along the trophic chain, with harmful consequences on the human population exposed to the consumption of contaminated fish and seafood [49]. Approximately 2000 people were intoxicated (many of whom died) showing typical signs and symptoms that characterized what various studies in this regard defined as the "Minamata syndrome". The damages caused by methylmercury mainly affects the brain, but also extends to other organs such as liver and kidneys. The most vulnerable and sensitive to the adverse effects of mercury are fetuses, newborn babies and children. The brain of the fetus is particularly sensitive and vulnerable to the action of this important neurotoxin. In fact, methylmercury ingested through Hg contaminated food is absorbed by the gastrointestinal tract and passes to the circulatory system, where, due to its strong affinity for the sulfhydryl groups, it is mainly transported inside the red blood cells linked to haemoglobin. Through the circulatory system methylmercury is distributed to all body districts and being highly lipophilic it may cross the blood-brain and placental barriers reaching the fetus and influencing its development with serious anomalies at neurological level such as mental retardation and brain paresis. Similar effects such as neurological disorders, permanent brain damage associated with memory, language, vision, hearing and motor skills, as well as death also occur in adults [48,49]. The severity of the damages caused by methylmercury is influenced both by its absorption from the gastrointestinal tract and by the high lipophilicity, characteristics that increase the biological half-life of this organic form in biological tissues, and therefore reduce the possibility of excretion from the body thus allowing its bioaccumulation [52].

Another episode of collective population poisoning due to methylmercury occurred in Iraq (1972-1973), where the human exposure took place through the consumption of contaminated bread produced with wheat treated with methylmercury as a fungicide [35].

Poisoned people showed neurological symptoms such as ataxia, dysarthria, deafness, tremors, and muscle hypotonia as well as mental retardation in children. Since the exposure to methylmercury mainly depends on the diet, some limit has been introduced. The World Health Organization (WHO) and the United States Environmental Protection Agency, indicated as the maximum tolerable intake of methylmercury the values of 1.6 μg kg^{-1} body weight per week [50,51].

In addition to methylmercury, people may also be exposed to elemental or inorganic mercury through inhalation of mercury vapor during occupational activities or spills, or through direct contact from mercury use. For example, in many developing regions the inhalation of mercury vapor, associated with Artisanal and Small-scale Gold Mining (ASGM) where mercury is used to extract gold from gold-bearing sediments and rocks, represents a significant source of occupational exposure to mercury. In this case, the miners burn an amalgam of mercury and gold to vaporize mercury and recover gold [55]. Mercury vapor is easily absorbed by inhalation in the respiratory tract and once arrived in the bloodstream, due to its high lipophilicity, it crosses the cell membranes, such as the blood-brain one and accumulates in the brain, causing damage to the central nervous system. Instead, a portion of mercury is oxidized to Hg^{2+} and accumulates mainly in the kidneys, where it exerts its toxicity. Additional symptoms due to the inhalation of mercury vapor are insomnia, memory loss, tremors, neuromuscular effects, and cognitive and motor dysfunction. Inorganic mercury in the human body follows the same path as organic mercury, accumulating mainly in the plasma fraction and then concentrating in the internal organs. It can mainly cause kidney and intestinal problems and is also corrosive to skin and eyes [56]. Therefore, in addition to being an environmental toxic substance, mercury poses a threat to global society. This is the reason why information on the relationships among Hg in the atmosphere, in the deposition, and the consequent contamination of ecosystems is a key challenge for the scientific community [25]. In this regards, future challenges should focus on increase the knowledge on how to limit mercury contamination on a global scale and identify appropriate strategies to prevent the adverse effects of mercury on ecosystems and human health.

Chapter 2

Mercury Monitoring Programs: from historical to new challenges at regional and global scale

2.1 Introduction

Mercury is considered a global pollutant due to its ability to be transported over long distances, far from the point emission source before being transformed into its various forms and reaching the various environmental compartments worldwide [3]. The linkage between long-range environmental contamination from mercury and potential impacts on human health represents one of the main reasons why Hg was added to the environmental political agenda in recent years, at national, regional, and global scale levels [10]. In fact, the scientific and political community is paying particular attention to adverse effects of mercury pollution and to the need of improving and extending monitoring activities. These latter represent a precious resource for a greater understanding of the Hg atmospheric gradient and of its global long-term distribution, in supporting relevant international mercury programs. Starting from the late 70's, several mercury monitoring sites had been established, as part of regional networks within North American, European, and Asian countries. Nevertheless the increase in knowledge about the unique properties of mercury has been brought out the need to strengthen existing monitoring programs through the establishment of a global network to improve the understanding of its behaviour and fate at global scale. In this scenario, a coordinated global observational network for atmospheric Hg, was established within the funded FP7 – GMOS project (Seventh Framework Program – Global Mercury Observation System), during the five years development of the project, from 2010 to 2015. Since the 2015 the coordinated network is continuing to operate in the framework of the GEO (Group of Earth Observation) program, and particularly within the GEO flagship on "*tracking persistent pollutants*", the GOS^{4}M (Global Observation System for Mercury) which supports the several articles of the Minamata Convention. Since mercury is a global issue that requires concerted global actions for effective protection of human health and environment, a top priority need for political and scientific programs is indeed the possibility to have a global

perspective on the problem of mercury pollution, through a legally binding global tool. An important international response has been the Minamata Convention on Mercury, which was the first global Convention on environment and health [10].

During the last years, there was a growing interest in increase monitoring sampling sites to assess Hg levels at different scales, such as those at global, regional, and national level. The European Commission in 2010, with Directive 2008/50/EC, established, as mandatory, the Hg monitoring within all the European air quality networks. As an example, in this chapter, the Italian "Reti Speciali" agreement, set to boost – among others – Hg measurements at national level, will be presented and described.

2.2 Coordinated Mercury Monitoring Programs on Regional Scale

In the past two decades, in order gain mercury data with a larger spatial representativeness, also covering remote locations and developing countries, multiple coordinated monitoring networks as well as long-term research programs, have been established in several regions and countries of the world, on a national, and global scale (Figure 2.1) [25].

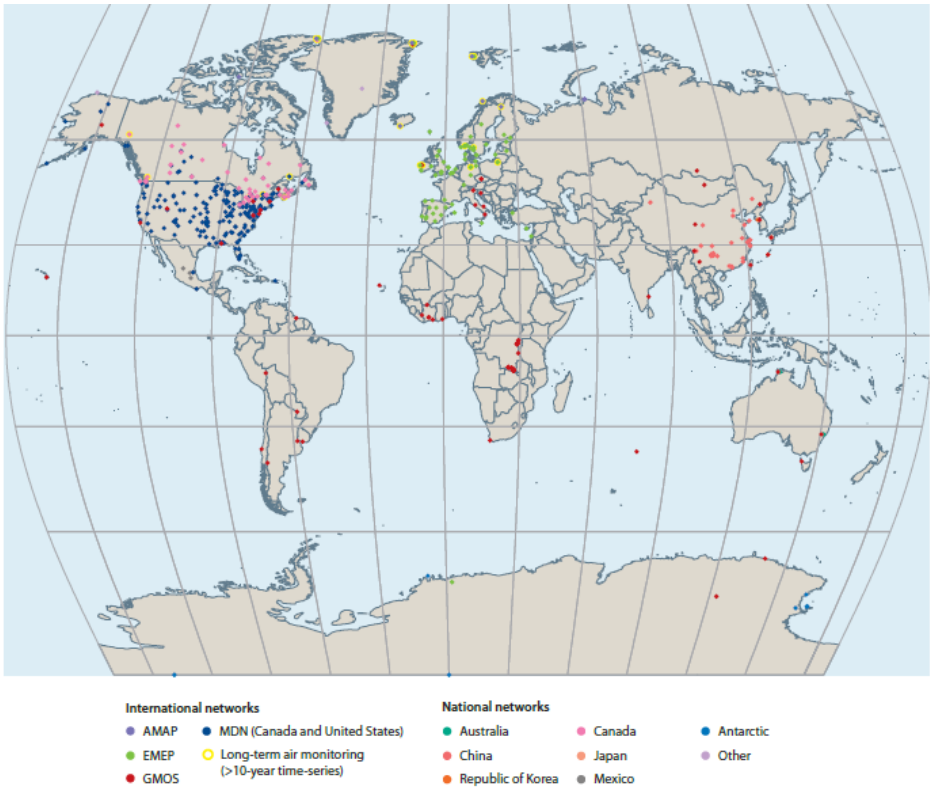

Figure 2.1 Global map of Hg monitoring networks [15].

In this line, several national networks exist and operate to support environmental international agreements and conventions through the development of common and shared procedures for measurements and reporting of high-quality data and for evaluation of trends and patterns worldwide. One of the most important national networks in North America is the Canadian Air and Precipitation Monitoring Network (CAPMoN), operated by Environment and Climate Change Canada (ECCC). The network was established in 1983 and was designed to monitor and study atmospheric pollutants, including total gaseous mercury and mercury in precipitation (wet and dry deposition) since 1996 [14,54]. Another monitoring program in Canada is the Canadian Northern Contaminants Program (NCP), which measures continuously atmospheric mercury at two remote stations, Alert (Nunavut) - since 1995 - and Little Fox Lake (Yukon) - since 2007, contributing to the understanding of long-range transport of mercury (UNEP Global Review of Mercury Monitoring Networks, 2016). In addition, in 1977 in North America, U.S. Agricultural Experiment Stations established the National Atmospheric Deposition Program (NADP) to measure atmospheric deposition and study its effects on the environment. NADP provides long-term records of total mercury concentrations and precipitation in the USA and Canada, to assess the long-term atmospheric mercury trends and to respond to future needs for environmental information on the effects of atmospheric deposition on terrestrial and aquatic ecosystems, biogeochemical cycling, climate change, and human health. Several networks joined the Program like the Mercury Deposition Network (MDN) and the Atmospheric Mercury Network (AMNet), which are focused on mercury pollution. MDN joined NADP in 1996 providing data on the concentration of total mercury in precipitation at sites located in North America, and information on the role of precipitation as a source of mercury in water bodies.

Afterwards, AMNet joined NADP in 2009 carrying out measurements on atmospheric mercury fractions (GEM, GOM and $PBM_{2.5}$) contributing to dry and total mercury deposition evaluation across North America, by facilitating a more complete scientific understanding of the mercury biogeochemical cycle and the ecological responses to mercury exposure through atmospheric pathways [15, 54, 55]. The Arctic Monitoring and Assessment Programme (AMAP) is a coordinated air monitoring program covering the Arctic areas of North America and Eurasia [15]. It was established in 1991 with the aim of monitor and assess climate change and pollution issues, including mercury and its long-

range transport to the Arctic from global sources [57]. In Europe, one of the first established international environmental measurement networks was the European Monitoring and Evaluation Programme (EMEP) [14]. It is a scientifically based and policy-driven program that was established by the Convention on Long-range Transboundary Air Pollution (CLRTAP). In addition to atmospheric measurements of sulphur and ozone, heavy metals, and particularly Hg which was listed as one of a priority pollutants as well as some persistent organic pollutants (POPs) have also been included in this monitoring program since 1999, with the main objective of regularly provide governments qualified scientific information on atmospheric pollutants. The operation of EMEP focuses on the combination of three elements: collection of emission data, measurements of air and precipitation quality, and deposition of air pollutions [57] EMEP is in charge of monitoring mercury in Europe and most of its monitoring stations are located in the northern, western and central parts of Europe while just some of them are located in the southern and eastern parts of Europe. A particularly interesting and important Hg monitoring site within EMEP is the Mace Head station, located in the west coast of Ireland, which measure TGM since September 1995 and maintains the longest time series of atmospheric Hg measurements with high time resolution in the temperate marine background atmosphere [14].

Asia, Japan, and Taiwan (China) have a large coverage of mercury monitoring stations compared to other countries in the region. Overall, the monitoring stations operating in Japan, Republic of Korea, Vietnam, Thailand, the Philippines, and Indonesia belong to the Asia-Pacific Mercury Monitoring Network (APMMN). Despite the coverage in Asia seems lower than in Europe and North America, joint efforts to establish a uniform monitoring network based on national systems in the region are ongoing [57]. However, the presence of national and regional monitoring networks operating in Europe, Canada, the United States and Asia is not sufficient for the creation of a coordinated mercury dataset on global scale capable of providing helpful information to obtain new insights on global emission trends, mercury deposition and re-emission flows. Therefore, a recognition of a coordinated observational network for mercury was necessary, in order to establish new measurement sites in Southern and Northern Hemisphere covering spatial gaps, establish the source-receptor relationships within the Hg cycle, allow models

validation at global scale, and then appreciate the interhemispheric transport as well as trends in background concentrations [28].

2.3 The GMOS Global Network

In November 2010, the Institute of Atmospheric Pollution of the National Research Council (CNR-IIA), with the financial support by the European Commission, promoted and coordinated the European Project Global Mercury Observation System (GMOS), with the aim to develop a global scale network of atmospheric Hg monitoring sites in the framework of this project (Seventh Framework Program – FP7). The goal of this monitoring network is to join existing regional and national Hg measurement networks (i.e., EMEP, AMAP) with new monitoring stations located in regions of the world where observational atmospheric Hg data were limited or completely absent such as the Southern Hemisphere and Tropical areas [28,39,56]. In fact, GMOS network was developed by integrating newly established GMOS sites, selected in regions of the world where atmospheric Hg observational data were scarce, with pre-existing sites [28]. To date, GMOS network includes and operates many monitoring stations located in Europe, North and South America, Asia, and Africa in coordination with national programs and regional agreements, providing observations from more than 40 ground-based monitoring spread around the world. Furthermore, to obtain an adequate understanding of the global mercury cycle, the GMOS observational program also includes ad-hoc oceanographic campaigns providing key information on mercury species concentrations in the marine boundary layer (MBL), in the maximum surface microlayer, and in the water column to evaluate the exchange rates of gaseous mercury at the air-water interface. In addition, the GMOS network focuses on tropospheric studies as well through aircraft measurements to assess mercury species on vertical profiling from the lower stratosphere to the lower troposphere both over industrial areas and regions characterized by natural emission sources (i.e., volcanos), for the identification and tracking of the plume to quantify and better understand the potential extent and relative importance of industrial, urban, and natural emissions. Therefore, data and information about Hg obtained by the GMOS were acquired through measurements carried out in land stations, in marine environments and air, and through the coordination of oceanographic campaigns and aircraft measurements, in order to intercept major intercontinental and continental air mass movements.

The GMOS ground-based stations are mostly located at background sites, distributed at both sea level and high-altitude locations, as well as in climatically diverse regions, including polar areas (Figure 2.1) [15]. Within the GMOS network, monitoring stations sites are classified as Master, since they provide mercury speciation measurements (GEM, GOM and $PBM_{2.5}$), and Secondary, that provide only total gaseous mercury (TGM) or GEM measurements. Moreover, both Master and Secondary sites collect precipitation samples for Hg analysis. The high-altitude monitoring station of the CNR-IIA, "Monte Curcio (MCU)", located in southern Italy, is part of the GMOS network. GEM levels revealed at MCU for one year, between 2019 - 2020, have been examined and results discussed in Chapter 4 of this thesis. Mercury measurements within the GMOS network have been carried out using high-quality techniques by harmonizing the GMOS measurement procedures with those already adopted at existing monitoring stations around the world, in order to assure high-quality observations in line with international quality assurance/quality control (QA/QC) standards. GMOS has answered not only to the need of having a global Hg monitoring network with comparable data worldwide but also to the necessity of providing international standards for inter-comparability [30]. In fact, to guarantee the full comparability of the observations collected in the network, Standard Operating Procedures (SOPs) and common QA/QC protocols have been implemented in all GMOS sites. These SOPs were developed based on the practical techniques incorporated within the existing European and American monitoring networks and then reviewed by GMOS partners and external partners before being adopted within the GMOS network. In addition, a centralized online system, named GMOS Data Quality Management (G-DQM), was designed and developed to ensure the fully integrated operation of the GMOS network, and the almost real-time acquisition of Hg atmospheric data.

The G-DQM system is also used to automate the QA process and it is available on the web with a user-friendly interface to manage all the QC steps from initial data transmission through final expert validation. Given the number and size of the data to be processed, G-DQM system is essential for processing data streams generated from the several monitoring stations. In addition it is useful for guaranteeing, controlling, and reporting the quality of mercury data-sets from the GMOS network providing reliable data on a global basis for both scientific and political communities. The G-DQM system

is a part of the GMOS Cyber-Infrastructure (GMOS-CI) that oversees data acquisition and data sharing among participating observers, ensures data validity and interoperability, their management, processing and sharing within GMOS network. It also allows site operators to be notified when their tools operate outside the parameters of the SOPs [60]. The GMOS-CI was developed following the Group on Earth Observations (GEO) data sharing and interoperability principles [14]. Data collected within GMOS network are then used to validate mercury models on a regional and global scale, to evaluate global mercury deposition and re-emission flows.

In this regard GMOS has been selected by GEO program to provide a valuable contribution to the development and the implementation of international policies and consequently for support United Nations Environment Programme (UNEP) for the implementation of the Minamata Convention. The GMOS network is currently part of the GEO strategic plan (2016–2025), aimed to develop a global observing system for Hg and Persistent Organic Pollutants (POPs). It is also a fundamental part of the GEO flagship on "tracking persistent pollutants" GOS^{4}M (Global Observation System for Mercury), which supports the development of a global monitoring network of mercury and the achievement of international programs and conventions, such as the Minamata Convention. This flagship also promotes research on new technologies that allow to perform long-term monitoring programs and to improve Hg spatial data coverage at sustainable costs. In this scenario, for increasing the GMOS geographical coverage through a consistent number of monitoring sites, reducing the costs associated to the extension of monitoring program and making the program itself more manageable and robust on global scale, a system of passive air samplers (PASs) for mercury based on nanostructured advanced materials was developed. These devices were firstly used for the development of a network for mercury monitoring in ambient air within a pilot project in cooperation with the World Health Organization (WHO), and founded by United Nations Environment Programme-Global Environment Facility (UNEP-GEF). The project entitled "*Development a plan for global monitoring of Human exposure to and environmental concentration of Mercury*" aims to harmonize approaches for mercury monitoring and to reinforce the capacity for mercury analysis on humans and in the environment, strengthening the GMOS network through the development of the complementary PASs network for mercury in ambient air. The GOS^{4}M flagship

supported this project and is encouraging its further development to reach the objectives of the Minamata Convention on Mercury with regard to Articles 19 and 22. The creation of the GMOS network, highlighted the importance of a close cooperation between the existing monitoring networks and the new ones, for supporting the implementation of a long-term monitoring, covering both hemispheres, and for ensuring comparability between different monitoring datasets produced with common standard methods, or with new technologies (i.e. PASs). The intention of the overall GMOS research strategy is to better understand emissions, transport, and storage of Hg on a global scale thus supporting the Minamata Convention, an important global legally binding instrument on mercury, promoted by UNEP and adopted by several countries aware of not being able to control and fight alone the cross-border effects of mercury.

2.4 The Minamata Convention on Mercury: a global commitment to protect human health and the environment

The Minamata Convention on Mercury is a global treaty that aim to protect human health and the environment from the adverse effects of mercury and represents an important advance in global environmental stewardship. It is named after the place in Japan where mercury-tainted industrial wastewater poisoned thousands of people, leading to severe symptoms that became known as the "Minamata disease" (Chapter 1) [14]. The Convention was promoted by the UNEP and the negotiations process to prepare a global legally binding instrument on mercury started in 2001, undertaking the global assessment of mercury and its compounds, its chemistry and health effects, sources, long-range transport, as well as prevention and control technologies relating to mercury. In 2003, following extensive evidences on the issues of mercury pollution, it turned out that actions taken to date had not been sufficient to address the concerns on adverse impacts of mercury, and that a global action against mercury pollution was necessary to reduce risks for human health and the environment. In 2009, UNEP decided to develop a global legally binding instrument on mercury and, after several intergovernmental negotiations, in January 2013 the text of the Minamata Convention on Mercury was agreed. In October of the same year the text was adopted and opened for signature until October 2014 in Kumamoto, Japan. Finally, on August 2017, the Minamata Convention on Mercury entered into force. Governments around the world who voluntarily decided to accede to

the Minamata Convention, have demonstrated their commitment to assume the consequent legal rights and obligations under the Convention in order to be able to face what remains a major global challenge through international cooperation on mercury monitoring and innovation.

The various countries participating in the Convention, aware of the cross-border effects of mercury, have decided to manage their actions regarding the reduction of emissions and releases of mercury into the environment through this legally binding instrument. The main goal of the Convention is guaranteeing the health of the environment, and that of current and future generations, especially of particularly vulnerable populations, such as pregnant women and children. For this reason, the Convention is a multilateral agreement that addresses the devastating effects of mercury through practical actions aimed at reducing global mercury levels and promoting the achievement of better living standards. The Convention recognizes mercury as a chemical substance of concern, given its long-range atmospheric propagation, its persistence in the environment, its ability to bioaccumulate in ecosystems and its considerably negative impact on human health and environment. Consequently, the key factor in defining the obligations under the Convention is the control of anthropogenic emissions of mercury during its life cycle. In fact, the objective of the Convention, as reported in its Article 1, is to protect human health and the environment from mercury anthropogenic emissions. The international regulatory framework provided by the Minamata Convention, and consisting of 35 Articles and 5 Annexes, includes a variety of provisions to control, reduce or eliminate major sources on mercury. As reported by Selin et al., 2018 [61] all the provisions of the Convention can be grouped in the followed areas:

- uses, emissions, and releases;
- support, awareness raising, and education;
- impacts and effectiveness

The text of the treaty establishes restrictions on primary extraction and international trade of mercury, prohibits the manufacture, import and export of a wide range of products with the addition of mercury, and provides for prohibitions or operating conditions for various manufacturing processes that use mercury. Furthermore, the text highlights the ban on creating new mercury mines and the phasing out of existing ones, discourages novel uses of mercury in industrial products and processes, and calls for the adoption of emission

and release control measures, as well as the regulation of activities such as artisanal and small-scale gold mining (ASGM). Finally, the Convention also contains provisions regarding the mercury storage and the management of mercury-containing waste so that these processes are carried out with respect for the environment.

The international treaty of Minamata Convention, through the Article 19, called "*Research, development and monitoring*", stresses the importance of improving monitoring activities on mercury for participating parties. In fact, Article 19 highlights the need for cooperation between the Parties to improve monitoring tools and methods, as well as current monitoring networks because effective monitoring systems covering all geographical regions and communities at risk are essential to obtain better information about mercury environmental cycle, its transport, deposition, transformation and fate in the environment. Moreover, it is important to distinguish between anthropogenic and natural emissions, and releases of mercury and of remobilization of mercury from historic deposition [14]. In this context, the Convention stresses the need to investigate the mercury cycle, its current sources and their impact on the environment and health since this baseline information regarding mercury emission, releases, deposition, distribution, and concentrations in humans and in the environment are essential for effectively control and reduce mercury globally. For this purpose, the Convention, with the aim of being able to evaluate the achievement of its objectives, established that a periodic evaluation of the effectiveness (Article 22) of the control measures, adopted by the various Parties regarding the mercury pollution problem, after its entry into force, be carried out. Observing the changes of mercury levels in the atmosphere on a large scale represent one way of assessing the success of global mercury reductions. In this context, despite the current method of measuring active mercury has proven to be a remarkably effective way to evaluate both spatial and temporal trends, their costs and their operating conditions in the field often limit their application in many areas of the world. For this reason, the passive air samplers (PASs) for mercury may represent a useful tool in supporting the obligations of the Minamata Convention.

2.5 The National Reference Centre for Mercury (CNRM)

The National Reference Centre for Mercury (CNRM), coordinated by the CNR-IIA, has been established in 2012 yr through a Memorandum of Understanding between the

Italian National Research Council and Ministry for Environment, Land and Sea Protection (MATTM), with the participation of the National Institute of Health (ISS), as part of the initiatives adopted by the Governing Council of the United Nations Environment Programme (UNEP) to tackle the problem of mercury pollution worldwide, and to support national and international organizations in the promotion and implementation of, and also the eventual compliance with, the provisions of the Minamata Convention. The establishment of an international reference centre for mercury and its coordination by Italy is of great strategic importance both nationally and internationally, as it will help strengthen the country's role in international and European environmental policies, and it will give impetus to future technological developments in the field of environmental monitoring and control of industrial emissions. The CNRM consists of four research Units:

(a) the Environmental Observing System;

(b) "Regional and global scale Modeling";

(c) "Emission Inventories and Cyber(e)-Infrastructure";

(d) "Health Impact Assessment"

which all together aim to provide support in the management of the activities related to the production, validation, reporting, and dissemination of high quality data, including those relating to health impacts. The CNRM also implements and coordinates an Italian network for monitoring the population exposure to mercury, from both anthropogenic and natural sources over time, following criteria established according to the UNEP Governing Council, in order to improve the understanding of the mercury cycle and develop effective policies and measures to reduce mercury pollution at global level. In this framework the GMOS global network play a key role in the coordination of the program for mercury and its compounds observation on a global scale useful on the one hand, for model evaluation and improvement for the analysis of future emission reduction scenarios, to support the Italian Ministry for the Environment Land and Sea, UNEP and other relevant bodies involved in the formulation of National Implementation Plans (NIPS), as described in the Minamata Convention. On the other hand, for the development of interoperable systems providing near real-time global mercury data to all stakeholders. An important part of the CNRM's role consists in the providing technical assistance, training and support concerning the Standard Operating Procedures in terms of

conventional and new technologies to be adopted and implemented worldwide, in order to support UNEP and nations in the implementation of several articles of the Minamata Convention with particular regard to Article 22 on “effectiveness evaluation”.

2.6 The Italian Special Network on Mercury

The Italian Legislative Decree 155/2010 “*Implementation of Directive 2008/50/EC on ambient air quality and cleaner air in Europe*” required the identification of “special” national stations for to improve the air quality monitoring, related to some key pollutants, such as $PM_{2.5}$ and PM_{10}, and their chemical speciation, ozone and its precursors, heavy metals including mercury, thus gaining a better knowledge on their mechanisms of formation and transport. In December 2010, the Ministry for Environment, Land and Sea protection of Italy (MATTM), the Institute of Atmospheric Pollution Research of the Italian National Research Council (CNR-IIA), the Italian National Agency for New Technologies, Energy and Sustainable Economic Development (ENEA), the Italian National Institute of Health (ISS) have entered into a collaboration agreement for the launch of the Italian Special Networks (Reti Speciali), in accordance with articles 6 and 8 of the Legislative Decree 155/2010 "*Special cases for assessing the quality of the ambient air*". After the evaluation of an ad-hoc scientific technical committee (CTS), the special stations for air quality monitoring meeting the specific requirements outlined in the Legislative Decree 155/2010, have been selected and then officially identified with the Ministerial Decree of the 29th of November 2012. In particular, in the Article 4 of the previously-mentioned Ministerial Decree, three monitoring rural/suburban background stations, specifically identified for measuring atmospheric mercury and its total deposition, are listed. The chosen monitoring stations are: Schivenoglia (SVG - Lombardy), Montelibretti (MLI - Lazio), and Monte Sant’Angelo (MSA - Apuglia). SVG and MSA are rural sites meanwhile the MLI is located in a suburban area. Moreover, based on the type of measurement carried out, SVG and MSA stations are defined secondary stations because, following the scheduled measurement programme, they have been providing TGM in ambient air and total mercury deposition. Instead, the MLI station, defined as a master site, has been providing mercury speciation analysis (GEM, GOM and PBM) for mercury in ambient air as well as measurements of mercury in both total and wet-only. The three sites of Schivenoglia, Montelibretti and Monte Sant’Angelo,

to meet the regulatory requirements of the Legislative Decree 155/2010, were also chosen as representative of the areas of Northern, Central and Southern Italy, respectively. At the Schivenoglia station, measurements of atmospheric Hg begun in February 2020, thus producing to date a limited Hg dataset to be examined in this thesis. Otherwise, available measurements for Monte Sant'Angelo and Montelibretti sites started in April 2018 and October 2018, respectively. For these two representative stations for the Italian Special Networks, atmospheric Hg trends, the influence of meteorological parameters, and the identification of some potential sources, have been examined and discussed as case studies in Chapter 4 of this thesis.

Chapter 3

Conventional and new sampling and analytical methods for mercury monitoring

3.1 Introduction

During the implementation of the GMOS network, one of the overall goals was the integration and harmonization of Hg measurements performed within the global network, together with measurements carried out within already existing external regional network to allow the exchange and joint evaluation of high-quality data. Integration of GMOS with other existing programs included the arrangement of inter-comparisons regarding measurement and analytical methods. This challenge was achieved with the development of common protocols regarding how the instruments should be necessarily performed in the field, to assure harmonization and comparability of that measurements from different sites worldwide. The following sections show the conventional techniques widely used as regards the active mercury measurements in the atmosphere and the analysis of total mercury in water. Regarding the conventional methods, harmonized Standard Operating Procedures (SOPs) as well as common Quality Assurance/Quality Control (QA/QC) protocols have been developed and implemented within GMOS according to measurement practices and methods followed within existing regional monitoring networks and based on the most recent literature [55,59,60]. The SOPs are also described in the following sections along with an ad-hoc system, named GMOS-Data Quality Management (G-DQM) system, aimed to automatically screen and validate raw data of Hg atmospheric measurements coming from different monitoring stations across the globe, also in near-real time way.

3.2 Conventional techniques for the determination of mercury in ambient air

The main method used to sample elemental mercury for atmospheric measurements around the world is based on gold amalgamation. This method highlights the ability of mercury to form amalgams with metals such as gold and is the basis of all the instrumental techniques used to sample mercury in the atmosphere. During the sampling phase, a gold surface is used to pre-concentrate Hg^0 which is then quantified by thermal desorption of

the amalgam at 550 °C. The Tekran mercury analyser model 2537 (Tekran Instrument Corp., Ontario, Canada) is the most common automatized instrument using the method of gold amalgamation to sample atmospheric mercury [64]. Tekran 2537 provides continuous analysis of gaseous mercury in air at sub-nanogram per cubic meter (ng m^{-3}) level. The mercury quantification trapped on the gold surface is based on the Cold Vapor Atomic Fluorescence Spectrometry (CVAFS), which requires a pure carrier gas such as argon during the analyte desorption and detection phase. In particular, the instrument consists of two gold cartridges arranged in parallel, also called traps or membranes (indicated with A and B), containing adsorbent material in ultra-pure gold representing the gold surface used for pre-concentrating Hg^0 during the sampling phase. Therefore, during the sampling phase the instrument samples, through forced aspiration, ambient air (containing mercury) on the gold trap, which selectively traps the elementary mercury vapors due to the formation of the amalgam (Figure. 3.1).

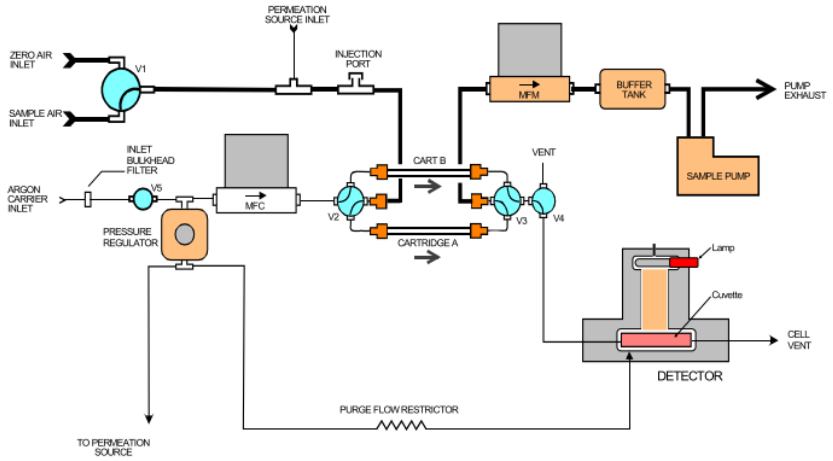

Figure 3.1 Schematic flow diagram of Tekran mercury analyser model 2537 [65].

The mercury, trapped and adsorbed on the gold surface, is thermally released in a carrier gas of ultra-high purity (usually argon) during the thermal desorption phase, when the amalgam is heated to 550 °C, and then sent to the CVAFS detector for quantification. The detected gaseous mercury is then expressed in ng m^{-3}, at standard temperature and pressure, with a detection limit of 0.1 ng m^{-3}. The two cartridges operate alternatively allowing alternate sampling and desorption cycles resulting in a continuous and

automated 5-minutes sampling of the inlet stream with no data gaps. In details, during the analysis cycle, the cartridge A collects mercury from the sample flow while the mercury vapors, previously trapped on the cartridge B, are thermally desorbed in the carrier gas flow to be sent to the CVAFS detector; the roles of the cartridges are then reversed at the end of the analytical cycle. Through the carrier gas, the mercury vapors arrive at the detector where they reach a quartz cuvette, which is irradiated by a low-pressure mercury vapor lamp. The lamp emits radiation at 253.7 nm exciting mercury atoms, which radiate again at the same wavelength. The produced fluorescence is proportional to the concentration of elemental mercury present in the cuvette and is selectively view from a photomultiplier tube (PMT) by means of a monochromatic filter at right angles to the incident light. After the baseline correction, the fluorescence signal (F) has an intensity that, as described by the following equation, is directly proportional to the intensity of the radiation emitted by the lamp source or excitation intensity (I_e) multiplied by the amount of mercury vapor in the cuvette (C_{Hg}):

$$F \propto I_e \, C_{Hg}{}^{0}$$

To obtain accurate measurements it is necessary to calibrate the instrument by automatic or manual calibrations. In both cases calibration is obtained with a known quantity of Hg^0 vapor of. Automatic calibration is based on the use of a permeation source located inside the instrument capable of calibrating the system automatically at a pre-set time. As regard manual calibration, mercury vapors are injected manually by the operator into the analyzer using an automatic gas-tight syringe, after being taken from a primary source of external elementary mercury at controlled temperature, such as that provided by the Tekran 2505 calibration unit. The Tekran 2505 unit is based on the principle of mercury vapor pressure as a function of temperature. Therefore, at a specific temperature value, in the vapor phase there is a precise concentration of saturated mass of mercury that can be taken from the syringe and used for the calibration of an analytical system. Furthermore, this primary source of elemental mercury is also useful for the evaluation of mercury analytical systems and the manual calibration procedure is used to verify the stability of the internal permeation source [66].

To concurrently detect the various atmospheric mercury species, such as GEM, GOM and PBM, in ambient air it is necessary to couple upstream of the Tekran 2537 analyzer, the Tekran 1130 module that allows the determination of GOM, and the Tekran 1135 module by which it is possible to determine particulate bound mercury (PBM). These three Tekran units are synchronized in their operation and once integrated they form a single automated Tekran 2537/1130/1135 system (Tekran Integrated System) (Figure 3.2), able to carry out a complete analysis of mercury speciation in the air. Speciation units are connected to the 2537 analyser through a heated polytetrafluoroethylene (PTFE) line (kept heated at 50°C, and 10 m in length) [61,64].

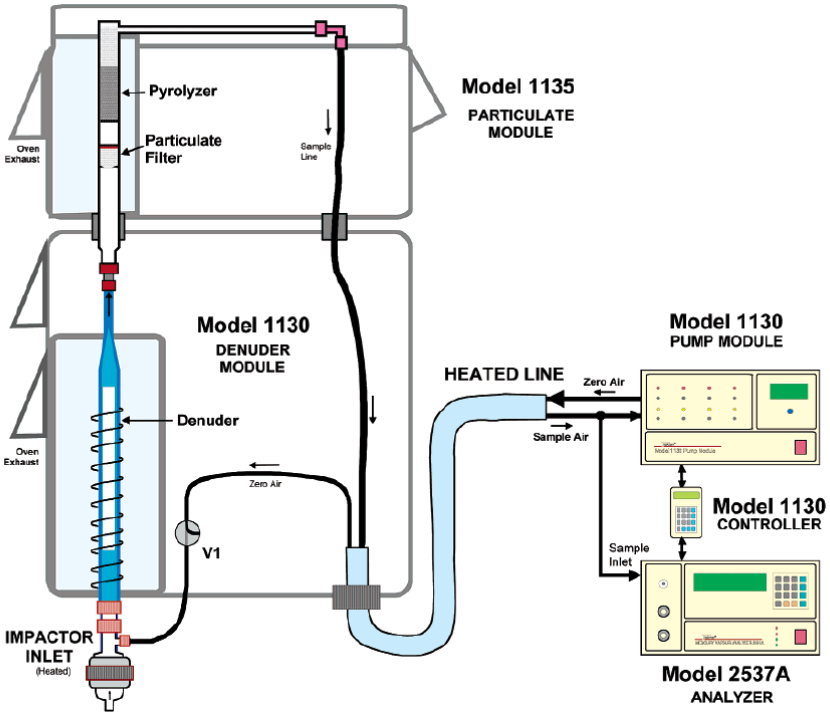

Figure 3.2 Schematic diagram of Tekran automated mercury speciation units 1130-1135 [67].

During the sampling phase, which usually lasts 2 hours, the device supplies GEM concentration values at 5-minute intervals; the sampling phase then follows a 1-hour desorption cycle during which GOM and PBM are quantified. In the sampling mode, a pump module draws ambient air into the glass elutriator inlet, maintaining a temperature of 50 °C for the entire system, thus avoiding humidity problems. The glass elutriator is connected to the module of the denuder (impactor inlet, Figure 3.2) (Tekran 1130 Unit)

and to that of the regenerable particulate filter (RPF) (Tekran 1135 Unit). The GOM is quantitatively collected onto KCl-coated quartz annular denuder (Tekran 1130), meanwhile PBM and GEM continue along the sampling line, until the PBM is collected on the RPF (Tekran 1135), and the GEM reaches the 2537 analyzer where it is trapped on the gold cartridges surface and then thermally desorbed. The released GEM is quantified by CVAFS.

The Tekran 1130 and 1135 units externally consist of a weatherproof container whereas inside there are the needed components, subjected to controlled temperature values, for GOM and PBM sampling. The detected PBM refers to mercury bound to the finer fraction of particulate, which is less than 2.5 μm diameter. This particulate-size selection is made possible by the fact that, when the ambient air flow is conveyed into the Tekran speciation system through the inlet of a glass elutriator, it passes through an impactor and then enters the denuder, thus eliminating coarse particles with a diameter greater than 2.5 μm. Around the impactor, an external heated boot, to reduce the relative humidity influence, can be placed. As previously mentioned, the glass elutriator is connected to the denuder module, ambient air flow reaches the annular denuder which is a key component of the instrument and is located inside the protective container of the Tekran 1130 module. The annular denuder consists of two coaxial quartz tubes and the internal surface of the external tube and the external surface of the internal tube are covered with a layer of KCl, which acts as an absorbent surface and favours the selective adsorption of GOM while GEM and PBM are unable to go through. At the end of the sampling phase, a zero-air flow passes through the annular denuder that is heated for 15 minutes at 500 °C so that the adsorbed GOM can be reduced to the elemental form (GEM). The collected GOM, once released as GEM, arrives at the Tekran 2537 analyzer through the sampling lines to be detected and quantified by CVAFS, by means the previously described steps. Generally, three 5-minute measuring cycles are required to completely remove the adsorbed mercury onto the denuder, since the desorption process is not instantaneous. The denuder coating is regenerated by the desorption phase and immediately after cooling the denuder is ready for another cycle. Periodically, the absorbent surface in the denuder is coated with a sub-saturated KCl solution. Connected to the module Tekran 1130, there is the module Tekran 1135 which, as mentioned, samples the PBM present in the air flow as it flows through its components, collecting these species of mercury on an RPF. The PBM fraction

captured by the RPF is then heated to 800 °C to desorb the captured particulate. The particulate thus reaches the pyrolyzer, which consists of a quartz tube of about 0.95 cm in diameter and 50 cm in length, filled with pieces of quartz which are kept at 800 °C to guarantee the complete decomposition of the PBM in elemental mercury (Figure 3.2) [68]. After cooling, in the quartz tail following the pyrolyzer, the formed GEM arrives to 2537 analyzer to be quantified by CVAFS.

Currently, Tekran 1130 and 1135 modules are the only commercially available systems for the automated measurement of gaseous mercury (GOM) and particulate bound mercury (PBM), respectively. Given the low concentration of GOM in the atmosphere, the 1130 module is based on a phase before the quantification phase by using quartz denuder coated with KCl to selectively collect GOM in air. Despite this, in recent years, several problems affecting measurements have been reported in literature such as events of unequal quantifications of all forms of GOM, interference events with water vapor and ozone. It seems, in fact, that the instrument underestimate the levels of GOM environmental conditions such as high levels of ozone and high relative humidity [64]. All measurement problems related to the exact GOM quantification also occur for the sampling of PBM during which biased measurements can occur since there are no certainties on the real composition of PBM. However, current analytical determination of PBM in a sample of ambient air consists in the collection of this fraction of mercury on a particulate filter, which then undergoes to analysis. For these reasons, research is aimed at developing efficient calibration methods for GOM species to certify Tekran system measurements and to understand the actual chemical composition of GOM and PBM. The CVAFS analytical technique, used by Tekran, allows to reach a lower detection limit and is more sensitive than Cold Vapor Atomic Absorption Spectrometry (CVAAS), which instead is the analytical technique behind the functioning of the Lumex RA-915 AM system. This is another instrument for the determination of atmospheric gaseous mercury. As previously mentioned, instruments using CVAFS technique require pure Ar or He gas, during the desorption and detection steps, while those using the CVAAS principle, require mercury free air or nitrogen. As for CVAFS, even CVAAS instruments detect mercury as GEM by UV radiation at 253.7 nm. Measurements with CVAAS, as described by the following equation, require determination of total UV intensity in absence of Hg^0 (I_0) and in presence of Hg^0 (I):

$$A = \ln\left(\frac{I_0}{I}\right) \propto {C_{Hg}}^0$$

The Lumex RA-915 AM Automatic Mercury Monitor is a fully automated instrument designed for the monitoring of Hg concentrations in background ambient air. The instrument provides direct continuous real-time measurements of mercury expressed as ng m^{-3} at standard temperature and pressure with a detection limit of 0.5 ng m^{-3}. Ambient air is drawn by a pump into a cell where a spectrometer detects mercury concentration using Zeeman atomic absorption spectrometry with Zeeman background correction. In detail, a Hg vapor lamp (radiation source) is placed in a magnetic field and generates a 254 nm light wavelength which is split into three polarized Zeeman components σ-, π and σ+. When the radiation propagates along the direction of the magnetic field, a photodetector reveals only the σ components of the electromagnetic radiation, one σ component within the mercury absorption line envelope (Hg absorption wavelength 254 nm) and the other one is outside it. The signals from both σ components are equal until no mercury vapors are detected in the cell [64]. When mercury is introduced into the cell, the difference in intensity between the two σ components increases as a function of the mercury concentration. In this way, Zeeman atomic absorption spectrometry allows the determination of mercury with extremely low detection limits (less than 1 ng m^{-3} Hg) without interference from other substances present in the ambient air. The Lumex RA-915 AM instrument may be calibrated by exposing to air containing Hg^0, generated from a constant mercury source, or using cells with saturated Hg^0 vapor.

3.3 Conventional techniques for the determination of mercury in water

An extremely sensitive instrument for the analysis of total mercury (THg) in aqueous matrices, such as wet deposition and seawater, is the Tekran liquid sample analyzer, which is a traditionally used instrument for the determination of THg in liquid samples or in solid matrices previously extracted and transformed into liquid matrices. The Tekran analyzer for liquid samples consists of an autosampler (Tekran 2620), a peristaltic pump (Tekran 2610) and a detector (Tekran 2600), which is based on CVAFS for the quantification of the mercury previously trapped with the double fusion technique in gold. The method used for this analysis is the EPA 1631 method "*Mercury in water by*

oxidation, purge, and trap, and cold vapor atomic fluorescence spectrometry" which describes how to treat the aqueous samples to be analyzed, highlighting the importance of the sample preparation phase for analysis purposes [69]. During both samples preparation and analysis, the working environment, all the glass materials and bottles containing the samples must be well cleaned to avoid problems of contamination in the measurements, which could compromise the analysis step. Before starting the analysis, a solution of bromine monochloride (BrCl) in the concentration of 1% v/v must be added to the liquid sample which contains mercury in different forms, mainly bivalent mercury. BrCl is a strongly oxidizing solution that converts all the mercury compounds present in the sample into Hg^{2+}, preserve the sample, and avoid mercury losses due to adhesion to the walls of the flask. The excess of BrCl and the products of the oxidation reaction Br_2 and Cl_2 are neutralized by adding a solution of hydroxylamine hydrochloride ($NH_2OH{\cdot}HCl$) before measurement. Subsequently, the aqueous sample in the test tube is positioned in the Tekran 2620 automatic sampling unit by means of a peristaltic pump. The peristaltic pump is equipped with five different channels which, during the analysis phase, support the flow of the sample, the reducing agent, the waste and ultrapure water, which occurs through two channels of the peristaltic pump. Then, a solution of the reducing agent stannous chloride ($SnCl_2$), contained in another tube connected to the sample tube by means of a Y fitting, arrives at the sample and quantitatively reduces the oxidized mercury contained in the sample to volatile Hg^0. At this point, the solution containing the volatile species of mercury reaches the phase separator (PS), which is necessary to divide the solution into gas and liquid. For this reason, the PS consists of a quartz tube containing a quartz rod along which flows the solution containing the formed elemental mercury while the carrier gas flows upstream to remove the elemental mercury from the solution and transport it in the detector module. The remaining solution is discarded. In the detector module, elemental mercury is subjected to the preconcentration phase on the two gold cartridges, which takes place by means of two-stage gold melting. In fact, the first cartridge, made of golden sand, serves for the preconcentration of mercury, while possible interferents such as organic solvents, halogens and water vapor pass through don't reaching the cuvette. This cartridge is heated to 550 °C allowing the thermal desorption of trapped mercury, which is then transported to the second cartridge that is the analytical cartridge made of pure gold particles and is responsible for the

quantification of mercury present in the sample. The mercury adsorbed on this cartridge and released by thermal desorption is transported to the quartz cuvette placed in the detector to be detected and quantified by CVAFS. A low-pressure mercury vapor lamp illuminates the cuvette, emitting radiation at 253.7 nm that excites the mercury atoms, which radiate back at the same wavelength. The fluorescence produced is proportional to the concentration of elemental mercury present in the cuvette and is selectively displayed by a photomultiplier tube.

3.4 Standard Operating Procedures

Conventional techniques for the active monitoring of mercury concentrations in the atmosphere and in deposition, described in the previous sections have been used in monitoring sites belonging to the GMOS network. Their field application is managed by specific common protocols called Standard Operating Procedures (SOPs), which were developed during the planning and implementation phase of the GMOS global network, in accordance with the measurement practices and methods adopted in well-established regional monitoring networks [58,68]. The SOPs have been designed to support sampling in the sites belonging to the GMOS network, were applied in order to harmonize the measurements obtained in the various sites of the network and to guarantee comparability among data obtained from all monitoring sites. Therefore, the SOPs are standardized protocols that provide both information on the method of determination of mercury in a specific environmental matrix, the procedures for use, and the technical maintenance on field of the automated instruments used in the network sites. The GMOS SOP "*Methods for the determination of TGM and GEM"* were based on the European standard (NEN-EN 15852 (en)) for TGM and GEM measurements, and on the Canadian Atmosphere Mercury Measurement Network (CAMNet)/Canadian Air and Precipitation Monitoring Network (CAPMoN) SOP for TGM measurements [71]. This SOP was developed within the GMOS network to be used as a reference guide for TGM and GEM continuous measurements and describes methods for determining TGM and GEM by using Tekran 2537 or Lumex RA-915 AM systems. Moreover, it includes the quality control protocols that have to be used during the execution of TGM/GEM measurements on field. For example, the SOP highlights how often the active TGM/GEM monitoring through automatic instruments requires some checking, such as a measuring cabin containing the

instrument, which is at controlled temperature and free from mercury, the adequate power supply necessary for the operation of the instruments, the presence of pure gases used during the desorption and detection step, and the presence of qualified operators for the installation and maintenance phases of the instruments over time. In addition, the air to be sampled is pulled inside the instrument by the sampling inlet and the sampling line. The sampling inlet must be installed in a position free from buildings and trees, placed at least 2 m above the ground so that the air flow around the sampling inlet is free and positioned for avoiding rain or snow from entering the sampling system. In addition, automatic calibration of Tekran 2537 by permeation source is recommended at least every 71 hours with a permeation time of 120 seconds, while manual calibration with manual injections should be performed quarterly, on annual basis, and is useful for checking the source of permeation and confirm its stability.

Besides this SOP, another GMOS SOP referring to "*Methods for the determination of speciated ambient Hg*" was generated. This latter specifically describes the methods of sampling and determination of simultaneous measurements in ambient air of GEM GOM PBM through the Tekran 2537/1130/1135 automated system. This SOP also contains procedures for the correct operation and maintenance of the integrated Tekran system itself and itis based on the United States Atmospheric Mercury Network (AMNet) Standard Operating Procedure [72]. The SOP recommend a 2-hour sampling period for GOM and PBM, during which GEM is continuously sampled at the recommended 5-minute intervals, except for remote sites where a 3-hour sampling period may be necessary. Following the sampling phase, a 1-hour desorption cycle for GOM and PBM quantification, during which each step requires a 5-minutes cycle, should be programmed as follows:

- 3 zero air flushes: the sampling system is flooded with zero air that acts as a carrier gas during subsequent analysis steps;
- 1 pyrolyzer heat cycle: the pyrolyzer is heated for converting any mercury compounds to elemental form;
- 3 particulate heat cycles: the regenerable particulate trap is heated to desorb PBM captured on the trap. The heating process reconditions the trap. The mercury released during this step is quantified by analyser 2537;

- 3 GOM denuder heat cycles: the denuder is heated, releasing the GOM trapped during sampling. The pyrolyzer and particulate trap continue to be heated during this step, allowing the eluted mercury to pass through without losses;
- 2 zero air flushes: the system is cooled and post-analysis zero levels are determined.

The sum of the concentration of the three particulate heat cycles, minus 3 times the value of the third zero air flush, represents the concentration of PBM, while the sum of the concentration from the three denuder heat cycles, minus 3 times the value of the third zero air flush, represents the concentration of GOM. Furthermore, the GMOS SOP suggests re-covering the absorbent surface of the denuder with a KCl solution after 15 days of use to avoid passivation [72] and also a thorough cleaning of all the components of the Tekran speciation system, for preventing the contamination of sampling equipment and ensuring the collection of the highest quality data. A volumetric flow rate of 10 L m^{-1} through the inlet is recommended with the Tekran 2537 unit which should pull at 1 L m^{-1} for GEM sampling while the 1130 pump module, which acts as support for the Tekran 1130 and 1135 units, instead pulls at 9 L m^{-1}. This volumetric flow rate can be reduced at high altitude sites because at lower atmospheric pressure it may be difficult to achieve 10 L m^{-1} at inlet. The Tekran system for speciated ambient Hg monitoring requires a continuous power supply and a mercury-free sheltered structure with a temperature-controlled system for the Tekran 2537 and the 1130 pump module. To guarantee the collection of high-quality data, a trained operator should visit the measurement site weekly, inspect the instrument and do proper maintenance.

Referring to mercury in deposition, the GMOS SOP "*Method for the determination of total mercury in precipitation*" was defined on the base of the Hg measurement standards set by the European Monitoring and Evaluation Programme (EMEP) and the North American Atmospheric Deposition Program (NADP) Mercury Deposition Network (MDN). It was developed within the GMOS network to be used as a reference guide for the determination of total mercury in precipitation at GMOS monitoring stations using wet-only or bulk deposition collectors [73]. The automated wet-only collectors present an automated system with a wetness sensor that opens the collector to the atmosphere only during precipitations because they only collect dissolved particles and components that are removed from the atmosphere through precipitation-related processes. Its use is recommended in sites where a power supply is available, a regular site operator is present,

and where the functionality of the collector is not impeded by extreme weather conditions. During the opening phase, however, it is probable that some dry particles (non sedimenting particles and gases) can enter this type of collector, whose collection efficiency can be influenced by various factors, such as wind speed, type of precipitation (rain or snow) and the aerodynamic properties of the sampler.

The bulk collector captures the total mercury deposition from the atmosphere, which includes all the gases and the wet and dry sediment particles because this kind of collector always remains open to the atmosphere regardless of precipitation. Therefore, bulk collector does not distinguish whether the collected atmospheric components have been removed through wet or dry deposition, but its use is important for measuring the total mercury deposition from the atmosphere or at sites where it is not possible to operate with a wet-only collector, due to operator or power constraints. Figure 3.3 shows a basic example for a deposition collector. During long sampling periods, further problems such as the volatilization of the mercury collected in the atmosphere, the adsorption of gas and particles to the walls of the funnel in the absence of precipitation, and the contamination of the collected sample with insects, bird droppings or other material in the sample ships may occur. All materials used for the sampling phase must be made of borosilicate glass or fluorocarbon polymers. In general, the precipitation collector system should consist of a cylindrical funnel with a circular horizontal opening of at least 8-10 cm inner diameter and a cylindrical vertical section of sufficient height to avoid sampling losses resulting from splashing. Through a glass capillary or a narrow tube, the funnel is connected to a bottle that stores the precipitation sample collected during the sampling period. The rim of the funnel shall be placed around 1.5 m above the ground level to avoid the contamination of the sample during heavy rain. In addition, a secondary capillary allows air to exit during sampling and acts as a drain during overflow. The sampling equipment need to be housed in a suitable container or cabinet to moderate the temperature of the sample preventing evaporation under high temperatures or freezing under low temperatures.

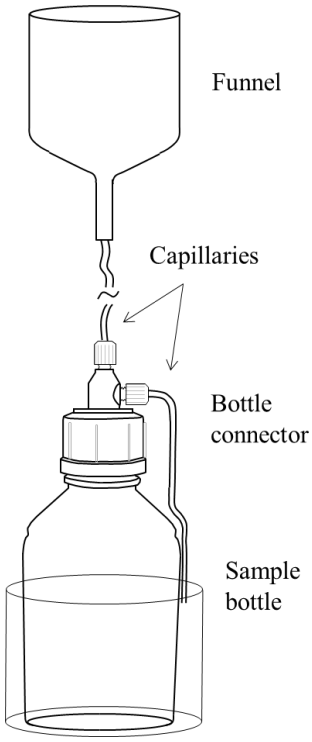

Figure 3.3 Example of a deposition collector [73].

The previously mentioned GMOS SOP "*Method for the determination of total mercury in precipitation*" describes how to prepare sampling materials in the laboratory, how carry out the sampling of precipitation in the field, and how to conduct the mercury analysis in the laboratory on the collected samples. Furthermore, the SOP for Hg in precipitation, specifies the designated laboratories, which oversee preparing the sampling materials, such as bottles, funnels and capillaries, and of sending the clean supplies to the involved GMOS monitoring stations. These laboratories, defined as primary analytical laboratories, are then responsible for the analysis of the deposition collected at the various GMOS sites. The GMOS designated laboratories are the CNR Air Pollution Research Institute (CNR-IIA), the Swedish Environmental Research Institute IVL, and the "Jozef Stefan" Institute (JSI). The SOP also suggests, if possible, the use of wet-only samplers or the co-location of wet-only and bulk samplers. Nevertheless, in conditions like insufficient power supply, absence of a regular site operator and extreme weather it is allowed the use of the bulk collector. The temperature of the sample container should be kept between 5 °C and 35 °C and can be monitored using a standard thermometer. The use of a standard meteorological rain gauge is recommended to verify the efficiency of

the sampling equipment. Regarding the preparation of sampling materials for precipitation collectors, the SOP specifies that it should take place in Class-100 clean rooms and that all parts of the precipitation collector in contact with the sample must be thoroughly cleaned before use. For the cleaning of rainfall sampling bottles (made of Teflon or glass), to obtain a complete removal of any trace of mercury, the SOP suggests the use of alkaline detergent, acetone, deionized water, 3.5% HNO_3 at 65-75 ºC for at least 6 hours, and 1% BrCl for at least 24 hours. Finally, 20 ml of high purity 0.8% L^{-1} of HCl are added to the bottles, to preserve the sample on field and then the bottles are sealed and inserted into three plastic or polyethylene zip-lock type bags. The same procedure without using BrCl and HCl is used for cleaning glass funnels and capillaries, which are stored in separate triple plastic or polyethylene zip-lock type bags. Samples need to be collected at least on a bi-weekly basis, although sample collection on a weekly or event basis is recommended. All bottles have to be handled carefully to avoid contamination during transport and storage.

3.5 Quality assurance and quality control procedures

To ensure the correct implementation of Standard Operating Procedures and avoid the production of poor-quality data within the network GMOS, common and rigorous quality assurance/quality control procedures (QA/QC) were specifically developed, for Hg measurements related to both ambient air and deposition [57,69].

The QA/QC procedures for the SOP GMOS "*Method for the determination of total mercury in precipitation*" include the use of field blanks that should be taken at least four times distributed throughout the year. Generally, two sampling bottles are required to carry out the field blank, one of which is empty and needs to be installed in the sampling apparatus and the second one contains a diluted HCl solution which is poured in the first bottle, through the funnel and the capillary, which is then analyzed in the laboratory. Any mercury content must be compared with that contained in the samples stored in a clean laboratory environment. The blank values must not exceed 20% of the concentrations normally measured at the site and the yearly average blank value is used to determine the detection limit. In addition, a laboratory blank must be determined, and certified reference materials and reagents must be tested regularly [73].

Regarding Hg atmospheric measurements, to guarantee, control and report the quality on the data collected in the various monitoring stations of the network GMOS and to ensure the comparability of the data collected between the atmospheric mercury datasets a centralized system, called GMOS-Data Quality Management (G-DQM) was developed. The novelty of this system is that it uses a web-based approach allowing real-time adaptive monitoring procedures thus preventing the production of poor-quality data [60]. Due to the size of Hg atmospheric datasets from the different monitoring stations of the network, their transfer to a central database, and their insertion within the G-DQM system, represent an important process of data management within the GMOS project. This system acquires atmospheric real-time mercury data from Tekran instruments and processes them automatically, checking whether the monitoring process adheres to standard procedures, in order to minimize the risk of data loss and to have inaccuracies in the data production [64,70]. The G-DQM system is oriented both to the process and to the product because it is based on a QA/QC methodology, where QA is related to the process about data collection, while the QC is applied to the final product of the monitoring. The QA process, through the G-DQM system, has been automated and made available on the web, meanwhile the QC process is supervised by the site operators, who must monitor the performance of the instrument, take corrective actions if necessary, identify data anomalies and confirm their refusal within their dataset [75]. Therefore, it's use represents a great improvement because it guarantees consistency, reduces human errors, avoids incorrect interpretations, bearing in mind that instrument failure or malfunction is always possible. In this regard, it is therefore essential to have a system capable of minimizing data loss and alerting operators in the event of non-standard instrumental performance.

The G-DQM system has been developed within the GMOS Cyber-Infrastructure (GMOS-CI), which is a research environment that supports advanced data acquisition, storage, management, integration, and visualization, built on an Information Technology (IT) infrastructure. The G-DQM system is plugged on this Cyber-Infrastructure and the integration of the QA/QC component into the GMOS-CI allows to deal with problems related to data and process integration, as well as the analysis of large datasets [60]. The G-DQM system starts working after the raw data of the Tekran instruments are stored in tables managed in the GMOS databases and processes these data using a set of validation

flags, derived from the recommendations of the instrument manufacturer and from the GMOS SOPs. Each flag refers to specific condition or criteria and each flagging criterion, by using thresholds, trigger the corresponding flags. Thus, the G-DQM system verify if data comply with these thresholds in order to tag the corresponding observations with flags that indicate valid, warning (suspicious) or invalid data. At the end of this quality screening, the system returns the same initial dataset as output where each data is marked with a tag identifying the quality of the data. For defining thresholds, the Research Data Management Quality (RDMQ) and the AMNet Quality Control (AMQC) programs were used as references. These two existing suites of software for data quality were developed independently by Environment Canada and by the National Atmospheric Deposition Network (NADP), respectively [74]. In other words, the G-DQM system works by performing an automated process that filters the raw data stored in the GMOS databases, which in turn refer to the three operating phases of the Tekran system: GEM or TGM measurements (GEM/ TGM), desorption cycle (DES) – if present - and Calibration cycle (CAL). At the end of this automated phase, the supervision of the reference site operator is required for a proper data quality control. Once the final valid dataset is approved, even by the reference site operator, it is stored and made accessible from the password protected GMOS web portal (http://www.gmos.eu/).

3.6 Improvements of the EPA method 1631E for the determination of mercury in water samples collected during an oceanographic sampling campaign (Med-Oceanor 2017)

The accurate determination of Hg levels in aqueous matrices (seawater, freshwater, rainwater) through highly sensitive analytical techniques such as the CVAFS could represents a potential drawback in the responsiveness to sample contamination. On the other hand, an accurate approach for determination of Hg levels in aqueous samples is necessary and represent an important challenging task that requires strict control of the potential contamination of the samples and of the particularly sensitive instruments to use. Contamination represents a very important issue to carry out reliable analysis at low Hg concentration levels, as those which involve water samples of background areas where low levels of mercury concentration, down to ng L^{-1}, can be detected. Mercury contamination may occur from many sources such as the unproperly-cleaning of storage

bottles or the use of reagents used for the sample preparation and analysis that can be contain Hg traces (resulting in blank contamination), which can compromise the results of analyses and leading the analyst to easily run into errors. Due to these contamination problems and to the low concentration of mercury that is usually detected in natural water samples collected far from anthropogenic sources, each stage of analysis, from the sampling to the quantification could represent a problem of major concern and thus rigorous precautions and scrutiny are required. In this regards, specific instructions and recommendations for each of these stages are included in the method "Mercury in water by oxidation, purge-and-trap, and cold vapor atomic fluorescence spectrometry" (EPA 1631E), issued by the United States Environmental Protection Agency (US-EPA) and worldwide used for the quantification of total mercury (THg) in natural waters [69].

As previously reported in the paragraph 3.3, the analytical method relies on chemical oxidation of Hg followed by purge-and-trap of gaseous Hg after chemical reduction, and on the detection by CVAFS for THg quantification. The traditionally used instrument for the determination of THg in liquid samples or in solid matrices previously extracted and transformed into liquid matrices is Tekran liquid sample analyzer. Nevertheless, some key modifications to the EPA method 1631E have been proposed [76], in order to minimize the Hg contamination of reagents, storage containers, and minimizing the carryover effect in the instrumental line of sampling. These customizations and technical improvements to the EPA method 1631E focus on the potential contamination issues during sampling and analysis of aqueous matrices in CVAFS instrumentation such as Tekran liquid sample analyzer. A key component of this Hg analyzer is the phase separator (PS) which as previously reported in the paragraph 3.3, allows for the removal of the gaseous mercury from the liquid phase using a counter current argon flow and its conveyance towards the trap system. Therefore, since a slight Hg contamination may result from the adhesion of Hg on the tubing walls and the frosted glass of the PS, especially when inorganic deposits are present, both components are major sources of memory effect and for a flow injection Tekran 2600, analyte carryover in the tubing system as well as over the PS may pose a treat for the next analyses. For this reason, in order to obtain reliable measurements a control of carryover contamination is necessary, although is challenging after repeated analyses or when high concentration samples are investigated. In fact, the operating procedures recommend the frequent replacement of

the tubing system and the thorough cleaning of the PS after analysis. Moreover, since as a consequence of the $SnCl_2$ oxidation the deposition of pale-yellow residues occurs, to tackle its formation that can potentially foster the entrapment of Hg from the samples, the use of $SnCl_2$ at the lowest effective concentration it is recommended. Unfortunately, the EPA method does not provide for any cleaning procedure aimed to remove the inorganic deposits from the inside tubing walls and the PS rod.

A practical recommendation for minimizing the risk of memory effect is reported in the Tekran liquid sample analyzer manual, which suggests running a rinse cycle at the end of the analyses by recirculating aqua regia (HNO_3/HCl 1:3) in the tubing system from the autosampler inlet to the PS output. However, the edited method proposes, for a rapid elimination of these deposits without the disassembling of the sampling line the recirculation for 20 minutes of ultra-purity HCl in the sample tubing and over the PS, such as a more effective treatment, since the use of HCl resulted able to dissolve the stannous deposits turning them into water-soluble species such as chlorinated complexes. Furthermore, in case of strong encrustation on the PS, an overnight soaking with concentrated HCl is suitable, allowing to attain an effective elimination of the deposits from the frosted glass. Beyond the strategy for the control of the memory effect, in the edited version of EPA method 1631E new protocols for the reduction of contamination in the storage bottles and reagents used for the preparation of BrCl solution have been provided. The selection of the sampler container material is a key point for an accurate determination of mercury at trace levels able to prevent the risk of contamination. In this contest, to avoid Hg contamination of samples during storage as well as losses due to Hg adhesion on the bottle walls, previous studies demonstrated that Fluorinated High-Density Polyethylene FLPE (e.g., Nalgene bottles) is suitable, because compared to other effective materials, like glass, FLPE bottles are splinter-proof and have tight-fitting caps [77]. The edited EPA method 1631E highlights that a rigorous cleaning protocol is required to pristine them and remove any Hg trace, even those eventually given by their factory production process and proposes a new procedure cleaning for 500 mL FLPE bottles (Figure 3.4).

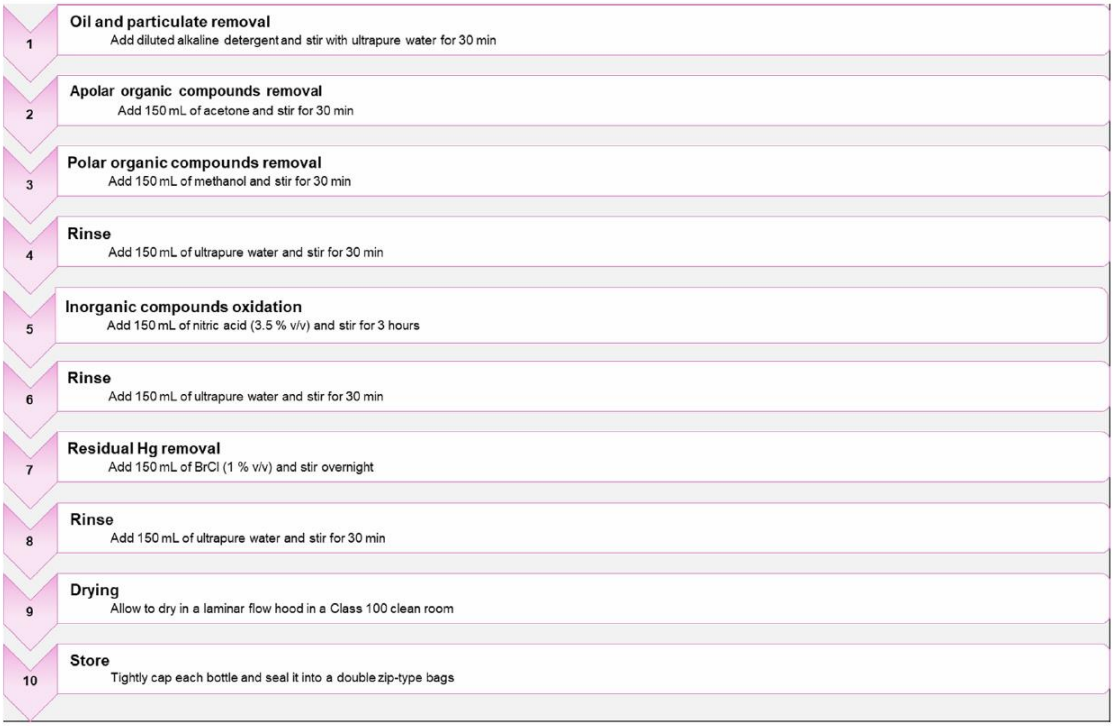

Figure 3.4 Customized procedure for the cleaning of FLPE sampling bottles [76].

This procedure developed and implemented during the thesis's, is a modified version of the one suggested in the EPA method 1631 which allows to reduce the time needed to clean each bottle because it provides a faster procedure to obtain Hg-free bottles, which require less than 24 hours, compared to the EPA method whose protocol for cleaning sampling equipment takes more than 48 hours. Moreover, to enhance the stirring process, the new cleaning procedure consists of 10 steps, which involves the use of an orbital shaker (e.g., KS 501 digital by IKA®-Werke GmbH & Co. KG, Germany) and suggests the use of alkaline detergent, acetone, methanol, deionized water, 3.5% v/v HNO_3 solution, and 1% v/v BrCl solution. After the cleaning procedure, 10 mL of 0.8% v/v ultra-purity HCl solution shall be added to each bottle to preserve the water sample after collection. The absence of Hg contamination in the cleaned bottles must be investigated by the analysis of blanks bottle obtained filling the empty bottle with 250 mL of ultrapure water and 2.5 mL of BrCl (1% of the ultrapure water volume). The THg content in each bottle must be measured after about 18 hours storage inside a HEPA-filtered laminar flow hood in Class 100 cleanroom. A bottle can be considered ready for use if THg concentration is lower than the detection limit of the EPA method 1631E, which is 20 pg. Therefore, the proposed protocol avoids the use of hot concentrated acids, such as the

HNO_3 4N at 65–75 °C reported by the EPA method, which can pose health risks to laboratory operators.

A further contamination source that have not to be underestimated coming from the use of the reagents involved in the analysis, which could lead to biased results. In this regard, EPA method 1631E suggests the use of reagent blanks to demonstrate that the amount of Hg is lower than the detection limit (20 pg). In detail, a reagent blank should be prepared and analyzed for each solution employed in the analysis such as the hydrochloric acid used to preserve the samples, the bromine monochloride used as an oxidizing agent, the hydroxylamine hydrochloride used to neutralize the excess of BrCl, the stannous chloride dihydrate, used as a reducing agent. Given method sensitivity and the low concentrations that can be detect in aqueous samples, the use of ultra-purity grade reagents, as for HCl, should be enough to ensure the absence of contamination. For the other reagents, the EPA method 1631E entitles further purification procedures including the purging of certain reagent solutions, such as $SnCl_2 \cdot 2H_2O$ or $NH_2OH \cdot HCl$, with mercury- free nitrogen or argon, which cannot be used for BrCl solution since this solution cannot be purified once it is prepared. Therefore, if contamination occur during the analysis of reagent blank, a new batch shall be prepared and tested again for potential contamination. The procedure for the preparation of BrCl, as suggested in the EPA method 1631E, requires the use of reagent grade KBr and $KBrO_3$. The modified version of EPA method 1631E [76] tested two different purity trademarks of KBr (Suprapur and ACS commercialized by Merck and Sigma Aldrich, respectively) and $KBrO_3$ (EMSURE and ACS commercialized by Merck and Fluka, respectively) to assess their contribution to the resulting BrCl solution. The use of these higher quality salts should be ensured the absence of Hg contamination but a significant THg level was detected in the BrCl solution prepared by reaction of the ACS KBr with ACS $KBrO_3$ and of the Suprapur KBr with EMSURE $KBrO_3$. Therefore, each salt was tested individually and higher THg levels were found in the ACS KBr and $KBrO_3$ compared with Suprapur KBr and EMSURE $KBrO_3$. A potential strategy proposed by edited EPA method 1631E to minimize Hg content in all the four salts involves the use of a muffle furnace at 300 °C for one week which proved to be a more effective treatment to remove contamination compared to the treatment at 220 °C for 48 h proposed by Leopold et al., 2010 [78]. In fact, the muffling at 300 °C for a one week did not affect the stability of the salts but force the release of Hg in the gaseous phase

purifying the salts. Moreover, after the salts have been purified, keeping them in the warm muffle to prevent the potential Hg reabsorption is recommended. In order to avoid contamination from external sources such as from the glass crucible used as a container for each reagent, the edited EPA method 1631 E suggest a cleaning by washing the glassware with concentrated HCl (36% w/w) followed by a rinse step with ultrapure water. Therefore, all these customizations have proved to be an effective strategy for reducing mercury contamination, which could potentially result in biased measurements. These modifications were successfully exploited in the interlaboratory comparison study RECETOX (Research Centre for Toxic Compounds in the Environment) - UNEP-Global Assessment of Laboratories Analyzing Mercury [79] by analyzing an aqueous standard test sample with unknown Hg concentration. The new analytical method improved during my Ph.D. thesis's work in different step as described above, has been implemented and used to analyze natural water samples collected at different sites along the route established during the Med-Oceanor oceanographic campaign organized in the Mediterranean Sea basin, and coordinated by CNR-IIA. Moreover, this new version of the method can also apply to the Hg analysis in solid matrices that require prior acid digestion of the samples. Details on this new approach of the analytical method has been published in Tassone et al., 2020 [76].

Chapter 4

Atmospheric mercury measurements by conventional methods and analytical techniques: case-studies across three selected Italian monitoring stations

4.1 Introduction

During the period of the Ph.D. studies, a large part of the research was focused on the application of those conventional sampling methods and analytical techniques previously described in Chapter 3. The three case-studies reported in this chapter, took place in three diverse sampling stations using different types of conventional instrumentation for the continuous monitoring and analysis of atmospheric mercury. The first and third case-studies reported in this chapter describe the results of atmospheric Hg measurements made during the sampling campaigns planned in the framework of the Italian Special Network "*Reti Speciali*" agreement, with specific reference to mercury assessment. The involved monitoring stations are Monte Sant'Angelo (MSA), in the Apulia region, and Montelibretti (MLI), in the Lazio region, which are representative of the Southern and Central Italian areas, respectively. In particular, the first case study reports the results of the TGM monitoring study carried out at the MSA site using the Lumex RA-915AM system. The second case study describes the results of the TGM measurements, carried out at the Climate-Obeservatory "Monte Curcio station (MCU)", in the Calabria region, southern of Italy, using a Tekran 2537X mercury analyser. Finally, the third case study shows the results of the monitoring study on the atmospheric Hg species (GEM, GOM and PBM), performed at the MLI station using the Tekran integrated system (model 2537X connected with the 1130 and 1135 speciation units). In respect to these monitoring studies, the collected data are presented in this chapter, discussed in terms of temporal variability (hourly, daily, monthly, and seasonal) and additionally investigated in respect to changes in meteorological conditions and source influences. A detailed description of the monitoring campaigns carried out is reported below for each case-study.

4.2 Data Processing and tools used for data interpretation

All data collected for each case-study were processed for quality issues. For that concerning Hg data recorded at MCU and MLI, where a Tekran analyzer operates, the first step for data analysis consisted with the specific application of the G-DQM system (Chapter 3), made possible to quality screened the measurements in compliance with the adopted SOPs procedures and the instrument quality maintenance instructions. Once finalized the quality validation step, each single dataset collected at the corresponding sampling stations, included also that obtained with the Lumex analyzer at MSA, was quality-screened using two statistically based control criteria. The first selection, or control criterion, is based on the use of the standard deviation (σ) to understand the variations of the data over time, identifying anomalous or unusual phenomena that could be associated to occasional but real events (i.e., wildfires, meteorological extreme events, etc.) and distinguish them from those that are instead due to electrical spikes for instrument malfunction. Therefore, the standard deviation (σ) for the concentration of data collected during the specific sampling campaigns has been calculated in order to determine the ± 3σ parameter useful for a first general quality data control. However, to avoid an unreasonable cut of data, only based on a "cold" statistical perspective, an additional inspection criterion for data quality- screening, was used. This second criterion verifies the percentage variation of a data with respect to the previous and subsequent values. In this way it was possible to identify as anomalous the values for which there was a variation in absolute value greater than 50%, which would mean a value increased/decreased more than 50% compared to the previous and/or to next ones, and recorded in a single hour. In other words, if the variation in values resulted to be less than 50% it is plausible that a real phenomenon is taking place such that the instrument is registering a gradual increase/decrease in values. The application of this second selection criterion, allowed to refine the overall quality-control of the whole dataset and then consider as anomalous only that data showing a percentage variation greater than ±50%. Datasets consisting of valid hourly-averaged of concentrations were then aggregated to daily averages, which were considered representative only if the 75% of the corresponding hourly-data were which means at least 18 over 24 hours for each daily period. In addition, the monthly mean values of available data were computed and considered as valid only for those months of the campaign that showed an availability of

more than 66% of the corresponding daily measurement data, at least 20 days for each month. A seasonal based analysis was additionally carried out. To this end the seasonal meteorological classification was applied. Therefore, Autumn is considered from September 1 to November 30, Winter from December 1 to February 28 (February 29 in a leap year), Spring from March 1 to May 31, and Summer from June 1 to August 31. Considering the seasonal classification above mentioned, for every measurement year at MSA and MCU stations, TGM seasonal-averaged concentrations were computed. In this case seasonal mean values were considered valid if obtained by at least two months of available data measurement values.

For the arrangement of tables and graphical representation of data, the Excel Application from the Microsoft Office Package was used. Regarding instead the production of the wind rose plots the specific *windRose* function, provided by the *openair* package within the free and open source RStudio tool. The wind speed (WS) and wind direction (WD) hourly data, recorded within each case-study, were used as input for the elaboration with RStudio. The *windRose* function can plot wind roses, summarizing all available data on WS and WD, for the whole measurement period examined at the involved sampling station, and additionally it makes possible to obtain individual wind roses at a selected year, month, or season, as a subset of the whole available dataset. Regarding the wind rose plots, they are presented in a circular format, where the length of each "spoke" around the circle indicates the amount of time that the wind blows from a particular direction. This information, reported as percentage % of WD frequencies, is represented by the inner grey circles. Each spoke is also broken down into colour-coded bands that show WS ranges.

To understand how the different investigated meteorological variables and the mercury concentrations, at each monitoring sites, were related the *corPlot* function was used. This function is provided by the *openair* package within the free and open source RStudio tool allowing to plot a correlation matrix, which provides the correlation between all pairs of considered data, to visualise relationships between variables. The correlation matrix shows the correlation coded by shape (ellipses), colour and the numeric value (Pearson correlation (r)). The shape can vary from a circle, for zero correlation, and a line at 45 degrees positive slope, for a perfect positive linear correlation.

The Student's t-test, with a significance level of 0.05, was additionally adopted to compare TGM concentrations observed in the presented case studies.

The evaluation and the interpretation of the Hg measurements was supported using different complementary tools which allowed to identify the occurrence and the impact at the involved station of some natural sources, such as wildfires and Saharan dust. In particular, the Navy Aerosol Analysis and Prediction System (NAAPS) model (https://www.nrlmry.navy.mil/), developed by the Naval Research Laboratory (NRL) was used to observe maps of smoke or dust surface concentration of specific days of the measurement campaign.

The MODIS true-colour images (http://rapidfire.sci.gsfc.nasa.gov/) was additionally employed, allowing to identify the location and the extension of each single fire hot-spot.

The evaluation and the interpretation of the Hg measurements at MCU and MLI was accomplished also using the Hybrid Single-Particle Lagrangian Integrated Trajectory model (HYSPLIT), available at the National Oceanic and Atmospheric Administration (NOAA) Air Resources Laboratory's (ARL). It was employed to calculate two-day backward trajectories in order to check the origin and pathway of the air masses collected at the investigated stations for specific interesting days of the measurement campaigns. These analyses were performed using the READY (Real-time Environmental Applications and Display sYstem) website at http://www.arl.noaa.gov/ready.html [80]. Where applicable the GFSG meteorological dataset, characterized by a grid-scale of 0.25 degrees, has been used as meteorological input, otherwise the GDAS (Global Data Assimilation System) meteorological dataset, with a broader 1degree grid scale, has been applied as second option. The trajectory arrival height was set at the elevation of the MCU and MLI stations, therefore equal to 1800 and 50 m above ground level, respectively. In both cases, a label interval of 6 hours has been introduced to better follow the air mass pathway with respect the temporal evolution.

4.3 Case study 1: Monte Sant'Angelo

4.3.1 Sampling site description

The sampling site of Monte Sant'Angelo (MSA, 41°39'55.61" N 15°56'42.14" E; 125 m a.s.l.), located in the Apulia region, province of Foggia, is classified as background station in a rural site, also identified as a coastal site, given its geographical position (see Figure

4.1). In the framework of the Italian Special Networks for Mercury, this station was established as a Secondary site in respect to the mercury measurements, consequently at MSA site only TGM concentrations were monitored during a measurement campaign.

Figure 4.1 Location of the Monte Sant'Angelo (MSA) sampling station.

4.3.2 Atmospheric sampling campaign and TGM measurements

At MSA monitoring station, TGM measurements in ambient air started in April 2018 and are still ongoing. For the purposes of the analysis reported in this thesis, atmospheric Hg levels and trends were investigated considering TGM data collected in the period from April 4th, 2018 to August 31st, 2020. At the MSA station, continuous TGM measurements were performed using the Lumex RA-915AM, with an air flow rate of 7-10 L min^{-1} and a detection limit of 0.5 ng m^{-3}. The TGM concentration was monitored with a resolution time of 1 second and measurements were then averaged every 5 minutes. The Lumex analyzer was calibrated every 48 h and an annual calibration was also performed in the laboratory. Moreover, meteorological parameters as air temperature (T), relative humidity (RH), wind speed (WS) and direction (WD), were acquired during the whole campaign, in order to deepen the different meteorological conditions of the sampling area and to investigate their influence on the seasonal and daily TGM temporal trends. Since MSA is unprovided of a weather station, the meteorological parameters herein processed refer to

Manfredonia (41°37’40.53” N 15°54’27.31” E, Apulia, Italy), which is about 16 km far from MSA station, and is equipped with an integrated meteorological station by with data are continuously recorded. Both TGM data, recorded at MSA, and meteorological parameters, recorded at Manfredonia, were courtesy provided by the Apulian Regional Agency for Environmental Protection and Prevention (ARPA Puglia).

4.3.3 TGM trends on hourly, daily, monthly, and seasonal basis in MSA

For the TGM concentration data collected at MSA site, considering the whole initial dataset, aggregated in hourly mean values, the resulting hourly mean value was equal to 1.72 ± 0.19 ng m^{-3} with a $\pm 3\sigma$ value of 0.56 ng m^{-3} ($n = 19053$). Therefore, the use of the first control criterion allowed to obtain a dataset of TGM concentration values ranging between 1.17-2.28 ng m^{-3}. In this way, 122 out of 19053 hourly values exceeding the lower and/or the higher thresholds have been identified.

However, the application of the second selection criterion, allowed to refine the overall quality-control of the whole dataset and then consider as anomalous only that data showing a percentage variation greater than ± 50%. In this way, 32 values have been thrown out from the initial dataset, instead of the 122 identified by applying the previously mentioned selection. In this way, a final valid dataset consisting of 19021 hourly-averaged TGM concentration values, recorded at the MSA station from April 2018 to August 2020, was obtained, on which the following analyses were carried out.

The dataset of the valid hourly-averaged TGM concentrations is shown in Figure 4.2. The interruptions of the sampling were due to the operations of instrument calibration or maintenance, as well as the above-described quality-screening procedure.

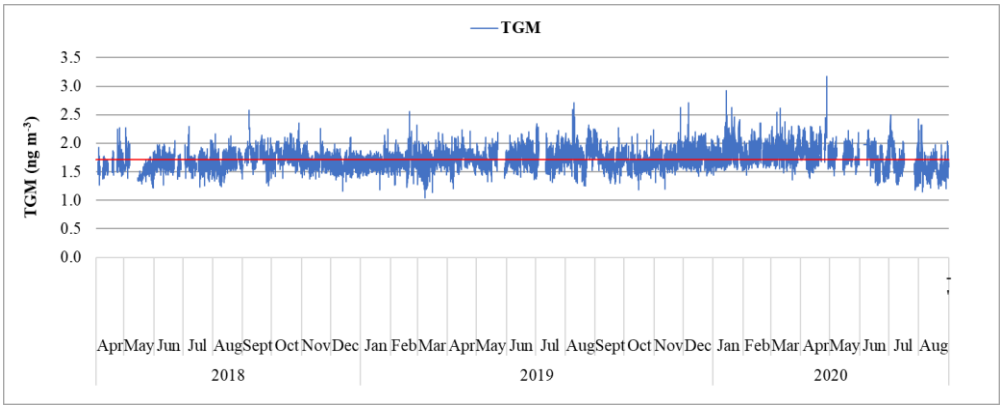

Figure 4.2 Hourly-averaged TGM concentration trend at MSA station detected throughout the campaign. The solid red line indicates the hourly average value of the TGM concentration (1.72 ± 0.18 ng m^{-3}) recorded during the entire measurement campaign.

The atmospheric hourly-averaged TGM concentrations in ambient air showed a quite constant trend over the whole campaign period at MSA site, with an hourly TGM concentrations ranging from 1.05 to 3.17 ng m^{-3} and an hourly mean value of 1.72 ± 0.18 ng m^{-3}. Hourly averages of TGM concentration were then aggregated to daily averages, which were considered representative only if the 75% of the corresponding hourly-data were available which means at least 18 over 24 hours for each daily period, removing only 68 days from the dataset. Daily mean TGM concentration values are showed in Figure 4.3.

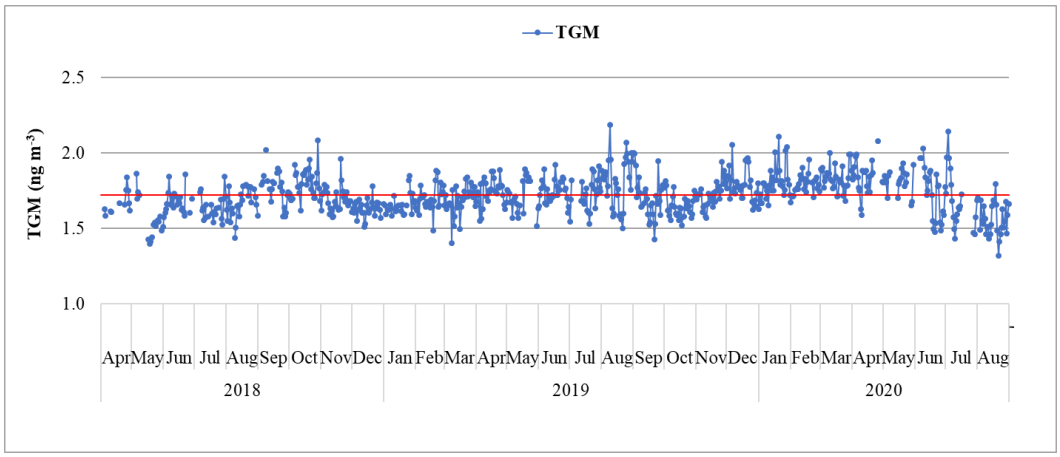

Figure 4.3 Trends of TGM daily averaged concentrations recorded at MSA station. The solid red line indicates the daily average value of the TGM concentration (1.72 ± 0.13 ng m^{-3}) recorded during the entire measurement campaign.

The mean daily values of TGM concentration resulted in the range from 1.32 to 2.19 ng m^{-3}, with a mean value of 1.72 ± 0.13 ng m^{-3}. Daily averages of TGM concentration were further converted to monthly averages, which were considered valid if the 66% of the corresponding daily data were available. Therefore, the monthly mean values of TGM concentration were computed and considered as valid only for those months of the campaign that showed an availability of more than 66% of the corresponding daily measurement data. Consequently, two months (April 2018 and May 2018) were removed for the purposes of our investigations. The mean values obtained for the TGM monthly-averaged concentrations for each year of whole study period (2018, 2019 and 2020) are showed in Figure 4.4 and reported in Table 4.1.

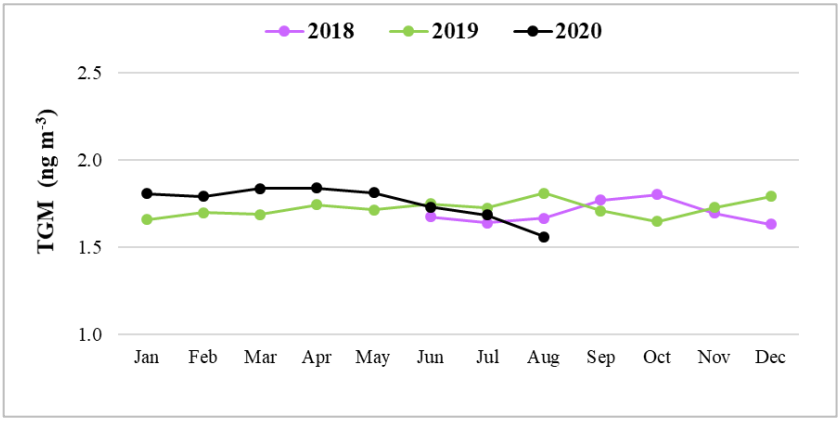

Figure 4.4 Trends of TGM monthly-averaged concentrations for each year of the sampling campaign at MSA station.

Month - Year	2018	2019	2020
	TGM (ng m^{-3})	TGM (ng m^{-3})	TGM (ng m^{-3})
January	-	1.66 ± 0.07	1.81 ± 0.11
February	-	1.7 ± 0.09	1.79 ± 0.06
March	-	1.69 ± 0.10	1.84 ± 0.08
April	-	1.74 ± 0.08	1.84 ± 0.11
May	-	1.71 ± 0.11	1.81 ± 0.08
June	1.67 ± 0.07	1.75 ± 0.07	1.73 ± 0.17
July	1.64 ± 0.08	1.73 ± 0.11	1.68 ± 0.19
August	1.67 ± 0.10	1.81 ± 0.17	1.56 ± 0.11
September	1.77 ± 0.11	1.71 ± 0.14	-
October	1.80 ± 0.10	1.65 ± 0.08	-
November	1.69 ± 0.08	1.73 ± 0.08	-
December	1.63 ± 0.05	1.79 ± 0.10	-

Table 4.1 Mean values and Standard deviation of the TGM monthly-averaged concentrations for each year of the sampling campaign at MSA.

The monthly based analysis on the variation of TGM concentration for each year of the whole sampling campaign showed that, for the year 2018, the highest TGM concentration was found in October (1.80 ± 0.10 ng m^{-3}) and the lowest in December (1.63 ± 0.05 ng m^{-3}). Regarding the year 2019, the highest TGM concentration was found during August (1.81 ± 0.17 ng m^{-3}) and the lowest during October (1.65 ± 0.08 ng m^{-3}). In year 2020, instead the highest value of TGM was recorded in both months of March (1.84 ± 0.08 ng m^{-3}) and April (1.84 ± 0.11 ng m^{-3}), and the lowest one in August (1.56 ± 0.11 ng m^{-3}).

A seasonal based analysis was additionally carried out. Considering the seasonal classification previously described for every measurement year at MSA station, TGM seasonal-averaged concentrations were computed. In this case seasonal mean values were considered valid if obtained by at least two months of available TGM measurement values (Figure 4.5 and Table 4.2).

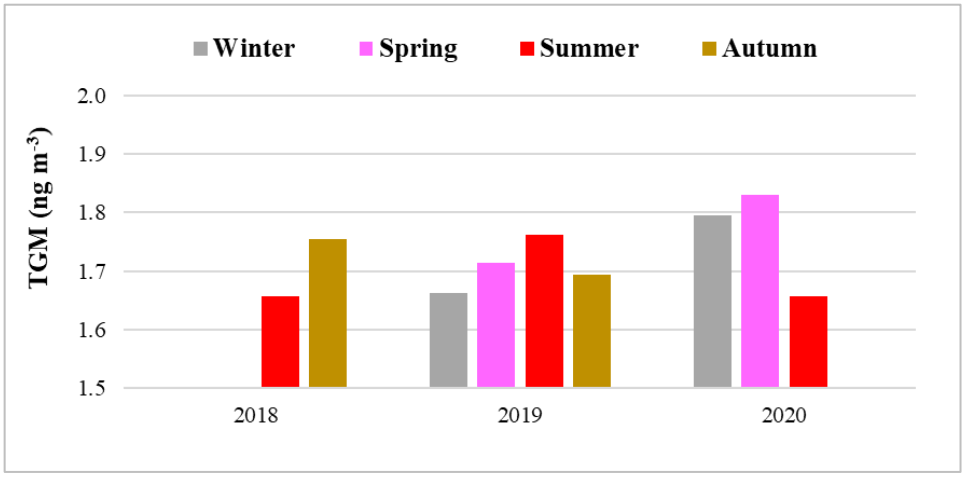

Figure 4.5 TGM seasonal-averaged concentrations at MSA station.

Season - Year	2018	2019	2020
	TGM (ng m^{-3})	TGM (ng m^{-3})	TGM (ng m^{-3})
Winter	-	1.66 ± 0.06	1.80 ± 0.01
Spring	-	1.71 ± 0.03	1.83 ± 0.01
Summer	1.66 ± 0.02	1.76 ± 0.04	1.66 ± 0.09
Autumn	1.76 ± 0.06	1.69 ± 0.04	-

Table 4.2 Mean value of TGM seasonal-averaged concentrations for each year of the campaign at MSA station.

As reported in Table 4.2 and in Figure 4.5, TGM showed seasonal variability in each investigated year. In 2018, TGM concentration in Autumn 2018 was significantly higher

than that in Summer 2018 (1.76 ± 0.06 ng m-3 and 1.66 ± 0.02 ng m^{-3}, respectively; $p < 0.05$). As regard year 2019, TGM concentration in Spring was significantly higher than those in Winter (1.71 ± 0.03 ng m^{-3} and 1.66 ± 0.06 ng m^{-3}, respectively $p < 0.05$) and in Autumn (1.71 ± 0.03 ng m^{-3} and 1.69 ± 0.04 ng m^{-3}, respectively $p < 0.05$). In the same way, TGM concentration in Summer 2019 was significantly higher than those in Winter 2019 (1.76 ± 0.04 ng m^{-3} and 1.66 ± 0.06 ng m^{-3}, respectively $p < 0.05$), in Autumn 2019 (1.76 ± 0.04 ng m^{-3} and 1.69 ± 0.04 ng m^{-3}, respectively $p < 0.05$) and in Spring 2019 (1.76 ± 0.04 ng m^{-3} and 1.71 ± 0.03 ng m^{-3}, respectively $p < 0.05$). Moreover, the TGM concentration in Autumn 2019 was significantly higher than those in Winter 2019 (1.76 ± 0.04 ng m^{-3} and 1.66 ± 0.06 ng m^{-3}, respectively $p < 0.05$).

TGM concentration in Spring 2020 was significantly higher than those in Winter 2020 (1.83 ± 0.01 ng m^{-3} and 1.80 ± 0.01 ng m^{-3}, respectively $p < 0.05$) and in Summer 2020 (1.83 ± 0.01 ng m^{-3} and 1.66 ± 0.09 ng m^{-3}, respectively $p < 0.05$). In addition, TGM concentration in Winter 2020 was significantly higher than in Summer 2020 (1.80 ± 0.01 ng m^{-3} and 1.66 ± 0.09 ng m^{-3}, respectively $p < 0.05$).

4.3.4 Seasonal average diurnal cycles of TGM concentrations

The average TGM concentrations diurnal cycle was investigated for each season and within each year of the measurement campaign. The daily hourly mean values of the TGM concentration over the available days for the investigated months were used to calculate the monthly-based average diurnal cycle TGM concentrations, from which the seasonally-based average diurnal cycle was then determined. In order to appreciate the diurnal cycle variability of TGM across seasons and for the years (2018, 2019, and 2020) of the measurement campaign, the computed hourly mean TGM concentrations, for each available season were plotted as shown in Figure 4.6.

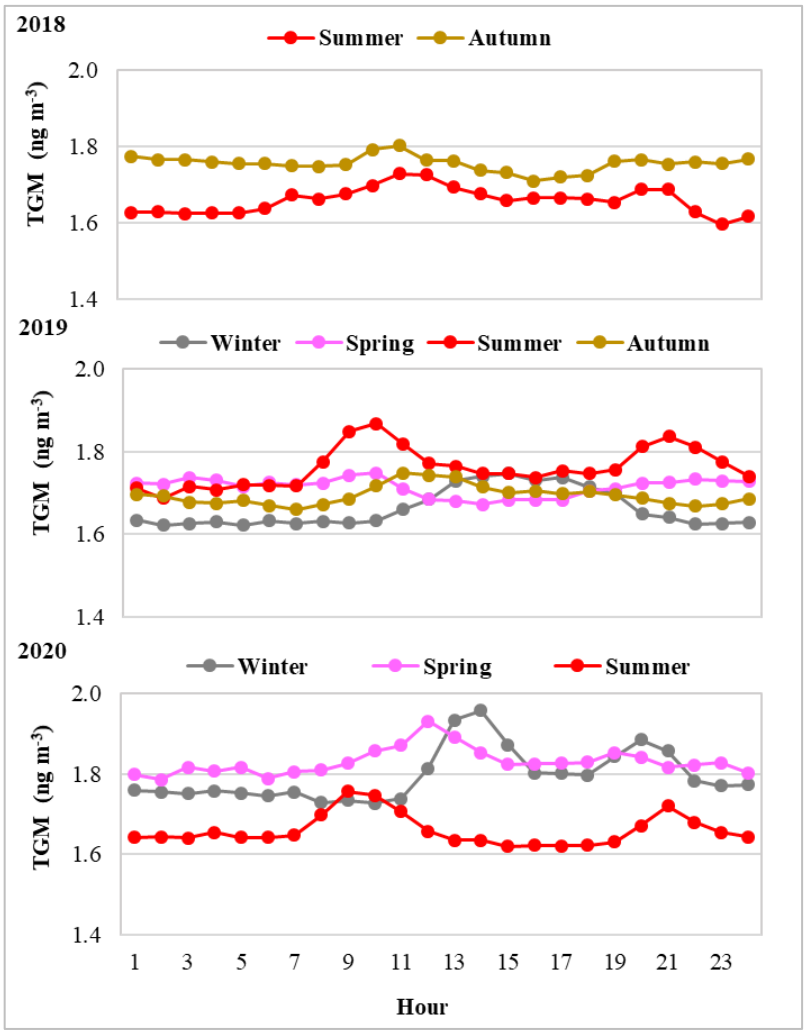

Figure 4.6 Average diurnal cycle the TGM concentrations computed over each available season for each year (2018, 2019, and 2020) of the sampling campaign at MSA.

This analysis made possible to highlight the maximum values reached by the hourly average TGM concentration along the typical diurnal cycle for the considered season. In correspondence of these hourly values, the percentage of increase, with respect to the related TGM seasonal average value, was calculated.

A deepen investigation over the average diurnal cycle of TGM concentrations was specifically carried out for summer and winter, due to the interesting variability remarked during these two seasons, being instead observed a quite steady variability for autumn and spring. In particular, the data availability makes possible to compare results obtained for the summer season of the years 2018, 2019 and 2020 (see Figure 4.7) whereas for the winter seasons were available only for the years 2019 and 2020 (Figure 4.8). As Figure 4.7 shows, the average diurnal cycle for TGM concentrations, recorded during summer

2018, displayed - between 07:00 and 14:00 and at 20:00-21:00 - hourly average values higher than the corresponding daily average value, which was 1.66 ng m^{-3}. In this time frame, the absolute maximum values over the entire daytime cycle were recorded at 11:00-12:00 and 20:00-21:00 characterized by an hourly average value of 1.73 ng m^{-3} and 1.69 ng m^{-3}, with an increase of 4% and 2%, respectively, compared to the average daily value of summer 2018 (1.66 ng m^{-3}).

For summer 2019, the average diurnal cycle of TGM concentrations, exhibited - between 08:00 and 13:00 and at 20:00-23:00 - hourly average values higher than the corresponding daily average value, which was 1.76 ng m^{-3}. In this time frame, the absolute maximum values over the entire daytime cycle were recorded at 10:00 and at 21:00, characterized by an hourly average value of 1.87 ng m^{-3} and 1.84 ng m^{-3}, with an increase of 6% and 4%, respectively, compared to the average daily value recorded for summer 2019 (1.76 ng m^{-3}).

Lastly, referring to summer 2020, the TGM concentrations along the average diurnal cycle showed - between 08:00 and 12:00 and at 20:00-23:00 - hourly average values higher than the corresponding daily average value which was 1.66 ng m^{-3}. In this period frame, the absolute maximum values over the whole daytime cycle were recorded at 09:00 and at 21:00, characterized by an hourly average value of 1.76 ng m^{-3} and 1.72 ng m^{-3}, with an increase of 6% and 4%, respectively, compared to the average daily value for summer 2020 (1.66 ng m^{-3}).

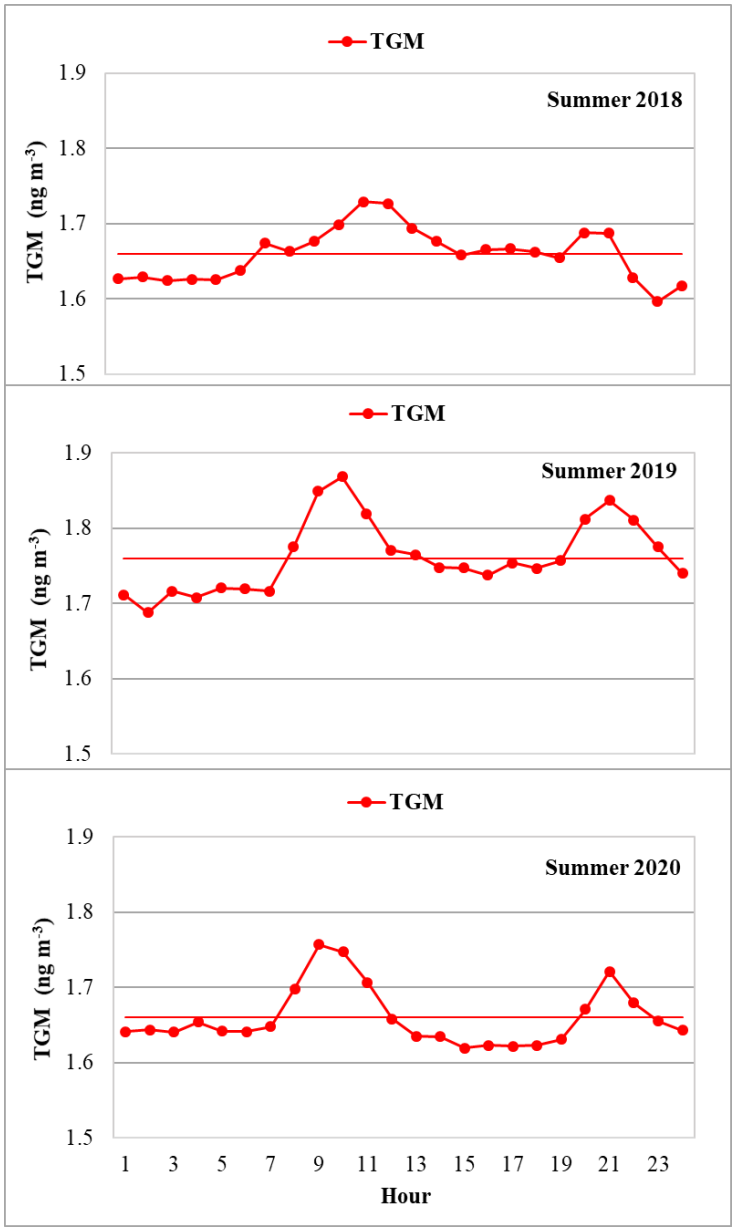

Figure 4.7 Average diurnal cycle for TGM concentrations recorded in summer 2018, 2019 and 2020 at MSA. In each plot, the solid red line indicates the average daily value of the TGM concentration recorded during the corresponding season.

The average diurnal cycle of TGM concentrations, referring to winter 2019 and 2020, are showed in Figure 4.8. The TGM concentrations for winter 2019 showed hourly average values higher than the corresponding daily average value which (1.66 ng m^{-3}), between 12:00 and 19:00. In this frame, the absolute maximum values, over the whole daytime cycle were, recorded between 13:00 and 18:00 characterized by an hourly average value

of 1.73 ng m^{-3} with an increase of 4% compared to the average daily value of winter 2019 (1.66 ng m^{-3}).

During winter 2020, the TGM concentrations showed - between 12:00 and 21:00 - hourly average values higher than the corresponding daily average value, which was 1.80 ng m^{-3}. In this period, the absolute maximum values over the entire daytime cycle were recorded between 14:00 and 20:00 characterized by an hourly average values of 1.96 ng m^{-3} and 1.89 ng m^{-3} with an increase of 9% and 5%, respectively compared to the average daily value for summer 2019 (1.80 ng m^{-3}).

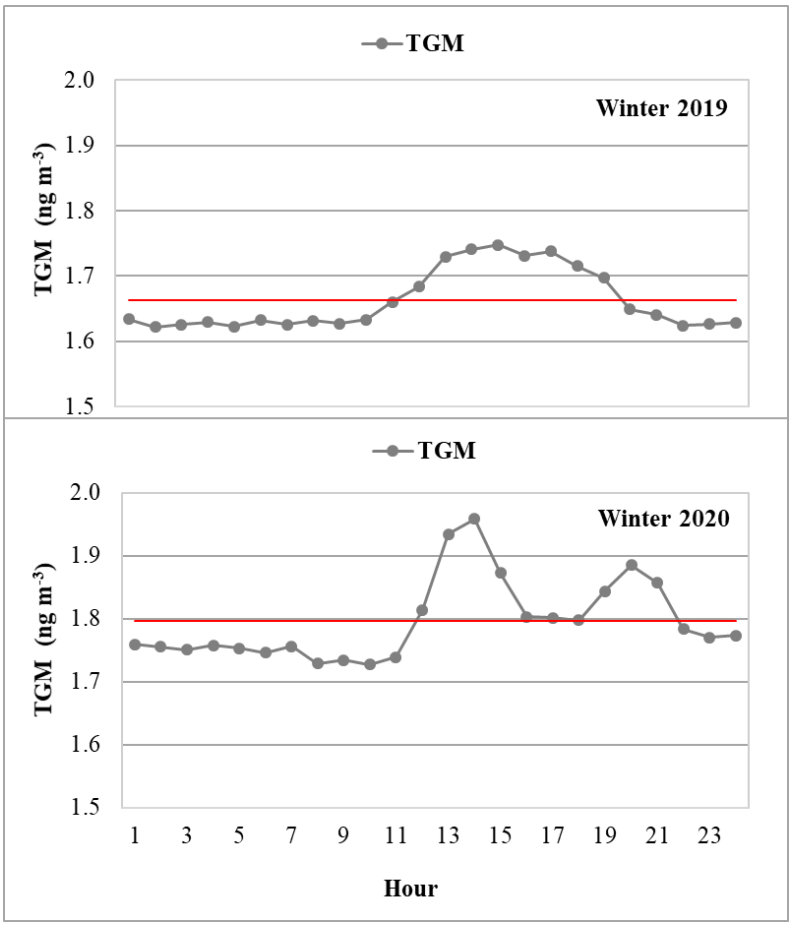

Figure 4.8 Average diurnal cycle for TGM concentrations recorded in winter 2019 and 2020 at MSA. In each plot, the solid red line indicates the average daily value of the TGM concentration recorded during the corresponding season.

4.3.5 Meteorological data analysis

For the meteorological dataset, the same collection period considered as valid for the TGM measurements at the MSA site (June 2018 - August 2020), also considered. The validated meteorological data of temperature, relative humidity, wind speed and wind

direction recorded at the Manfredonia station, about 16 km far from MSA, during whole measurement campaign were aggregated and showed on hourly basis, in order to better analyze the meteorological conditions at the investigated sampling site. The hourly time series of air temperature, relative humidity, and wind speed, recorded over period from June 2018 to August 2020, are summarized in Figure 4.9.

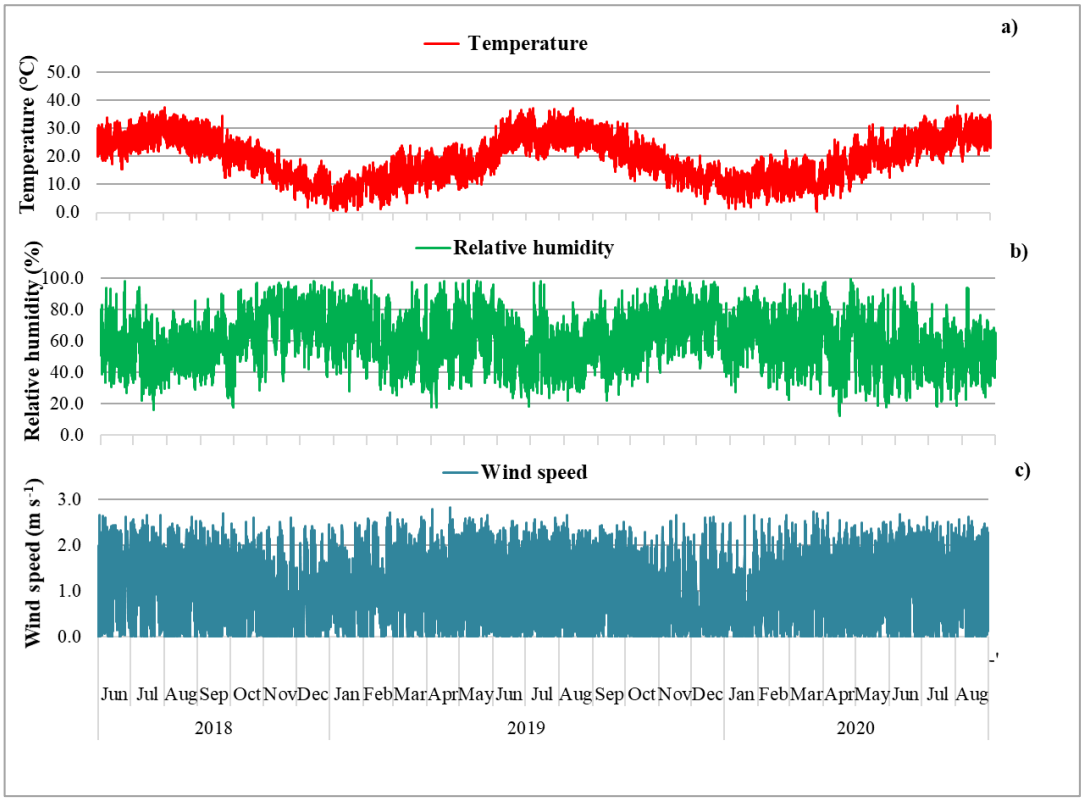

Figure 4.9 Hourly time series of a) air temperature (°C), b) relative humidity (%) and c) wind speed (m s^{-1}), recorded at the MSA station.

The main descriptive statistics such as average, Standard Deviation (± SD), the range from the minimum to the maximum of the recorded values for the meteorological parameters measured during whole campaign were reported in Table 4.3. In detail, during the considered study period (June 2018 – August 2020) the weather conditions were characterized by an average hourly temperature of 18.92 ± 7.86 °C (range 0.32 °C - 37.95 °C) and an average hourly relative humidity of 61.20 ± 16.49% (range 11.91 – 100%). The wind blew with an average hourly intensity of 0.97 ± 0.72 m s^{-1} (range 0 m s^{-1} and 2.83 m s^{-1}).

Meteorological parameters	Average ± SD	Range
Air temperature (°C)	18.92 ± 7.86	0.32 - 37.95
Relative humidity (%)	61.20 ± 16.49	11.91 - 100
Wind speed ($m\ s^{-1}$)	0.97 ± 0.72	0 - 2.83

Table 4.3 Descriptive statistics (average ± SD, range with min and max values) of the meteorological parameters (air temperature, relative humidity, and wind speed) recorded over the whole observing period, from June 2018 to August 2020.

By using the RStudio tool and the openair *windRoses* function, the wind rose plot reported in Figure 4.10 was obtained, as representative of the whole sampling campaign. In this case WS and WD data recoded from June 2018 – August 2020 was used as input. During the whole measurement campaign, the prevailing wind directions resulted to be South-South-East (SSE) and North-West (NW). Figure 4.10 show the wind rose overlapped with an overview map of the sampling area, which highlight the position of the MSA station, where TGM measurement were performed, and the Manfredonia site, where the weather station is located.

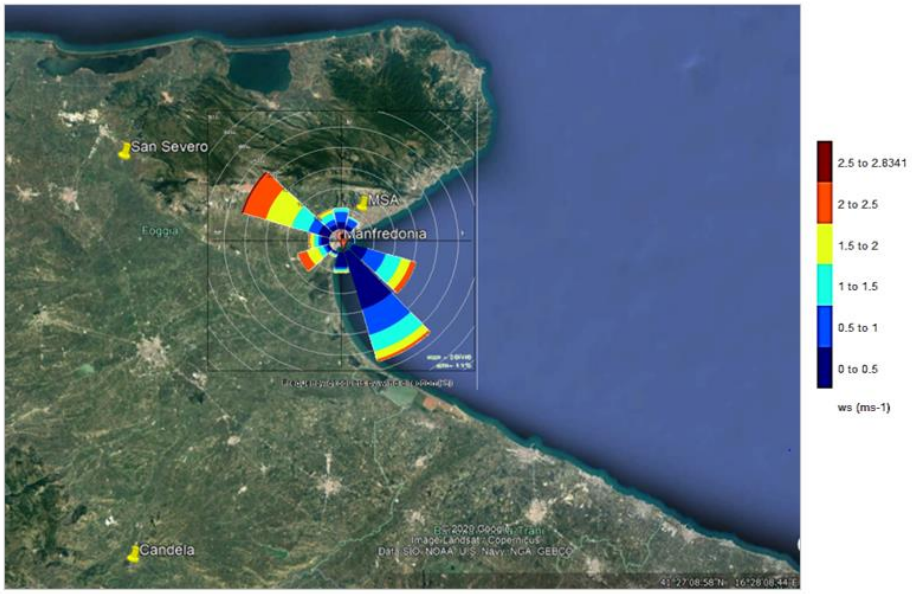

Figure 4.10 Wind rose throughout the sampling campaign overlapped with an overview map of the sampling area (MSA: TGM sampling station; Manfredonia: weather station site).

To appreciate how the wind conditions varied both throughout the seasons over the whole campaign, and the seasons for each specific investigated year the wind rose plots were made for the whole seasonal basis (Figure 4.11 a) and for the annual/seasonal basis (Figure 4.11 b) basis. All these plots confirmed the general prevalence of already

mentioned wind directions (SSE and NW). In fact, from the plots below it can be noticed that during winter the component coming from SSE prevailed with a higher frequency in respect to that coming from NW.

In addition, during spring and summer, the component from NW was featured by stronger winds (WS > 2.5 m s^{-1}).

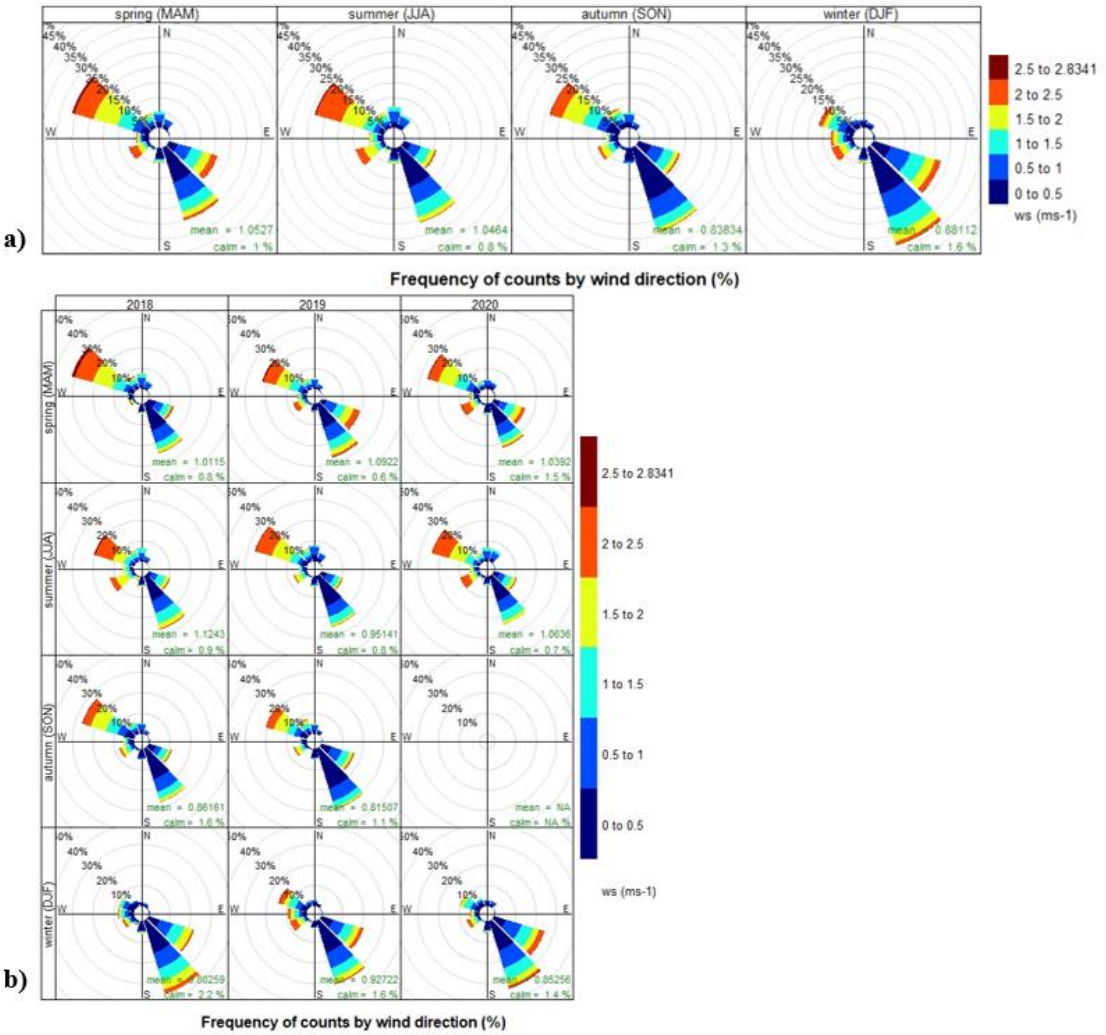

Figure 4.11 Representation of the wind roses for the whole seasonal basis a) and for the annual/seasonal basis b) throughout the campaign.

4.3.5.1 Summer and winter average diurnal cycle for both TGM concentrations and meteorological data

For each available year of the measurement campaign carried out at the MSA station, the trends of both the TGM concentration and the meteorological parameters simultaneously recorded were observed, in respect to the summer and winter average diurnal cycle.

Figure 4.12 shows that in correspondence with recorded TGM maximum value there was an increase also in the hourly average temperature value which reached a value of 30.76 °C at 12:00, compared to average daily value for the summer 2018, which was 26.92 °C. At the same time, at 12:00, it can be observed a decrease in the hourly average value of relative humidity, which showed a value of 44.02%, compared to the average daily seasonal value of 54.46%. Instead, in correspondence with the evening TGM maximum value there was a decrease in the hourly average temperature value, which reached a value of 26.49 °C at 21:00. At the same time, an increase in the hourly average value of relative humidity was observed, showing a value of 58.31%. It is also worth noting that TGM maximum value were recorded in correspondence of a large change in wind speed and wind direction. The direction could be linked to the location of some potential source surroundings the sampling area. In particular, since this case-study refer to a coastal site, the direction of wind was influenced by the land/sea breezes. In fact, it can be noticed that early in the morning, wind blew from the direction around 160-180° (SSE), which given the station location, means air masses blowing from the sea. As the temperature rises, the thermal gradient between land and sea changes in such a way as trigger a wind direction blowing from land, corresponding to NW, (WD in the range 250-300°, see Figure 4.12). A similar mechanism recurs, in the opposite way, during the evening, when WD come back to values around 180°, from sea, with a corresponding increase in relative humidity and decrease of both temperature and wind speed. The observed diurnal cycle for WS values highlights the dilution function it can exert to the concentrations of a pollutant in the atmosphere. Specifically, TGM levels resulted to decrease with the increase of WS. A positive correlation was observed between TGM concentration and temperature ($r = 0.67$), between TGM concentration and wind speed ($r = 0.47$), as well as between TGM concentration and wind direction ($r = 0.11$), whereas a negative correlation was observed between TGM concentration and relative humidity ($r = - 0.74$). Moreover, a negative correlation was observed between temperature and relative humidity ($r = - 0.97$) whereas a positive correlation was observed between wind speed and wind direction ($r = 0.85$).

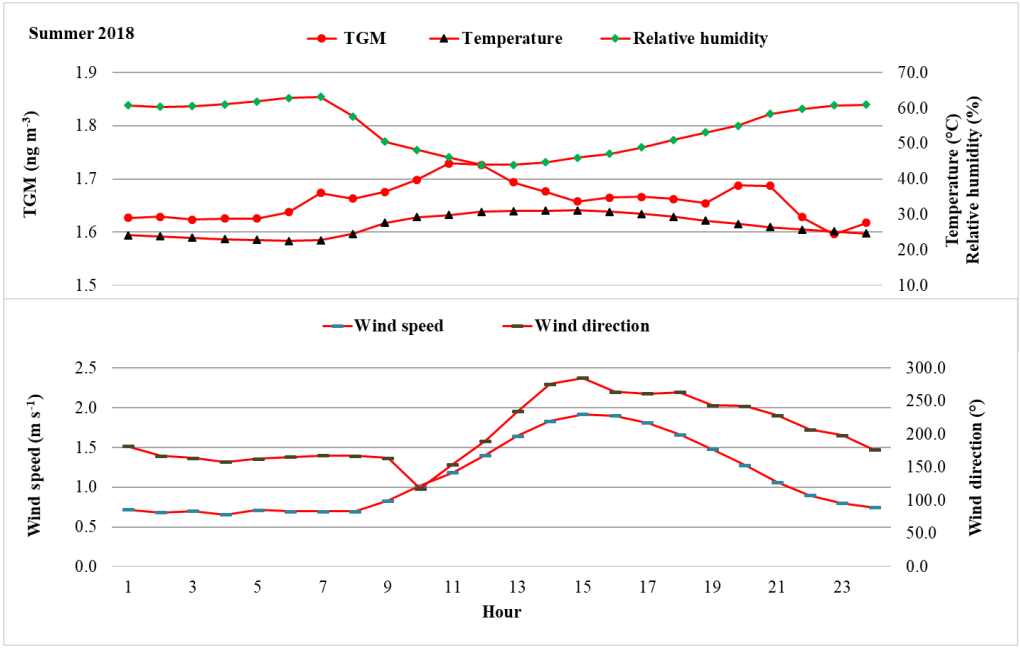

Figure 4.12 Average diurnal cycle for TGM concentrations and meteorological parameters, during summer 2018.

This behaviour was found to occur in a similar way also for the next summer, for which specific graphs and data values have been anyway reported for completeness.

Figure 4.13 shows that in correspondence with the diurnal TGM maximum value there was an increase also in the hourly average value of the temperature, which reaches a value of 29.74 °C, compared to average value for summer 2019, which was 27.35 °C, and a decrease in the hourly average value of relative humidity, which showed a value of 46.62%, compared to the average seasonal value of 52.34%. Instead, in correspondence with the evening TGM maximum value there was a decrease in the hourly average value of the temperature which is 27.28 °C and an increase in the hourly average value of relative humidity of 56.23%. A positive correlation was observed between TGM concentration and temperature (r = 0.42), between TGM concentration and wind speed (r = 0.8) whereas a negative correlation was observed between TGM concentration and wind direction (r = - 0.20) and between TGM concentration and relative humidity (r = - 0.31). Moreover, a negative correlation was observed between temperature and relative humidity (r = - 0.92) whereas a positive correlation was observed between wind speed and wind direction (r = 0.88).

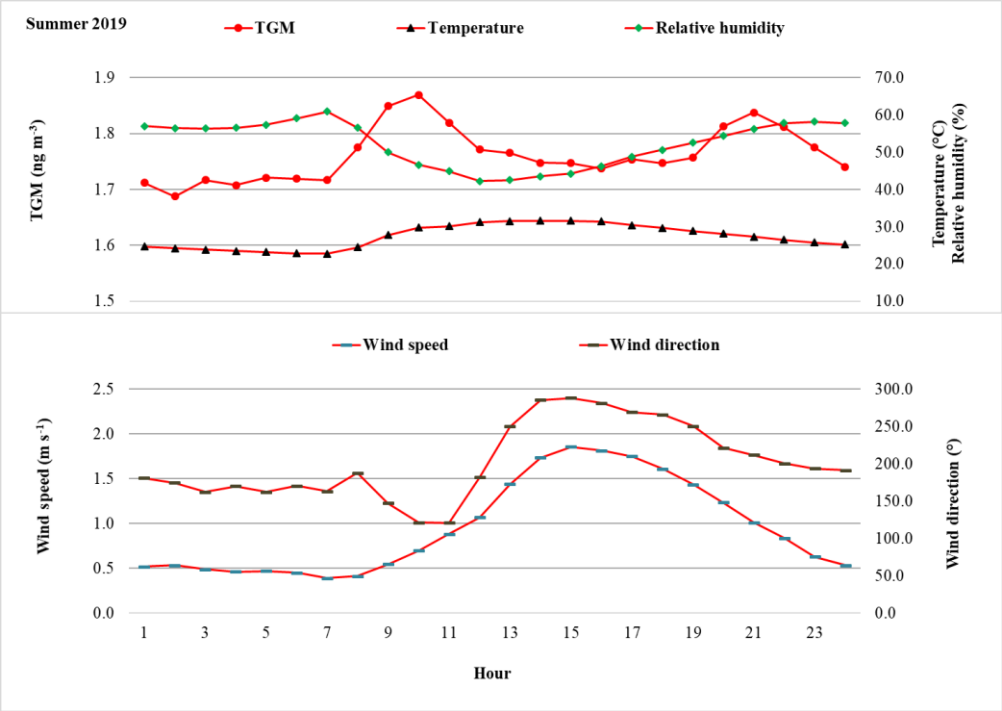

Figure 4.13 Average diurnal cycle for TGM concentrations and meteorological parameters, during summer 2019.

Figure 4.14 shows that in correspondence with the diurnal TGM maximum value there was an increase in the hourly average value of the temperature, which reached a value of 27.77 °C, compared to the seasonal daily average value, which was 26.12 °C. A decrease in the hourly average value of relative humidity was also observed with a value of 47.69%, compared to the average daily seasonal value which is 52.19%. Instead, in correspondence with the evening TGM maximum value there was a decrease in the hourly average temperature value (25.62 °C), C and an increase in the hourly average value of relative humidity (56.64%). A positive correlation was observed between TGM concentration and temperature (r = 0.10) whereas a negative correlation was observed between TGM concentration and relative humidity (r = - 0.20), between TGM concentration and wind direction (r = - 0.68) and between TGM concentration and wind speed (r = - 0.34). Moreover, a negative correlation was observed between temperature and relative humidity (r = - 0.92) whereas a positive correlation was observed between wind speed and wind direction (r = 0.77).

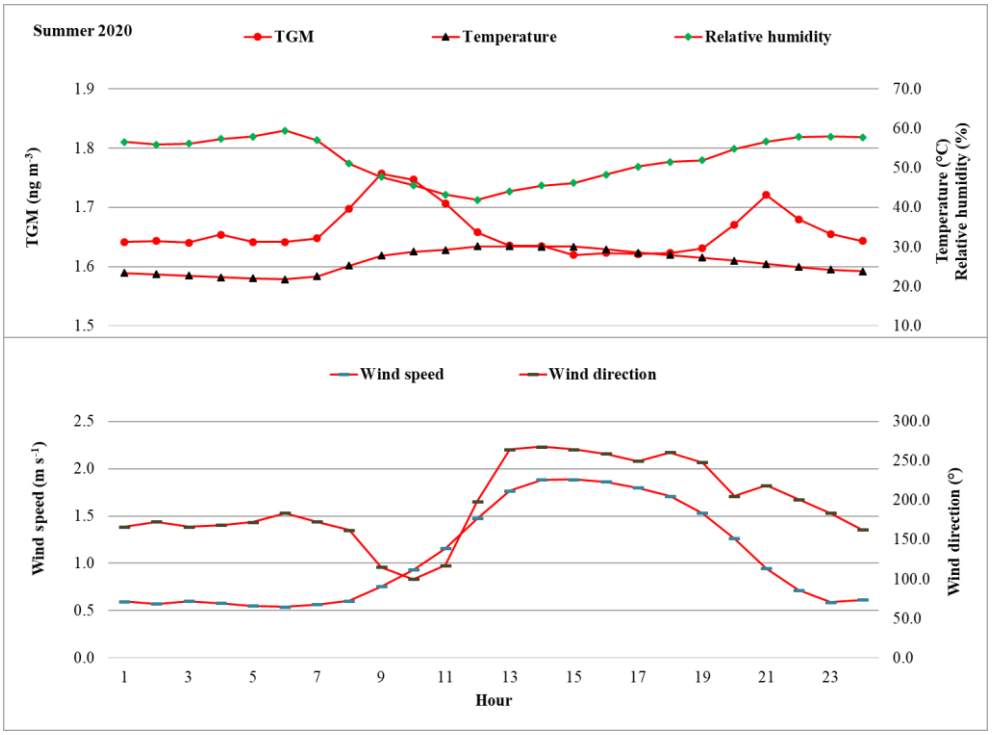

Figure 4.14 Average diurnal cycle for TGM concentrations and meteorological parameters, during summer 2020.

The same investigations were also made in respect to the winter average diurnal cycle, for which similar results were found with the difference that the TGM maximum values were recorded in the afternoon (around 13:00-18:00) instead of early or late morning as occurred during summer. The reason may be attributed to the weaker solar radiation during the winter season, which influence the air temperatures and in turns the potential re-emissions of elemental mercury from the sea/ground surface. This difference can be noticed also in the WS and WD diurnal trends, whose change in values and direction occurred after midday whereas in the summer period it was registered well before midday. In correspondence with this period there was an increase in the hourly average temperature value which reaches a value of 12.43 °C, compared to the seasonal average value which is 9.04 °C, and a decrease in the hourly average value of relative humidity, which showed a value of 56.67%, compared to the average averaged value for winter 2019, which was 68.28%. A positive correlation was observed between TGM concentration and temperature (r = 0.92), between TGM concentration and wind direction (r = 0.51) and between TGM concentration and wind speed (r = 0.96) whereas a negative correlation was observed between TGM concentration and relative humidity (r = - 0.95). Moreover, a negative correlation was observed between temperature and relative

humidity (r = - 0.99) whereas a positive correlation was observed between wind speed and wind direction (r = 0.46).

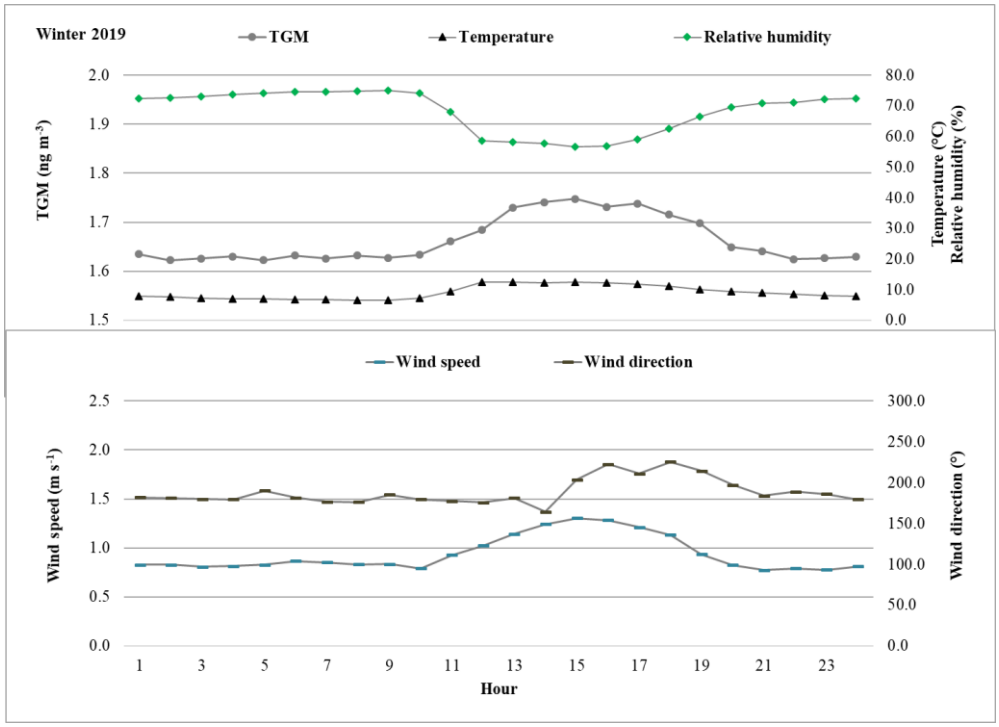

Figure 4.15 Average diurnal cycle for TGM concentrations and meteorological parameters, during winter 2019.

Figure 4.16 shows that in correspondence with the first TGM maximum value there was an increase in the hourly average temperature value which reaches a value of 13.97 °C, with respect to the average value for winter 2020, which is 10.56 °C, and a decrease in the hourly average value of relative humidity, which showed a value of 55.92%, compared to the average seasonal value, which was 66.93%. Instead, in correspondence with the evening TGM maximum value there was an increase in the hourly average value of the temperature, which was 11.28 °C and a decrease in the hourly average value of relative humidity, which showed a value of 65.80%. A positive correlation was observed between TGM concentration and temperature (r = 0.76), between TGM concentration and wind direction (r = 0.32) and between TGM concentration and wind speed (r = 0.59) whereas a negative correlation was observed between TGM concentration and relative humidity (r = - 0.75). Moreover, a negative correlation was observed between temperature and relative humidity (r = - 0.99) whereas a positive correlation was observed between wind speed and wind direction (r = 0.65).

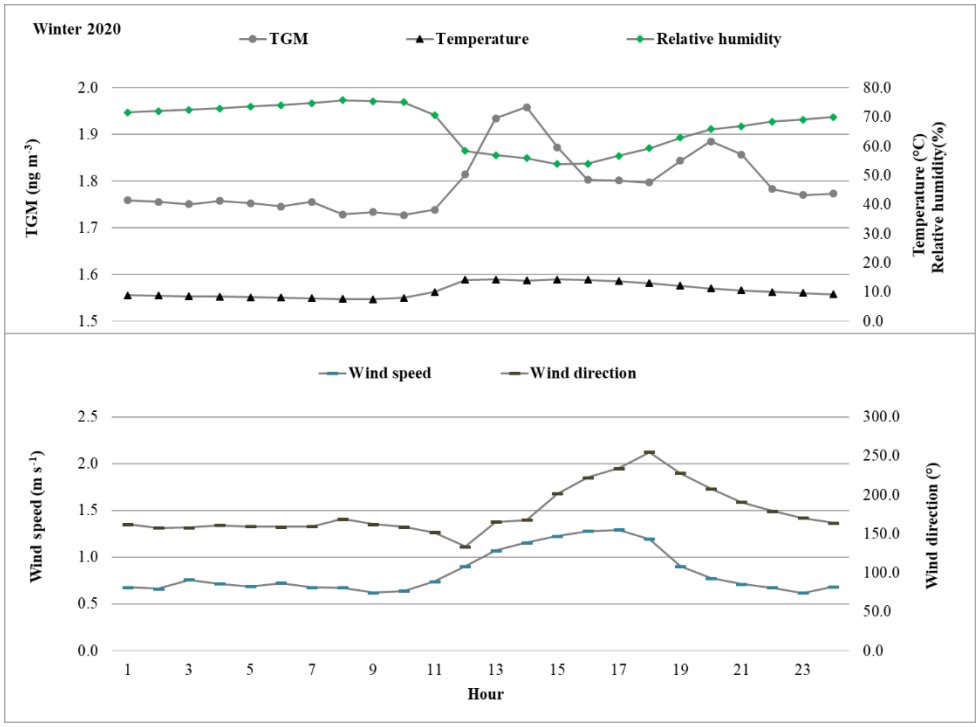

Figure 4.16 Average diurnal cycle for TGM concentrations and meteorological parameters, during winter 2020.

To visualise relationships between all recorded variables at MSA monitoring station during the whole measurement campaign, in Figure 4.17 the correlation matrix, providing the correlation between all pairs of investigated data at considered monitoring station, is showed. In this Figure, the additional dendrogram, plotted on the right side of the matrix, represents the relationships of similarity among the investigated variables for MSA station.

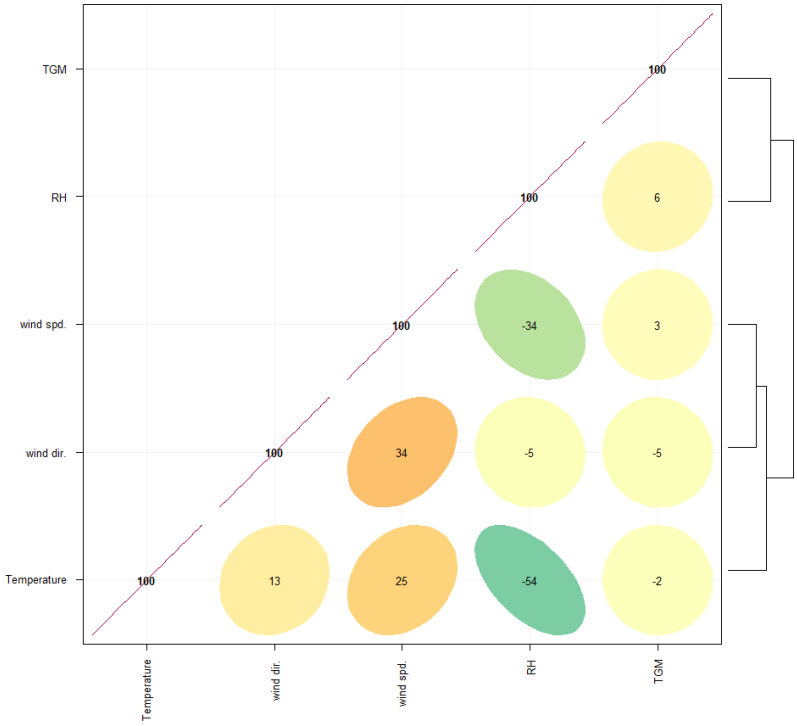

Figure 4.17 Correlation matrix and dendrogram showing the Pearson correlation values (r) and the similarities among the investigated variables at MSA station.

As showed in the Figure 4.17, a positive correlation was observed between TGM concentration and relative humidity (r = 0.6) and between TGM concentration and wind speed (r = 0.3) whereas a negative correlation was observed between TGM concentration and temperature (r = - 0.2) and between TGM concentration and wind direction (r = - 0.5).

4.3.5.2 High TGM concentrations events and identification of potential influencing sources at MSA

For a first investigation on the potential influencing sources on the TGM levels recorded at MSA an analysis of the latest inventory of national Hg emissions, with provincial downscaling, drawn up in 2015 by ISPRA (Higher Institute for Environmental Protection and Research), was carried out for the province of Foggia. The analysis showed that in 2015 the highest levels of emissions caused by public energy plants (thermoelectric power plants) were recorded in the municipalities of San Severo and Candela and about 40 km and 70 km far away from the MSA station, respectively (Figure. 4.18). The reported emissions related to the San Severo and Candela power plants were 6.27 and 3.05 kg yr^{-1}, respectively. The emission inventory also reports minor emissions linked to productive

processes located at Foggia and Poggio Imperiale, whose emissions values for the year 2015, were 0.34 and 0.05 kg. The proximity of this Hg emission point sources and the correspondence between their location and the direction of wind blowing from NW, which was found to one of the prevalent directions, could explain this kind of anthropogenic influence over the TGM levels.

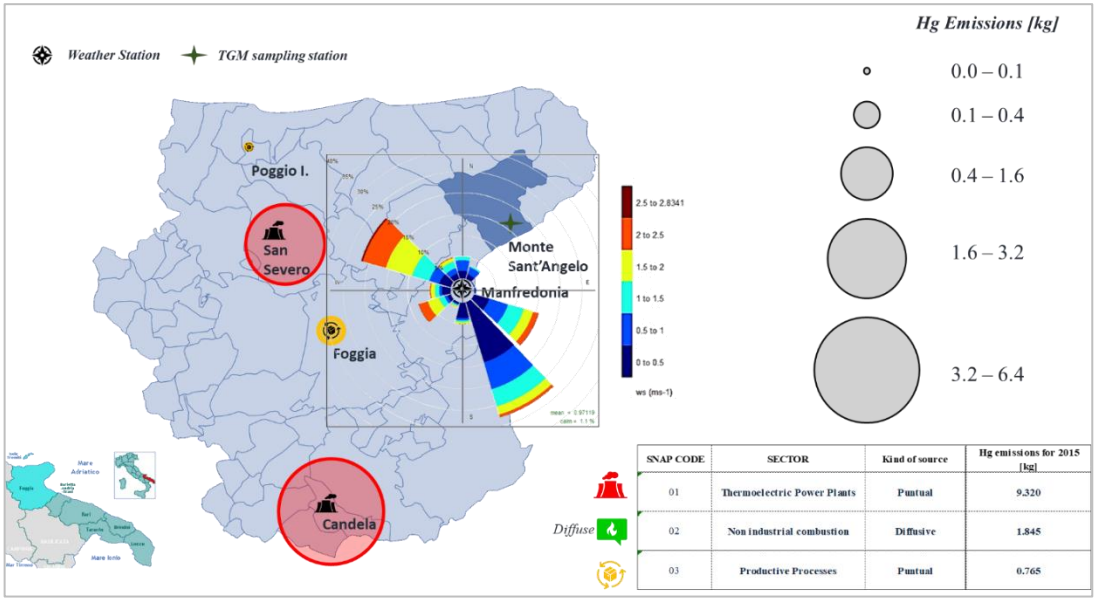

Figure 4.18 Point sources of Hg emissions in the proximity of the sampling station.

After the investigation on the Hg emissions point sources a specific analysis was performed in correspondence to those periods when the daily averaged TGM concentrations resulted to be greater than, or equal to, the 95th percentile, computed over the whole dataset with daily TGM concentrations recorded at MSA, which was found to be 1.94 ng m^{-3}. Checking days with daily mean values equal or larger that the computed 95th percentile, several specific events were identified distributed as follow: autumn 2018 (4 events), summer 2019 (11 events), autumn 2019 (2 events), winter 2020 (10 events), spring 2020 (7 events), and summer 2020 (3 events). Their occurrence is highlighted in Figure 4.19, where TGM levels identified as peak values (≥95th) were reported separately to all the remaining values (less than the 95th) and recognised as baseline values of the TGM dataset (tgm_baseline).

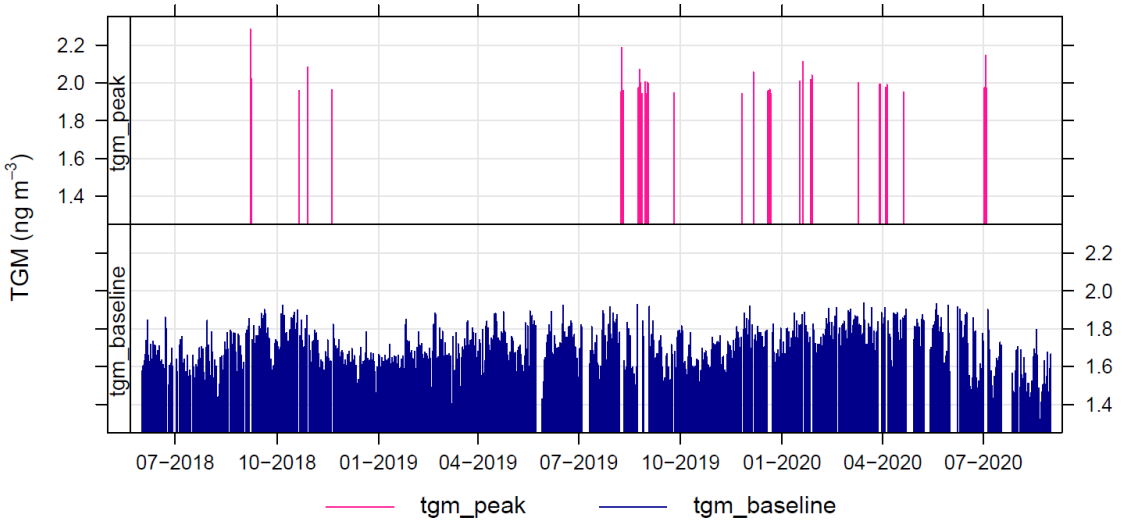

Figure 4.19 Events with daily averaged TGM concentrations identified as peak values (≥95th) reported separately from all the remaining TGM values (<95th), here recognised as baseline values.

For a thorough discussion about these specific events, special attention was given to discriminate the possible influence of natural sources as wildfires emissions, which are important mercury emissions sources contributing significantly to the atmospheric mercury load. The day-by-day identification and verification of the considered events was carried out by interpreting the results obtained from the analysis of satellite maps provided by both the NAAPS and MODIS tools. These analyses have confirmed the presence of fire events in autumn 2018 (for 2 events), summer 2019 (for 11 events), winter 2020 (for 1 event), spring 2020 (for 4 events), and summer 2020 (for 3 events). This context highlights that in winter 2020 the detected episodes of high TGM concentration values seem not to be caused by fires as a source whereas in spring 2020 and autumn 2018 wildfires resulted to affect about half the number of events with the highest TGM concentrations highlighted in this study. Moreover, in summer 2019 most of the episodes characterized by high TGM values were determined, or otherwise influenced, by the presence of fires. Figure 4.20 reports the smoke surface concentration NAAPS-based maps and the MODIS maps for some of the days previously identified and chosen as representative for the fire events, which, as confirmed by both the NAAPS and MODIS maps, affected the measurement campaign carried out at the MSA station. Specifically, the following three days has been considered: September 8th, 2018, with an average daily TGM concentration value of 2.02 ng m^{-3}, and chosen as representative of the fire episode

occurred in autumn 2018; August 10th, 2019 with an average daily TGM concentration value of 1.96 ng m^{-3}, and chosen as representative of the fire episode occurred in summer 2019; and July 2nd, 2020 with an average daily TGM concentration value of 1.97 ng m^{-3}, chosen as representative of the fire episodes occurred in summer 2020. In respect to these specific and extreme events, it was noticed that the average daily concentration found for the August 10th, 2019 (1.96 ng m^{-3}) was even higher than the seasonal average concentration value for the whole summer 2019, which was 1.76 ng m^{-3}. Similarly, for the average daily concentration recorded the July 2nd, 2020 (1.97 ng m^{-3}), resulted higher than the seasonal average concentration value for summer 2020, which was 1.66 ng m^{-3}. In addition, for both the above-mentioned days, an increase in the average daily temperature value was observed. In detail, on August 10th, 2019, a daily average temperature value of 28.52 °C was recorded, higher than the seasonal average temperature value which was 27.35 °C, and on July 2nd, 2020, a daily average value of temperature was found to be equal to 28.89 °C, higher than the average seasonal temperature value, which was 26.12 °C. These observations for the summer seasons, available during the measurement campaign, support the hypothesis of the potential influence of the wildfire episodes on the highest daily-average values of both TGM and temperature levels recorded at the sampling stations.

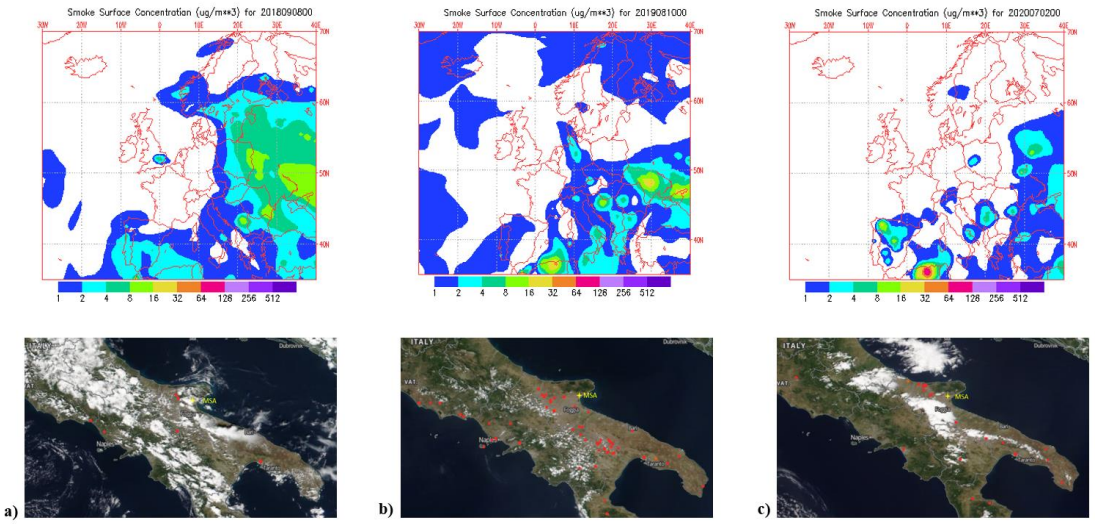

Figure 4.20 For the following days: a) September 8th 2018, b) August 10th 2019, and c) July 2nd 2020, chosen as representative of wildfire events, the smoke surface concentration maps provided by the NAAPS model, and the MODIS maps were reported in upper and in lower panels of this figure, respectively.

4.4 Case study 2: Monte Curcio

4.4.1 Sampling site description

The Monte Curcio (MCU) Environmental-Climate Observatory (1796 m a.s.l.; 39°18’57.2” N 16°25’23.6” E; http://mtcurcio.iia.cnr.it/), established during the GMOS global network and consolidated in the framework of the PON Project I-AMICA (Infrastructure of High Technology for Integrated Climate and Environmental Monitoring), consists in a large infrastructure of the CNR-IIA of Rende Division. It operates since 2015 and is part, as regional sampling station, of the Global Atmosphere Watch (GAW) program, established by the World Meteorological Organisation (WMO), which is a United Nations agency aimed to systematic long-term monitoring atmospheric chemical and physical parameters, at local and global scale [81]. The MCU station was further established as a Master site within the GMOS station contributing to Hg speciation measurements [30]. MCU stations is located within the Sila National Park in the Calabria region (Southern Italy), within an extended plateau of tens of km, whose mean altitude is about of 1200–1300 m a.s.l. Figure 4.21 shows the geographical location of the MCU Observatory, which is strategic being in the middle of the Mediterranean, around 30 and 60 km far from the Tyrrhenian and the Ionian Sea, respectively, and at an altitude allowing the advantage to intercept long-range transported air masses.

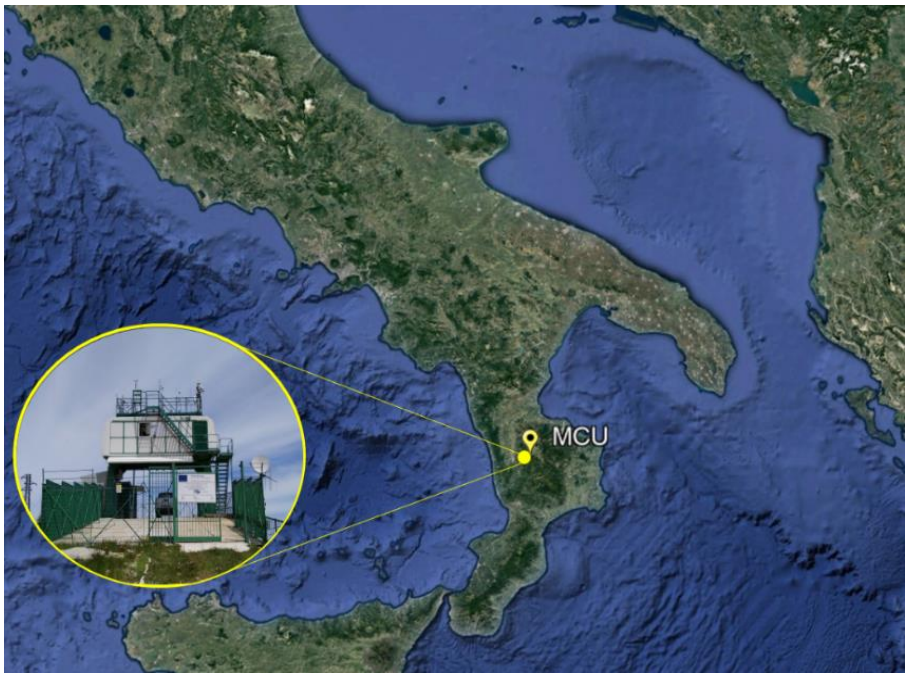

Figure 4.21 Location of the Environmental-Climate Observatory of Monte Curcio (MCU).

In fact, the operative station is situated on a southern Appenine mountain peak with completely free horizon, therefore allowing to gain atmospheric monitoring measurements with a large spatial representativeness. Moreover, this station is characterized by no access by road, and it is 200 m from a ski resort and from the cable car arrival point of the surrounding ski area. However, there are some important urban centers as the cities of Cosenza and Rende at tens of kilometers far from the station. Therefore, it is not defined as a remote site, but as rural high-altitude monitoring site not influenced by local anthropogenic sources of contamination. Being a high-altitude station, MCU is also characterized by snowfalls, low temperatures, and storms during winter while the weather is mainly fair, and the temperature increases until about 30 °C during summer and it was.

4.4.2 Atmospheric sampling campaign and TGM measurements

For the purposes of this Ph.D. thesis an intensive sampling campaign performed from May 21st, 2019 to August 31st, 2020, has been considered. At the MCU station TGM atmospheric concentrations, expressed in ng m^{-3} at standard temperature and pressure (STP, 273.15 K, 1013.25 hPa), were continuously measured at 5-minute intervals and collected using an automated Hg analyzer Tekran 2537X (Tekran Inc., Toronto, ON, Canada). During the considered sampling period, this analyser continuously measured atmospheric TGM, with an airflow rate of 1.5 L min^{-1}, and a detection limit is 0.1 ngm^{-3}. As previously described in Chapter 3, the automated analyzer Tekran 2537X works by collecting, through a Teflon sampling line, pre-filtered ambient air onto gold traps, which are thermally desorbed for quantification of mercury by cold vapor atomic fluorescence spectrometry (CVAFS) at wavelength 253.7 nm [67]. To ensure the proper functioning of this analyzer and the production of data with good quality, during the whole sampling period of monitoring campaign the measurements were performed following the SOPs and QA/QC established and adopted within the GMOS network. During the whole sampling campaign, in addition to TGM measurements, local meteorological parameters, such as air temperature (T) and relative humidity (RH), were continuously recorded with 1-minute time resolution by the meteorological station (Lastem LSI), with which the MCU Observatory is equipped. Unfortunately, the anemometer for measuring wind speed

(WS) and direction (WD) did not work properly during the case-study period, therefore, WS and WD data were not available for this research work. However, in order to investigate on the prevalent direction characterizing the MCU site, available WS and WD data, recorded in the previous years (January 2015 – November 2019) by the same weather station located at MCU were used. The available WS and WD hourly data were used as input to produce some wind rose charts which resulted useful to show overall which are the prevailing wind directions at MCU and how the general wind conditions vary by seasons.

4.4.3 TGM trends on hourly, daily, monthly, and seasonal basis

All data collected at MCU station, both TGM and meteorological ones, were processed for quality issues. The obtained valid dataset consists of TGM concentrations recorded, with a resolution of 5 minutes, from May 2019 to August 2020. Figure 4.22, shows the TGM concentrations recorded with a time resolution of 5 minutes at MCU (n = 98563) highlighting the occurrence of some interruptions, due to instrument calibration/technical maintenance or data invalidation detected with the G-DQM system.

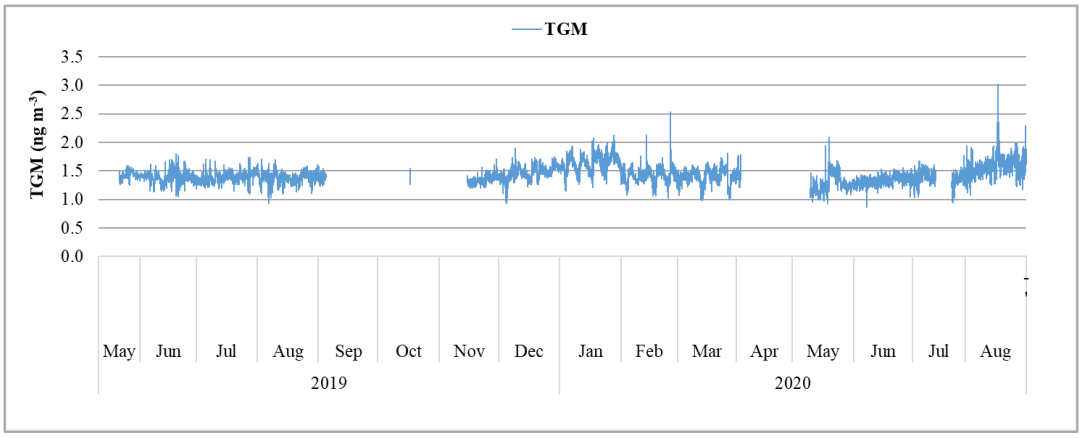

Figure 4.22 Trends of TGM concentrations recorded with a time resolution of 5 minutes at the MCU station, from May 2019 to August 2020.

TGM concentration were converted to hourly averages and then to daily averages, following the data processing procedures that consider as valid the daily average if at least 75% of the corresponding hourly measurement data are available. By applying this criterion to the TGM dataset obtained at MCU, 127 days were not considered

representative due to the lack of sufficient hourly data. The remaining 341 valid daily-averaged TGM data are reported in Figure 4.23.

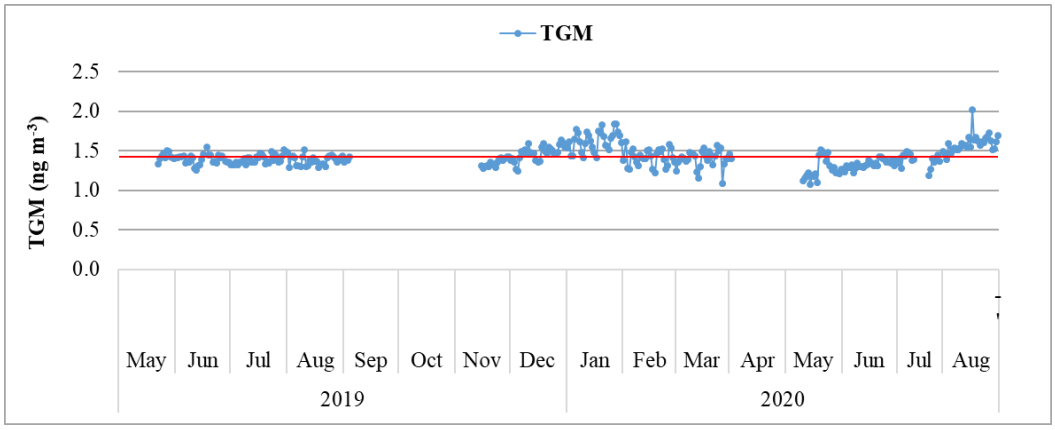

Figure 4.23 Daily-averaged TGM concentrations at the MCU station. The solid red line indicates the daily average value of the TGM concentration (1.43 ± 0.13 ng m^{-3}) recorded during the entire measurement campaign.

The atmospheric daily-averaged TGM concentrations exhibited a quite constant trend over the whole sampling campaign considered at MCU site. TGM daily values showed a variability from 1.08 ng m^{-3} to 2.02 ng m^{-3}, with an average value of 1.43 ± 0.13 ng m^{-3}. Daily-averaged TGM concentrations were then aggregated on monthly basis which were considered valid if at least the 66% of the corresponding daily data resulted available, in the MCU, the application of this criterion consequently led to the elimination of five months (May, September, and November 2019, and April 2020), for which it was not possible to obtain a representative monthly-averaged value. Otherwise, the remaining valid monthly data were reported in Figure 4.24.

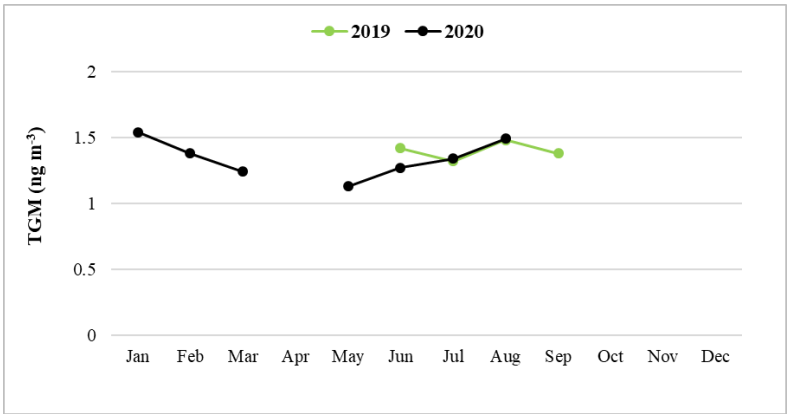

Figure 4.24 Monthly-averaged TGM concentrations at the MCU station.

Table 4.4 summarizes the representative values for the monthly-averaged TGM concentrations, recorded at MCU station during 2019 and 2020. For each available month the corresponding values for standard deviation, were also reported.

Month - Year	2019	2020
	TGM (ng m^{-3})	TGM (ng m^{-3})
January	-	1.54 ± 0.13
February	-	1.38 ± 0.10
March	-	1.24 ± 0.11
April	-	-
May	-	1.13 ± 0.13
June	1.42 ± 0.06	1.27 ± 0.05
July	1.32 ± 0.06	1.34 ± 0.08
August	1.48 ± 0.06	1.49 ± 0.11
September	1.38 ± 0.09	-
October	-	-
November	-	-
December	-	-

Table 4.4 Monthly-averaged values for TGM concentrations and the corresponding standard deviation values, obtained for 2019 and 2020.

The analysis of the monthly variation of TGM concentrations showed that during 2019 the highest average monthly TGM value was recorded in August (1.48 ± 0.06 ng m^{-3}) and the lowest in July (1.32 ± 0.06 ng m^{-3}) whereas during 2020 the highest and lowest average monthly TGM values were found in January (1.54 ± 0.13 ng m^{-3}) and May (1.13 ± 0.13 ng m^{-3}), respectively. Despite the limited dataset available, the seasonal-averaged TGM values have been computed, considering them as valid if determined by at least two months of TGM measurement values.

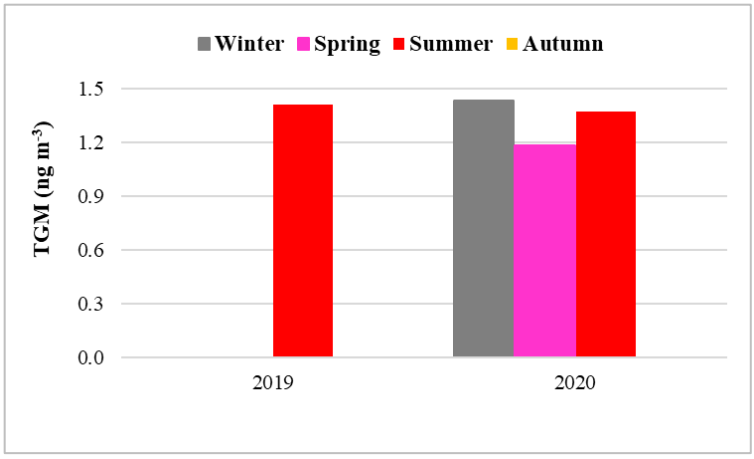

Figure 4.25 Seasonal-averaged TGM concentrations at the MCU station.

In this way, for the year 2019 it was possible to define only one season (summer) whereas for 2020, average values for three seasons (winter, spring, and summer) were properly computed (see Figure 4.25). The higher seasonal average for TGM concentration was recorded in winter 2020, with value of 1.43 ± 0.09 ng m^{-3}, and the lower one in spring 2020, with a value of 1.18 ± 0.08 ng m^{-3} (Table 4.5).

Season - Year	2019	2020
	TGM (ng m^{-3})	TGM (ng m^{-3})
Winter	-	1.43 ± 0.09
Spring	-	1.18 ± 0.08
Summer	1.41 ± 0.08	1.37 ± 0.11
Autumn	-	-

Table 4.5 Seasonal-averaged TGM concentrations for 2019 and 2020.

The seasonal average TGM concentration in Summer 2019 was significantly higher than that recorded in Summer 2020 (1.41 ± 0.08 ng m^{-3} and 1.37 ± 0.11 ng m^{-3}, respectively; $p < 0.05$).

4.4.4 Seasonal average diurnal cycles of TGM concentrations

For those seasons resulted to have enough data to be considered representative for the sampling MCU station, the seasonal average diurnal cycle of TGM concentrations have been processed and then plotted in Figure 4.26.

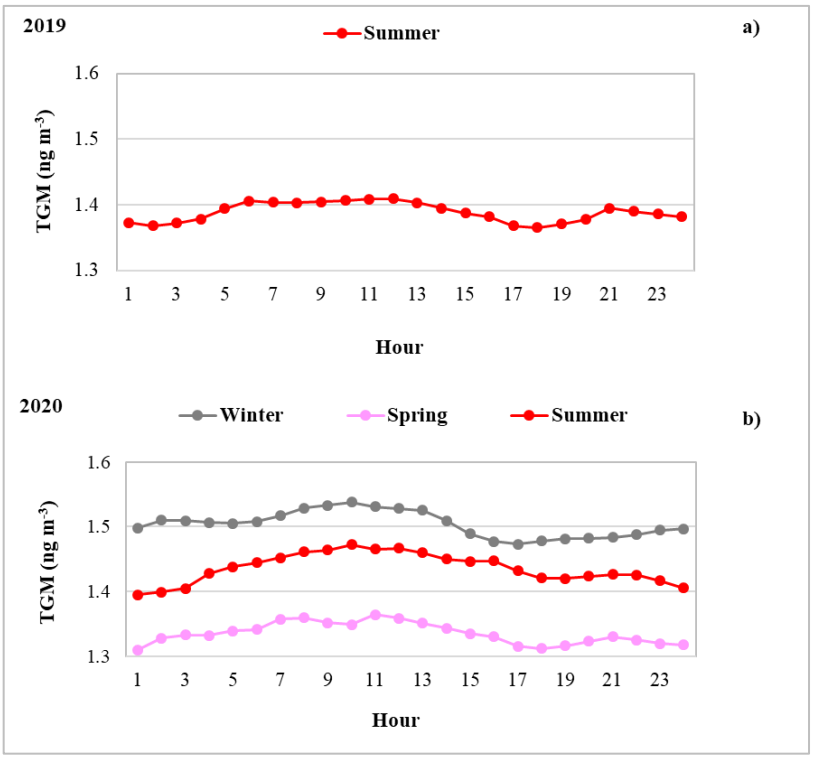

Figure 4.26 Seasonal average diurnal cycle of TGM recorded at MCU during: a) 2019 and b) 2020.

For each investigated season, the carried out analysis made it possible to highlight the maximum values reached by the hourly TGM average concentrations along the related seasonal-averaged diurnal cycle.

The analysis of the seasonal average diurnal cycle of TGM concentrations was then focused on the summer and winter seasonal periods available for the measurement campaign performed at the MCU station. In particular, the summer seasons of the years 2019 and 2020, and the winter season of the year 2020, have been investigated. In detail, during summer 2019, the average diurnal cycle of TGM concentrations exhibited - between 05:00 and 14:00 - hourly average values higher than the corresponding daily average value, which was 1.39 ng m^{-3}. In this time frame, the absolute maximum value over the entire daytime cycle was recorded at 06:00 and at 10:00-12:00 (Figure 4.27 a)), both characterized by hourly average values of 1.41 ng m^{-3}, corresponding to an increase of 1%, compared to the average value of summer 2019 (1.39 ng m^{-3}). During summer 2020 (Figure 4.27 b)), the average diurnal cycle of TGM concentrations showed - between 05:00 and 17:00 - hourly average values higher than the corresponding daily average value, which was 1.44 ng m^{-3}. In this time frame, the absolute maximum value over the whole daytime cycle was recorded at 10:00 and another around 11:00-12:00, both

characterized by the same hourly average values of 1.47 ng m^{-3} and an increase of 2%, compared to the average value for summer 2020.

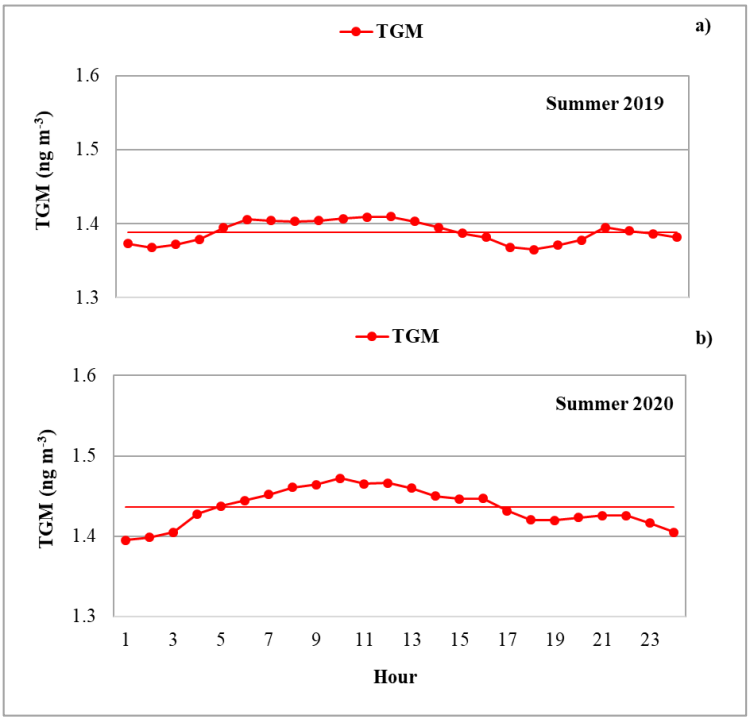

Figure 4.27 Average diurnal cycle of TGM concentrations for: a) summer 2019, and b) summer 2020. In each plot, the solid red line indicates the average daily value of the TGM concentration recorded during the corresponding season.

Regarding winter 2020, the average diurnal cycle TGM concentrations (see Figure 4.28) between 06:00 and 14:00 exhibited a long-lasting plateau with hourly average values higher than the corresponding daily average value, which was 1.50 ng m^{-3}. In this time period, the absolute maximum value over the entire daytime cycle was recorded at 10:00 and another around 11:00-12:00, which was characterized by a hourly average value of 1.54 ng m^{-3} and 1.53 ng m^{-3} and an increase of 3% and 2%, respectively, compared to the average value for winter 2020.

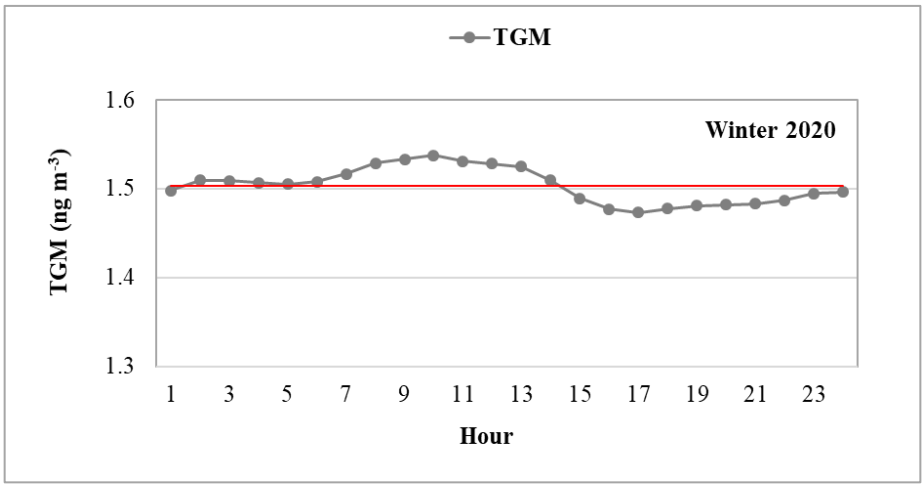

Figure 4.28 Average diurnal cycle of TGM concentrations during winter 2020. The solid red line indicates the average daily value of the TGM concentration recorded during the corresponding season.

4.4.5 Meteorological data analysis

The validated raw meteorological data of air temperature and relative humidity recorded at MCU station during whole measurement campaign, from May 2019 to August 2020, were aggregated on hourly basis and reported in Figure 4.29, in order to better analyse the meteorological conditions at the investigated sampling site shows the hourly time series.

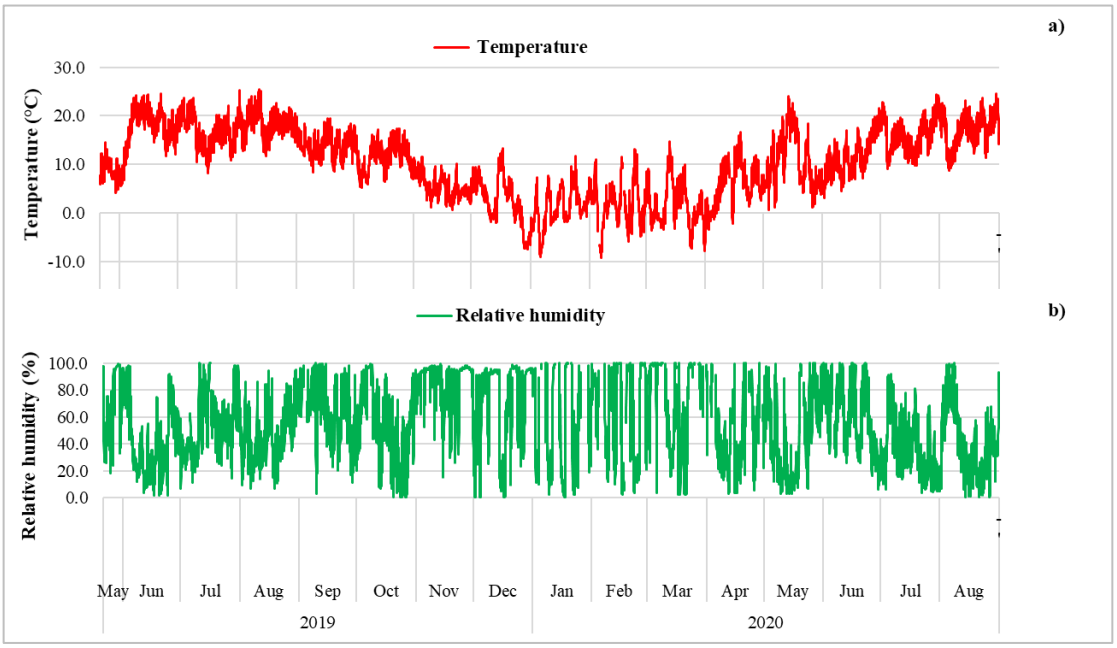

Figure 4.29 Hourly time series of a) air temperature (°C) and b) relative humidity (%) recorded at the MCU station.

During the measurement campaign, local weather conditions were mainly characterized by an average hourly temperature value of 10.04 ± 7.24 °C, ranging between -9.30 and 25.50 °C, and an average hourly relative humidity value of 52.79 ± 29.08%, ranging between 0.10 and 100 % (see Table 4.6). The correlation analysis between temperature and relative humidity showed a negative correlation (r = - 0.54).

Meteorological parameters	Average ± SD	Range
Air temperature (°C)	10.04 ± 7.24	- 9.30 - 25.50
Relative humidity (%)	52.79 ± 29.08	0.10 - 100.00

Table 4.6 Descriptive statistics (average ± SD, range with minimum and maximum values) for air temperature and relative humidity recorded over the whole observing period from May 21st, 2019 to August 31st, 2020.

The same basic descriptive statistics (average ± SD, range with minimum and maximum values) for the available meteorological parameters at MCU station, air temperature and relative humidity, were also computed about each single season for which corresponding seasonal-averaged TGM values are available. Results obtained for the considered meteorological parameters are summarized in Table 4.7.

Season	Meteorological parameters	Average ± SD	Range
Summer 2019	Air temperature (°C)	17.34 ± 1.53	15.49 - 19.64
	Relative humidity (%)	46.63 ± 3.93	39.54 - 54.13
Winter 2020	Air temperature (°C)	1.83 ± 0.56	1.24 - 2.89
	Relative humidity (%)	54.30 ± 3.56	48.61 - 61.21
Spring 2020	Air temperature (°C)	6.64 ± 1.09	5.47 - 8.51
	Relative humidity (%)	51.44 ± 4.62	43.11 - 59.33
Summer 2020	Air temperature (°C)	14.74 ± 1.58	12.99 - 17.20
	Relative humidity (%)	43.56 ± 4.29	36.45 - 48.16

Table 4.7 Descriptive statistics for air temperature and relative humidity recorded at MCU station, during 2019 and 2020, split by seasons for which TGM measurements are available.

The obtained results highlight seasonal trends for which the air temperature exhibited the highest value in summer 2019 (17.34 ± 1.53 °C) and the lowest value in winter 2020 (1.83 ± 0.56 °C). Conversely the relative humidity showed a higher level in winter 2020 (54.30 ± 3.56%) and a lower one during summer 2020 (43.56 ± 4.29%) (see Table 4.7). As already mentioned, unfortunately the anemometer reported some technical faults so that WS and WD measurements were not recorded during the investigation period considered for the case-study of this thesis (May 2019 – Aug 2020). However, to investigate the general

prevailing wind conditions at the MCU station, the wind rose plots have been performed with data available for WS and WD, referring to the long-term period from January 2015 to November 2019. Figure 4.30 (left panel) summarizes the results showing how the wind directions varied at the MCU station as a function of wind speed. The wind rose highlights the three prevailing wind direction, from which the wind blow, recorded at MCU: the NE direction, with a frequency of more than 10%, the WSW one, with the same frequency of about 10%, and then the westerlies (W) direction, with the highest recorded frequency of 15%. The prevailing west-south-westerlies (WSW) wind direction also showed the largest frequency associated with the higher recorded wind speed values, between 8 and 20.7 m s^{-1}.

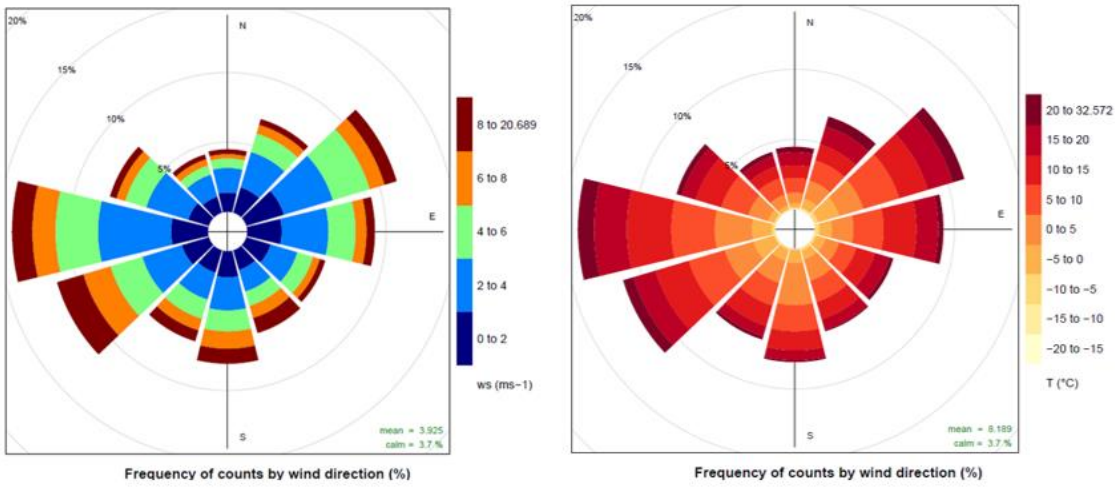

Figure 4.30 Wind roses showing wind direction as a function of wind speed (left panel) and as a function of temperature (right panel) obtained considering WS, WS and T available data at MCU station for the period from January 2015 to November 2019.

In addition, a wind rose chart obtained plotting WD data as function of temperature, was performed even considering the meteorological available data at the MCU station from January 2015 to November 2019. This chart, reported in Figure 4.30 (right panel) highlights that, among the three prevailing wind directions already detected at the MCU station, the prevailing westerlies (W) direction showed the largest frequency associated with the higher temperature values, from 20 to 33 °C. Over the same observing period (January 2015 to November 2019), the wind roses on a seasonal basis were also produced considering the wind direction as a function of both wind speed and temperature (see Figure 4.31). The obtained wind roses display a quite larger variability within seasons. In

particular, it was observed that in summer the wind mainly blew from the north-easterlies (NE) direction, with a frequency of 15%, and that it was generally weak, with wind speed values falling in the blue and green ranges, referring to values of 2-4 and 4-6 m s^{-1}, respectively. However, in winter the wind blew mainly from the southerlies (S) and south-westerlies (SW) directions, also associated with values of wind speed, above 8 m s^{-1}. The same direction also showed a higher frequency associated with higher temperature values between 5 and 10 °C. Wind roses by seasons, obtained as function of air temperature (see Figure 4.31 – lower panel), highlight the large variability of temperature, whose recorded levels, reached values above 20 °C during the summer, whereas come also down below -15 °C during the winter season.

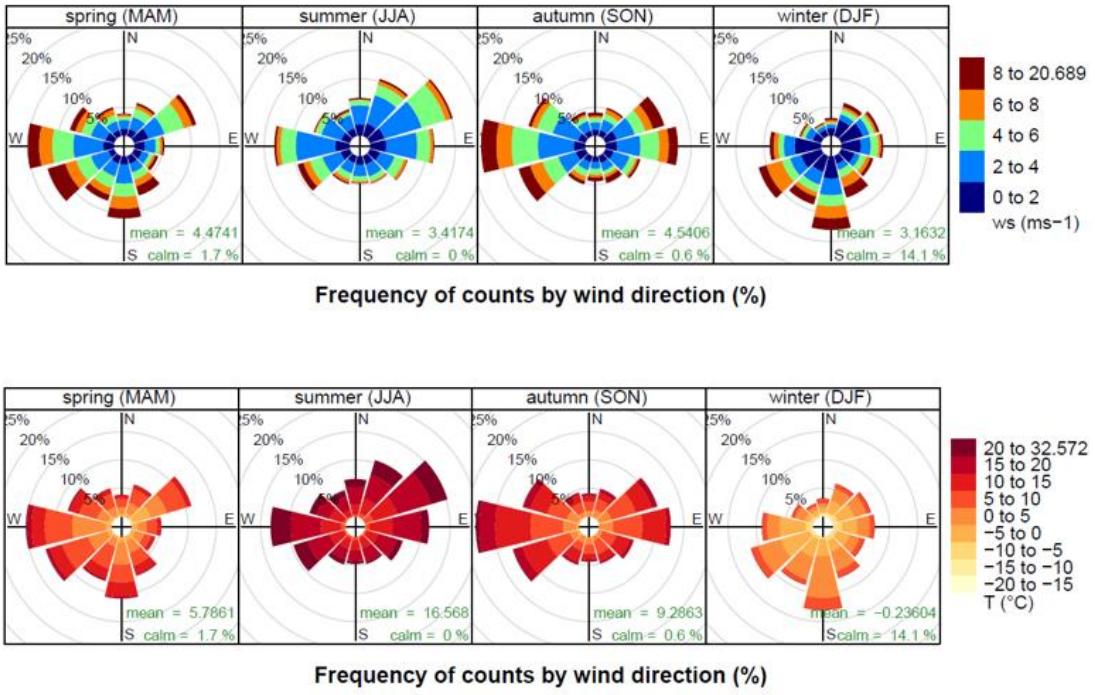

Figure 4.31 Seasonal wind roses showing wind direction as a function of wind speed (upper panel) and air temperature (lower panel), obtained considering WS, WS and T available data at MCU station for the period from January 2015 to November 2019.

4.4.6 Summer and winter average diurnal cycle for both TGM concentrations and meteorological data

For the years 2019 and 2020 of the measurement campaign carried out at the MCU station, the trends of both the TGM concentration and the meteorological parameters, such as air temperature and relative humidity, were observed, as average diurnal cycle for

the summer and winter seasons. The average diurnal cycle of TGM concentrations recorded during summer 2019 exhibited between 05:00 and 14:00 hourly average values higher than the corresponding daily average value, which was 1.39 ng m^{-3}. In this time period, the absolute maximum value over the entire daytime cycle was recorded at 06:00 and at 10:00-13:00 both characterized by hourly average values of 1.41 ng m^{-3}, corresponding to an increase of 1%, compared to the average daily value of the summer (1.39 ng m^{-3}). Figure 4.32 highlights that, in correspondence of both absolute maximum values recorded at 06:00 and at 13:00, there were a decrease and an increase of the hourly average values for the air temperature, which reached values of 16.40 °C and 19.64 °C, respectively, compared to the seasonal average value for summer 2019, which was 17.34 °C. Moreover, in correspondence of these maximum values, decreases in the hourly average values of relative humidity, were detected with values of 46.29% and of 42.74%, respectively, compared to the seasonal-averaged value, which was equal to 46.63%.

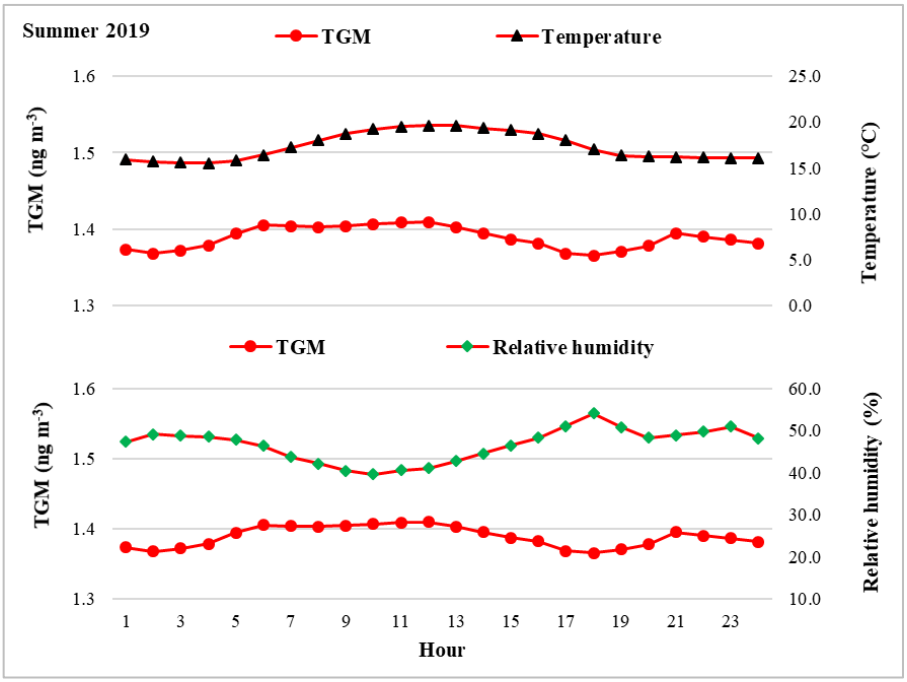

Figure 4.32 Average diurnal cycle of TGM concentrations and of meteorological parameters, during summer 2019.

A positive correlation was observed between TGM concentration and temperature (r = 0.57) whereas a negative correlation was observed between TGM concentration and relative

humidity (r = - 0.81). Moreover, a negative correlation was observed between temperature and relative humidity (r = - 0.69).

Similarly, during summer 2020, the average diurnal cycle of TGM concentrations displayed - between 05:00 and 17:00 - hourly average values higher than the corresponding daily average value, which was 1.44 ng m^{-3}. In this time frame, the absolute maximum value over the entire daytime cycle was recorded at 10:00 and another around 11:00-12:00, both characterized by hourly average values of 1.47 ng m^{-3} and an increase of 2%, compared to the average value for summer 2020. Figure 4.33 shows that in correspondence with the absolute maximum values at 10:00 and at 12:00 there were increases in the hourly average values of the air temperature, which reached values of 16.50 °C and 17.07 °C at 12:00, compared to the seasonal average value for summer 2020, which was 14.74 °C. Moreover, in correspondence of these maximum values there were decreases in the hourly average values of relative humidity showing values of 37.97% and of 36.45%, compared to the seasonal average value of 43.56%.

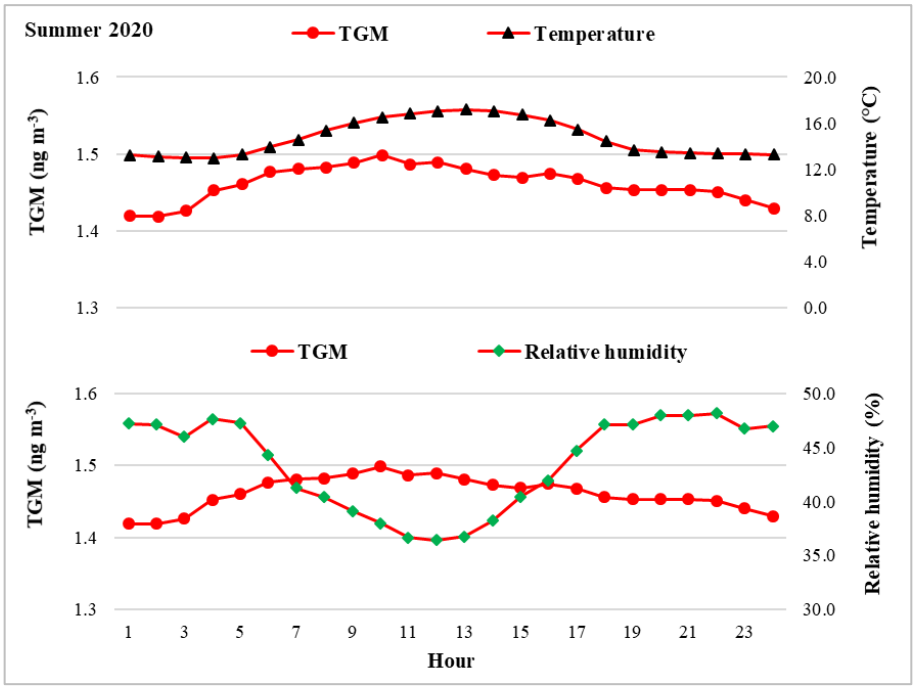

Figure 4.33 Average diurnal cycle of atmospheric TGM concentrations and of meteorological parameters, during summer 2020.

A positive correlation was observed between TGM concentration and temperature (r = 0.80) whereas a negative correlation was observed between TGM concentration and relative

humidity (r = - 0.81). Moreover, a negative correlation was observed between temperature and relative humidity (r = - 0.94).

As regard to winter 2020, the average diurnal cycle of TGM concentrations - between 06:00 and 14:00 - showed hourly average values higher than the corresponding daily average value, which was 1.50 ng m^{-3}. In this time frame, the absolute maximum values, over the entire daytime cycle, were recorded at 10:00 and another around 11:00-12:00, which were characterized by a hourly average value of 1.54 ng m^{-3} and 1.53 ng m^{-3}, and an increase of 3% and 2%, respectively, compared to the average daily value for winter 2020 (1.50 ng m^{-3}). As it can be noticed in Figure 4.34, in correspondence with the TGM absolute maximum value around 12:00, an increase in the hourly average value of the temperature was registered, which reached the value of 2.89 °C, compared to the seasonal average value for winter 2020, which was 1.83 °C. Moreover, in correspondence of this maximum value there was a decrease in the hourly average value of relative humidity, which recorded a value of 50.70%, compared to the seasonal average of 54.30%.

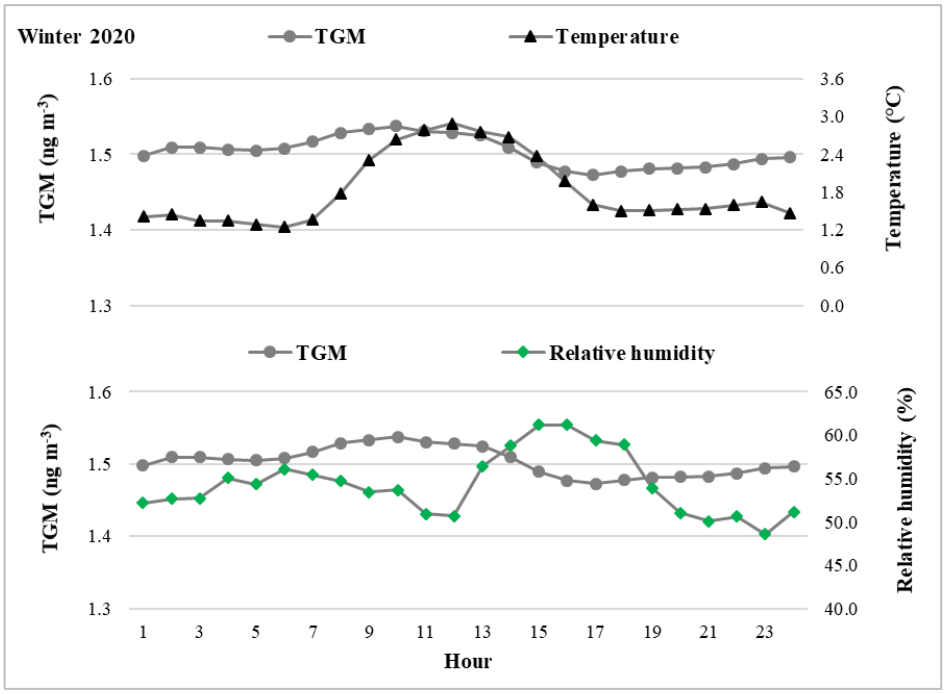

Figure 4.34 Average diurnal cycle of TGM concentrations and of meteorological parameters, during winter 2020.

A positive correlation was observed between TGM concentration and temperature (r = 0.51) whereas a negative correlation was observed between TGM concentration and relative

humidity (r = - 0.21). Moreover, a positive correlation was observed between temperature and relative humidity (r = 0.12).

In summary, it can be asserted that, by observing each single seasonal-events available at the MCU station, the average diurnal cycle of TGM is featured, both in summer and in winter, by increasing values around midday, which resulted directly and inversely related to air temperature and relative humidity, respectively.

4.4.7 Comparison between the average diurnal cycle of TGM concentrations at MSA and MCU sites

Considering the data availability for the measurement campaigns carried out at both the MSA and MCU monitoring stations, a comparison of the seasonal variability highlighted by the already detected trends for TGM was performed. Graphical trends, summarized in the following chart (Figure 4.35) allowed to easily compare the already obtained average diurnal cycle of TGM, recorded at both MSA and MCU stations. For both sites, the whole monitoring period was grouped in four seasons and the comparison was made possible for those seasons for which measurements were simultaneously carried out at the MSA and MCU stations. In particular, the seasons available for both monitoring periods were summer 2019, summer 2020 and winter 2020. It can be easily noticed from the charts (Figure 4.35) that TGM trends at MCU were steadier than MSA. The only increases detected at MCU station were in the order of 1-2%, in respect to the seasonal-averaged values. It is instead remarkable the great variability of the TGM diurnal cycle observed at MSA, during which the observed increases were in the order of 3-6%. In detail, as regard to the investigated seasons at both sites, the TGM concentration recorded in Summer 2019 at MSA was significantly higher than that observed in Summer 2019 at MCU (1.76 ± 0.05 ng m^{-3} and 1.39 ± 0.01 ng m^{-3}, respectively; $p < 0.05$). With respect to Summer 2020, the TGM concentration at MSA was significantly higher than that observed at MCU (1.66 ± 0.04 ng m^{-3} and 1.44 ± 0.02 ng m^{-3}, respectively; $p < 0.05$). Moreover, for that concerning Winter 2020 the TGM concentration in at MSA was significantly higher than that in Winter 2020 at MCU (1.80 ± 0.04 ng m^{-3} and 1.47 ± 0.02 ng m^{-3}, respectively; $p < 0.05$). These outcomes may be justified considering that MSA is a coastal site, then influenced by the breeze regimes that, as already observed, determines a larger variability in wind regimes. In fact, each day the MSA station is

influenced by air masses, coming from both land and sea, which are intrinsically different in chemical composition and physical properties. The specific location of MCU on the peak of the Apennines and its relevant distance from potential sources are the reason for the weaker variability of TGM levels here detected. The latter would additionally be the reason why the background TGM concentrations at MCU, in the range of 1.4 – 1.6 ng m^{-3}, were found lower that that recorded at MSA, whose values varied from 1.7 to 2.0 ng m^{-3}.

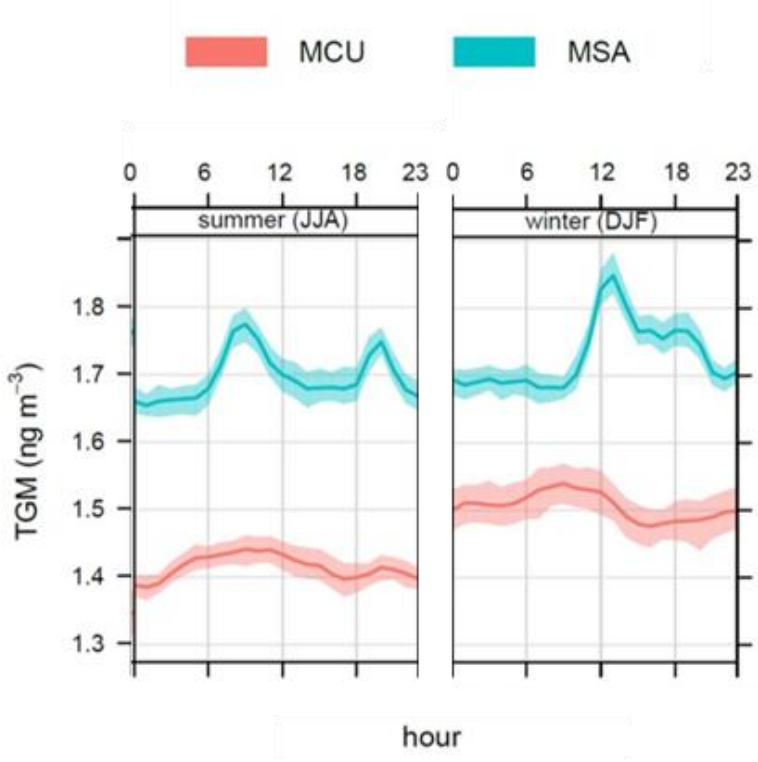

Figure 4.35 Seasonal average diurnal cycle of atmospheric TGM concentrations recorded at MSA and MCU stations, for the seasons during which the TGM measurements were jointly available.

4.4.8 High TGM concentrations events and identification of potential influencing sources at MCU

During the measurement campaign, the higher Hg values attributable to specific events were detected and analysed in detail below. The specific events corresponding to the higher TGM values were identified for some days in winter 2020 (13 events) and in summer 2020 (4 events). Since the MCU station is located in a high-altitude rural area, special attention was given to discriminate the potential influence of natural sources, such as wildfires emissions and Saharan dust both usually affecting the atmosphere of the Mediterranean basin. As previously described, the day-by-day identification of each detected event was carried out by interpreting the results obtained examining the satellite

maps provided by the NAAPS and MODIS tools together with the analysis of the backward trajectories provided by the HYSPLIT model. The verification analysis carried out with NAAPS and MODIS maps confirmed the wildfire occurrence during August 2020, and in particular for those days previously identified as days characterized by a daily-averaged TGM concentration greater than the 95th percentile (1.68 ng m^{-3}) which were: August 17th, 25th, 26th and 31st 2020. To examine these events more thoroughly, TGM data recorded during August 2020 were plotted in Figure 4.36 with the finer available time resolution, equal to 5 minutes.

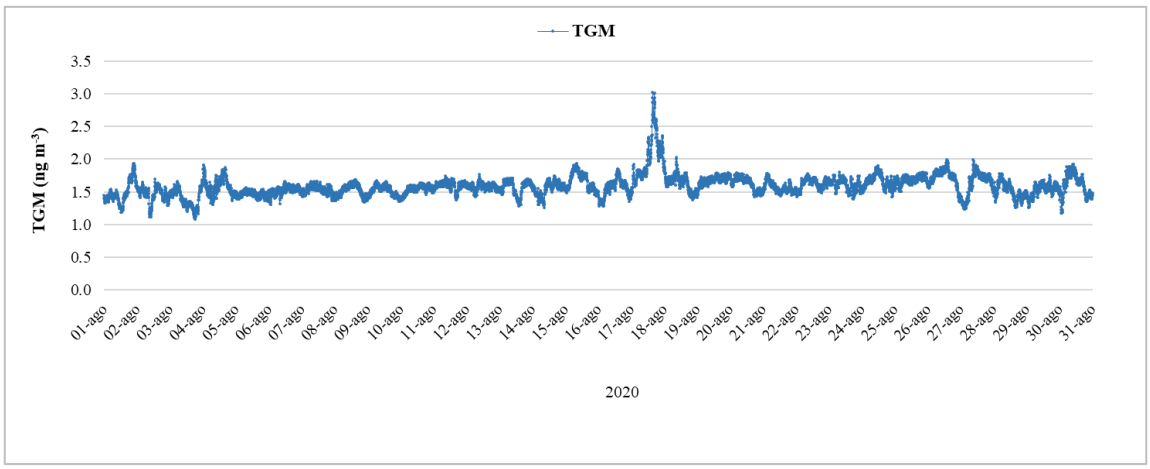

Figure 4.36 Five-minute TGM concentrations collected during August 2020 at MCU.

August 17th and 31st, 2020 with mean daily TGM concentration values equal to 2.02 and 1.69 ng m^{-3}, respectively, were chosen as representative for the discussion of the influence of a summer wildfire event over the TGM levels revealed at MCU. The daily-averaged concentrations of TGM recorded in these days resulted higher than the seasonal-averaged TGM concentration for summer 2020, which was 1.44 ± 0.02 ng m^{-3}. Furthermore, on August 17th and 31st , 2020 the daily-averaged air temperature value were 17.29 ± 1.68 °C and 19.68 ± 3.41 °C, respectively, therefore higher than the seasonal-averaged temperature value, which was instead 14.74 ± 1.58 °C. The smoke surface concentration NAAPS-based maps as well as the MODIS maps corresponding to these days were reported in Figure 4.37.

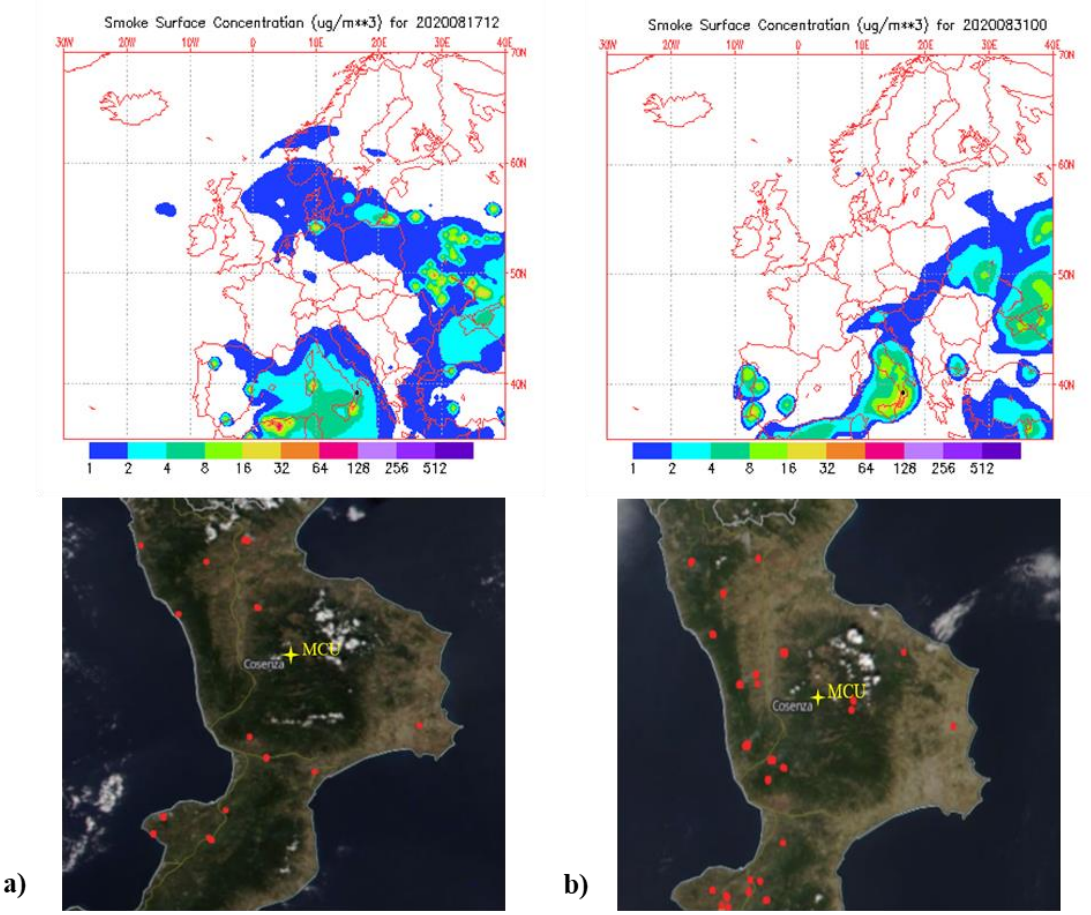

Figure 4.37 For the day considered as representative of wildfire event: a) August 17th and b) 31st 2020, the NAAPS (upper side) and the MODIS (lower side) maps are reported. In the upper panel, the location of MCU station was indicated by a black spot.

The smoke surface concentration from the NAAPS-based map corresponding to August 17th 2020 (Figure 4.37 a) - upper side), shows that at ground level, in correspondence of the area where MCU station is located, the model estimates a smoke concentration between approximately 4 and 8 µg m^{-3}, while the smoke surface concentration from the NAAPS-based map corresponding to August 31st 2020 (Figure 4.37 b) upper side, shows that at ground levels, the model estimates a smoke concentration between approximately 32 and 64 µg m^{-3}. The MODIS-maps (Figure 4.37 a) and b) – lower side), both display that during the examined period some wildfires were active in proximity of the MCU sampling area.

The observation of the daily averaged TGM concentration allowed to focus attention on the increase of TGM values recorded between the days of January 26th and 28th, 2020, which increased from a value of 1.69 ng m^{-3} to a value of 1.84 ng m^{-3}.

The days with values higher than the 95th percentiles, identified during January 2020. To additionally examine these events more thoroughly, TGM data recorded only during January 2020 were plotted in Figure 4.38 with the finer available time resolution, equal to 5 minutes.

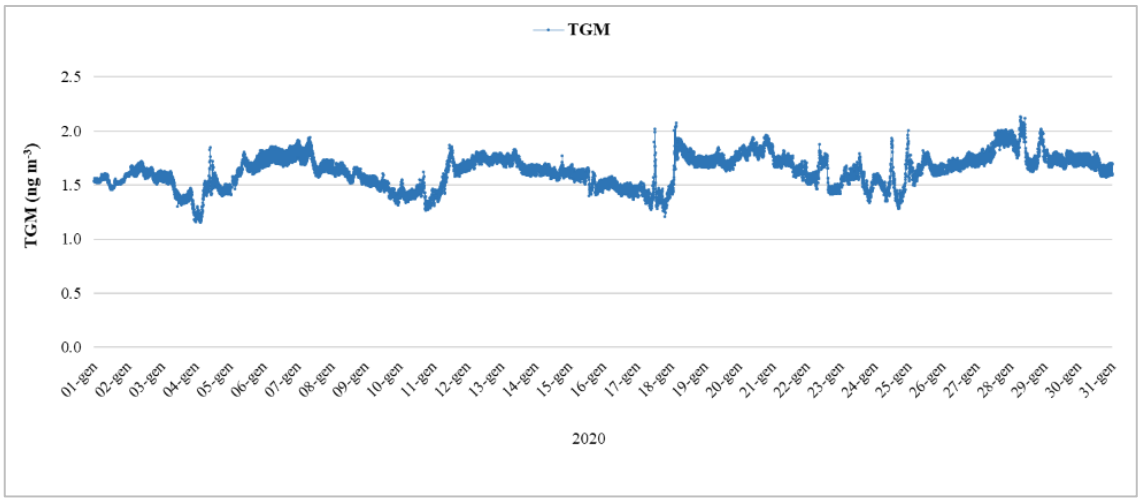

Figure 4.38 Five-minute TGM concentrations collected during January 2020 at MCU

The specific analysis of both the dust surface concentration and the Aerosol Optical Depth (AOD), together provided by the NAAPS model, allowed to identify the presence of the Saharan dust intrusion in concomitance with the increase in the average daily values of TGM observed at the MCU station in the period of January 26th - 28th, 2020. To better investigate this event, the dynamics at synoptic level of the air masses were deepen by performing specific runs simulating the two-day backward trajectory ensemble and the trajectory frequencies, both performed with the NOAA HYSPLIT model, whose a description is reported in paragraph 4.2. Both the NOAA-HYSPLIT two-day backward trajectory (Figure 4.39 a) and the trajectory frequencies (Figure 4.39 b) confirmed that air masses collected January 26th at MCU station were coming from North Africa as early as January 24th, 2020 at 00:00 UTC. The NAAPS-based maps have been generated for January 26th, where an increase in the concentration of TGM occurred lasting for the following two days. The obtained NAAP simulation maps, providing the AOD (Figure 4.39 c) and the dust surface concentration (Figure 4.39 d) supported the evidence of the intrusion of air mass enriched with dust and their fallout on the ground surrounding the MCU station area.

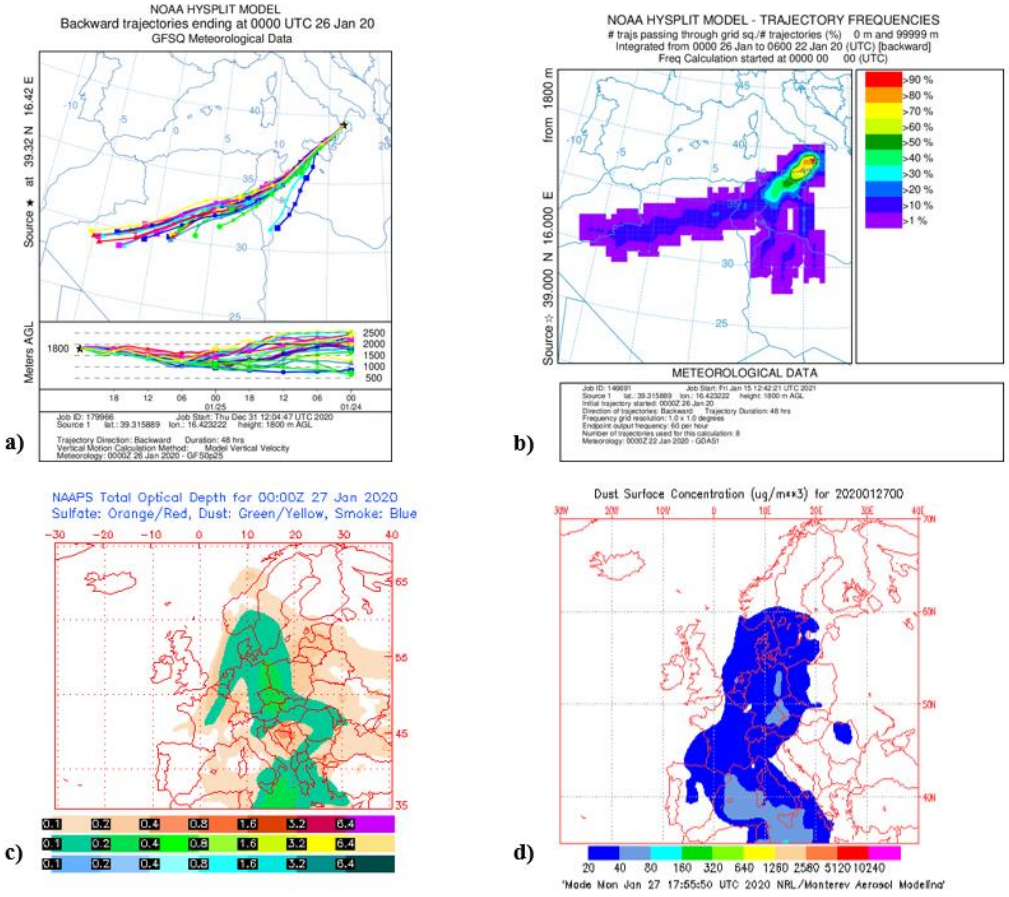

Figure 4.39 The charts refer to: a) the NOAA-HYSPLIT two-day backward trajectories for January 26th 2020; b) the NOAA-HYSPLIT trajectory frequencies for January 26th 2020; c) the NAAPS-based map with Aerosol Optical Depth for January 27th 2020; and d) the NAAPS-based map with Dust surface concentration for January 27th 2020.

4.5 Case study 3: Montelibretti

4.5.1 Sampling site description

The Montelibretti (MLI) sampling site 42°06'17"N 12°38'15"E; 48 m a.s.l.) is represented by a background station ("A. Liberti") located in a suburban area about 25 km northeast of Rome, in the Lazio region. The station is managed by the CNR-IIA and is located inside the CNR Research Area in a green area with trees and bushes, about 50 m from the nearest local road and 500 m from a busy road, thus not directly influenced by traffic but affected by local vehicular emissions and often impacted by pollutants transported from the metropolitan area [82]. The nearest town is Monterotondo that is located 5 km west [76,77]. Figure 4.40 shows the geographical location of the MLI which is one the Italian monitoring station that has been actively participating to the EMEP co-operative Programme for Monitoring and Evaluation of the Long-range Transmission of Air

Pollutants in Europe program since the beginning (around the 80s). Recently, it has been also established as a Master site within the Italian Special Network for Mercury, whose measurements programmes foresee at MLI the speciation of mercury in the atmosphere and the determination of mercury in both wet and total deposition.

Figure 4.40 Location of the Montelibretti sampling site.

For the purposes of this Ph.D. thesis, the ambient air sampling campaign carried out at MLI station for a period of five months, from October 16th, 2018 to February 28th, 2019, was considered. Although the observing sampling period was shorter, the aim of the research study was to investigate the average simultaneous trends of the atmospheric mercury species, GEM, GOM, and PBM, detected by the Tekran automated mercury integrated system, of which the MLI station, differently from the other case-studies already discussed, is equipped (see Figure 4.41).

Figure 4.41 Automated Tekran mercury speciation units (highlighted by the red circle) at MLI station.

4.5.2 Atmospheric sampling campaign and measurements of Hg species

At MLI station, a set of continuous speciated atmospheric Hg measurements have been performed using the conventional integrated system by Tekran, composed of the three units 2537X, 1130, and 1135 for the simultaneous collection and analysis of the different atmospheric Hg species, GEM, GOM, and PBM [67]. The integrated Tekran speciation system Tekran running at MLI has been configured to collect 2 hours GOM and PBM samples on a quartz KCl-coated annular denuder and quartz filter assembly, respectively, with a 1-hour desorption step, while GEM has been sampled and detected every 5 minutes, following the SOPs established and adopted within the GMOS network [58,65]. Consequently, different precautions were taken. To avoid passivation with time the KCl-coated denuder was replaced by a new one on a bi-weekly basis, to reduce the relative humidity influence an external heated boot was placed around the impactor, and an automatic calibration of the Tekran analyzer with a frequency of a 71 h was set, using the internal permeation source. Moreover, the Tekran 2537X instrument was calibrated just prior to the study using a Tekran model 2505 primary calibration unit. The flow rate was of 1 L min^{-1}, the detection limit for GEM was 0.1 ng m^{-3}. Local meteorological parameters such as air temperature (T), relative humidity (RH), wind speed (WS) and wind direction (WD) were continuously recorded during the whole campaign by the meteorological station (Davis Vantage Pro-2) of which is equipped the MLI station. The availability of

the meteorological parameters allowed to assess their influence on the concentration variation of the Hg species monitored during the campaign.

4.5.3 Hg speciation measurements on bi-hourly, daily, and monthly basis

All data collected at MLI station, both those regarding atmospheric mercury species and the meteorological ones, were processed for quality issues. All GEM, PBM and GOM measurement raw data resulting from the Tekran speciation units were firstly processed to check their quality, using the GMOS-Data Quality Management (G-DQM) system. The resulting valid dataset of GEM concentrations recorded at the MLI station with a sampling time resolution of 5 minutes (n= 15998) is showed in Figure 4.42. The whole observing period lasted from October 2018 to February 2019, during which some interruptions occurred, due to the operations of instrument calibration or maintenance, as well as the data invalidation resulting from the quality screening with the G-DQM system.

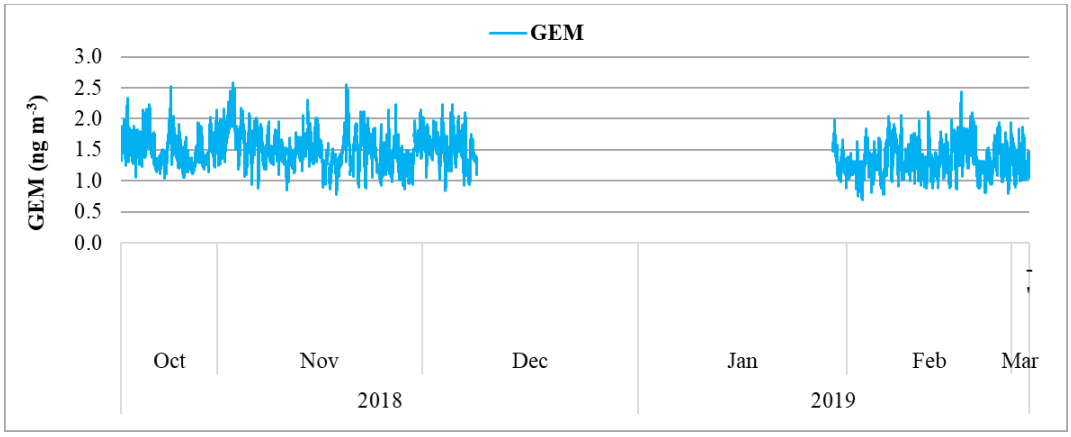

Figure 4.42 GEM concentrations recorded with a resolution of 5 minutes at the MLI station.

The dataset obtained for the study period, containing the valid GEM values with 5-minute resolution, has been then aggregated to hourly averaged GEM values (n= 84), whose trend is represented in Figure 4.43.

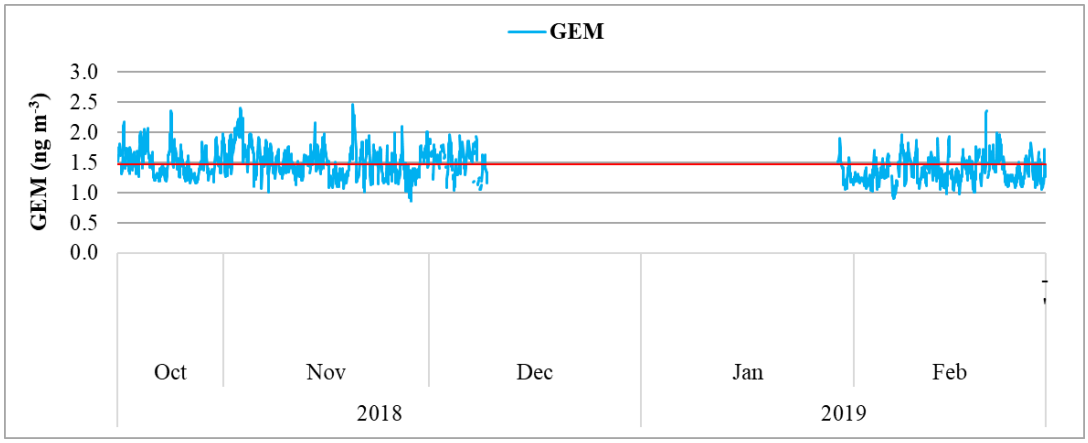

Figure 4.43 Hourly trend of GEM concentrations recorded at the MLI station. The solid red line indicates the hourly average value of the GEM concentration (1.47 ± 0.24 ng m^{-3}) recorded during the entire measurement campaign.

Being the MLI equipped with the integrated Tekran units, able to detect both the three atmospheric Hg species, for this case-study, besides the GEM concentrations measured with a 5-minute time resolution, GOM and PBM, with a two-hour sampling resolution have been additionally detected. In order to obtain comparable values of the different atmospheric Hg species detected at MLI station, the values of GEM concentration values have been averaged over the corresponding 2 hours, during which both GOM and PBM have been collected, as set in the configuration of the Tekran integrated system. Concurrent trends of GEM, GOM and PBM concentrations, referring to the same two-hour sampling period, for the whole measurement campaign, are those reported in Figure 4.44.

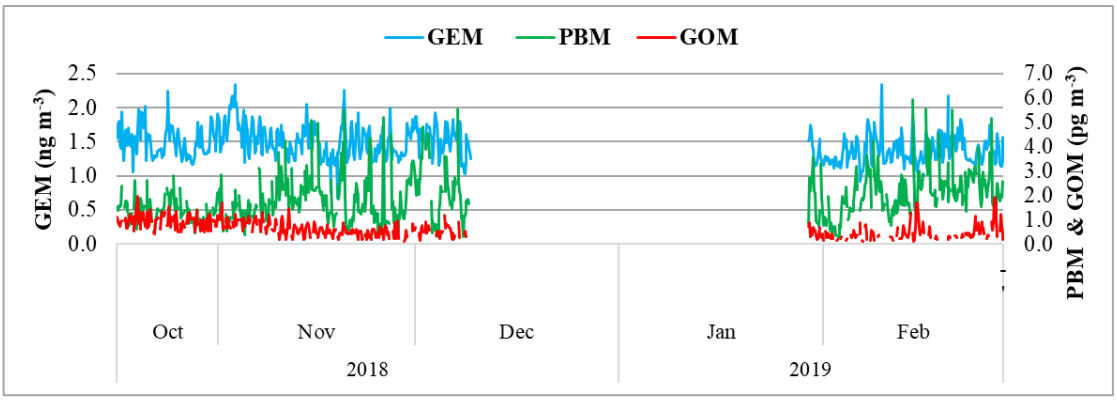

Figure 4.44 Concurrent trends of GEM, GOM and PBM concentrations referring to the same two-hour sampling period.

The hourly values have been aggregated in the daily-averaged concentrations, considered valid if the 75% of the corresponding hourly data were available (Figure 4.45). Consequently, 57 days of the measurement campaign carried out at the MLI station have been eliminated from the valid daily-based dataset. The daily averaged concentration values of GEM showed a variability ranging from 1.22 ng m^{-3} to 2.05 ng m^{-3}, with an average value of 1.47 ± 0.16 ng m^{-3} over the whole sampling campaign. Over the same period, the GOM average daily concentration was 0.60 ± 0.26 ng m^{-3}, with a range from 0.23 to 1.22 ng m^{-3}, while the PBM average daily value was 1.87 ± 0.67 ng m^{-3} with recorded values between 0.57 and 4.11 ng m^{-3}.

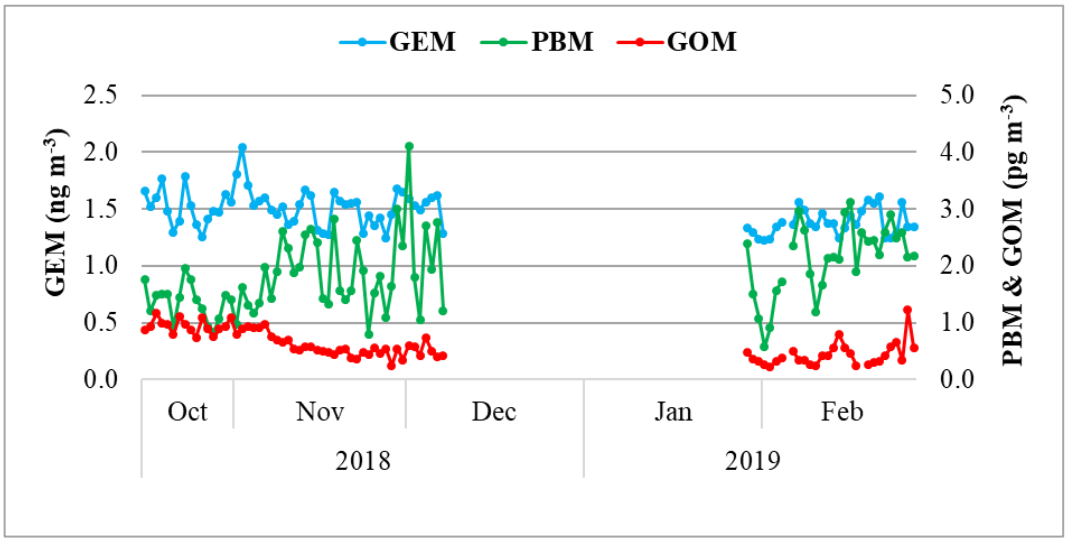

Figure 4.45 Daily averaged trends of GEM, GOM and PBM recorded at the MLI station.

Daily averages of GEM, GOM and PBM concentrations have been additionally converted to monthly averages, which were considered valid if determined by 66% of the daily data available. Consequently, two months (December 2018 and January 2019) were removed from the monthly-based dataset, because they did not result representative to compare and discuss the monthly variability of the Hg atmospheric species at MLI. Monthly-based Hg species measurements, representative of the sampling campaign at MLI, resulted to be those related to the months of October 2018, November 2018, and February 2019. The analysis of the variation of Hg species concentrations showed for October 2018 the average values of 1.51 ± 0.16 ng m^{-3}, 1.37 ± 0.33 pg m^{-3}, 0.93 ± 0.12 pg m^{-3}, for GEM, GOM, and PBM, respectively. With regards to November 2018, the monthly-averaged

concentration for GEM was 1.52 ± 0.17 ng m^{-3}, while for PBM and GOM the values were 1.79 ± 0.58 pg m^{-3} and 0.62 ± 0.21 pg m^{-3}, respectively. For February 2019, average values of 1.38 ± 0.12 ng m^{-3}, 2.13 ± 0.65 pg m^{-3}, 0.44 ± 0.21 pg m^{-3}, were recorded for GEM, PBM, and GOM, respectively (Table 4.8).

Months	**GEM**	**PBM**	**GOM**
	Average ± SD	Average ± SD	Average ± SD
	(ng m^{-3})	(pg m^{-3})	(pg m^{-3})
October 2018	1.51 ± 0.16	1.37 ± 0.33	0.93 ± 0.12
November 2018	1.52 ± 0.17	1.79 ± 0.58	0.62 ± 0.21
February 2019	1.38 ± 0.12	2.13 ± 0.65	0.44 ± 0.21

Table 4.8 Monthly-averaged concentrations of GEM, PBM and GOM recorded at MLI station.

Monthly variation of GEM, GOM and PBM was studied by means of One-Way Analysis of Variance (ANOVA). GEM showed a higher mean concentration during November 2018, and a lower one during February 2019 ($F = 6.30$; $p < 0.05$Referring to GOM, its levels were higher during February 2019 and lower in October 2018 ($F = 30.65$; $p < 0.05$). Otherwise, PBM levels were higher during October 2018, and lower during February 2019 ($F = 8.72$; $p < 0.05$).

4.5.4 Meteorological data analysis

Validated meteorological data of air temperature, relative humidity and wind speed recorded at MLI station during the whole measurement campaign, from October 2018 to February 2019, were aggregated into hourly data and plotted in Figure 4.46 in order to better analyze meteorological conditions at the investigated sampling site.

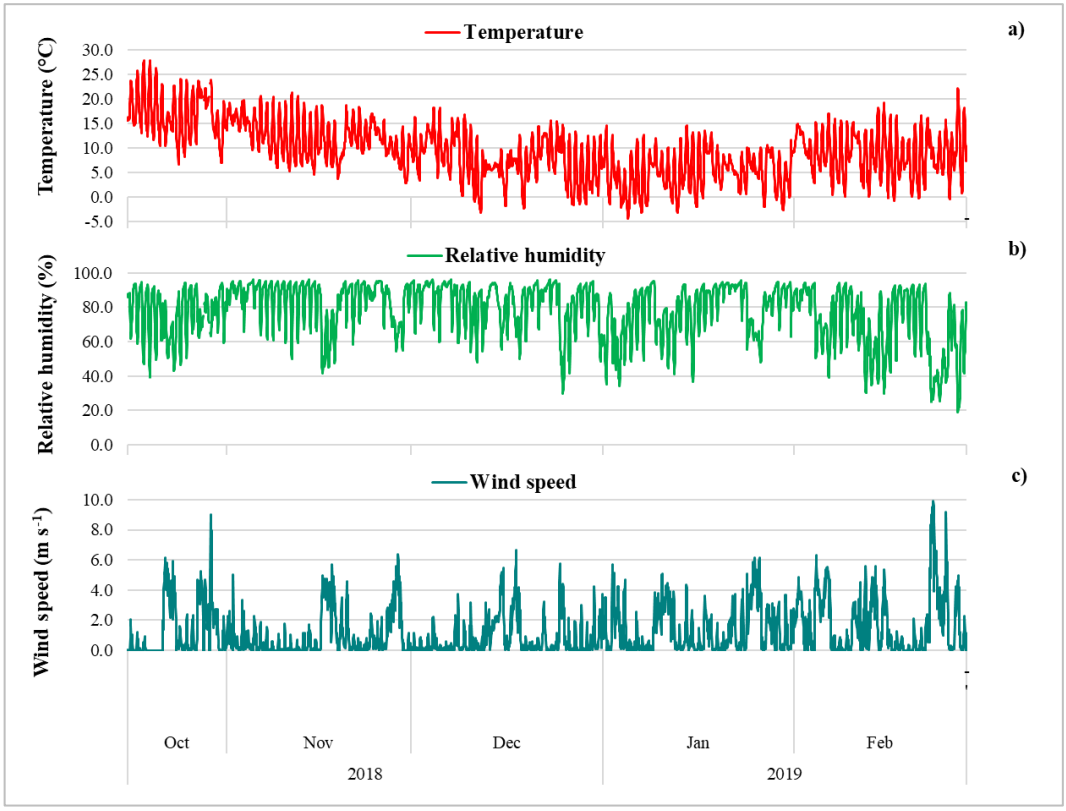

Figure 4.46 Hourly time series of a) air temperature (°C), b) relative humidity (%), and c) wind speed (m s^{-1}) recorded at the MLI station.

Local weather conditions were mainly characterized by an average hourly temperature value of 10.27 ± 6.23 °C, ranging between -4.46 and 27.83 °C, an average hourly relative humidity value of 77.31 ± 16.29%, ranging between 18.67 and 96.00% and an average hourly wind speed value of 1.21 ± 1.58 m s^{-1}, ranging between 0 and 9.93 m s^{-1} (Table 4.9). The correlation analysis between temperature and relative humidity showed a negative correlation (r = - 0.31) whereas a positive correlation was observed between temperature and wind speed (r = 0.17). Moreover, a negative correlation was observed between relative humidity and wind speed (r = - 0.57).

Meteorological parameters	Average ± SD	Range
Air temperature (°C)	10.27 ± 6.23	- 4.46 - 27.83
Relative Humidity (%)	77.31 ± 16.29	18.67 - 96.00
Wind speed (m s^{-1})	1.21 ± 1.58	0 - 9.93

Table 4.9 Descriptive statistics (average ± SD, range with min and max values) of air temperature, relative humidity, and wind speed recorded at the MLI station over the whole observing period - from October 2018 to February 2019.

Wind speed and wind direction, as well as air temperature available data have been used as input to perform the wind rose charts, which show how both the wind speed (Figure 4.47 – left panel) and air temperature (Figure 4.47 – right panel) varied, at the MLI station. Over the whole measurement campaign, from October 2018 to February 2019, the prevailing wind directions at MLI were found to be those from the south-south-westerlies (SSW) and the north-north-westerlies (NNW). This last direction also displayed a larger frequency associated with the higher wind speed values, above 6 m s^{-1}. Otherwise, the wind rose with the air temperature as function of the wind direction highlighted that the air masses associated with the higher temperatures (30 - 39 °C) came mainly from south-south-west (SSW).

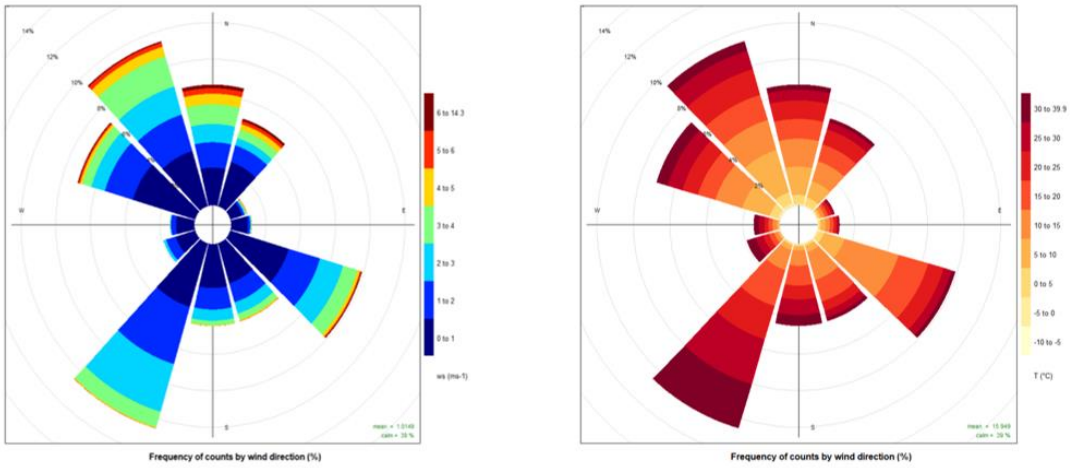

Figure 4.47 Wind roses showing wind direction as a function of wind speed (left-panel) and air temperature (right-panel) throughout the campaign at MLI station.

4.5.5 High GEM, GOM or PBM concentration events and identification of potential influencing sources at MLI

The observation of daily averaged trends of GEM, GOM and PBM (Figure 4.45), allowed to detect peak values for each of the three Hg atmospheric species recorded at MLI during the measurement campaign. In correspondence of these highest recorded values, a detailed analysis has been carried out and reported below, in order to identify the potential event that contributed to their increase. The interpretation of satellite maps, like those provided by NAAPS and MODIS tools as well as the analysis of air masses performed by the HYSPLIT modelling, which specifically allows visualizing the long-range transport of air masses and tracking the spatial sources, supported the daily characterization of the identified events. Therefore, the different GEM, GOM, and PBM peak concentrations have been attributed to plausible sources. In correspondence with the increase of the daily averaged GEM concentrations, recorded in the period between October and November 2018, an episode of Saharan dust occurred. The HYSPLIT model running with the ending date set at 00:00 UTC, of November 2nd, 2018, provided two-day backward trajectories represented as ensemble over the default HYSPLIT layout (Figure 4.48 a), even as ensemble but over the Google Earth map layer (Figure 4.48 b), and in terms of trajectory frequencies (Figure 4.48 c). From the obtained charts it was evident that the air masses intercepted in early November 2018 at MLI were coming from the North Africa (see Figure 4.48).

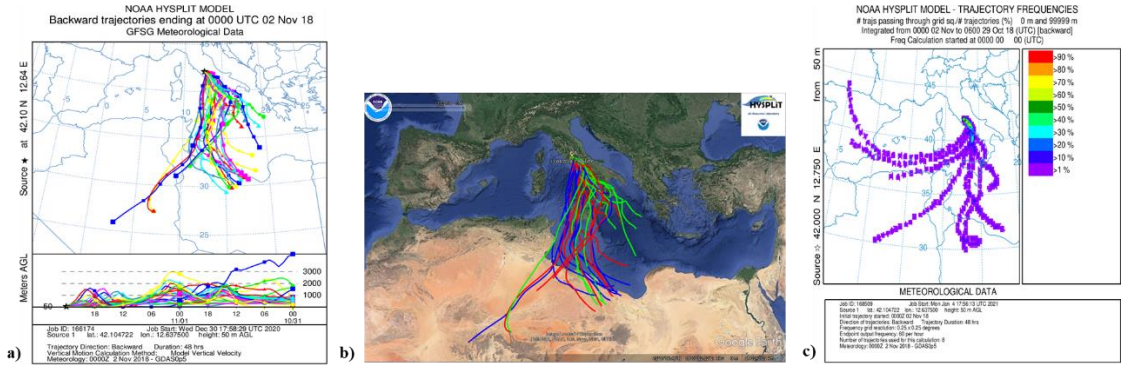

Figure 4.48 Two-day backward trajectories provided by the HYSPLIT model for the identification of a North African Saharan intrusion for the day November 2nd, 2018. The two-day backward trajectories are herein reported: a) as ensemble over the default HYSPLIT layout, b) even as ensemble but over the Google Earth map layer, and c) in terms of trajectory frequencies.

In conjunction with the above identified Saharan dust intrusion, a marked increase in the daily-averaged GEM concentration was observed, which on November 3rd 2018 reached the value of 2.05 ng m^{-3}, the highest GEM concentration recorded throughout the measurement campaign at MLI station (see Figure 4.45). The occurrence of this event and its temporal permanence over the considered sampling station, has been further supported by the NAAPS model, through which it was also identified the ending date of this event on November 4th 2018, at 00:00 UTC. In Figure 4.49 the Total Optical Depth and the Dust surface concentration, are reported for the day November 3rd, 2018.

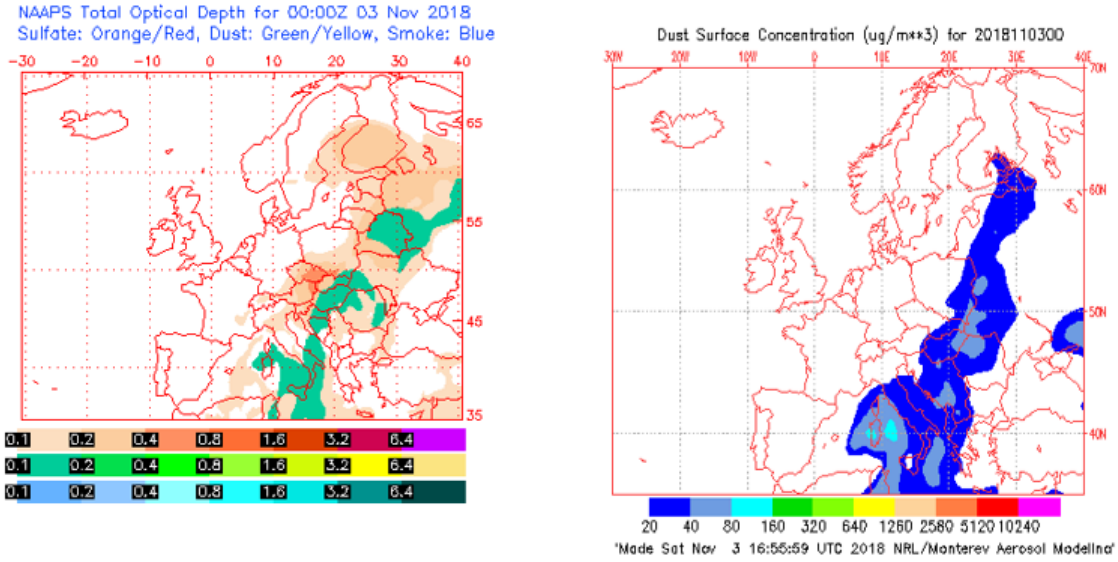

Figure 4.49 NAAPS-based maps showing the Total Optical Depth (left-panel), and dust surface concentration (right-panel) for the day November 3rd, 2018.

The specific wind conditions have been additionally investigated for the days affected by this Saharan dust event (1-5 November 2018). In particular, Figure 4.50 shows how the wind speed and the air temperature varied both as a function of the wind direction at the MLI station during the day November 2nd, 2018, confirming a prevalent wind direction from west-south-west.

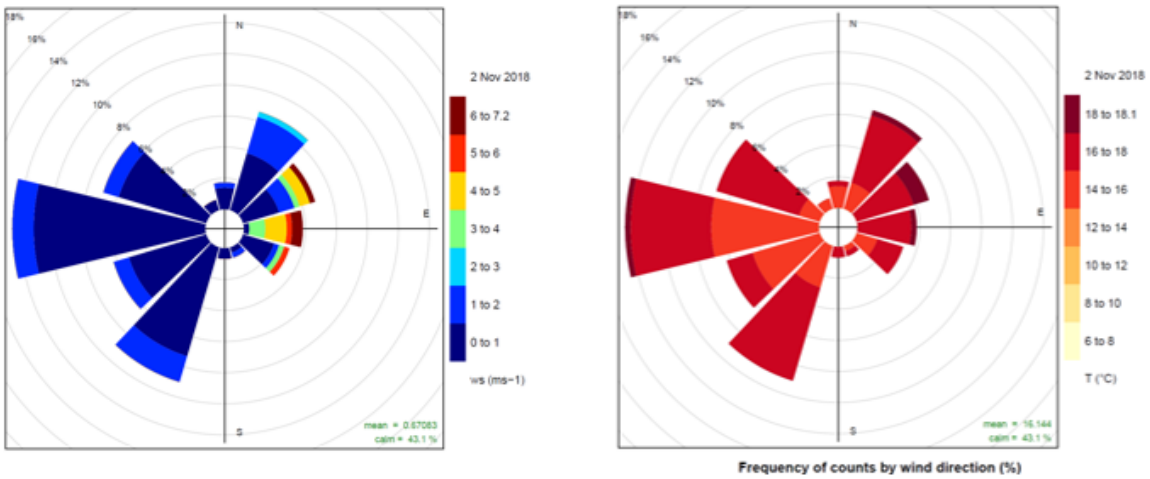

Figure 4.50 Wind roses showing the wind speed (left-panel) and the air temperature (right-panel), both as a function of the wind direction detected at MLI station for November 2nd, 2018.

Regarding GOM trend, its highest daily-averaged concentration recorded during the sampling campaign, with a peak value of about 1.22 pg m^{-3} has been recorded on 27th February 2019. To better characterize this event, the temperature, relative humidity, and wind speed recorded at MLI station from February 1st to March 5th have been considered for chart representation (see Figure 4.51). This figure highlights that, in respect to the reported period, on February 27th the higher hourly-averaged value of temperature (22.18 °C) and the lower hourly-average value of relative humidity (18.67%) were simultaneously recorded while the hourly-averaged value of wind speed was 3.63 m s^{-1}.

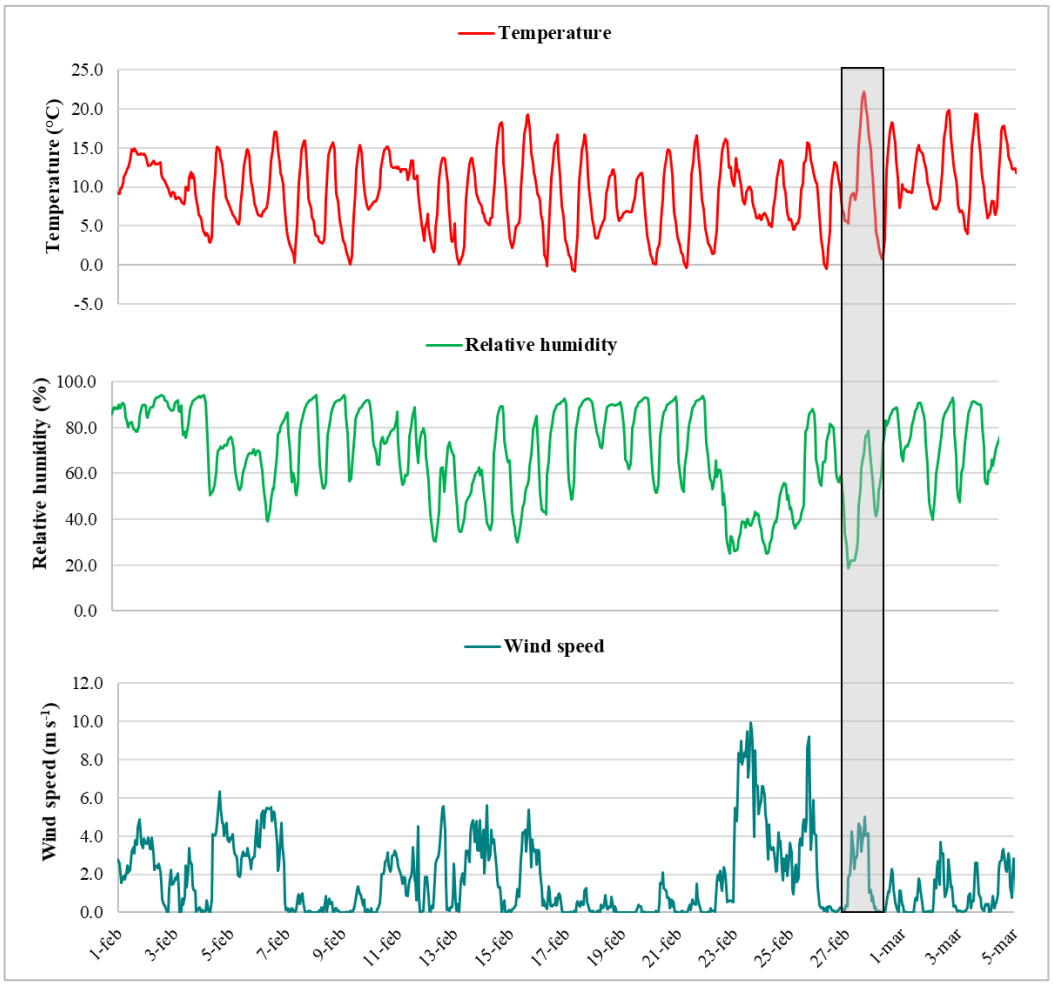

Figure 4.51 Hourly trends of temperature, relative humidity, and wind speed at the MLI station from February 1st to March 5th, 2019 with February 27th pointed out by the grey box.

Figure 4.52 shows how the wind speed and the air temperature varied at the MLI station both as a function of wind direction for the specific day of February 27th 2019.

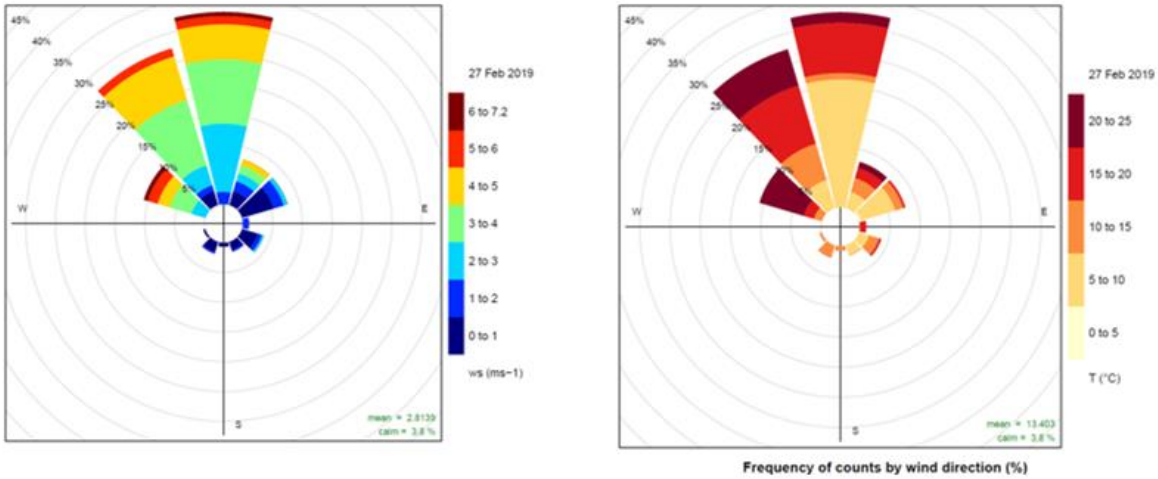

Figure 4.52 Wind roses showing wind speed (left-panel) and air temperature (right-panel) both as a function of the wind direction recorded at MLI station for February 27th 2019.

In particular, the wind rose chart showing air temperature as a function of wind direction (Figure 4.52-right panel) highlights that the air masses coming from North and North-West have a wide percentage of high temperatures, above 15 °C, despite the average temperature during the month of February was 8.91 °C. Furthermore, air masses specifically coming from the North-West direction exhibited a 5% percentage of data with temperatures between 20-25 °C, thus supporting the hypothesis for the probable occurrence of a fire. The verification analysis carried out with both NAAPS and MODIS maps, confirmed the fires event on February 27th, 2019, in the surrounding area of MLI (see Figure 4.53).

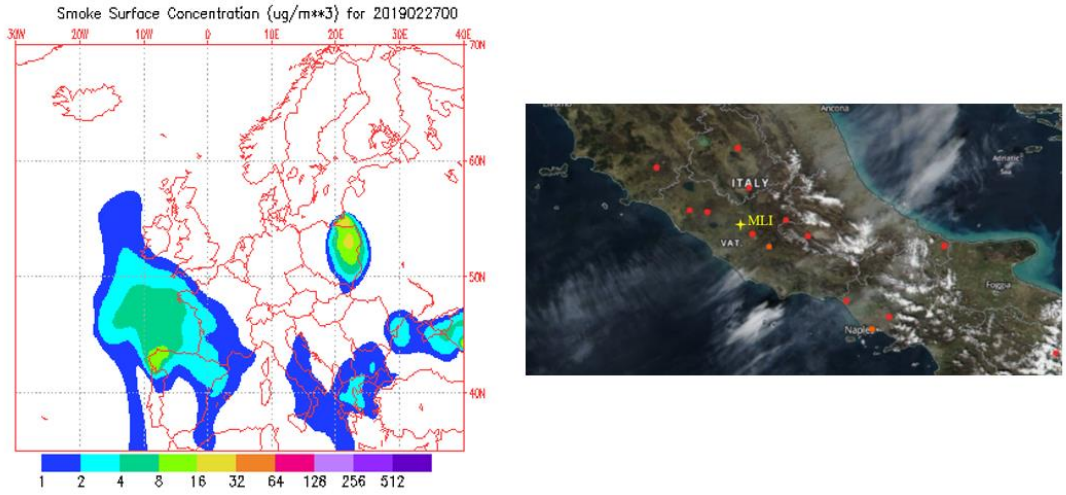

Figure 4.53 NAAPS-based map reporting the smoke surface concentration (left-panel) and MODIS map with hotspot fire detection (right-panel) for the day February 27th, 2019.

Regarding PBM, a peak about 4.11 pg m^{-3} was recorded on December 2nd, 2018, as daily averaged concentration value (see Figure 4.45). To investigate the potential influencing sources on this higher PBM levels recorded at MLI an analysis of the latest inventory of national Hg emissions, with provincial downscaling, drawn up in 2015 by ISPRA. The analysis of the provincial emissions, summarized for the macro-sectors in Table 4.10, revealed that in 2015, among the point Hg emissions source, the thermoelectric power plant located at Civitavecchia, about 80 km away from MLI, is one of the biggest contributing sources with well 94.88 kg of Hg. As confirmed by both the wind rose chart and the two-day backward trajectories reported in Figure 4.54, the correspondence of the wind direction observed at MLI blowing from NW and the interception of air masses passing across the Civitavecchia location before to be detected at MLI the day of December 2nd, 2018, could suggest this kind of anthropogenic over the observed higher PBM levels.

SNAP CODE	SECTOR	Kind of source	Hg emissions for 2015 [Kg]
01	Thermoelectric Power Plants	Puntual	97.229
02	Non industrial combustion	Diffusive	69.104
03	Productive Processes	Diffusive & Puntual	48.553
04	Waste treatment and landfills	Diffusive	0.012

Table 4.10 Hg emissions, divided by the main macro-sectors, for 2015 and for the province of Rome.

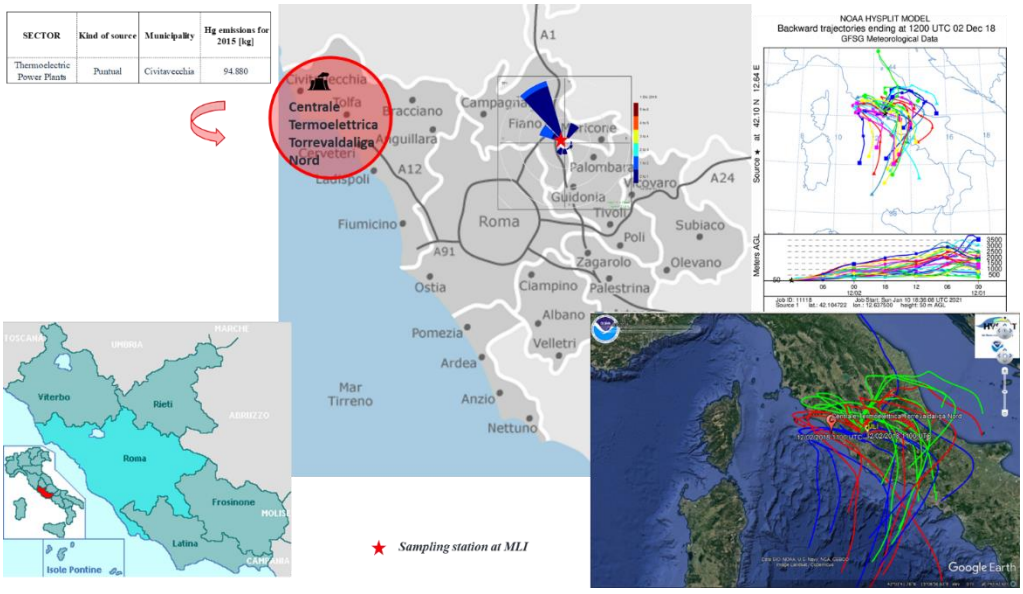

Figure 4.54 Power plant of Civitavecchia location with its Hg emissions estimates (ISPRA, 2015), the two-day backward trajectories and wind rose charts for the day of December 2nd, 2018, both overlapped to the map of the province of Rome.

4.6 Highlights from the in-situ campaigns by conventional methods and instrumentation

The work described in the case-studies reported in this chapter provides information on measurements of atmospheric mercury concentrations at background stations located in a rural/costal site as the MSA sampling station, in a rural site at high-elevation as the MCU mountain site, and in a suburban site as the MLI sampling station. The daily averaged TGM concentrations recorded over the available period of measurements are showed, for each site in Figure 4.55. Over the whole observing period, for each involved

stations, the daily averaged TGM concentration resulted to be equal to 1.72 ± 0.13 ng m^{-3}, 1.43 ± 0.13 ng m^{-3}, and 1.47 ± 0.16 ng m^{-3} at MSA, MCU and MLI stations, respectively.

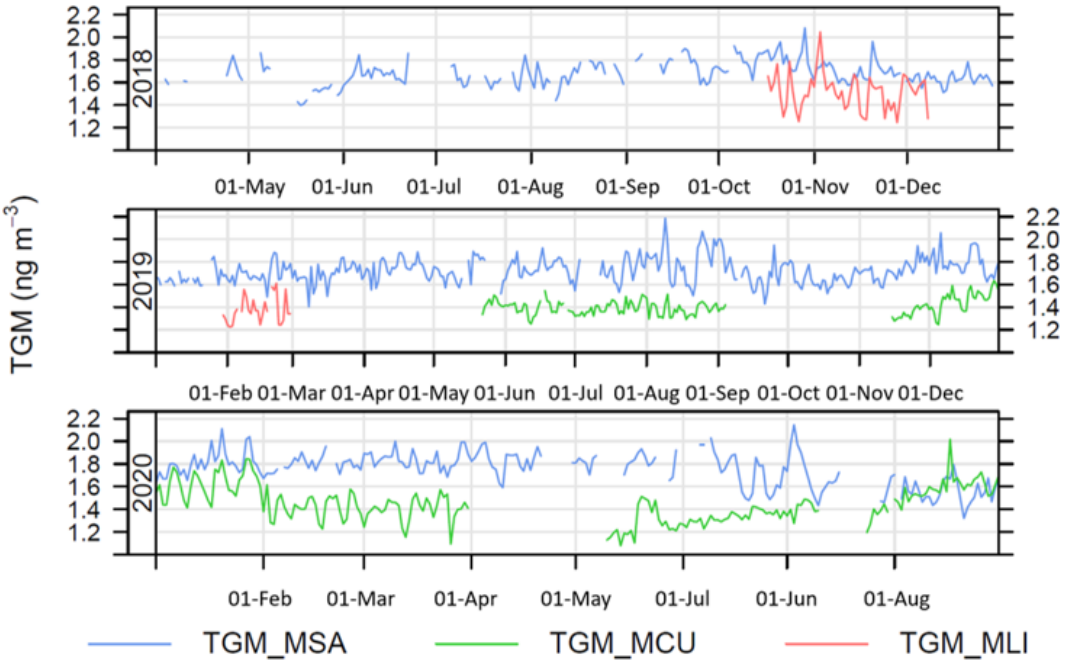

Figure 4.55 Comparison of the daily averaged TGM concentrations recorded at MSA, MCU and MLI stations, over the available measurement period.

At each monitoring site, the local meteorological parameters were also collected and examined to explore the variability of atmospheric mercury trends with respect to changes in meteorological conditions and additionally to support the discussion on the most likely Hg source and on the main Hg driving mechanisms. During the measurement campaigns, a series of events were identified in which the concentrations of atmospheric mercury increased compared to the seasonal average daily values. The study of the local and long-term atmospheric patterns, with their influences, supported by the NOAA-HYSPLIT model, for the calculation of the air masses backward trajectories, coupled with the use of satellite maps, like those provided by both NAAPS and MODIS tools, provided results that evidenced the relevant impact of Saharan dust intrusion and wildfire events over the Hg atmospheric measurements, with respect to their background levels recorded at the same stations. The investigation of the Hg emissions provided by ISPRA for the main Italian anthropogenic point sources, a detailed analysis of their location in respect to the sampling area, allowed to additionally identify their potential influence over the recorded atmospheric Hg concentrations.

In particular, it was interesting to note that at MSA and MLI sites the atmospheric mercury concentration levels were influenced by both natural and anthropogenic sources, whereas at MCU the mercury concentration levels were mainly influenced only by the natural ones.

Chapter 5

Innovative sampling and analytical methods for mercury monitoring

5.1 Introduction

The characteristics of conventional automated instrumentation employed for active monitoring of environmental mercury often limit the ability to monitor it on a global scale by narrowing their spatial range of use only to certain areas such as those having electricity sources, easily accessible sites, or regions where it is possible to bear the maintenance costs [85]. In fact, over the years it has been demonstrated how the use in the field of active automated air samplers is not always easy and where possible is subject to a compromise between costs and needs. In addition to their high purchase cost, which prevent their use in simultaneous large-scale monitoring studies, conventional instruments present others disadvantages such as bulky dimensions, transport and installation on difficult to access sites, constant need of external electrical power supply and gas cylinders, mechanical pumps for ambient air aspiration, appropriate operating temperature and professional maintenance by well-trained operators [72,73,74]. Consequently, although their measurements in near real time guarantees a relatively fine temporal resolution of Hg concentrations, all the described characteristics limit the range of global data on atmospheric mercury concentrations available to the scientific research community to understand important characteristics of mercury biogeochemical cycle [25]. Over time, the need for improvement and spatial expansion of monitoring studies, even in remote areas, has directed the scientific community towards the development of innovative monitoring techniques for quantification of environmental mercury. In this context, passive sampling has been proposed as an interesting alternative that can also enhance existing active monitoring techniques to fill the lacking spots on mercury monitoring in the world. This need for improvement and for easy to use, low maintenance and low-cost sampling equipment has been particularly felt in the context of atmospheric mercury monitoring, given the importance that the atmosphere and atmospheric processes exert on mercury and on its global distribution [3,12]. The following sections list the advantages of innovative passive sampling techniques and the different types of passive air samplers developed to date, for the determination of total gaseous mercury in the

atmosphere, whose results obtained during an international inter-comparison sampling campaign, are presented and discussed in this thesis.

5.2 Innovative techniques for the determination of mercury in air

To date, as regards the monitoring of environmental pollutants such as mercury, passive sampling is one of the main research areas. In addition to the conventional methods based on active sampling, innovative methods are currently reported in literature. These new devices do not require the use of electricity or mechanical pumps and show numerous advantages that allow to face many problems in the Hg atmospheric monitoring. Although the conventional instruments for active atmospheric mercury monitoring provide continuous concentration data with a fine temporal resolution, in many cases their use limits the spatial resolution of the measurements. In fact, instrument requirements and technical features do not always allow to gain an adequate spatial resolution also extended to areas in the world far from sources of emissions or difficult to reach, such as high altitude sites, Polar Regions and remote islands [85].

5.3 Passive Air Samplers (PASs)

Passive Air Samplers (PASs) for mercury are innovative sampling devices developed in response to the limitations of conventional instrumentation and to the necessity of expanding the knowledge on long-range transport of mercury, to have available monitoring data from remote areas and to support the implementation of the Minamata Convention. Generally, PASs are compact and portable devices, and smaller than those of conventional instrumentation, so that they can be easily handled, transported, and installed in situ. Furthermore, PASs do not require external power supply (a limiting factor in many areas for active instruments), gas cylinders and mechanical pumps for working and, therefore, they are silent sampling devices suitable for monitoring studies both indoors and outdoors [88]. Moreover, PAS samplers can be deployed in different positions without requiring continuous and expert installation, supervision, and maintenance by the operators. The advantages over conventional instrumentation allow to overcome the lacks shown by the active sampling technique and to integrate existing monitoring approaches [24,74,76]. The properties of the PASs make passive sampling more appropriate and suitable for screening studies and for the monitoring of long-term

mercury concentrations, as well as in background sites, even in dangerous and extreme environments, such as wild and remote areas. Compared to automated analyzers, which are usually positioned in a single point of a specific area, PAS samplers are suitable for determining the spatial distribution of gaseous pollutants over large areas. In fact, many passive devices can be distributed or positioned simultaneously over various interesting points of a given area, improving the coverage especially of large areas, and thus the spatial resolution of mercury concentrations data, allowing a simultaneous spatial mapping of mercury concentration on regional and global scale, and thus complementing conventional active measurement approaches [85]. Therefore, passive sampling for atmospheric mercury measurements represents a cheaper and simpler alternative with respect to active samplers in monitoring plans requiring large-scale concentration estimates also in remote areas, do not requiring well-trained instrument operators, requiring estimates of the more spatially representative global mercury distributions, providing for information over the collection of samples for long periods of time. In fact, passive sampling allows a coarser temporal resolution than the active one, and quantifies the cumulative exposure to atmospheric mercury as total or average concentration over longer exposure periods [89]. For this reason, PASs provide time-averaged concentration of gaseous mercury over the time scale of weeks to months, also based on the requests of the monitoring study and the type of evaluation to be performed. During prolonged periods of exposure, and until the PASs are removed from their sampling site, it is not necessary to revisit the site, but it is important that the absorption capacity of Hg is ensured. For this purpose, knowing the characteristics device specifications is essential. The PASs operating principle is based on the collection of a gaseous pollutant on an absorbent surface by diffusion processes, which are regulated by the first Fick's Law [86]:

$$SR = \frac{DA}{L} = \frac{m}{tC}$$

where *SR* represents the sampling rate, which quantifies the volume of air that is effectively stripped of target compound per unit time; *D* is the molecular diffusion coefficient of the target compound in air; *A* represents the collection surface area; *L* is the thickness of the diffusion layer; *m* represents the mass of sorbed compound; *t* is the deployment time; and *C* represents the ambient concentration of the target pollutant. The

theoretical calculation of the sampling frequency of a passive sampler for a specific compound consists of the product of the molecular diffusion coefficient (which is detailed for each compound in a specific medium, as it is determined by its chemical and physical properties), and the geometry of the sampling device, represented by the parameter A/L. The equation shows that the rate with which the target compound migrates on a collection surface increases with increasing area and decreasing diffusive path length [90]. By quantifying the mass absorbed during exposure for a certain period, at a known concentration of the considered pollutant, the equation allows to experimentally determine the speed with which the chemical spreads through the passive sampler. Before the PASs can be used in the field, a calibration procedure is necessary to obtain the SR value of the sampler.

Passive air samplers for mercury monitoring collect the gaseous mercury without involving the active movement of air through it. They are based on the use of an absorbent material or collection surface (Figure 5.1)

that has a high affinity for the target compound, thus creating a concentration gradient responsible for spreading the target pollutant from a certain volume of stagnant air to the material itself, while turbulence is reduced. In this case, depending on the type of material, the target compound is the mercury species present in the air being the sum of all the gaseous compounds (TGM) or exclusively Hg^0 (GEM), while the particulate mercury difficultly crosses the barrier of diffusion and is therefore excluded.

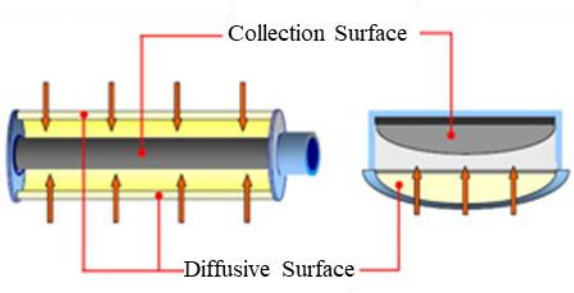

Figure 5.1 Schematic representation of passive air samplers (adapted from [91]).

At the end of the deployed period to ambient air, the samplers are removed from the exposition sites and are disassembled into their various components to analyze their collection surface. Given the advantages previously listed, the collection and potential shipment to specialized laboratories for analysis can also be easily performed. The

analysis of the collection surface allows to quantify the sorbed mercury mass, which is then elaborated using the first Fick's Law to calculate the time-averaged mercury concentration in ambient air at the selected measurement site. The greater data spatial resolution favoured by the mapping of the areas of interest with the distributions of passive samplers with high spatial density, could also facilitate the identification and characterization of known and unknown sources of mercury. Active sampling, performed with a single measuring instrument, often does not easily allow the distinction of specific emission sources and the attribution of concentration variability to temporal or spatial factors. For example, in recent years, PASs have also found wide application as a tool for assessing air quality in urbanized areas. Although the reliability and accuracy of passive samplers have been questioned in the past, current studies identify them as a viable option and an effective alternative to conventional active samplers in exposure and health effects studies, highlighting that they can provide comparable performance in terms of sensitivity and reproducibility to active samplers [88]. The analysis techniques of PASs can vary according to the type of passive sampler and its sorbent material. The most common techniques are thermal desorption and extraction. Thermal desorption consists in heating the sorbent material and in the consequent release of the target compound, which will be then quantified. This technique does not alter the sorbent material, which keeps unaltered and can be also regenerated and reused. On the other hand, extraction allows the target compound to be separated from the collection surface by adding solvent or acid, destroying the sorbent material, which consequently cannot be regenerated and must be replaced. The analysis phase is followed by the subsequent quantification phase of the target compound, which can be performed using common analytical approaches such as CVAAS or CVAFS [86]. Some analyzers available on commerce, such as Nippon MA3000 (Nippon Instruments Co.) and DMA-80 (Milestone), work with thermal desorption and subsequent quantification of the Hg sorbed onto the collection surface. In addition to these analyzers, some research groups, have been able to design and realize their own passive devices, but also to define their laboratory analysis system, which was then implemented in conventional mercury analyzers. For instance, the researchers from the Institute of Atmospheric Pollution of the National Research Council (CNR-IIA), for the desorption and quantification of the mass of mercury absorbed by the absorbent surface of their own PASs have developed a laboratory system implemented in a

conventional mercury analyzer. Such a system consists of a refractory material lab-made furnace capable to reach 550 °C for promoting mercury desorption from the passive membrane, contained into a cylindrical gas chamber and connected to the CVAFS analyzer Tekran 2537. Moreover, several studies were carried out aimed at developing new low-cost passive mercury samplers characterized by different geometry and composition of sorbent material. As a result, various types of PASs for mercury are commercially available, which usually consist of a placed adsorbent material inside a container protected by a membrane on a discoid geometry or column geometry surrounded by a cylindrical diffusive barrier. Further studies are aimed at testing the effectiveness of these sampling devices on a global scale to meet the obligations of the Minamata Convention on mercury.

The following section describes, specifically, the types of PASs for mercury used in an inter-comparison study object of this thesis, and described in the next chapter. These devices are characterized by different geometry and composition of sorbent material, but they all based on the use of a solid trapping material with a high affinity for mercury [73,74,77].

5.4 CNR-PAS

The passive air sampler for gaseous elemental mercury proposed by the researchers of the National Research Council of Italy – Institute of Atmospheric Pollution Research CNR-IIA (CNR-PAS) was developed in the framework of the Global Environment Facility (GEF)-funded UNEP project "Development of a Plan for Global Monitoring of Human Exposure to and Environmental Concentrations of Mercury", at the end of 2014. The aim of the project was to harmonize the approaches and to strengthen the analytical ability, at a global level, for the accurate monitoring of the mercury concentrations, both in the ambient air and in the human biological components. In this regard, in order to develop a global Mercury Monitoring Plan for the implementation of the International Convention of Minamata on Mercury, the project was agreed by the Chemicals and Health Branch of the United Nations Environment Programme (UN Environment), in collaboration with the CNR-IIA and the World Health Organization – European Centre for Environment and Health (WHO – ECEH), involved in mercury monitoring in ambient air and biological compartments, respectively. The CNR-PAS developed in this context

is an axial passive sampler for gaseous elemental mercury (axial diffusion badge), designed exploiting the nanostructured pattern of a sorbent surface for the unassisted collection of atmospheric mercury [90]. The initial prototype of this passive sampler consisted of a sorbent membrane that through a locking ring was maintained on the bottom of a borosilicate glass vessel, which was sealed by a cap. For the exposure to ambient air, the cap had to be replaced with a perforated cap equipped with a diffusive membrane consisting of an anti-convection micro-porous nylon screen, useful for gas diffusion, particulate stopping and sorbent layer preserving. The sorbent material was made up of densely packed titania nanoparticles ($TiO_2 \leq 25$ nm diameter) including smaller gold nanoparticles (AuNPs). For the realization of this sorbent material the photocatalytic properties of the titania-anatase have been exploited; it is able to reduce $HAuCl_4$ into elemental gold under ultraviolet irradiation (UVR) and in the presence of polyvinylpyrrolidone (PVP) as capping reagent. Titanium (IV) oxide nanoparticles, commercially available in the anatase phase were suspended into an aqueous solution of PVP/$HAuCl_4$ (0.1 M PVP, 0.5 mg mL^{-1} $HAuCl_4$), which was irradiated with UV light for 1 hour. At this point, the yellow-coloured aqueous suspension of TiO_2NPs, containing $HAuCl_4$ and PVP under UV-light irradiation, turned into a blue-purple colour, by highlighting the formation of gold nanoparticles. The functionalization step of the TiO_2NPs was checked by UV-Vis spectrophotometry (UV-Spectrometer Shimadzu 2600). The product obtained was centrifuged and rinsed with ultrapure water to remove PVP excess and the resulting precipitate was vortexed, diluted with ultrapure water and subsequently deposited on thin quartz slices by drop casting. About 10 mg of sorbent material were deposited on each quartz substrate (sorbent carrier). To remove any traces of polymer and mercury eventually collected during the preparation phase, the membrane was heated first to 80 °C and then to 450 °C under clean airflow. Scanning Transmission Electron Microscopy (STEM), High-Resolution Transmission Electron Microscopy (HR-TEM), Atomic Force Microscopy (AFM), and Optical Microscopy (OM) were the different techniques used for the morphological study of the sorbent material, which presented a homogeneous distribution of the nanoparticles with size ranging between 5 to 40 nm, centered around the mean value of 32.6 nm [90].

Regarding the environmental deployment, to allow the axial diffusion from the diffusive nylon membrane (diffusive barrier) to the sorbent surface, CNR passive devices have to

be deployed with the passive membrane facing downward. Moreover, during each sampling period they have to be hooked to a housing shelter developed by CNR-IIA laboratories. At the end of the sampling period, the chemical analysis of the passive membrane allows to determine the average concentration of sorbed mercury during deployment time to ambient conditions. As previously mentioned, in addition to the passive samplers, the CNR-IIA has also designed and built a thermal desorption system to quantify Hg collected by their own PASs, consisting of a quartz cylindrical housing (Spaziani, Italy) for the sorbent membrane, placed in a heater furnace (De Marco, Italy) for thermal desorption (Figure 5.2) and connected to a common analytical system for mercury detection by CVAFS, as the mercury vapor analyzer Tekran 2537A (Figure 5.3).

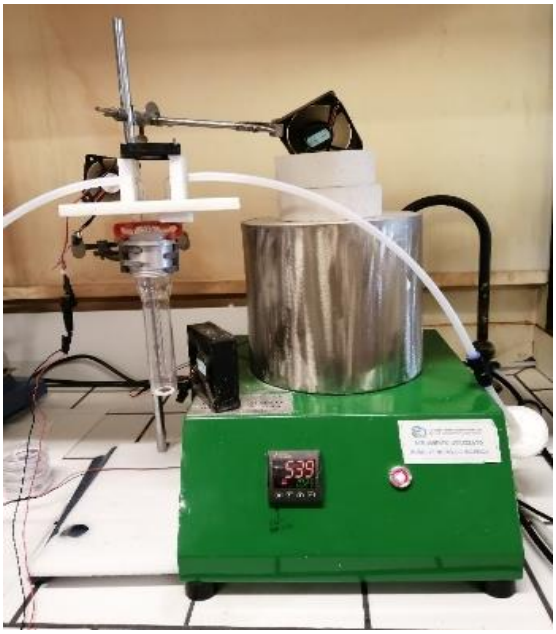

Figure 5.2 The quartz cylindrical housing for the sorbent membrane and the furnace for thermal desorption.

The sorbent membrane contained into the passive sampler is taken out of the glass vessel and placed into the quartz cylindrical housing heated to 550 °C into the furnace for the desorption of the trapped Hg. Successively, the mercury vapor contained into the air stream is quantified by CVAFS in the Tekran analyzer. This system, instead of the argon carrier customarily required by the analyser Tekran 2537, exploits filtered ambient air to flow the desorbed Hg vapors from sorbent membrane to the mercury analyser [90]. Once the passive membrane analysis phase has been completed, all the components of the

passive device can be reused, including the collection surface (sorbent material), supporting their lower production cost and reduced production of environmental waste. To be returned as blank, the passive membrane requires two or three 5-minute cycles of the analyzer. At the end it can be reassembled in a clean glass vessel and reused for another environmental exposure. Using CNR-PAS loaded with a known Hg concentration the method accuracy of the lab-made analytical system was periodically verified and the Tekran system calibrated by automatic and manual procedures.

Figure 5.3 Thermal desorption system for the analysis of CNR-PASs.

The sorbent material of CNR-PAS was tested during different field campaign exercises in various sites of the GMOS network and showed very good performances for mercury collection, given the strong affinity of mercury with gold, the high adsorption capacity resulting from the nanostructured model of the absorbent layer, and the reusability of the entire passive device after desorption analysis. The calibration phase of the PASs must be carried out before performing the field-testing of the passive devices, to be able to calibrate them and determine an experimental value of the sampling frequency, SR, which represents the volume of air that is effectively stripped of mercury. The calibration of the CNR-PAS was carried out using a quartz chamber (Figure 5.4), suitable for containing passive air samplers, where increasing quantities of mercury vapors were injected under dry air, taken from the Tekran 2505 Primary Calibration Source using a gas-tight syringe. A Tekran analyser model 2537 was connected to the quartz chamber to continuously measure the concentration of mercury inside the chamber, during the execution of the various tests that were carried out at different deployment times. The results of the

analysis of the tested PAS sorbent membranes were elaborated using the first Fick's Law, and the SR value of 0.0147 ± 0.0007 m^3 day^{-1} was obtained as an average experimental at 20 °C [90]. Furthermore, to determine the effect of meteorological conditions, such as ambient temperature and relative humidity on the sampling rate, additional laboratory tests were carried out through which the passive membrane adsorption was studied, at different concentrations of Hg^0 vapor, by exposing the membrane to the pollutant for 15 minutes. The temperature values, which were ranged between -20 and 60 °C were obtained by placing the measuring chamber into a refrigerator and a thermal bath. A mass flow controller was used to control and generate relative humidity changes, by flowing dry air and increasing the concentrations of water vapors inside the measuring chamber. The relative humidity was investigated in the range of 0 – 70%. The results obtained by these experiments were + 0.1% per Celsius degree, as regards the temperature, and + 0.06% per % of RH unit, as regards the relative humidity. Therefore, temperature and relative humidity only showed minor effects. Nevertheless, further laboratory tests are needed to investigate the effect of wind speed on the sampling frequency of the gaseous mercury and to obtain a more thorough calibration of these passive devices.

Figure 5.4 Quartz chamber for the controlled exposure of CNR-PASs during calibration.

5.4.1 Improvements of CNR-PAS over time

Over the years, although the comparison among CNR-PASs and conventional instruments gave acceptable results during several field exercises, in various sites of the GMOS network, this innovative prototype has undergone changes to improve its performance in the field. These changes were made starting from the production phase to

the exposure phase, to avoid problems with sampler contamination and mercury losses from the sampler cap. In particular, to reduce the potential contamination during the opening and replacement of the cap and, thus, to ensure that the membrane never comes into contact with the surrounding air, a double cap system was introduced. This cap system consists of a bottom cap, containing the diffusive membrane always screwed to the glass vessel, and a top cap, which in turn is screwed to the bottom one only when the passive sampler is not deployed to ambient air (Figure 5.5).

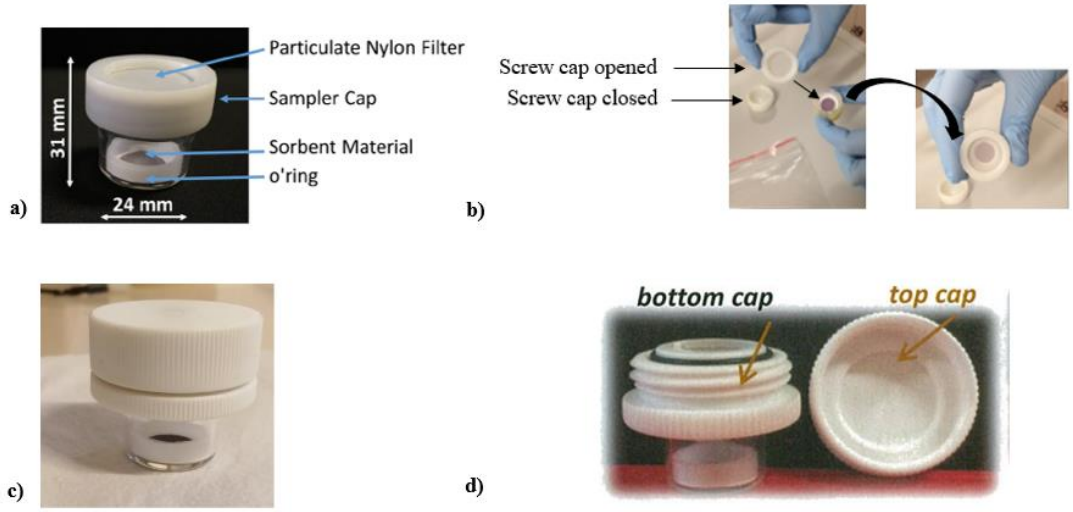

Figure 5.5 a) Passive air sampler structure before improvements, ready for deployment (with screw cap opened in the middle); b) screw cap opened in the middle used during the sampling time and screw cap closed of the sampler device, employed before and after the sampling period; c) passive air sampler structure after improvements; d) double cap system with a bottom cap that contains the diffusive membrane always screwed to the glass vessel, and an top cap that in turn is screwed to the bottom one only when the passive sampler is not deployed to ambient air.

Moreover, to make the entire passive sampler air-tight, two O-rings were added. The first one was placed between the glass vessel and the bottom cap, while the second one was placed between the two caps of passive sampler (Figure 5.6).

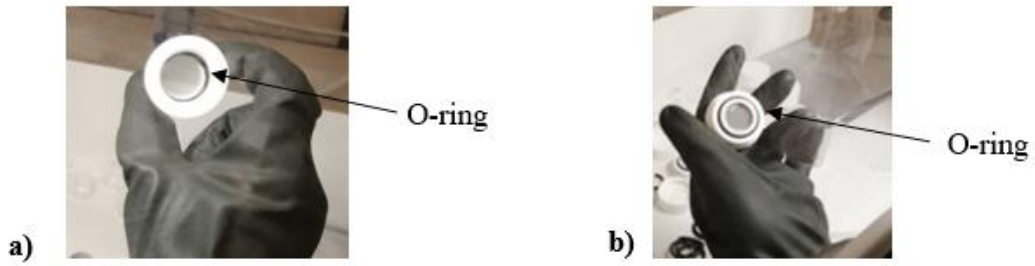

Figure 5.6 a) O-ring between the glass vessel and the bottom cap; b) O-ring between the bottom and the caps.

A new strategy for the storage of the samplers has also been planned and applied to avoid contamination problems. In fact, instead of the previous plastic bags used for PASs storage, the new approach has provided the use of heat- and zip-sealed aluminium bags containing a lab-made cartridge realized perforating a common laboratory sample-holder and placing a passive membrane inside. This cartridge acts as a scrubber to collect any traces of mercury present in the aluminium bag (Figure 5.7).

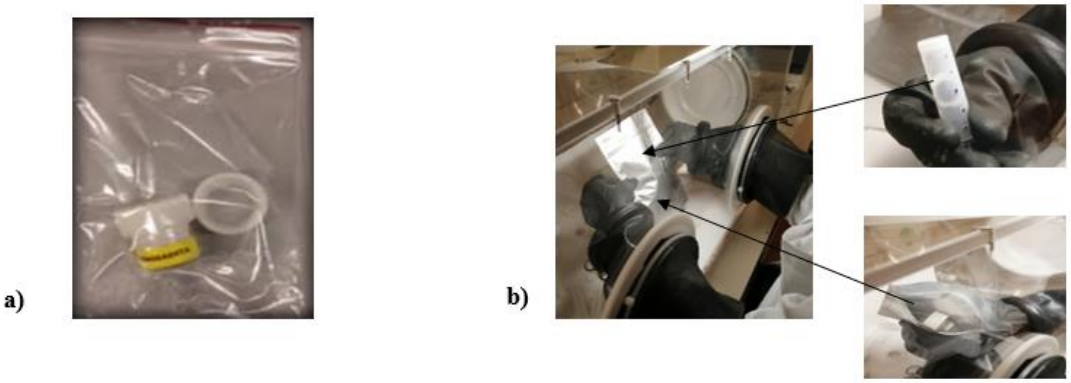

Figure 5.7 a) Plastic bag; b) Aluminium bag containing a lab-made cartridge and a passive sampler.

As regard the deployment of the passive devices to ambient air, the metallic material of shelter circular top structure housing PASs was replaced by a non-conducting material such as High-Density Polypropylene (HDPP), to protect the samplers from solar radiation during sampling phase. Moreover, a HDPP bell has been added to the circular top structure, surrounding the passive samplers to protect them from atmospheric agents, as wind and rain. The lab-made shelter is consisted of eight seats used for the deployment passive devices. As well as all components of the CNR-PAS, also the shelter is reusable (Figure 5.8).

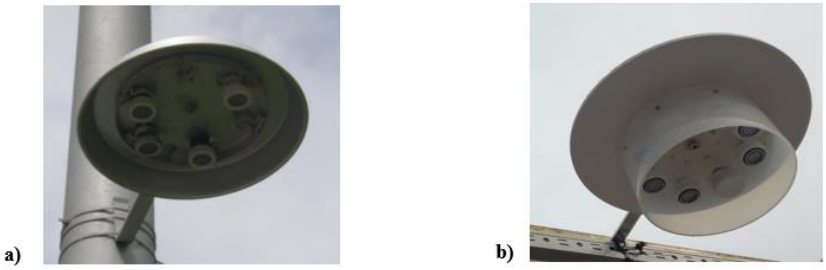

Figure 5.8 Shelter housing for the environmental deployment of CNR-PASs, a) metal structure and b) HDPP structure after improvements.

Further improvements concerned the reassembly phase of the PASs. In fact, each passive sampler was disassembled into its various components, which were cleaned by using diluted $HClO_4$ (used as an oxidizer) and ultrapure water, except for the absorbent layer. The subsequent assembly of these parts into new sampling devices ready to be reused was carried out in a glove box to avoid contamination after the cleaning phase (Figure 5.9).

Figure 5.9 Glove box for assembling phase of CNR-PASs.

The current version of the passive sampler and the shelter for outdoor exposure were both tested in the field, through an inter-comparison campaign aimed at evaluating the PAS analytical performance monitoring sites which are described in the next chapter. The passive membrane is the same as that present in the initial passive prototype and consists of the fibrous quartz filter as sorbent carrier, coated with the sorbent material made of densely packed nanoparticles of TiO_2 finely functionalized with smaller gold nanoparticles (AuNPs). It is placed on the bottom of a borosilicate glass vessel through a locking ring and the glass vessel is sealed by a double cap system, to minimize the operator handling and avoid contamination due to the cap opening. Overall, samplers are 3.1 cm height and with a diameter of 2.4 cm (w/o the cap), while the effective diffusion path length is 2.8 cm with an area of 3.1 cm^2 [90].

5.5 IVL-PAS

The passive air sampler for gaseous mercury created by the Swedish Environmental Research Institute IVL (IVL-PAS) was developed within the EU project, Global Mercury Observation System GMOS. It consists of a sorbent carrier, made of cellulose (Whatman)

filters coated with a sorbent material, made of activated carbon impregnated with iodine solution (75 µl 0.1%) that is inserted in a badge-type device, which makes it an axial diffusion badge. At one end of this badge, an open cap contained an anti-convection steel mesh net (FALP membrane) is fitted, which allows the diffusion of gases and acts as mechanical protection, while at the other end a solid cap is fitted (Figure 5.10). Samplers are 1.2 cm height with a diameter of 2.5 cm, while the effective diffusion path length is 1.15 cm, with an area of 4.9 cm^2 [91].

Figure 5.10 The Badge type IVL-PAS [91].

During non-exposure phase and shipment, each sampler is stored in a plastic tube, which in turn is placed in a plastic bag to avoid contamination. In addition, IVL laboratories also developed the holder-protective metallic shields, which consist of a top metallic disc, no side shield, with four seats where passive devices are positioned during the period of exposure to ambient air, to be protected from atmospheric agents (Figure 5.11). This passive sampler holder-protective shield is reusable. Determination of mercury concentration in the IVL-PASs is performed by wet-digestion with chemical reduction, gas-liquid separation, and gold amalgamation with CVAFS detection; therefore, the sorbent material and the sorbent carrier are not reusable. In detail, the carbon filters are carefully removed from each sampler and individually boiled in an acid solution (HNO_3/H_2SO_4) for 5 – 6 hours. BrCl is added to the cold solution as an oxidant and subsequent reduction is performed, by adding $SnCl_2$ prior to analysis. Moreover, prior to addition of $SnCl_2$, excessive BrCl is reduced using hydroxylamine hydrochloride. Liquid-gas separation is performed using a purge system with Hg pre-concentration on a gold

trap. Finally, the sample gold-trap is analyzed in an IVL-custom made desorption system connected to a CVAFS detector (Tekran 2500 unit) [91].

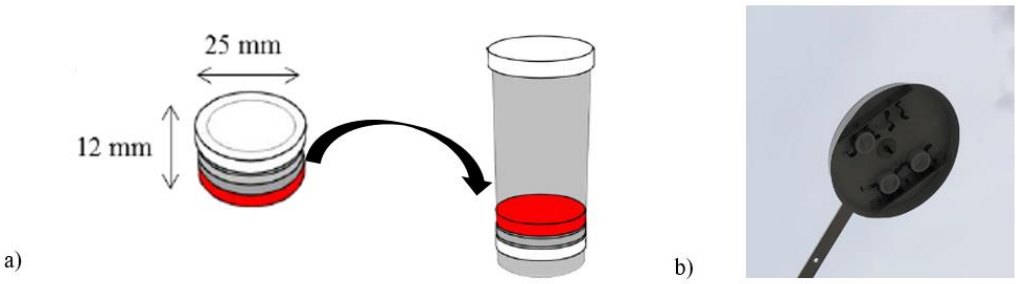

Figure 5.11 a) The passive airtight sample storing container; b) the passive sample holder-protective shield [91].

5.6 *Mer*PAS®

The passive air sampler for gaseous mercury, designed and developed by researchers at the University of Toronto (*Mer*PAS®) and produced by Tekran corporation, consists of sulfur-impregnated activated carbon (HGR-AC, Calgon Carbon Corporation, 0.6 grams) as sorbent material, housed in a porous stainless-steel mesh cylinder as sorbent carrier [86]. The cylinder is kept into a porous high-density polyethylene radial diffusive body, the commercially available White Radiello® (Sigma Aldrich), which acts as a diffusive barrier controlling the diffusion rate from the atmosphere to the sorbent material (Figure 5.12).

Figure 5.12 MerPAS® [86].

The sampler diffusive body is, in turn, integrated within a compact PET protective shield, capped with a tape-sealed solid lid, which is replaced with a screened lid to be used during exposure to the ambient air. Integrated, compact PET protective shelter is used for storage

and transport. Lid is tape-sealed, and sampler placed in plastic bag. To prevent rain from entering the sampler, the mesh screened lid is faced downward during deployment. *Mer*PAS® can be deployed at ambient air using the screw and bolt dowel embedded with the PET shield, without the need of any sampler holder (Figure 5.13), mounting it bracket with top threaded post and cap-nut.

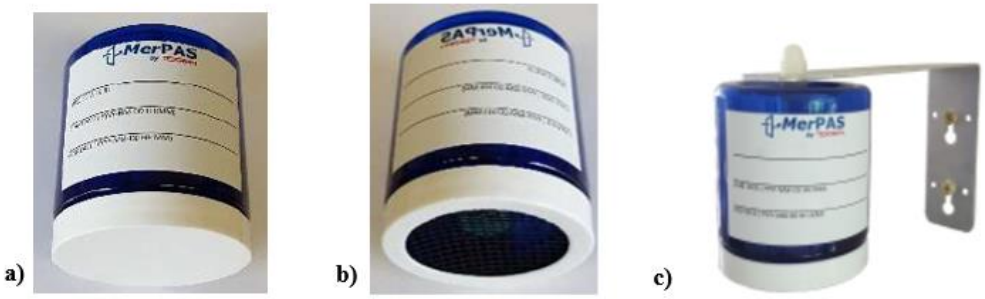

Figure 5.13 a) MerPAS® with the tape-sealed solid lid, b) with the screened lid to be used during exposure to the ambient air, and c) mounted on the bracket during deployment.

*Mer*PASs® are 7.6 cm height with diameter of 7.2 cm, while the effective diffusion path length is 0.77 cm (without air boundary layer), with areas of ~7.5 cm^2 on outer sorbent surface, ~30 cm^2 on diffuser surface. Analysis of mercury concentration trapped by activated carbon sorbent, carried out at the Tekran laboratory in Toronto, takes place through a Nippon MA-3000 system used for automated combustion, gold amalgamation, and detection by atomic absorption spectroscopy. Standard reference materials and liquid Hg standards (2 to 8 ng) added to activated carbon were analysed during analysis. Standard reference materials were bituminous coal (NIST 2684b, NIST 2685) and an activated carbon sample generated in-house at the University of Toronto. After analysis phase, the sorbent material is not reusable while sorbent carrier, diffusive barrier and the compact PET protective shelter with a mesh screened lid, are reusable.

Chapter 6

Gaseous mercury concentration data collected by new technologies: an intensive field inter-comparison campaign employing three Passive Air Samplers (PASs)

6.1 Introduction

This chapter reports the case study performed during this Ph.D. thesis and related to the use of three passive air sampling devices for mercury as a potential alternative system approach to the conventional sampling methods currently commercially available, in order to increase the spatial resolution of Hg data around the world, to make the adoption of these devices sustainable for the creation of a long-term global monitoring network and to implement existing conventional monitoring systems. As previously mentioned, conventional active or automated air samplers, currently commercially available and used to measure atmospheric concentrations of mercury, draw a known volume of air through a pair of Hg (usually gold) absorbent traps, which are periodically desorbed for Hg quantification [65,80]. Their operation in near real time guarantees a relatively fine temporal resolution of Hg concentration measurements but the bulky dimensions, the needs of power supply, gas cylinders and maintenance by well-trained operators, in addition to the high purchase and management costs, make them difficult to manage from a logistical and economic point of view, limiting their application on a large scale. Compared to the conventional active sampling, the use of innovative passive sampling results in various advantages. In fact, passive samplers usually are compact, small in size, portable and easy to install and, therefore, can be easily transported to remote sites. Given their relatively low production cost unlike a conventional automatic analyser, which is often placed in a single point of a given area, PASs can be exposed simultaneously at multiple points of a given area allowing the identification of mercury sources and their characterization through finely resolved spatial mapping over large areas, implementing existing monitoring systems [25,74,75,76].

Once exposed in the field, PASs have a low operating cost since they do not require neither electricity or pumps to operate nor continuous supervision or maintenance by

trained operators. For these reasons, passive devices represent an adequate sampling solution for remote sites and areas that are difficult to reach or for areas where greater spatial coverage is required to integrate mercury concentration data. The PASs are also suitable for monitoring studies that do not require high time resolution data, as they provide a time-averaged concentration of gaseous mercury over a time scale of weeks to months. PASs availability and affordability, and their ability to provide results with acceptable precision and accuracy are key points of their usefulness in the monitoring studies, where promising to fill the gap in the monitoring of atmospheric mercury worldwide. The case study reported below was one of the activities carried out during the Ph.D. and it was focused on the field comparative evaluation of three PASs, regarding their ability to record precisely and accurately atmospheric background Hg concentrations at two monitoring sites, located in Italy (Southern Italy) and Canada (Southern Ontario), over a three-month period. At these monitoring sites, the performances of these sampling devices were assessed for accuracy through comparison with active sampling data, for precision and for sensitivity (e.g. the method detection limit, MDL), as well as in terms of the linearity of uptake over extended deployment periods. In particular, the research work focused on the deployment, at Italian site, of the different passive devices involved in the inter-comparison campaign exercise and on the quantitative analysis and data elaboration of the passive samplers developed by CNR-IIA. The following sections contain a detailed description of the wide inter-comparison study carried out and the results obtained of the PASs field application.

6.2 Study characteristics

The comparison study included the CNR-PAS with gold nanoparticles as a sorbent, developed by the Italian National Research Council [90], the IVL-PAS using an activated carbon-coated disk, developed by the Swedish Environmental Research Institute [91] and the *Mer*PAS® using a sulfur-impregnated activated carbon sorbent, developed by University of Toronto and commercialized by Tekran Instrument Corp. [89] (Figure 6.1). A detailed description of the characteristics of the three PAS design involved in this study was reported in the previous chapter. Each participating research group designed, produced, and supplied their PASs along with deployment instructions that were sent by international courier from each participating laboratory to the two chosen sampling sites

where the devices were exposed to ambient air, following the producer operating instructions and the agreed sampling plan for carrying out the inter-comparison study. Shortly, after the end of the last deployment, the samplers were returned to the participating laboratories by international courier to perform chemical analysis and report volumetric air concentrations and basic QA/QC results to an independent blind third party, in order to control for bias. Furthermore, as required by the study protocol, for each monitoring site at the same time as the deployment of the PASs, the GEM concentrations recorded by the instruments based on active air sampling, averaged for the different periods of PAS deployment, were reported. This made it possible to compare the performance of the passive devices mentioned above through the assessment of the accuracy with respect to the active sampling data, precision and method detection limit (MDL), as well as in terms of the linearity of uptake over extended deployment period.

Figure 6.1 The three passive air samplers for gaseous mercury compared in this study: a) CNR-PAS, b) IVL-PAS, and c) *Mer*PAS®.

6.3 Sampling sites

In order to evaluate the performance of the three different PASs during the inter-comparison exercise, Rende (Italy) and Toronto (Canada) were selected as monitoring sites. These sites are mostly background sites not affected by local sources where the atmospheric mercury concentrations are continuously monitored by means of the conventional active Tekran 2537. Moreover, during the campaign air temperature, relative humidity, wind speed and wind direction were measured at both sites. The Italian sampling site was a monitoring station close to the CNR Institute of Atmospheric Pollution Research (39°21'27.2"N 16°13'53.7"E) in Rende, in the area surrounding the Institute that is a suburban site, where mercury concentration in the atmosphere mostly remains in background values, between 1 and 2 ng m^{-3}. The meteorological data in Rende were recorded by a meteorological station located in proximity of deployment area, and

data were continuously acquired using a thermo-hygrometer LSI LASTEM DMA875 for the monitoring of temperature and relative humidity. A pluviometer LSI LASTEM DQA030 for the acquisition of precipitation depth and an LSI LASTEM DNA821 anemometer for the acquisition of wind speed and direction, were also employed. As regards the weather conditions, an average temperature of 12.0 ± 4.6 °C (range 0.9 – 30.6 °C) and relative average humidity of 60.4 ± 18.1% (range 13.6 – 97.9%), were measured in Rende site. Moreover, over the study period the wind blew mainly from SSE with an average speed of 1.2 ± 0.9 m s^{-1}, in a range between 0 and 6.9 m s^{-1}. The total rainfall was 1.71 mm and no precipitation fell as snow.

The Canadian sampling site was located on the ground of the Downsview office of Environment and Climate Change Canada, in a Northern suburb of Toronto (43°46'49.65"N 79°28'2.46"W). In Toronto, meteorological parameters were obtained from a co-located integrated weather station (Vaisala WXT520) operated by the Ontario Ministry of Environment, Conservation and Parks. The weather conditions recorded throughout spring season showed a mean temperature of 0.6 ± 6.6 °C (range 15.8 – 21.5 °C), a wind speed averaged of 2.4 m s^{-1} (range of hourly averages from 0 to 11 m s^{-1}) and an average relative humidity of 64.7 ± 15.7% (range 18.5 – 92.1%). The prevalent (20.5% of the time) wind vector was from the west, between 260 and 285°. During the PAS deployment period the total precipitation was 225 mm, of which 168 mm fell as rain and the remainder as snow.

6.4 Sampling plan and PASs deployment

The three PAS types were deployed side-by-side nearby existing active air monitoring systems at Rende (Italy) and Toronto (Canada) during late winter and early spring of 2019, for a total period of three months. In particular, at both sites the inter-comparison campaign was carried out from February 5th to April 30th, 2019, by deploying PASs according to the sampling plan (Table 6.1). In each site, the sampling plan provided 11 overlapping PAS deployment periods that ranged in length from 2 to 12 weeks. In detail, the sampling plan included four sampling rounds of 2 weeks, three rounds of 4 weeks, two rounds of 6 weeks, one round of 8 weeks and one round of 12 weeks.

Site	Deployment	1 w	2 w	3 w	4 w	5 w	6 w	7 w	8 w	9 w	10 w	11 w	12 w	Sampling start and stop
Rende	1st 2-week		4											5 Feb to 19 Feb
	2nd 2-week				4									19 Feb to 5 Mar
	3rd 2-week						4							5 Mar to 19 Mar
	4th 2-week										4			2 Apr to 16 Apr
	1st 4-week				4									5 Feb to 5 Mar
	2nd 4-week								4					5 Mar to 2 Apr
	3rd 4-week												4	2 Apr to 30 Apr
	1st 6-week						4							5 Feb to 19 Mar
	2nd 6-week												4	19 Mar to 30 Apr
	1st 8-week								4					5 Feb to 2 Apr
	1st 12-week												4	5 Feb to 30 Apr
Toronto	1st 2-week		4											5 Feb to 19 Feb
	2nd 2-week				4									19 Feb to 5 Mar
	3rd 2-week						4							5 Mar to 20 Mar
	4th 2-week										4			2 Apr to 16 Apr
	1st 4-week				4									5 Feb to 5 Mar
	2nd 4-week								4					5 Mar to 2 Apr
	3rd 4-week												4	2 Apr to 30 Apr
	1st 6-week						4							5 Feb to 20 Mar
	2nd 6-week												4	20 Mar to 30 Apr
	1st 8-week								4					5 Feb to 2 Apr
	1st 12-week												4	5 Feb to 30 Apr

Table 6.1 Sampling deployment plan for PASs in Rende and Toronto. For each deployment round the sampling start and end dates are reported. These dates refer to 2019. The bolded numbers in the boxes refer to the number of PASs of each type deployed during every round (3 samplers and 1 field blank).

All PAS deployments were triplicated, with the addition of a field blank for each type of PAS to check the potential for contamination during transport, storage and handling of the samplers. Therefore, for each deployment round three replicates and a field blank were deployed in order to determine the repeatability and the lower detection limit of the samplers that was calculated as three times the standard deviation of the blanks of each time-period. At both monitoring sites a total of 22 PAS deployment periods were carried out, during which a total of 88 PASs of each type were deployed. Sixty-six devices were used as samplers while 22 devices were used and considered in the measurements as field blanks (FBs). At each monitoring site a total of 11 field blanks were used, one for each deployment round, therefore 4 field blanks for the 2-week deployment, 3 field blanks for the 4-week deployment, 2 field blanks for the 6-week deployment, 1 field blank for the 8-week deployment, and 1 field blank for the 12-week deployment. At both sites, personnel were involved in the deployment and retrieval of PASs over the 12 weeks of

the study, but it was always the same personnel that handled all three PASs at any one of the seven deployment and retrieval dates. The personnel involved in the management of all PASs throughout the campaign distributed, recovered and treated the samplers following the instructions provided by each participating research group, thus ensuring the samplers were treated in the same way at both monitoring stations. At Rende and Toronto sites, the samplers were deployed on a metal support rack parallel to the ground and about 4 m height to facilitate free air circulation. All PASs were deployed close together within 2 m of each other and from the inlet of the active air sampler and when not deployed, samplers were stored on-site at room temperature. At both sites, the deployment set up was quite similar (Figure 6.2).

Figure 6.2 Deployment set up in Rende (left) and Toronto (right).

While the three PASs were treated the same as much as possible, there were some unavoidable differences. The CNR-PAS did not need to undergo extended travel to the Rende site and the *Mer*PAS® was only transported by car between different locations within the city of Toronto (Tekran facilities, University of Toronto Scarborough Campus, ECCC sampling site in Downsview). The IVL-PASs made return air trips by international courier to both sampling sites and were deployed at both sites by personnel with no experience with this sampler. At Rende, CNR-PASs were deployed by personnel with some familiarity working with this sampler; the same occurred at Toronto with the *Mer*PAS®. The shelters for CNR and IVL-PASs were mounted on the metallic support as well as the *Mer*PAS® devices, which were secured using the embedded screw and bolt dowel directly. As regards the exposure to ambient air of CNR-PASs, for every round each passive device was taken from heat- and zip- sealed aluminium bag used for its storage and transport immediately before deployment. The top cap of CNR-PASs used as

samplers was removed and placed in the corresponding aluminium bag together with mercury scrubber cartridge for the whole exposure period and the device was positioned in a shelter seat with the diffusive membrane facing downwards. After exposure, CNR-PASs used as samplers were removed from the seat, closed with the corresponding top cap, and placed into the aluminium bag, together with the mercury scrubber cartridge. The passive devices used as field blanks were deployed closed, without ever being open, removed at the end deployment and then placed in the corresponding aluminium bag, together with the mercury scrubber cartridge. IVL-PASs were deployed and removed following a procedure similar to CNR-PASs. After removing the IVL samplers from the two plastic bags and plastic container used for their storage and transport, they were placed in the seats of their shelter with the steel mesh net facing downwards. After exposure to ambient air, IVL-PASs used as samplers were removed, placed in the plastic container and then into the two plastic bags. Instead, the IVL-PAS used as field blanks were not deployed at the actual field sites but were only briefly transported to the deployment site during a sample change-over. Therefore, the IVL-PASs used as field blanks were never removed from theirs plastic container and plastic bags. During the remainder of the 12 weeks of the study, they were stored indoor. As regard *Mer*PAS® exposure, the samplers were secured to the metallic support of the deployment set up using the embedded screw and bolt dowel after removing the plastic bag used for storage and transport and the tape from seal, and after having replaced the solid lid with the screened lid. The solid lid was placed in the plastic bag for the duration of the exposure. After exposure, the screened lid was replaced by the solid lid, and the tape-sealed device were placed in a protective Ziploc bag. Instead, the *Mer*PAS® field blanks were deployed in the same way on metallic support but sealed with the solid lid and after exposure were placed in a Ziploc bag. Therefore, at both monitoring sites the CNR-PAS and *Mer*PAS® field blanks were deployed in the field alongside each triplicate without opening their cap or lid. Additionally, five storage blanks of the CNR-PAS in each monitoring site were used to check contamination for mercury during the PAS storage and transport meanwhile there were only five such storage blanks of the *Mer*PAS® in Rende and none in Toronto.

6.5 Active air sampling

During the inter-comparison exercise, at both sites the gaseous mercury atmospheric concentrations were measured and monitored in continuous using both passive and active sampling method. The simultaneous use of both methods for sampling atmospheric mercury has made it possible to evaluate the performance of the passive devices in terms of comparison with Tekran active measurements and to provide comparable data globally. The gaseous mercury concentrations were obtained at 5-minute intervals using Tekran 2537X and 2537A automated mercury analyzers (Tekran Inc., Toronto, ON, Canada) at both sites. At Rende site, a Tekran 2537X unit was used. In Toronto, in order to be able to quantify the duplicate precision of the active air sampling technique two systems, namely a Tekran 2537X and 2537A (5037 and 0075 units, respectively) were operating in parallel. The sampling was performed with airflow rates of 1.5 and 1.0 L min^{-1} at Rende and Toronto, respectively. To ensure that Tekran systems were operating consistently, before and during the inter-comparison campaign flow verifications and calibrations were carried out by external injections of mercury and by using the instrument internal mercury permeation source for automatic calibration at 72-hour and 23-hour intervals in Rende and Toronto respectively, throughout the monitoring period. Calibration results and data acquisition obtained at both monitoring sites were quality controlled according to established quality assurance and quality control procedures (QA/QC). In order to check the mercury concentration data collected by Tekran 2537X at Rende site and to monitor the performance of the instrument in terms of baseline shifts, sample volume cell bias and difference between the gold traps (for verifying that it adhered to standard procedures) in a way that minimizes losses and inaccuracies in data production, the GMOS-Data Quality Management (G-DQM) was used [60]. Instead, for qualitatively check all data collected by Tekran analyzer at Toronto site, the Toronto QA/QC system based on the Research Data Management Quality (RDMQ) standards defined in Steffen et al., 2012 [74] was used, which invalidate data based on cell bias and sample volume, also monitoring for baseline and deviation amongst other warning flags.

6.6 Analysis of PAS sorbents for determination of Hg concentration and statistical analysis

At the end of the sampling campaign, all passive devices collected at each monitoring site were delivered to the development laboratories for the analysis of the sorbent material. The quantitative determination of the mercury mass trapped by the three type of PASs involved in the inter-comparison study were carried out using analysis methods and instrumentations described in the previous chapter. Successively, from the Hg mass resulted from the analysis of sorbent material, according to the equation derived from Fick's law the average Hg atmospheric concentrations in the atmosphere measured by each sampler (*C*; ng m^{-3}) was calculated:

$$C = \frac{m}{t \times SR}$$

where *m* is the mass of sorbed Hg (ng) corrected for the blank contamination, *t* is the deployment time of the PAS (days) and *SR* is the sampling rate of the PAS (m^3 day^{-1}). For the calculation of the volumetric concentration the constant values of the SR for each PAS type were used, which were experimentally previously derived. For the CNR-PASs, the SR value was of 0.0147 m^3 day^{-1} with an uncertainty of 0.0007 m^3 day^{-1}, which is a value slightly different from the previously reported one [90] probably due to further improvements of CNR-PAS geometry. For the IVL-PASs, the SR was 0.028 m^3 day^{-1} in Rende and 0.029 m^3 day^{-1} in Toronto (calculated using the diffusivity for Hg according to Massman [93]. The SR of the *Mer*PAS® was 0.111 ± 0.017 m^3 day^{-1} which is a function of the *Mer*PAS® radial design. Due to small modifications between the *Mer*PAS® and the original sampler, this SR value derived from a number of calibration experiments performed by Tekran, and deviates slightly from previously published values [76,77]. The uncertainty of the SR of each PAS type is directly propagated to the volumetric air concentration. During the sampling campaign exercise, the sampler's deployment for every exposure period were carried out in triplicate in order to assess the precision of each PAS device after analysis as a relative standard deviation (RSD%). For each type of PASs, devices used as samplers and those used as field blanks during deployment to ambient air were analysed in the same way. Both analytical and field blanks were used for QA/QC of mercury analytical data during the analyses of the sorbent. To ensure

sorbent materials were free from Hg contamination analytical blanks were analyzed before deployment and sampling. To ascertain whether there was contamination during sampler assembly, shipping, transport, deployment, retrieval and storage some field blanks were used. Storage blanks were used to assess any contamination due to the transport and storage only, particularly during deployment and retrieval operations. In addition to the precision, the method detection limits (MDLs) expressed in ng were obtained as three times the standard deviation of the amount of mercury in field blanks; the practical quantification limits (PQLs) expressed in ng were calculated as ten times the standard deviation of the amount of mercury in field blanks; the limits of detection (LOD) expressed in ng m^{-3} were obtained by dividing MDL by the product of sampling rate (SR) and deployment time (days) and the limits of quantification (LOQ) in ng m^{-3} were calculated by dividing PQL by the product of sampling rate (SR) and deployment time (days).

The relative accuracy of the three type of PASs was evaluated calculating the percentage differences between Hg concentrations measured by Tekran analyzer ($[Hg]_{Tekran}$) and those derived from each of the paired PASs ($[Hg]_{PAS}$). These percent concentration differences were calculated as:

$$\%\, difference = \frac{[Hg]_{Tekran} - [Hg]_{PAS}}{[Hg]_{Tekran}}$$

The calculated absolute concentration differences were used for subsequent analysis. A variance partitioning analysis was used to quantify the proportion of the overall variability in absolute percentage concentration difference values (calculated in the previous Eq.), that is explained by deployment site, deployment time, Tekran identity (in the case of Toronto), and PAS type. This variance partitioning analysis was based on n=99 total observations of absolute percent concentration differences. To perform the variance partitioning analysis a linear mixed effects model was applied by using R package [94]. In this model, absolute percent concentration differences are predicted as a function of a single fixed effect (i.e., the model intercept, which represents the overall mean percent concentration difference), and four random effects (i.e., four nested factors including PAS type, within Tekran IDs (alternatively, the deployment location), within deployment

periods, within deployment site (i.e., one of Rende or Toronto). The proportion of variation in concentration differences that owes to each of the four nested factors was then quantified [95]. Based on these results, it was then calculated and compared mean absolute concentration percentage differences across both PAS types and sites, while accounting for the non-independence of samples, unbalanced sample sizes across sites and PASs, and potentially confounding effects of a) sampling deployment times and b) sites. Successively, a second linear mixed effects model where absolute concentration differences were predicted as a function of PAS type, site, and a PAS-by-site interaction term as fixed factors was used. This mixed model statistically accounted for non-independence of samples, by including deployment period and Tekran identity as nested random effects and it allowed to calculate and statistically compared least square mean concentration difference values (and associated standard errors) across each PAS type, site, and each PAS-by-site combination. This analysis therefore allowed to assess whether least square mean concentration differences values in any of these groups, differed significantly from one another, or differed significantly from zero.

6.7 Results and discussion

In this section, the results of the field application of PASs and of the comparison of their performance with those of the Tekran continuous monitoring systems were reported. For the passive sampling, the reported values for each deployment rounds refer to the time-averaged concentration of mercury adsorbed by samplers deployed during the specific deployment round. The gaseous mercury concentration values reported for active sampling were obtained using the continuous Tekran mercury analyzers and determined by averaging the values recorded every 5-minutes by instrument during every PAS deployment period of whole campaign.

6.7.1 Gaseous mercury concentration obtained by active sampling

At both sites, the values recorded by conventional instruments with 5 minutes resolution were validated using standard quality assurance and quality control procedures (QA/QC) and the complete series of the valid Hg concentration data were illustrated in (Figure 6.3). For each site, the interruptions to the sampling were due to instrument calibration or maintenance.

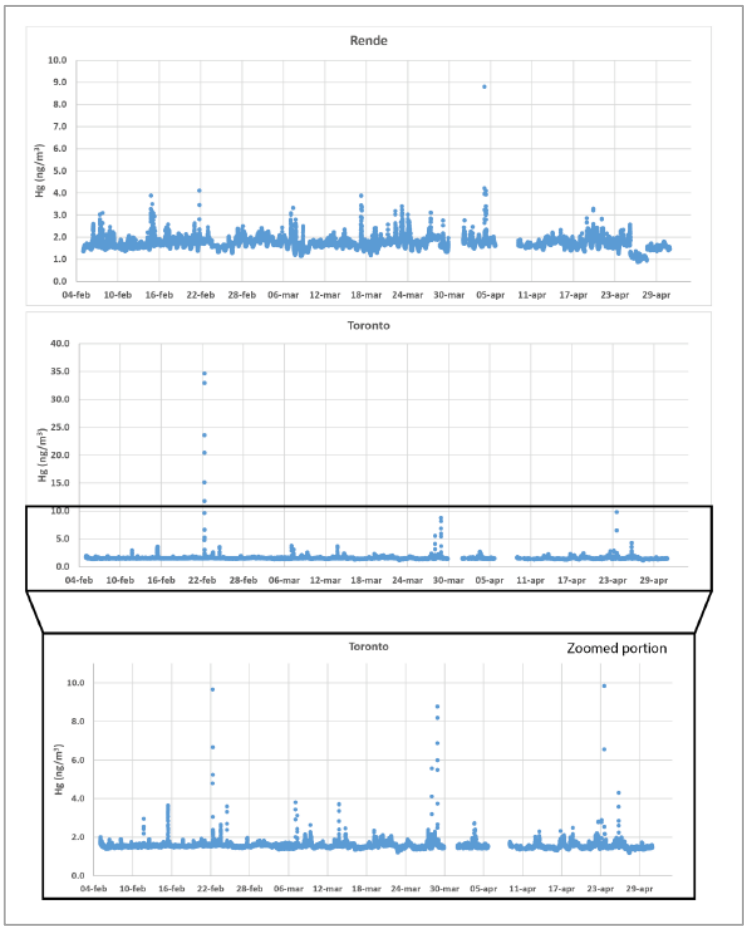

Figure 6.3 Concentration of gaseous mercury at Rende and Toronto using active instrumentation.

At Rende, the active mercury concentration values obtained resulting in 98.9% of valid data. These data showed that the mean measured Hg concentration at Rende during the 11 PAS deployment periods was quite constant, with a mean value of 1.66 ± 0.28 ng m^{-3} and 1.79 ± 0.19 ng m^{-3}. The active sampling measurements showed that the average Hg concentration at Rende over the 12 weeks was 1.72 ± 0. 25 ng m^{-3}, with a range from 0.88 to 8.80 ng m^{-3} (Figure 6.3). At Toronto, RDMQ standards were used for data quality assessment which together with the measurement gaps during daily calibration periods, to the hourly standard additions and instrument maintenance resulted in 82.5% of valid data coverage throughout the entire deployment period for the primary 2537X analyzer. During campaign, the mean Hg concentration for each deployment varied only slightly, between 1.51 ng m m^{-3} and 1.63 ng m^{-3}. As previously reported (Section 6.3.2), at Toronto site in addition to Tekran 2537X analyser, a secondary co-located 2537A analyser was used to validate primary mercury analyzer precision. However, given that primary Tekran analyzer 2537A showed an 8% shift in the mass-flow meter calibration during the study

and since it was not possible to determine when the shift occurred, for PAS comparison only the primary 2537X data were used. Nevertheless, the data from Tekran 2537A analyzer were included in the statistical analysis of this study (described in paragraph 6.6). The active gaseous Hg concentration ranged between 1.17 and 34.6 ng m^{-3} (Figure 6.3), resulting in an average value of 1.57 ± 0.45 ng m^{-3}. Over the study period five short periods of high mercury concentrations (over 4 ng m^{-3}) were observed with the maximum reaching 34.6 ng m^{-3}. Although unusual, the elevated values were observed on both primary and secondary analyzers and lasted between 10 and 35 minutes and are accepted as valid. The Toronto site is located in a northern suburb of Canada largest urban center and a possible explanation for the elevated episodes could be associated to of nearby industrial mercury emissions.

6.8 Comparison of Passive Air Sampler Performance

6.8.1 Blanks and Detection Limits

The mercury concentration in field blanks were similar between the different passive samplers at monitoring sites, with values of less than 0.2 ng, 0.2 ng and 0.4 ng in the CNR-PAS, IVL-PAS and *Mer*PAS®, respectively as showed in Table 6.2. The averages of those values are displayed in the top row of panels in Figure 6.4. The obtained values of mean, standard deviation (SD) and percentage relative standard deviation (%RSD) of mercury levels in field blanks of the three PASs for each deployment period at Rende and Toronto showed that during the campaign, the blank levels of the CNR-PAS are the lowest recorded, especially for exposure in Rende. The *Mer*PAS® showed no difference in the blank levels between Rende and Toronto, whereas the CNR-PAS and IVL-PAS showed a slight difference between the two sites. Moreover, in the case of *Mer*PAS® and CNR-PAS field blanks which were deployed together with samplers in the field for variable lengths of time due to there was no indication that the field blank contamination increased with increasing deployment time in the field, the average values for each site (which showed in bold font in Table 6.2) were used for the blank correction of the amount of mercury measured in exposed PASs. This observation is consistent with blank contamination arising during handling and transport and not during the placement at the deployment location.

	Length	*n*	*Mer*PAS®		IVL-PAS		CNR-PAS	
			Mean ± SD	**RSD**	**Mean ± SD**	**RSD**	**Mean ± SD**	**RSD**
Rende	2 weeks	4	0.228 ± 0.012	5%	0.495 ± 0.079[b]	16%	0.144 ± 0.014	10%
	4 weeks	3	0.244 ± 0.014	6%	0.482 ± 0.110[c]	23%	0.155 ± 0.029	19%
	6 weeks	2	0.263[a]	-	0.576 ± 0.072	12%	0.151 ± 0.014	9%
	8 weeks	1	0.213	-	0.440	-	0.175	-
	12 weeks	1	0.315	-	0.390	-	0.174	-
	all	**11**	**0.229 ± 0.055**	**24%**	**0.490 ± 0.090**	**18%**	**0.154 ± 0.019**	**12%**
Toronto	2 weeks	4	0.200 ± 0.041	21%	-	-	0.136 ± 0.052	38%
	4 weeks	3	0.258 ± 0.040	16%	-	-	0.275 ± 0.053	19%
	6 weeks	2	0.240 ± 0.068	28%	-	-	0.231 ± 0.023	10%
	8 weeks	1	0.243	-	-	-	0.211	-
	12 weeks	1	0.322	-	-	-	0.195	-
	all	**11**	**0.238 ± 0.052**	**22%**	**0.430 ± 0.077[d]**	**18%**	**0.203 ± 0.070**	**34%**

[a] *n*=1 only, [b] *n*=3 only, [c] *n*=2 only, [d] *n*=12

Table 6.1 Mean, standard deviation (SD) and percentage relative standard deviation (%RSD) values of mercury levels (ng) in field blanks of the three passive samplers for each deployment period, at Rende and Toronto. *n* indicates the number of field blanks of a certain deployment length and the number reported in bold font are the average values for each location used for the blank correction. In Toronto, the field blanks of the IVL-PAS were not deployed alongside the exposed samplers.

As previously reported, some samplers of CNR-PASs and *Mer*PAS® were used as storage blanks. As regarding the CNR-PAS, the values of storage blanks (0.066 ng ± 0.010 ng, n = 5 - Toronto, 0.042 ng ± 0.009 ng, n = 5 - Rende) were considerably lower than the levels of field blanks (0.20 ng ± 0.07 ng, n = 5 - Toronto, 0.15 ng ± 0.02 ng, n = 5 - Rende), which implies that the deployment and retrieval of those samplers does introduce some contamination. The Hg amount quantified in *Mer*PAS® storage blanks (0.187 ng ± 0.009 ng, n = 5, Rende) is only marginally lower than the amount in field blanks (0.23 ng ± 0.06 ng, n = 10, Rende). The relative standard deviation (RSD) of levels in field blanks was also similar between the three samplers. In the IVL-PAS RSD value (~18%) was slightly lower than in the *Mer*PAS® and CNR-PAS (~23% on average), probably due to the fact that IVL-PAS field blanks were all treated the same, whereas the *Mer*PAS® and CNR-PAS field blanks had slightly different handling processes, because they were deployed alongside the exposed samplers. As regard the CNR-PAS, the RSD of that deployed in Rende was notably lower (12%) than to that deployed in Toronto (34%). For every type of PAS, the amount of mercury detected in the corresponding field blanks was used for the calculation of the method performance metrics as the method detection limit (MDL), the practical quantification limit (PQL), the limits of detection (LOD) and limit of

quantification (LOQ). Because the field blank levels were different in the two deployment sites, the previously parameters for the three passive air samplers were determined for Rende and Toronto sites separately and the numerical results obtained at each monitoring site were showed in Figure 6.4 and reported in Table 6.3. The MDL and PQL values are derived from the variability in the field blank levels. Therefore, they are similar between the three samplers (middle row of panels in Figure 6.4). Although the RSD of the field blank levels is smaller for the IVL-PAS (~18%) than the other two devices (~23%), the larger absolute SD means that IVL-PAS has MDL and PQL values of ~0.25 ng and ~0.8 ng, respectively, that were higher than to those other two samplers which were 0.13 and 0.45 ng for the CNR-PAS on average, 0.16 and 0.54 ng for the *Mer*PAS®.

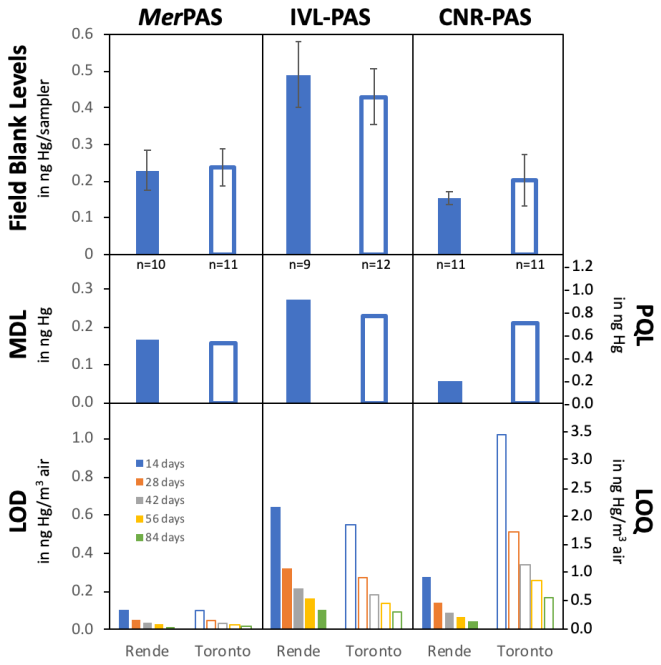

Figure 6.4 Mean and standard deviation of field blank levels, method detection limit (MDL), practical quantification limit (PQL), limit of detection (LOD) and quantification (LOQ) for the three PASs deployed in Rende and Toronto.

	Length of Deployment (days)	*Mer*PAS®		IVL-PAS		CNR-PAS	
		Rende	Toronto	Rende	Toronto	Rende	Toronto
MDL (ng)		0.17	0.16	0.27	0.23	0.06	0.21
PQL (ng)		0.55	0.52	0.90	0.77	0.19	0.70
LOD ($ng\ m^{-3}$)	14	0.11	0.10	0.64	0.55	0.28	1.02
	28	0.05	0.05	0.32	0.27	0.14	0.51
	42	0.04	0.03	0.21	0.18	0.09	0.34
	56	0.03	0.03	0.16	0.14	0.07	0.26
	84	0.02	0.02	0.11	0.09	0.05	0.17
LOQ ($ng\ m^{-3}$)	14	0.35	0.33	2.14	1.82	0.92	3.40
	28	0.18	0.17	1.07	0.91	0.46	1.70
	42	0.12	0.11	0.71	0.61	0.31	1.13
	56	0.09	0.08	0.54	0.46	0.23	0.85
	84	0.06	0.06	0.36	0.30	0.15	0.57

Table 6.2 Method detection limit (MDL), practical quantification limit (PQL) and limits of detection (LOD) and quantification (LOQ) for the for *Mer*PAS®, IVL-PAS, and CNR-PAS for both sites.

The bottom row of Figure 6.4 displays the LODs and LOQs for each of the five deployment times used in this study, whose corresponding numerical values were reported in Table 6.3. From these representations it is possible to observe how in terms of volumetric air concentrations, the LODs and LOQs decrease with the sampled air volume, which, in turn, increases with a sampler sampling rate and deployment period. Given the *Mer*PAS® has a sampling rate that is ~4 to ~8 times higher than others two and accordingly samples mercury from a much larger air volume during similar deployment times, larger differences between the *Mer*PAS® and the other two PASs, are evident. Therefore, despite the absolute amounts of Hg in field blanks were similar between the samplers, the amount in field blanks relative to the amounts in exposed samplers was different (Table 6.4).

Deployment	*Mer*PAS®		IVL-PAS		CNR-PAS	
	Rende	Toronto	Rende	Toronto	Rende	Toronto
1st 2-week	8%	8%	43%	37%	31%	42%
2nd 2-week	8%	8%	43%	36%	31%	32%
3rd 2-week	8%	8%	40%	29%	30%	28%
4th 2-week	8%	9%	43%	36%	30%	47%
1st 4-week	4%	4%	28%	23%	18%	37%
2nd 4-week	4%	4%	23%	21%	16%	32%
3rd 4-week	4%	4%	27%	23%	17%	33%
1st 6-week	3%	3%	21%	17%	13%	18%
2nd 6-week	3%	3%	21%	17%	13%	19%
1st 8-week	2%	2%	16%	15%	11%	13%
1st 12-week	1%	1%	10%	10%	7%	11%
2-week (n=8)	7.9 ± 0.4%		38 ± 5%		34 ± 7%	
4-week (n=6)	4.2 ± 0.1%		24 ± 3%		26 ± 9%	
6-week (n=4)	2.7 ± 0.1%		19 ± 2%		16 ± 3%	
8-week (n=2)	2.1 ± 0.1%		15.2 ± 0.7%		12.0 ± 1.2%	
12-week (n=2)	1.38 ± 0.01%		10.0 ± 0.2%		9 ± 2%	

Table 6.3 Mercury amount in field blanks expressed as percentage of the amount in exposed samplers. In the top of the table, the average of the triplicated deployments was reported, while in the bottom panel reports the percentages averaged over deployment length.

For each type of PAS deployed in a specific site and for every deployment round, the average value of the triplicated deployments was calculated by dividing the average Hg amount in field blank by the average Hg amount in triplicate samplers deployed in that specific round. The values reported highlight that field blank contamination in the *Mer*PAS® does not exceed 8% of the quantified mercury amount in an exposed sampler (range 1 to 8%). Instead in both IVL-PAS and CNR-PAS was similar and ranged between 7 - 47%, with higher values during short periods of deployment (Table 6.4). This means that during a two-week deployment the *Mer*PAS® has a LOD of 0.11 ng m^{-3} and a LOQ of 0.35 ng m^{-3}, which are ~6 times lower than those of the IVL-PAS and the CNR-PAS. The blank contamination and therefore also MDL/PQL and LOD/LOQ were study-specific, therefore were determined during this study and need to be determined during every study anew. The CNR-PASs deployed at Rende showed lower and more consistent blank levels compared to those deployed in Toronto. In fact, for a two-week deployment

CNR-PASs at Rende showed LODs values of 0.28 ng m^{-3}, four times lower to those deployed in Toronto that were 1.02 ng m^{-3}, as well as the LOQs values that were 0.9 ng m^{-3} at Rende and 3.4 ng m^{-3} at Toronto (Table 6.3).

6.8.2 Precision

In this study, analytical and sampling precision was quantified through 22 triplicated deployments for each PAS ranging in length from two to twelve weeks. Therefore, the use of a very large number of triplicate deployments allowed a thorough characterization of the measure of precision for the different PASs as relative standard deviation (RSD %) of the mean value of Hg amount quantified in three samplers. The replicate precision of three type of PASs deployed simultaneously was determined both before and after blank correction during the 22 different deployments. The precision of the quantified mercury amount in a PAS before blank correction is a combined measure of the consistency and reproducibility of the PAS manufacturing, deployment and handling and the laboratory analytical process (Table 6.5).

Location	Deployment	*Mer*PAS®		IVL-PAS		CNR-PAS	
		Mean ± SD (ng)	RSD (%)	Mean ± SD (ng)	RSD (%)	Mean ± SD (ng)	RSD (%)
Rende	1st 2-week	2.99 ± 0.11	4	1.15 ± 0.09	8	0.50 ± 0.02	3
	2nd 2-week	3.00 ± 0.06	2	1.15 ± 0.09	8	0.50 ± 0.02	4
	3rd 2-week	2.92 ± 0.27	9	1.21 ± 0.09	7	0.51 ± 0.03	5
	4th 2-week	3.02 ± 0.11	4	1.15 ± 0.09	8	0.52 ± 0.01	3
	1st 4-week	5.72 ± 0.29	5	1.74 ± 0.15	8	0.84 ± 0.12	14
	2nd 4-week	5.72 ± 0.14	2	2.10 ± 0.62	29	0.96 ± 0.02	2
	3rd 4-week	5.44 ± 0.18	3	1.82 ± 0.32	17	0.89 ± 0.03	3
	1st 6-week	8.71 ± 0.23[a]	3	2.39 ± 0.26	11	1.15 ± 0.11	9
	2nd 6-week	8.69 ± 0.11	1	2.38 ± 0.24	10	1.20 ± 0.05	4
	1st 8-week	11.41 ± 0.43	4	3.12 ± 0.25	8	1.38 ± 0.15	11
	1st 12-week	16.61 ± 0.30	2	4.80 ± 0.33	7	2.13 ± 0.35[a]	16
Toronto	1st 2-week	2.84 ± 0.14	5	1.17 ± 0.05	4	0.48 ± 0.04	7
	2nd 2-week	3.12 ± 0.11	4	1.19[b]		0.64 ± 0.06	10
	3rd 2-week	2.90 ± 0.20	7	1.49 ± 0.20	13	0.73 ± 0.07	10
	4th 2-week	2.80 ± 0.10	4	1.18 ± 0.01[a]	1	0.43 ± 0.03	6
	1st 4-week	5.50 ± 0.05	1	1.91 ± 0.10	5	0.55 ± 0.01	3
	2nd 4-week	5.64 ± 0.30	5	2.09 ± 0.27	13	0.63 ± 0.01	2
	3rd 4-week	5.67 ± 0.14	2	1.89 ± 0.13	7	0.62 ± 0.03	4
	1st 6-week	8.28 ± 0.33	4	2.52 ± 0.21	8	1.10 ± 0.09	9
	2nd 6-week	8.48 ± 0.23	3	2.54 ± 0.32	13	1.05 ± 0.08	7
	1st 8-week	11.12 ± 0.15	1	2.91 ± 0.04	1	1.59 ± 0.26	16
	1st 12-week	17.11 ± 0.27	2	4.36 ± 0.11	2	1.91 ± 0.10[a]	5

[a] duplicate only, [b] no replication

Table 6.4 Mean, standard deviation (SD) and percentage relative standard deviation (%RSD) of the amounts of Hg (ng) quantified in deployed PASs before blank correction for each of the 22 deployments. The values refer to triplicates, unless otherwise specified.

The precision of the quantified mercury amount in a PAS after blank correction additionally accounts for the consistency and reproducibility of the blank contamination (Table 6.6).

Location	Deployment	*Mer*PAS®		IVL-PAS		CNR-PAS	
		Mean ± SD (ng)	RSD (%)	Mean ± SD (ng)	RSD (%)	Mean ± SD (ng)	RSD (%)
Rende	1st 2-week	2.76 ± 0.12	4	0.66 ± 0.13	19	0.34 ± 0.02	7
	2nd 2-week	2.77 ± 0.08	3	0.66 ± 0.13	20	0.35 ± 0.03	8
	3rd 2-week	2.69 ± 0.28	10	0.72 ± 0.13	18	0.36 ± 0.03	9
	4th 2-week	2.79 ± 0.12	4	0.66 ± 0.13	19	0.36 ± 0.02	7
	1st 4-week	5.49 ± 0.30	5	1.25 ± 0.17	14	0.69 ± 0.12	18
	2nd 4-week	5.49 ± 0.15	3	1.61 ± 0.62	39	0.81 ± 0.03	4
	3rd 4-week	5.21 ± 0.19	4	1.33 ± 0.33	25	0.73 ± 0.04	5
	1st 6-week	8.48 ± 0.24[a]	3	1.90 ± 0.28	15	1.00 ± 0.11	11
	2nd 6-week	8.46 ± 0.12	1	1.89 ± 0.26	14	1.05 ± 0.05	5
	1st 8-week	11.18 ± 0.43	4	2.63 ± 0.27	10	1.23 ± 0.15	12
	1st 12-week	16.38 ± 0.31	2	4.31 ± 0.34	8	1.97 ± 0.35[a]	18
Toronto	1st 2-week	2.60 ± 0.15	6	0.74 ± 0.09	12	0.28 ± 0.08	28
	2nd 2-week	2.88 ± 0.12	4	0.76 ± 0.08[b]	10	0.43 ± 0.09	21
	3rd 2-week	2.66 ± 0.21	8	1.06 ± 0.21	20	0.53 ± 0.10	19
	4th 2-week	2.56 ± 0.11	4	0.75 ± 0.08[a]	10	0.23 ± 0.07	33
	1st 4-week	5.26 ± 0.07	1	1.48 ± 0.13	9	0.35 ± 0.07	20
	2nd 4-week	5.40 ± 0.33	6	1.66 ± 0.28	17	0.43 ± 0.07	17
	3rd 4-week	5.43 ± 0.15	3	1.46 ± 0.15	10	0.42 ± 0.08	18
	1st 6-week	8.04 ± 0.33	4	2.09 ± 0.22	11	0.90 ± 0.12	13
	2nd 6-week	8.24 ± 0.24	3	2.11 ± 0.33	16	0.85 ± 0.10	12
	1st 8-week	10.88 ± 0.16	1	2.28 ± 0.09	3	1.38 ± 0.27	19
	1st 12-week	16.87 ± 0.27	2	3.93 ± 0.13	3	1.70 ± 0.12[a]	7

[a] duplicate only, [b] no replication

Table 6.5 Mean, standard deviation (SD) and relative standard deviation (RSD) of the amounts of Hg (ng) in deployed PASs after blank correction for each of the 22 deployments. The values refer to triplicates, unless otherwise specified. SDs are calculated by propagating the SD of both the amounts in Table 6.4 and of the field blank levels in Table 6.2.

Since the field blanks did not show a dependence on deployment length for any sampler but did display differences between Rende and Toronto deployments for some samplers, the blank correction was performed using the average value of all field blanks deployed at one sampling site. The precision of the blank-corrected amount was determined by propagating the standard deviations of the Hg amount in exposed samplers and of the Hg amounts in field blanks. The precision (RSD%) for the three type of samplers, averaged for different deployment lengths, at the two sites and across all replicated deployments were showed in Figure 6.5 and the numerical data were reported in Table 6.7.

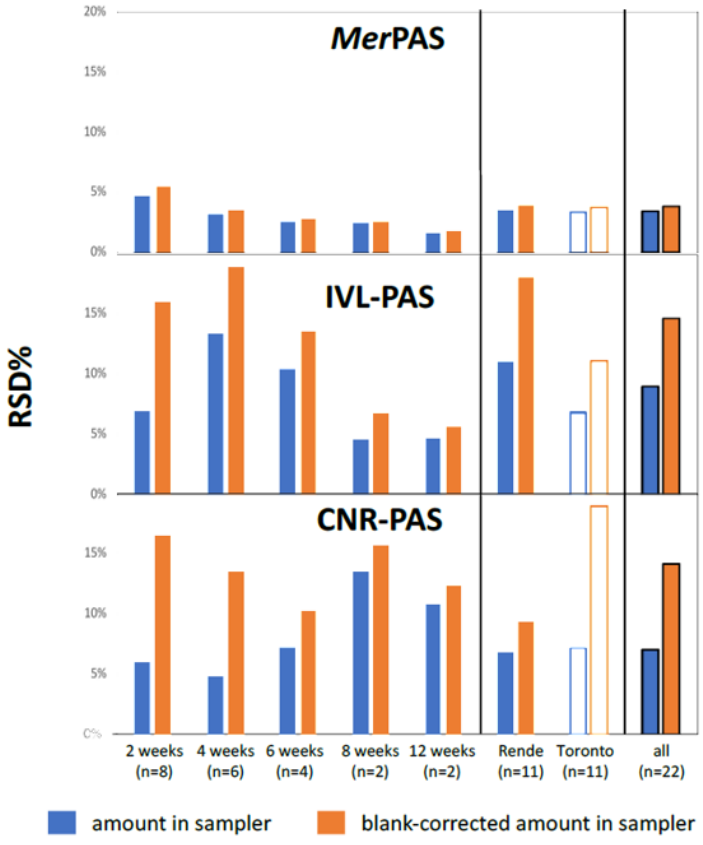

Figure 6.5 Precision expressed as the relative standard deviation in percent of the amounts of Hg quantified in triplicate PASs, both before (blue) and after blank correction (orange), averaged over different deployment lengths, across different sites and over all replicated deployments. In some cases, a sampler was lost and therefore some deployments were only duplicated.

	n	*Mer*PAS®		IVL-PAS		CNR-PAS	
		***m*PAS**	***m*PAS-*m*FB**	***m*PAS**	***m*PAS-*m*FB**	***m*PAS**	***m*PAS-*m*FB**
2-week deployments	8	4.7	5.5	7.0	16	6.0	17
4-week deployments	6	3.3	3.6	13	19	4.8	14
6-week deployments	4	2.7	2.8	11	14	7.3	10
8-week deployments	2	2.6	2.7	4.7	6.8	13.4	16
12-week deployments	2	1.7	1.7	4.7	5.7	10.7	12
Rende deployments	11	3.5	4.0	11	18	6.9	9.3
Toronto deployments	11	3.4	3.8	6.8	11	7.2	19
all deployments	22	3.5	3.9	9.1	15	7.0	14

Table 6.6 Values of average replicate precision (in %) of the amount of Hg quantified in a PAS (m_{PAS}) and of the blank-corrected amount of Hg in a PAS (m_{PAS}-m_{FB}). n indicates the number of deployments of a certain type.

As reported in Table 6.7 across all 22 replicated deployments, *Mer*PAS®, IVL-PAS and CNR-PAS devices had an average precision of 3%, 9% and 7%, respectively. Replicate precision was generally similar in Rende and Toronto deployments for *Mer*PAS® and CNR-PAS devices, while only the IVL-PAS had on average slightly lower precision in Rende (~11%) than in Toronto (~ 7%). Moreover, with increasing deployment length the replicate precision of the *Mer*PAS® declined slightly (from ~5% for the 2-week samples to ~2% for the 12-week samples). It is possible to assume that larger amounts of Hg to be quantified more reliably than smaller amounts explaining such a trend. The *Mer*PAS®, for example, collected about 3 ng of Hg in a two-week period, but about 17 ng in a 12-week deployment. The IVL-PAS showed an improve in precision with longer deployment between the 4-week (~13%) and the 12-week samples (~5%). However the relatively good precision of the 2-week samples which was ~7%, did not fit this pattern. The precision of the CNR-PAS was not related to deployment length, with the lowest precision for the 8-week deployments (~13%) and the highest precision for the 4-week deployments (~5%). The precision was 4%, 15% and 14% for *Mer*PAS®, IVL-PAS and CNR-PAS, respectively when evaluated on the blank-corrected mercury amounts in replicate samplers and it was worse than for the non-blank corrected amount, due to the variability of the field blank levels adds uncertainty (Table 6.7). This increase in

uncertainty upon blank correction strongly depends on how large the blank contamination is relative to the amount in exposed samplers explaining why the increase is much smaller for the *Mer*PAS® with respect to the other two samplers and also why the increase is larger for shorter deployment periods. As reported in Table 6.4, the blank correction for IVL-PAS and CNR-PAS deployed for 2 weeks was fairly large ranging from 28 to 47% of the amount quantified in exposed samplers. Therefore, the uncertainty of the deducted amount added notably to the uncertainty of the blank-corrected value. Regarding the CNR-PAS, the blank-correction substantially doubled the average relative standard deviation between replicates. However, the CNR-PAS also showed how sampler precision can be greatly improved by consistent field blank levels. The blank correction of the CNR-PASs deployed in Rende added less uncertainty (from 7% to 9%) than the blank-correction of those deployed in Toronto (from 7% to 19%) due to the smaller variability in the field blank levels measured in Rende (Table 6.7, Figure 6.4).

6.8.3 Accuracy

According to the Fick's law the average air concentrations during each of the 22 deployment periods was derived by dividing the blank corrected amounts in a PAS by the product of the deployment period and the sampling rate. The concentration values obtained for both deployed sites were reported in Table 6.8.

Location	Deployment	*Mer*PAS®		IVL-PAS		CNR-PAS	
		Mean ± SD (ng/m^3)	RSD (%)	Mean ± SD (ng/m^3)	RSD (%)	Mean ± SD (ng/m^3)	RSD (%)
Rende	1st 2-week	1.78 ± 0.16	9	1.66 ± 0.20	12	1.67 ± 0.09	5
	2nd 2-week	1.78 ± 0.15	9	1.66 ± 0.21	13	1.69 ± 0.10	6
	3rd 2-week	1.71 ± 0.18	10	1.84 ± 0.19	10	1.74 ± 0.10	5
	4th 2-week	1.80 ± 0.16	9	1.67 ± 0.20	12	1.76 ± 0.08	4
	1st 4-week	1.77 ± 0.16	9	1.57 ± 0.15	10	1.68 ± 0.18	10
	2nd 4-week	1.77 ± 0.15	9	2.05 ± 0.39	19	1.96 ± 0.06	3
	3rd 4-week	1.68 ± 0.15	9	1.70 ± 0.25	15	1.78 ± 0.07	4
	1st 6-week	1.82 ± 0.15[a]	8	1.60 ± 0.16	10	1.61 ± 0.12	8
	2nd 6-week	1.82 ± 0.15	8	1.61 ± 0.15	9	1.69 ± 0.07	4
	1st 8-week	1.80 ± 0.15	9	1.67 ± 0.12	7	1.49 ± 0.13	9
	1st 12-week	1.76 ± 0.15	9	1.83 ± 0.10	5	1.60 ± 0.18[a]	12
Toronto	1st 2-week	1.65 ± 0.16	10	1.77 ± 0.18	10	1.35 ± 0.28	21
	2nd 2-week	1.87 ± 0.16	8	1.86 ± 0.17[b]	9	2.12 ± 0.22	10
	3rd 2-week	1.60 ± 0.17	11	2.42 ± 0.24	10	2.40 ± 0.20	8
	4th 2-week	1.67 ± 0.16	9	1.90 ± 0.17[a]	9	1.11 ± 0.33	30
	1st 4-week	1.69 ± 0.15	9	1.79 ± 0.16	9	0.85 ± 0.21	25
	2nd 4-week	1.73 ± 0.16	9	2.03 ± 0.22	11	1.04 ± 0.17	17
	3rd 4-week	1.76 ± 0.15	9	1.84 ± 0.17	9	1.03 ± 0.18	18
	1st 6-week	1.68 ± 0.16	9	1.65 ± 0.17	10	1.42 ± 0.14	10
	2nd 6-week	1.82 ± 0.15	8	1.80 ± 0.20	11	1.41 ± 0.13	9
	1st 8-week	1.74 ± 0.15	9	1.51 ± 0.13	9	1.67 ± 0.20	12
	1st 12-week	1.81 ± 0.15	8	1.61 ± 0.13	8	1.38 ± 0.08[a]	6

[a] duplicate only, [b] no replication

Table 6.7 Mean, standard deviation (SD) and percentage relative standard deviation (%RSD) of the volumetric concentrations (ng m^{-3}) of Hg in air for each of the 22 deployments as derived by the three PASs. The values refer to triplicates, unless otherwise specified. Standard deviations are calculated by propagating the standard deviation of the amounts in Table 6.5 and assumed uncertainty of the SRs.

Each participating laboratory provided the sampling rate and its estimated uncertainty for their own PAS. The uncertainty of the *Mer*PAS® sampling rate was assumed to be 15%, that of the CNR-PAS was 4.7%, whereas the SR uncertainty of the IVL-PAS was assumed to be 6% and 13% during the deployments in Rende and Toronto, respectively. The uncertainty of the concentration values in Table 6.8 was obtained by propagating the

estimated uncertainty of the SR and the standard uncertainty of the blank-corrected amounts Table 6.6. The average value of the relative uncertainty of the volumetric concentrations of both sites, determined by values reported in Table 6.8 was very similar between the three PASs; in fact it was of 9% for *Mer*PAS® and CNR-PAS and of 8% for the IVL-PAS. However, these values cannot be directly compared with each other, as the self-reported uncertainty of the SRs was not established the same way by the three study participants.

The accuracy of the PAS-derived time-averaged mercury air concentrations reported in Table 6.8 was obtained by comparing them to the average value derived by the active Tekran instruments that have operated alongside the passive devices in monitoring sites. Tekran values were considered as a benchmark for pragmatic reasons, knowing full well that this measurement itself may provide biased results [82,83,84]. In fact, during and after flow and detector accuracy audits of the active instruments were performed at both sites. As showed in Table 6.9 that summarizes the average bias and the average absolute difference between the averaged concentrations measured by the Tekran analyzers and the various passive samplers, the accuracy of all three PASs is much better during the deployments in Rende than the deployments in Toronto. The IVL-PAS and CNR-PAS results in Rende show no bias, whereas the *Mer*PAS® results were slightly positively biased (~3%). Moreover, the average absolute discrepancies were quite small in Rende, with values of ~3% for the *Mer*PAS® and ~7% for the IVL-PAS and CNR-PAS. At Toronto site, *Mer*PAS® and IVL-PAS air concentrations were biased high, on average 10% and 17%, respectively, showing a positive bias whereas the CNR-PAS levels were on average 9% lower than the Tekran results. In the same site, the average absolute discrepancies range from 10% of the *Mer*PAS® to 18% for the IVL-PAS and 25% for the CNR-PAS.

		***Mer*PAS®**	**IVL-PAS**	**CNR-PAS**
Rende	Bias (%)	2.8	-0.5	-1.4
(n=11)	Absolute discrepancy (%)	2.9	7.1	6.1
Toronto	Bias (%)	10.2	17.0	-8.8
(n=11)	Absolute discrepancy (%)	10.2	17.8	24.9

Table 6.8 Average bias and average absolute discrepancy between the time-averaged volumetric air concentrations of Hg derived by PASs and Tekran.

The discrepancies of the PAS results from the average concentrations measured by the Tekran analyzers for each of all the 22 sampling periods at both sites are illustrated in Figure 6.6. This Figure additionally shows that there is no apparent relationship between the accuracy of the PASs and the length of the deployment period in Rende. Positive or negative discrepancies indicate a PAS-derived concentration higher or lower than the Tekran value, respectively. Moreover, for the *Mer*PAS®, at Toronto site, there is also no relationship between discrepancies and deployment length. The high bias tends to be consistent indicating that the SR was likely higher than the applied value of 0.111 m^3 day^{-1}. During the longer deployments in Toronto (6 weeks and up), the discrepancy of the IVL- and CNR-PAS from the Tekran results tend to be smaller and in fact, for the IVL-PAS the discrepancies tend to get smaller with increasing deployment times. This makes sense considering that the uncertainty introduced by the blank-correction becomes much smaller with longer deployments. The three 4-week deployments of the CNR-PAS in Toronto are consistently biased very low (by about 50 %), whereas the two sampling periods with very high bias are both 2-week deployments, so, it is difficult to decipher a consistent pattern in the discrepancies

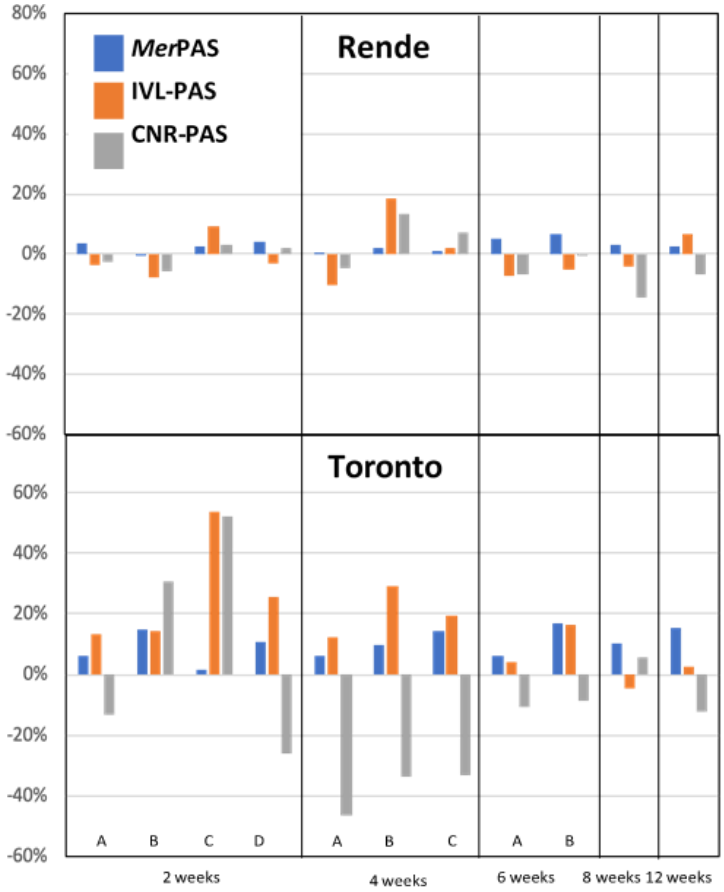

Figure 6.6 Discrepancies of the time averaged air concentrations of mercury during 22 deployment periods as derived by the three PAS from the average concentration obtained by an active Tekran system used at the same time. Deployments in Rende and in Toronto are displayed in the upper and in the lower panel, respectively. Positive or negative discrepancies indicate a PAS-derived concentration higher or lower than the Tekran value, respectively.

The variance partitioning analysis coupled with mixed effects models, (Figure 6.7) confirmed that all PAS-derived concentrations were significantly closer to the Tekran values for the deployments at Rende site than they were for the deployments at Toronto site. The significance level by which the mean absolute concentration difference of a "dataset" differs significantly from 0, (i.e., whether PAS-derived concentrations deflect significantly from Tekran-measured concentrations) is indicated by asterisks in Figure 6.7. In Rende, the mean concentration differences for all three PASs individually, and when the data were grouped among all PASs, were not significantly different from 0. Instead, in Toronto both when all three PASs were taken individually, and when the data were grouped among all PASs all of the mean concentration differences were significantly different from 0.

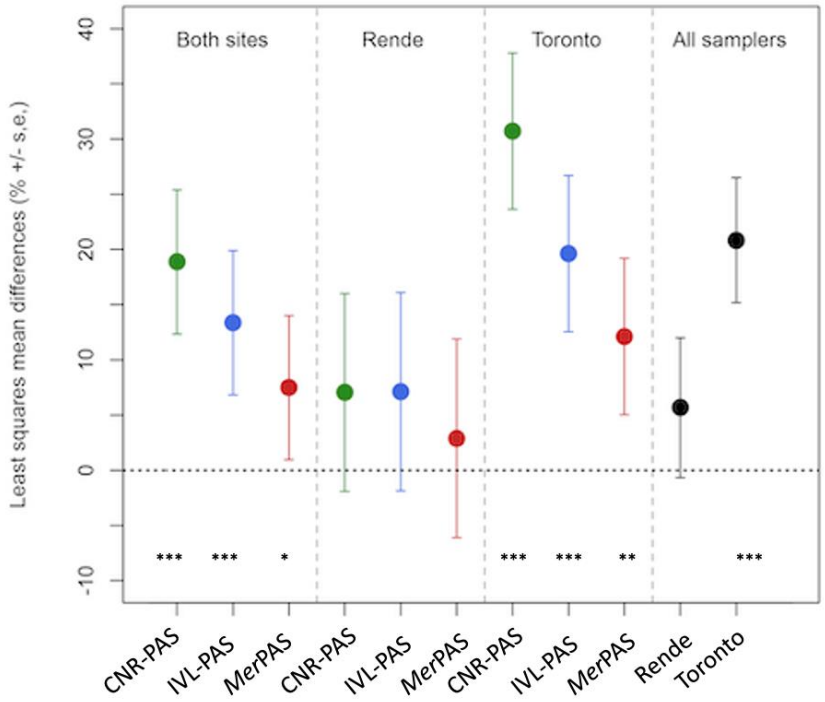

Figure 6.7 Least square means and standard errors of the differences in concentrations measured by the PASs and by the Tekran units. Results are shown either for each PAS individually (colored markers: green, blue and red for CNR-PAS, IVL-PAS and MerPAS®, respectively) or for the three PAS together (black markers). The asterisks indicate the significance level at which a mean absolute concentration difference of a "dataset" differs significantly from 0 (where *** denotes $p \leq 0.001$; ** denotes $p \leq 0.01$; and * denotes $p \leq 0.05$).

Given that the same concentrations measured by different methods resulted not be significantly different in Rende implies that the uncertainty of the concentrations derived from all three PASs deployed in Toronto must have been underestimated, that is the assumed uncertainty of the SR applied in the calculation of the concentrations must have been too small. Whether meteorological conditions during a deployment deflect largely from those prevailing during the calibration of a PAS, as they did for all three PASs during a Toronto winter, it is possible top hypothesize that SR is subject considerably higher uncertainty, than if calibration and application occur under similar environmental conditions. The variance decomposition analysis attributed roughly half of the variance in percentage differences to the PAS type (48.3%) and most of the other half of total variance by differences observed between Toronto and Rende (site = 46.8%) (Table 6.10).

Variable	Proportion explained
Site	**0.4678**
Period	0.0000
PAS ID	**0.4834**
Tekran ID	0.0474
Unexplained	0.0015

Table 6.9 Variance decomposition analysis partitioning variability in the percent concentration differences between Tekran® and PASs, across four nested levels. Factors explaining the largest proportion of the variation are highlighted in bold.

According to the mixed effects model, there were significant differences for both site (Rende vs. Toronto; $p < 0.001$) and PAS type ($p = 0.006$) (Table 6.11).

Term	Sum Sq.	Mean Sq.	Num D.F.	Den. D.F.	*F* value	*p* value
PAS ID	**1903.6**	**951.8**	**2**	**83**	**5.37**	**0.006**
Site	**5036.6**	**5036.6**	**1**	**83**	**28.43**	**<0.001**
PAS ID*Site	838.6	419.3	2	83	2.37	0.100

Table 6.10 Results of a mixed effects model predicting percent concentration differences between Tekran and PASs. Significant terms are highlighted in bold, and the model was fit while accounting for deployment time and location as random effects (where these random effects exerted a significant effect on concentration differences, $\chi^2=8.7$, $p=0.003$).

In the post-hoc least squares comparison Table 6.12, differences amongst PAS types were not significant from one another at Rende ($p = 0.458$ to 0.992). At Toronto, the percentage difference between Tekran and PAS concentrations was not significant between the IVL-PAS and *Mer*PAS® samplers ($p = 0.312$), but both the IVL ($p = 0.013$) and *Mer*PAS® ($p < 0.001$) had concentrations significantly closer to Tekran values than did the CNR sampler.

Factors compared	PAS 1	Site 1	PAS 2	Site 2	Estimated difference (%)	*t* value	*p* value
PAS	CNR-PAS	-	IVL-PAS	-	5.5	1.59	0.116
PAS	**CNR-PAS**	-	***Mer*PAS®**	-	**11.4**	**3.28**	**0.002**
PAS	IVL-PAS	-	*Mer*PAS®	-	5.9	1.69	0.095
Sites	-	**Rende**		**Toronto**	**-15.1**	**-5.33**	**<0.001**
PAS-by-Sites	CNR-PAS	Rende	IVL-PAS	Rende	-0.1	-0.01	0.992
PAS-by-Sites	CNR-PAS	Rende	*Mer*PAS®	Rende	4.2	0.74	0.464
PAS-by-Sites	**CNR-PAS**	**Rende**	**CNR-PAS**	**Toronto**	**-23.7**	**-4.81**	**<0.001**
PAS-by-Sites	**CNR-PAS**	**Rende**	**IVL-PAS**	**Toronto**	**-12.6**	**-2.56**	**0.012**
PAS-by-Sites	CNR-PAS	Rende	*Mer*PAS®	Toronto	-5.1	-1.03	0.307
PAS-by-Sites	IVL-PAS	Rende	*Mer*PAS®	Rende	4.2	0.75	0.458
PAS-by-Sites	**IVL-PAS**	**Rende**	**CNR-PAS**	**Toronto**	**-23.6**	**-4.8**	**<0.001**
PAS-by-Sites	**IVL-PAS**	**Rende**	**IVL-PAS**	**Toronto**	**-12.5**	**-2.54**	**0.013**
PAS-by-Sites	IVL-PAS	Rende	*Mer*PAS®	Toronto	-5	-1.02	0.312
PAS-by-Sites	***Mer*PAS**	**Rende**	**CNR-PAS**	**Toronto**	**-27.8**	**-5.66**	**<0.001**
PAS-by-Sites	***Mer*PAS**	**Rende**	**IVL-PAS**	**Toronto**	**-16.7**	**-3.41**	**0.001**
PAS-by-Sites	*Mer*PAS	Rende	*Mer*PAS®	Toronto	-9.2	-1.88	0.064
PAS-by-Sites	**CNR-PAS**	**Toronto**	**IVL-PAS**	**Toronto**	**11.1**	**2.76**	**0.007**
PAS-by-Sites	**CNR-PAS**	**Toronto**	***Mer*PAS®**	**Toronto**	**18.6**	**4.64**	**<0.001**
PAS-by-Sites	IVL-PAS	Toronto	*Mer*PAS®	Toronto	7.5	1.87	0.065

Table 6.11 Statistical comparison of least square mean differences in concentrations, across different passive sampler models, sites, and all passive air sampler (PAS) model-by-site combinations. Comparisons here are based on a linear mixed effects model (presented in Table 6.9) predicting concentration differences as a function of sampler, site, and a sampler-by-site interaction, while accounting for sampling location and time as random effects. Significant differences are highlighted in bold.

6.8.4 Linearity of uptake

Passive sampler performances depend on having an uptake capacity that is sufficiently high for mercury to remain in a linear uptake phase throughout the entire deployment period. It is possible test the passive sampler performances by assessing the linearity of uptake by plotting the blank-corrected amount quantified in the samplers m_{PAS} against the sampler deployment time Δt, even this disregards the variability in the GEM concentrations between different deployments. The influence of the GEM concentration

variability can be eliminated by plotting the amount in a sampler against the product of Δt and the average air concentration during the deployment of that sampler C_{air} [99]. In this study, the data from the Tekran instruments as the input for C_{air} were used. Using the data in this way amounts to a process of sampler calibration, as the slope of the linear relationship between m_{PAS} in ng and Δt C_{air} in units of days ng m^{-3} corresponds to the SR of the PAS in m^3 day^{-1}. The uptake plots for all three passive samplers at the two sampling sites and the linear regression lines fitted to the displayed data were showed in Figure 6.8.

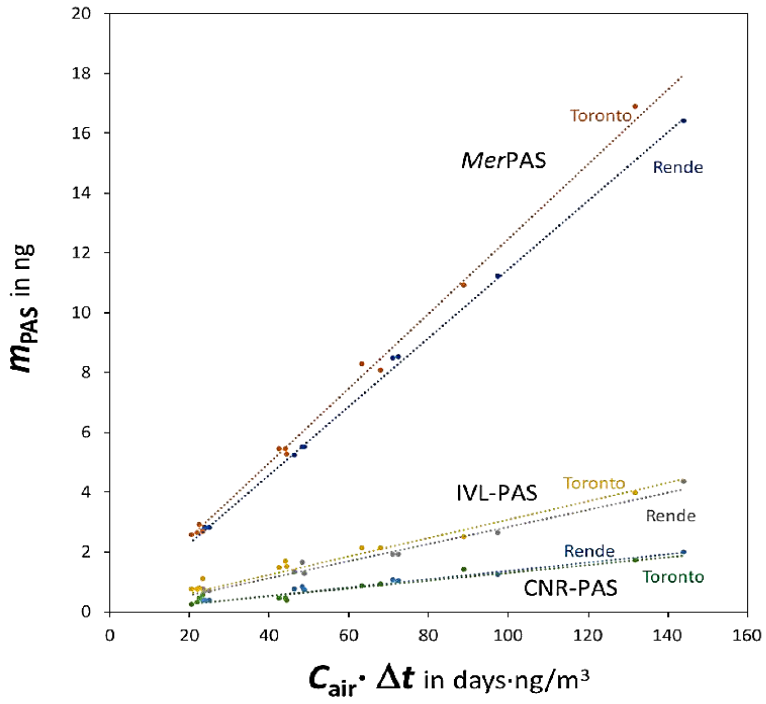

Figure 6.8 Plot of the blank-corrected amount of Hg quantified in the three types of PAS deployed in Rende and Toronto against the product of the deployment time of a sampler Δt and the average ambiet air concentration during the deployment of that sampler C_{air}, as determined independently by a Tekran active sampling system.

The numerical data of the slopes with standard error of the regression line, which has been forced through the origin, and the coefficient of correlation r^2 were reported in Table 6.13. The slopes determined are also the sampling rates applicable to the PASs at the two sites during the period of the study.

Sampler	Location	*SR* (m^3 day^{-1})	Relative SE (%)	r^2	*a priori* SR (m^3 day^{-1})	SR difference (%)
*Mer*PAS®	Rende	0.1144 ± 0.0006	0.5	0.9997	0.111	+3
	Toronto	0.1247 ± 0.0014	1.1	0.9988	0.111	+12
IVL-PAS	Rende	0.0284 ± 0.0006	2.2	0.9951	0.03	-5
	Toronto	0.0309 ± 0.0009	3.0	0.9911	0.03	+3
CNR-PAS	Rende	0.0139 ± 0.0003	2.2	0.9951	0.0147	-6
	Toronto	0.0131 ± 0.0007	5.5	0.9710	0.0147	-11

Table 6.12 Numerical results of the linear regressions showed in Figure 6.8. The slope of the regression line corresponds to the SR of a PAS at the considered site.

As reported in both representations, all uptake were linear with high r^2 values and small relative standard errors of the slope of the linear regressions that were 1% for *Mer*PAS®, 2 to 3% for IVL-PAS, 2 to 5% for CNR-PAS. Figure 6.8 also confirms that forcing the regression through the origin was justified, indicating that the blank correction was largely effective for all three samplers. Consistent with what should be expected from the sampler performance at the two sites, the regressions were generally better for deployments in Rende than in Toronto, suggesting that the PASs had better performances during deployments in Rende than in those in Toronto. Overall, it is clear that all three samplers perform as true linear uptake samplers at both locations over a three-month period. Moreover, in Table 6.13 is showed a comparison between the site- and deployment specific SRs obtained from the regressions with the generic a priori ones that were used in the calculation of the volumetric air concentrations from the PASs. Deviations between these SRs should be roughly similar to the bias of the PAS-derived air concentrations, reported in Table 6.9. In the case of the *Mer*PAS®, they are indeed very similar (+2.8% vs. +3.1% at Rende, +10.2 vs. +12.3% at Toronto). In the case of the IVL-PAS (-0.5% vs. -5.4% at Rende, +17.0% vs. +3.0% at Toronto) and CNR-PAS (-1.4% vs. -5.7% at Rende, -8.8% vs. -10.7% at Toronto) they are less similar, although the direction of bias is the same (Table 6.9 and Table 6.13). The deviations are not exactly the same, because the longer deployments have a stronger impact on the slope of the lines in Figure 6.8 than shorter ones, whereas when the average bias given in Table 6.9 was calculated, each sample counted the same, irrespective of deployment length. It also

possible compare the relative size of the fitted SRs at the two locations. Both *Mer*PAS® and IVL-PAS the SR was 9% higher in Toronto than in Rende, while the SR of the CNR sampler shows an opposite behavior, being 5% lower in Toronto than in Rende. Local conditions can be responsible for differences in SR between deployment at different sites or different period. In particular, an increase in the molecular diffusivity of Hg in air with temperatures can lead to a higher SR at higher temperatures, whereas an increase in wind speed can reduce the thickness of the stagnant air boundary layer surrounding a PAS's diffusive barrier and therefore also lead to a higher SR [100]. During the study period, Toronto was much colder than Rende with an average during the 12 weeks deployment period of 1 °C and 12 °C, respectively and this scenario would be consistent with a lower SR in Toronto as was observed for the CNR-PAS. Moreover, wind speeds in Toronto were approximately double those in Rende with an average of 2.4 m s^{-1} and 1.2 m s^{-1}, respectively and this scenario would be consistent with higher SR in Toronto as was observed by IVL-PAS and *Mer*PAS®.

6.8.5 Possible explanation for the different performance in Rende and Toronto

The PASs performance in Rende and Toronto were different. As showed by the assessment of accuracy in Figure 6.6 and in Figure 6.7, the three type of passive devices performed better during deployments in Rende than in those in Toronto. However, this did not apply to all performance indicators because for instance, magnitude and variability in field blanks were comparable between the two deployment sites for the IVL-PAS and the *Mer*PAS®, while only the CNR-PAS had much more variable field blank contamination in Toronto (Figure 6.4). Moreover, replicate precision prior to blank correction for *Mer*PAS® and CNR-PAS was very similar at the two monitoring sites (Figure 6.5). Instead in the case of the IVL-PAS, the replicate precision was better in Toronto. This suggest that operator handling is unlikely to be responsible for the differences in performance at the two sites. During the deployment period, which comprised the three months of February to April 2019 a major difference between the two sites was the harshness of the weather conditions. In fact, in Toronto, winter and early spring can be very cold and experience large temperature fluctuations over short time periods as well as precipitation in different forms (rain, snow, freezing rain, sleet). In this regard, as mentioned above, both temperature and the wind speed can influence the rate

of diffusion to the passive sampling sorbent, causing variability in the SRs, also because it is possible that in adverse weather conditions, the path of Hg towards the absorbent can be potentially prevented by the formation of frost on the surface of the diffusion barriers or by the snow that blown could agglomerate on the samplers. However, it will often not be possible to weather conditions as demonstrated when deviations occur in opposite direction during overlapping deployments. For example, the third 2-week and the second 4-week deployments overlap but the CNR-PAS shows positive bias in the former and negative bias in the latter. Moreover, in Toronto the higher fraction of missing or rejected data from the Tekran that operated at this site is another possible source of the discrepancies between Tekran and PAS concentrations in Toronto (Figure 6.6). Whereas in Rende, generally 98.9% was covered by valid Tekran data, the data coverage for the PAS deployment reached 82.5% for the Tekran "5037" units providing the reference value in Toronto. The reason for the lower percentage in Toronto is a sampling method that relies on daily calibrations (2.4% daily loss of coverage) and hourly (8.3% daily loss of coverage) spikes; these alone already account for a 10.7% per day loss of coverage, yet improve confidence in the data. The distribution of the standard addition spikes throughout the day however means they are unlikely to result in any bias of the results. The remainder was due to regular maintenance, and a power outage. A different, but equally valid, sampling method in Rende ran calibration every 3 days and no spikes. For individual deployments data coverage ranged as low as 66% for the fourth 2-week deployment in Toronto. However, the discrepancy between PASs and Tekran are not unusually large during that deployment period (Figure 6.6). A final difference between the two study locations is the occurrence of several short spikes of elevated GEM concentrations in Toronto. If these had been caused by a local source in immediate vicinity of the sampling site, it is conceivable that spatial GEM concentration gradients may have been present within the assembly of PASs and Tekran inlets. However, no relationship between the occurrence of such spikes and the discrepancies in PAS results is apparent. In any case, it is more likely the spikes were caused by sources sufficiently far from the sampling site to not result in concentration gradients on the scale of a few meters.

6.9 Highlights from the inter-comparison campaign

In this case study, the results of a field-based inter-comparison campaign and a controlled, blind performance comparison among different mercury PASs, at two monitoring sites located in Italy (Rende) and Canada (Toronto), over a three-month period were reported. The PASs involved in this study were developed by the Italian Institute of Atmospheric Pollution Research (CNR-IIA) [88], the Swedish Environmental Research Institute (IVL) [91] and the University of Toronto [89]. The geometry of CNR-PAS and IVL-PAS makes them both axial diffusion samplers, while the *Mer*PAS® is a radial sampler. All three passive samplers are based on the unassisted molecular diffusion of the target species from the ambient air onto an absorbent membrane. Each participating research group supplied their PASs along with deployment instructions, performed the chemical analysis and reported volumetric air concentrations and basic QA/QC results to an independent third party. At the two monitoring sites the performances of the PASs were assessed for accuracy through comparison with active sampling data, for precision and for sensitivity, as well as in terms of the linearity of uptake over extended deployment periods. The results showed that the performance of the PASs was significantly better in Italy, with all of them providing concentrations that are not significantly different from the average of the active sampling results. In Canada, where weather conditions were much harsher and more variable during February-April deployment period, differences were observed among PASs. The results showed that *Mer*PAS® is the most sensitive, precise and accurate at both sites. All key performance indicators for the three passive air samplers determined in this study were reported in Table 6.14.

	***Mer*PAS®**	**IVL-PAS**	**CNR-PAS**
MDL (ng)	0.16	0.25	0.13
LOD (2 weeks) (ng m^{-3})	0.10	0.59	0.65
LOQ (2 weeks) (ng m^{-3})	0.34	1.98	2.16
LOD (12 weeks) (ng m^{-3})	0.02	0.10	0.11
LOQ (12 weeks) (ng m^{-3})	0.06	0.33	0.36
Replicate precision (before blank correction) (%)	3	9	7
Replicate precision (after blank correction) (%)	4	15	14
Concentration bias (relative to Tekran), n = 22 (%)	+6.5	+8.2	-5.1
Absolute discrepancy (relative to Tekran), n = 22 (%)	6.5	12.5	15.5
Linear uptake over 12 weeks	Yes	Yes	Yes

Table 6.13 Summary of the key metrics describing the performance of the three PASs for Hg as determined in this study.

Table 6.14 shows the average of all values obtained from the Rende and Toronto deployments and highlights that the *Mer*PAS® is currently the best performing passive device, having the lowest LODs, the highest precision and the best accuracy based on the discrepancy from the Tekran system. The better performance of the *Mer*PAS® is due to the sampler larger size and radial diffusion configuration, which leads to much higher SRs than the other samplers, IVL-PAS and CNR-PAS, which are axial diffusion samplers and also much smaller in size. Therefore, *Mer*PAS® results in blank levels than are lower to the sequestered quantities of mercury compared to the other two PAS, with axial diffusion geometries. In fact, a higher SR value means that the amount of Hg absorbed into a *Mer*PAS® during a deployment is much higher than the blank contamination level compared to the other two samplers, which have very similar blank contamination levels. Consequently, as the blank correction becomes relatively smaller with a longer distribution, sampler performance tends to be better during the 8- and 12-week deployments. From the performance comparison at the two monitoring sites is evident

that inconsistent and relatively high blank contamination levels could hinder the performance of a PAS. For CNR-PAS, higher and more variable blank levels in Toronto result into much higher LOD values as showed in Table 6.9 and much poorer precision after blank correction compared to Rende site. Therefore, a reduction in the magnitude and variability of blank contamination and/or a change in the sampler size and configuration that increases the SR could represent ways for improvement for passive device. Moreover, the study showed that the SRs of the CNR-PAS at the two sites are more similar compared to the other two PASs. This is a promising result which may suggest that SR has a relatively small dependence on meteorological factors, though this will still need to be confirmed by calibrating the sampler under a wide variety of meteorological circumstances. The summary of the key metrics describing the performance of the passive devices used in this study shows that IVL-PAS and CNR-PAS are remarkably similar in their performance characteristics with very similar LOD values and replicate precision (Table 6.14). Overall, the average bias of the CNR-PAS is small largely because fairly large discrepancies occur in either direction and, therefore, cancel each other out. Overall, the IVL-PAS derived air concentrations agree better with the Tekran derived data than those of the CNR-PAS (12.5 vs. 15.5%). The *Mer*PAS® derived air concentrations were on average 6.5% higher than the Tekran-derived values, and this positive bias was evident at both deployment sites, although more pronounced in Toronto. The usefulness of a passive mercury sampler depends on its ease-of-use and robustness under field conditions, its availability and affordability, and most notably, its ability to provide results of acceptable precision and accuracy. Therefore, this study through a systematic comparison of the performance of three mercury passive samplers highlighted the usefulness of each of them as regard monitoring mercury, confirming that PASs represent a good alternative or supplemental system to the traditional monitoring techniques allowing to fill the gaps in the monitoring of Hg worldwide due to limitations imposed by the use of conventional instrumentation.

Chapter 7

Conclusions and future remarks

Mercury (Hg) is a highly toxic pollutant, which implies negative consequences on both environment and human health. Its global load in the atmosphere, due not only to natural sources but also to decades of emissions deriving from anthropogenic activities, has highlighted the demand for actions aimed at reducing its emissions at European and global scale. Due to its properties, once mercury has entered the environment, it remains there adopting different physical and chemical forms reaching all of the environmental compartments to a greater or lesser extent: air, soil, water, sediments. Further, its long residence time (0.5–2 years) in the atmosphere, due to its high volatility and low solubility in water, make possible that, once released into the atmosphere, it is easily transported over long distances, even reaching remote regions. For these reasons in recent years, the scientific community attention is focusing on the need of a global perspective in research, monitoring and policymaking. In fact, mercury has been added to the environmental political agenda at national, regional, and global levels. Scientific and political communities are therefore engaged in assessing the current state of mercury environmental pollution and the consequent impact of its emissions on human health and the environment. An increase in mercury levels in ambient air could in fact results in an increase in direct human exposure and an increase in the flow of mercury entering terrestrial and aquatic ecosystems, with post-depositional consequences that, as extreme case, could determine circumstances like those occurred in the historical episode, known as the Minamata disaster. In this context, the Minamata Convention on Mercury was adopted with the aim of protecting human health and the environment from Hg releases and emissions (Article 1), highlighting the importance of environmental monitoring (Article 19), and requesting the Parties to formally assess, through the provision of "comparable monitoring data on the presence and movement of mercury and mercury compounds in the environment", how effective the structure and implementation of the Convention is, in achieving its main objective (Article 22). Therefore, it is evident that an accurate mercury assessment is useful for understanding its transport and deposition

mechanisms in ecosystems, and it is necessary to pay particular attention to the atmosphere which is an important pathway for Hg distribution throughout various environmental compartments. These efforts, in addition to building on existing regional and global monitoring networks, also require research and development of innovative monitoring technologies. Indeed, despite the current active air sampling instruments have been proven to be effective instruments for monitoring atmospheric mercury, they do not allow a high spatial resolution data coverage, due to their high purchase and management costs, request for high purity gas, and highly trained technical personnel for operation and maintenance. In this context, during this Ph.D. period the research study has been focused on atmospheric mercury monitoring, carried out using direct measurements during field campaigns, through both conventional and innovative methodologies. For each of these approaches specific case-studies have been performed and herein presented and discussed. The conventional active analyzers were employed to record the concentrations of atmospheric mercury at three monitoring background stations, located at different Italian sites. Measurements were carried out following the Standard Operational Procedures (SOPs) developed and employed within the GMOS global network, and based upon the European standard (NEN-EN 15852) for TGM and GEM measurements and the Canadian CAMNet/CAPMoN SOP for TGM measurements, and on the United States Atmospheric Mercury Network (AMNet) Standard Operational Procedure for Hg speciation. SOPs describe methods for determining total gaseous mercury (TGM) and gaseous elemental mercury (GEM) in ambient air using the Tekran 2537 or the Lumex RA 915 AM and mercury species (GEM, and oxidized Hg species and Hg bound particular matter) using the Tekran integrated system (Tekran 2537/1130/1135). The Tekran system uses CVAFS to quantify ambient mercury concentrations, while the Lumex system uses Zeeman CVAAS. Total gaseous mercury (TGM) is the sum of gaseous elemental mercury (Hg^0; GEM) and gaseous oxidised mercury (GOM), which may constitute from both inorganic and organic gaseous mercury species. Automatic TGM instruments (i.e., Tekran and Lumex) use the amalgamation technique to trap gaseous mercury in the air. Exactly determined air volumes are pulled through a cartridge containing an adsorbent (a gold surface), onto which all gaseous mercury quantitatively is adsorbed. Mercury is then thermally desorbed as GEM (Hg^0) and detected by CVAFS or alternatively by CVAAS. The mass of Hg^0 as a function of the detector response is

obtained by calibration using known amounts of Hg^0 vapour. The accuracy of the measurement depends on the accuracy of the calibration and the air volume measurements. The CVAFS method is more sensitive compared to CVAAS, but instruments based on this analytical technique require pure Ar or He gas during the desorption and detection step, whereas CVAAS instruments use mercury free air or nitrogen. Both CVAFS and CVAAS instruments detect mercury as GEM by UV radiation at 253.7 nm. The observations carried out using conventional instruments during the Ph.D. case studies allowed to evaluate the temporal variability of the atmospheric mercury concentrations on hourly, daily, monthly, and seasonal basis. In detail, the investigated Italian sites were Monte Sant'Angelo (MSA) and Montelibretti (MLI) monitoring stations, belonging to the Special Network "Reti Speciali" agreement on mercury, and Monte Curcio (MCU) monitoring station, which is a research infrastructure managed by the CNR-IIA, belonging to the GMOS network. As regard to the atmospheric mercury measurements at MSA and MCU stations, the atmospheric concentrations of TGM were monitored using a Lumex and a Tekran analyzers, respectively, while at MLI station, the atmospheric mercury species (GEM, GOM and PBM) were simultaneously monitored, through a Tekran integrated system. During the study research, with respect to all datasets collected with active traditional instrumentation, a particular attention has been paid to the quality data control developed according to conventional measurement practices and methods followed within existing regional and global monitoring networks to achieve a high degree of harmonization. Over the obtained valid Hg datasets for MCU and MLI, and also over the GEM dataset recorded at MSA by a Lumex, other control criteria, widely used in the scientific community, have been then applied, to obtain statistically representative data at a broader time resolution (hourly, daily, monthly and seasonally). During the performed monitoring campaigns, the recorded TGM, GEM, GOM and PBM higher concentrations were considered to deepen the specific conditions that led to the observed increases. In particular, the highest TGM daily average concentration was observed at MSA station whereas the lowest at MCU. Successively, through the evaluation of the local meteorological parameters, recorded at the investigated stations, and with the support of satellite maps, provided by NAAPS and MODIS, as well as of the air masses backward trajectories, obtained by running the NOAA-HYSPLIT model, made it was possible to identify the plausible mercury sources

affecting the recorded measurements. Within natural sources, specific events of wildfires and Saharan dust intrusions, were detected to influence the peak concentrations of TGM/GEM at both the three involved stations, as well as the specific event with a peak in GOM levels observed at MLI. Otherwise, regarding anthropogenic sources, some Italian thermoelectric power plants, located in the proximity of the sampling stations, were identified to be the most likely reason of higher background TGM concentrations at MSA as well as of a specific episode that led a marked increase in PBM levels recorded at MLI.

Besides the conventional instrumentations, the research study has been focused on passive air samplers (PASs) monitoring systems that although do not operate in real time, are potentially suitable for overcoming the limitations of active monitoring systems that could play a key role in improving the monitoring of atmospheric gaseous mercury thanks to their low cost, ease of transport and use and the ability to operate without electricity.

From a global perspective, is indeed essential for providing a good spatial resolution of mercury measurements worldwide to develop technologies and new sensing systems for rapid Hg detection. These new devices should be robust, traceable and should not require either a gas carrier, a significant energy supply or highly qualified technical expertise. By allowing for simultaneous, cost-effective measurements at a multitude of sites, passive air samplers (PASs) could play an important role in this context if it can be shown to be suitable for monitoring long-term background concentrations, concentration gradients in and around Hg sources, and personal exposure levels. Indeed, passive devices enable the simultaneous spatial Hg measurements in different areas, thus creating a map of the Hg concentration surrounding the emission sources and allowing for the extension of monitoring network for mercury, in order provide more complete boundaries of the presence of mercury as well as a better understanding of the environmental factors that interact globally and regionally the global biogeochemical cycle of this pollutant.

In this context, an in-depth study has been dedicated to the development and construction of passive samplers for gaseous mercury (PASs), with specific regard to those engaged by the CNR-IIA. These last consist of a layer of Titania nanoparticles (TiO2NPs, $\leq$ 25 nm diameter) finely decorated with gold nanoparticles (AuNPs), and drop-casted on a thin quartz slice, which was incorporated into a common axial sampler which consists of a borosilicate glass vessel equipped with a double cap system to minimize operator

handling and avoid contamination due to the cap opening. This CNR-PAS has been settled in the framework of the project "*Development of a Plan for Global Monitoring of Human Exposure to and Environmental Concentrations of Mercury*". To assess the analytical performance of these new devices an intensive inter-comparison campaign has been carried out to make a direct comparison on field between the CNR-PAS sampler with other two types of passive samplers, referring both to atmospheric mercury measurements performed by active sampling systems for monitoring. The other two passive sampling devices involved in the inter-comparison campaign were that developed by the Swedish Environmental Research Institute IVL (IVL-PAS), which consists of a disk coated with an activated carbon sorbent inserted in a badge-type device, and that known as *Mer*PAS®, developed by the University of Toronto and commercialized by Tekran, consisting of sulfur-impregnated activated carbon (HGR-AC, Calgon Carbon Corporation), housed in a stainless-steel mesh cylinder inserted into a commercially available White Radiello® (Sigma Aldrich) diffusive body. All three passive samplers are based on the unassisted molecular diffusion of the target species from the ambient air onto an absorbent membrane and the geometry of CNR-PAS and IVL-PAS makes them both axial diffusion samplers while the *Mer*PAS® is a radial sampler.

The inter-comparison campaign was carried out over a three-month period, at two monitoring sites located in Italy (Rende) and Canada (Toronto), where the performances of the PASs have been assessed for accuracy through comparison with active sampling data, for precision and for sensitivity, as well as in terms of the linearity of uptake. The results of this study through a systematic comparison of the performance of three mercury PASs highlighted their usefulness for monitor mercury. In Italy, the performance of the PASs was significantly better since all provided concentrations were not statistically significantly different from the average of the active sampling results, while in Canada, where weather conditions were much harsher and more variable during the deployment period could influence the PASs performance differences were observed amongst passive devices investigated. The results showed that *Mer*PAS® is the most sensitive, precise and accurate device at both monitoring sites, probably due to the sampler larger size and radial diffusion configuration, which leads to much higher Sampling Rate (SR) than IVL- and CNR-PAS. Moreover, as regards CNR-PAS the results obtained showed that SR values of this sampler were more similar at two sites with respect to the IVL-PAS and *Mer*PAS®,

suggesting that SR has a relatively small dependence on meteorological factors, although this will still need to be confirmed by calibrating the sampler under a wide variety of meteorological circumstances. Consequently, the good and promising results obtained from this study made it possible to consider the PASs as a valid and promising alternative to traditional monitoring techniques, even if the only potential use in place of conventional methods still requires further investigations in the field, also aimed at confirming their robustness against the influence of meteorological parameters. The development and employment of innovative technological systems for the measurement of Hg in ambient air such as PAS within the global GMOS network, in support of the Minamata Convention on Mercury, allows the strengthening of the monitoring network itself by increasing the number of survey sites selected and allowing the sustainability at lower costs of the long-term management of the monitoring network on a global scale. Furthermore, the use of PASs improves the spatial resolution of mercury measurements in order to consider all possible geographic and meteorological conditions and, used in a complementary way with traditional instrumentations, offer a better understanding of the mercury cycle in the environment.

Contributions

List of paper, oral or poster presentations of some results reported in this thesis that have been presented in various conferences and congresses during the Ph.D. studies:

- F. Sprovieri, A. Naccarato, A. Fino, A. Macagnano, E. Zampetti, P. Papa, A. Joshua, A. Tassone, M. Martino, S. Moretti, N. Pirrone, "Assesing mercury air levels using passive air samplers (PASs) as part of the GMOS network in the framework of the UNEP GEF project". Poster, 14th International Conference on Mercury as a Global Pollutant (ICMGP 2019), Cracovia, 08-13 september 2019
- F. Sprovieri, A. Naccarato, A. Fino, A. Macagnano, E. Zampetti, P. Paolo, A. Joshua, A. Tassone, M. Martino, S. Moretti, N. Pirrone "Assessing mercury air levels using passive air samplers (PASs) as part of the GMOS network in the framework of the UNEP GEF project". Abstract Volume -Poster ABSTRACTS – ICMGP 2019 - 14th International Conference on Mercury as a Global Pollutant, Cracovia (Polonia), 08-13 september 2019
- Naccarato, A., Tassone, A., Martino, M., Moretti, S., Macagnano, A., Zampetti, E., Papa, P., Avossa, J., Pirrone, N., Nerentorp, M., Munthe, J., Wängberg, I., Stupple, G. W., Mitchell, C. P. J., Martin, A. R., Steffen, A., Babi, D., Prestbo, E. M., Sprovieri, F., and Wania, F.: A field intercomparison of three passive air samplers for gaseous mercury in ambient air, Atmos. Meas. Tech. Discuss. [preprint], https://doi.org/10.5194/amt-2020-455, in review, 2020"
- A. Tassone, S. Moretti, M. Martino, N. Pirrone, F. Sprovieri, A. Naccarato "Modification of the EPA method 1631E for the quantification of total mercury in natural waters", Methodsx, 2020, 7:100987 DOI: 10.1016/j.mex.2020.100987

List of further paper, oral or poster presentations presented at various conferences and congresses during the Ph.D. studies:

- M. Martino, A. Naccarato, A. Tassone, S. Moretti, F. Sprovieri, N. Pirrone "Organomercury compounds in biological samples: analytical approach for a thorough determination". Conference Proceedings of the CNR-Institute of atmospheric pollution research, Montelibretti (Roma), 9-10 May 2018, Edizioni Ambiente, ISBN: 978-88-6627-254-0

- A. Tassone, A. Naccarato, S. Moretti, M. Martino, F. Sprovieri, N. Pirrone "Analytical approaches for the determination of total and speciated mercury in environmental waters". Conference Proceedings of the CNR-Institute of atmospheric pollution research, Montelibretti (Roma), 9-10 May 2018, Edizioni Ambiente, ISBN: 978-88-6627-254-0
- A. Naccarato, A. Tassone, S. Moretti, M. Martino, F. Sprovieri, N. Pirrone, A. Tagarelli "Microextraction techniques and microwave-assisted extraction: a new combined approach for the analysis of the pollutants associated to the airborne particulate matter". Conference Proceedings of the CNR-Institute of atmospheric pollution research, Montelibretti (Roma), 9-10 May 2018, Edizioni Ambiente, ISBN: 978-88-6627-254-0
- S. Moretti, A. Naccarato, V. Andreoli, A. Tassone, M. Martino, N. Pirrone, F. Sprovieri "Investigation of carbonaceous compunds and trace elements occurrence in particulate matter at Monte Curcio observatory". Conference Proceedings of the CNR-Institute of atmospheric pollution research, Montelibretti (Roma), 9-10 May 2018, Edizioni Ambiente, ISBN: 978-88-6627-254-0
- A. Naccarato, J. Castagna, S. Moretti, M. Bencardino, F. Carbone, F. D'Amore, M. Martino, A. Tassone, N. Pirrone, F. Sprovieri "Investigation of particulate matter collected during three cruise campaigns in the Mediterranean Sea: composition and source apportionment". Poster, VIII Convegno Nazionale sul Particolato Atmosferico (PM2018), Matera, 23-25 May 2018
- A. Naccarato, A. Tassone, M. Martino, R. Elliani, F. Sprovieri, N. Pirrone, A. Tagarelli, "A New Green Method For The Quantification Of Benzothiazoles, Benzotriazoles And Benzosulfonamides In Airborne Particulate Matter By Microwave-Assisted Extraction Coupled With Solid Phase Microextraction Gas Chromatography Tandem Mass Spectrometry", Poster, XXVIII Congress of the Analytical Chemistry Division, Bari 22 – 26 September 2019

Bibliography

[1] N. Pirrone, P. Costa, J. M. Pacyna, and R. Ferrara, “Mercury emissions to the atmosphere from natural and anthropogenic sources in the Mediterranean region,” *Atmos. Environ.*, vol. 35, no. 17, pp. 2997–3006, 2001.

[2] G. Liu, Y. Cai, and N. O’Driscoll, *Environmental Chemistry and Toxicology of Mercury*. 2011.

[3] C. T. Driscoll, R. P. Mason, H. M. Chan, D. J. Jacob, and N. Pirrone, “Mercury as a global pollutant: Sources, pathways, and effects,” *Environ. Sci. Technol.*, vol. 47, no. 10, pp. 4967–4983, 2013.

[4] P. M. Outridge, R. P. Mason, F. Wang, S. Guerrero, and L. E. Heimbürger-Boavida, “Updated Global and Oceanic Mercury Budgets for the United Nations Global Mercury Assessment 2018,” *Environ. Sci. Technol.*, vol. 52, no. 20, pp. 11466–11477, 2018.

[5] F. Beckers and J. Rinklebe, “Cycling of mercury in the environment: Sources, fate, and human health implications: A review,” *Crit. Rev. Environ. Sci. Technol.*, vol. 47, no. 9, pp. 693–794, 2017.

[6] N. Batrakova, O. Travnikov, and O. Rozovskaya, “Chemical and physical transformations of mercury in the ocean: A review,” *Ocean Sci.*, vol. 10, no. 6, pp. 1047–1063, 2014.

[7] M. Sedlar, M. Pavlin, A. Popovieč, and M. Horvat, “Temperature stability of mercury compounds in solid substrates,” *Open Chem.*, vol. 13, no. 1, pp. 404–419, 2015.

[8] N. Pirrone and R. Mason, “Mercury fate and transport in the global atmosphere: Emissions, measurements and models,” *Mercur. Fate Transp. Glob. Atmos. Emiss. Meas. Model.*, no. Ii, pp. 1–637, 2009.

[9] R. M. Hazen *et al.*, “Mercury (Hg) mineral evolution: A mineralogical record of supercontinent assembly, changing ocean geochemistry, and the emerging terrestrial biosphere,” *Am. Mineral.*, vol. 97, no. 7, pp. 1013–1042, 2012.

[10] Unep, “Minamata Convention on Mercury - Text and Annexes,” *UNEP, 2013a*, p. 69, 2013.

[11] E. G. Pacyna, J. M. Pacyna, and N. Pirrone, “European emissions of atmospheric

mercury from anthropogenic sources in 1995," *Atmos. Environ.*, vol. 35, no. 17, pp. 2987–2996, 2001.

[12] N. E. Selin, "Global biogeochemical cycling of mercury: A review," *Annu. Rev. Environ. Resour.*, vol. 34, pp. 43–63, 2009.

[13] N. Pirrone *et al.*, "Global mercury emissions to the atmosphere from anthropogenic and natural sources," *Atmos. Chem. Phys.*, vol. 10, no. 13, pp. 5951–5964, 2010.

[14] AMAP, "Technical Background Report for the Global Mercury Assessment," *Arct. Monit. Assess. Program.*, p. 263, 2013.

[15] *Technical Background Report for the Global Mercury Assessment 2018. Arctic Monitoring and Assessment Programme, Oslo, Norway/UN Environment Programme, Chemicals and Health Branch, Geneva, Switzerland.* 2018.

[16] E. G. Pacyna, J. M. Pacyna, J. Fudala, E. Strzelecka-Jastrzab, S. Hlawiczka, and D. Panasiuk, "Mercury emissions to the atmosphere from anthropogenic sources in Europe in 2000 and their scenarios until 2020," *Sci. Total Environ.*, vol. 370, no. 1, pp. 147–156, 2006.

[17] E. G. Pacyna, J. M. Pacyna, F. Steenhuisen, and S. Wilson, "Global anthropogenic mercury emission inventory for 2000," *Atmos. Environ.*, vol. 40, no. 22, pp. 4048–4063, 2006.

[18] "UNEP-GRID-Arendal, httpswww.grida.noresources5709." .

[19] I. M. Hedgecock and N. Pirrone, "Mercury and photochemistry in the marine boundary layer-modelling studies suggest the in situ production of reactive gas phase mercury," *Atmos. Environ.*, vol. 35, no. 17, pp. 3055–3062, 2001.

[20] A. Saiz-Lopez *et al.*, "Photoreduction of gaseous oxidized mercury changes global atmospheric mercury speciation, transport and deposition," *Nat. Commun.*, vol. 9, no. 1, pp. 1–9, 2018.

[21] W. F. Fitzgerald, C. H. Lamborg, and C. R. Hammerschmidt, "Marine biogeochemical cycling of mercury," *Chem. Rev.*, vol. 107, no. 2, pp. 641–662, 2007.

[22] M. S. Gustin, H. Biester, and C. S. Kim, "Investigation of the light-enhanced emission of mercury from naturally enriched substrates," *Atmos. Environ.*, vol. 36, no. 20, pp. 3241–3254, 2002.

[23] L. Whalin, E. H. Kim, and R. Mason, “Factors influencing the oxidation, reduction, methylation and demethylation of mercury species in coastal waters,” *Mar. Chem.*, vol. 107, no. 3, pp. 278–294, 2007.

[24] J. O. Nriagu, “Mechanistic steps in the photoreduction of mercury in natural waters,” *Sci. Total Environ.*, vol. 154, no. 1, pp. 1–8, 1994.

[25] N. Pirrone *et al.*, “Toward the next generation of air quality monitoring: Mercury,” *Atmos. Environ.*, vol. 80, pp. 599–611, 2013.

[26] P. Mahato, S. Saha, P. Das, H. Agarwalla, and A. Das, “An overview of the recent developments on Hg2+ recognition,” *RSC Adv.*, vol. 4, no. 68, pp. 36140–36174, 2014.

[27] M. S. Gustin, S. E. Lindberg, and P. J. Weisberg, “An update on the natural sources and sinks of atmospheric mercury,” *Appl. Geochemistry*, vol. 23, no. 3, pp. 482–493, 2008.

[28] F. Sprovieri, N. Pirrone, R. Ebinghaus, H. Kock, and A. Dommergue, “A review of worldwide atmospheric mercury measurements,” *Atmos. Chem. Phys.*, vol. 10, no. 17, pp. 8245–8265, 2010.

[29] S. E. Lindberg and W. J. Stratton, “Atmospheric mercury speciation: Concentration and behavior of reactive gaseous mercury in ambient air,” *Environ. Sci. Technol.*, vol. 32, no. 1, pp. 49–57, 1998.

[30] F. Sprovieri *et al.*, “Atmospheric mercury concentrations observed at ground-based monitoring sites globally distributed in the framework of the GMOS network,” *Atmos. Chem. Phys.*, vol. 16, no. 18, pp. 11915–11935, 2016.

[31] E. G. Pacyna *et al.*, “Global emission of mercury to the atmosphere from anthropogenic sources in 2005 and projections to 2020,” *Atmos. Environ.*, vol. 44, no. 20, pp. 2487–2499, 2010.

[32] C. J. Lin and S. O. Pehkonen, “The chemistry of atmospheric mercury: A review,” *Atmos. Environ.*, vol. 33, no. 13, pp. 2067–2079, 1999.

[33] C. D. Holmes, D. J. Jacob, and X. Yang, “Global lifetime of elemental mercury against oxidation by atomic bromine in the free troposphere,” *Geophys. Res. Lett.*, vol. 33, no. 20, pp. 1–5, 2006.

[34] R. P. Mason and G. R. Sheu, “Role of the ocean in the global mercury cycle,” *Global Biogeochem. Cycles*, vol. 16, no. 4, pp. 40-1-40–14, 2002.

[35] N. O. Guangliang Liu, Yong Cai, *Chemistry and toxicology of mercury environmental chemistry and toxicology edited by Guangliang Liu, Yong Cai, Nelson O'Driscoll*, John Wiley. 2012.

[36] W. R. Simpson *et al.*, "Halogens and their role in polar boundary-layer ozone depletion," *Atmos. Chem. Phys.*, vol. 7, no. 16, pp. 4375–4418, 2007.

[37] S. E. Lindberg *et al.*, "Dynamic oxidation of gaseous mercury in the arctic troposphere at polar sunrise," *Environ. Sci. Technol.*, vol. 36, no. 6, pp. 1245–1256, 2002.

[38] I. M. Hedgecock and N. Pirrone, "Chasing Quicksilver: Modeling the Atmospheric Lifetime of Hg 0(g) in the Marine Boundary Layer at Various Latitudes," *Environ. Sci. Technol.*, vol. 38, no. 1, pp. 69–76, 2004.

[39] F. Sprovieri, I. M. Hedgecock, and N. Pirrone, "An investigation of the origins of reactive gaseous mercury in the Mediterranean marine boundary layer," *Atmos. Chem. Phys.*, vol. 10, no. 8, pp. 3985–3997, 2010.

[40] M. Horvat, J. Kotnik, M. Logar, V. Fajon, T. Zvonarić, and N. Pirrone, "Speciation of mercury in surface and deep-sea waters in the Mediterranean Sea," *Atmos. Environ.*, vol. 37, no. SUPPL. 1, 2003.

[41] C. J. Lin, P. Pongprueksa, S. E. Lindberg, S. O. Pehkonen, D. Byun, and C. Jang, "Scientific uncertainties in atmospheric mercury models I: Model science evaluation," *Atmos. Environ.*, vol. 40, no. 16, pp. 2911–2928, 2006.

[42] Q. Wan *et al.*, "Atmospheric mercury in Changbai Mountain area, northeastern China II. The distribution of reactive gaseous mercury and particulate mercury and mercury deposition fluxes," *Environ. Res.*, vol. 109, no. 6, pp. 721–727, 2009.

[43] R. Winfrey and W. M. Rudd, "ENVIRONMENTAL FACTORS AFFECTING THE FORMATION OF METHYLMERCURY IN LOW pH LAKES," *Environ. Toxicol. Chem.*, vol. 9, pp. 853–869, 1990.

[44] F. Sprovieri, N. Pirrone, K. Gärdfeldt, and J. Sommar, "Mercury speciation in the marine boundary layer along a 6000 km cruise path around the Mediterranean Sea," *Atmos. Environ.*, vol. 37, no. SUPPL. 1, pp. 63–71, 2003.

[45] N. Pirrone *et al.*, "Dynamic processes of mercury over the Mediterranean region: Results from the Mediterranean Atmospheric Mercury Cycle System (MAMCS)

project," *Atmos. Environ.*, vol. 37, no. SUPPL. 1, pp. 21–39, 2003.

[46] I. M. Hedgecock, N. Pirrone, G. A. Trunfio, and F. Sprovieri, "Integrated mercury cycling, transport, and air-water exchange (MECAWEx) model," *J. Geophys. Res. Atmos.*, vol. 111, no. 20, pp. 1–13, 2006.

[47] D. Mergler *et al.*, "Methylmercury exposure and health effects in humans: A worldwide concern," *Ambio*, vol. 36, no. 1, pp. 3–11, 2007.

[48] M. Nakamura *et al.*, "Methylmercury exposure and neurological outcomes in Taiji residents accustomed to consuming whale meat," *Environ. Int.*, vol. 68, pp. 25–32, 2014.

[49] K. Eto, M. Marumoto, and M. Takeya, "The pathology of methylmercury poisoning (Minamata disease): The 50th Anniversary of Japanese Society of Neuropathology," *Neuropathology*, vol. 30, no. 5, pp. 471–479, 2010.

[50] T. W. Clarkson and L. Magos, "The toxicology of mercury and its chemical compounds," *Crit. Rev. Toxicol.*, vol. 36, no. 8, pp. 609–662, 2006.

[51] A. M. Scheuhammer, M. W. Meyer, M. B. Sandheinrich, and M. W. Murray, "Effects of environmental methylmercury on the health of wild birds, mammals, and fish," *Ambio*, vol. 36, no. 1, pp. 12–18, 2007.

[52] T. W. Clarkson, "The three modern faces of mercury," *Environ. Health Perspect.*, vol. 110, no. SUPPL. 1, pp. 11–23, 2002.

[53] P. Jitaru and F. Adams, "Toxicity, sources and biogeochemical cycle of mercury," *J. Phys. IV JP*, vol. 121, pp. 185–193, 2004.

[54] S. Balshaw, J. Edwards, B. Daughtry, and K. Ross, "Mercury in seafood: Mechanisms of accumulation and consequences for consumer health," *Rev. Environ. Health*, vol. 22, no. 2, pp. 91–113, 2007.

[55] K. Sundseth, J. M. Pacyna, E. G. Pacyna, N. Pirrone, and R. J. Thorne, "Global sources and pathways of mercury in the context of human health," *Int. J. Environ. Res. Public Health*, vol. 14, no. 1, 2017.

[56] K. M. Rice, E. M. Walker, M. Wu, C. Gillette, and E. R. Blough, "Environmental mercury and its toxic effects," *J. Prev. Med. Public Heal.*, vol. 47, no. 2, pp. 74–83, 2014.

[57] United Nations Environment Programme, "Global Review of Mercury Monitoring Networks," no. November, pp. 1–48, 2016.

[58] D. A. Gay, D. Schmeltz, E. Prestbo, M. Olson, T. Sharac, and R. Tordon, “The Atmospheric Mercury Network: Measurement and initial examination of an ongoing atmospheric mercury record across North America,” *Atmos. Chem. Phys.*, 2013.

[59] F. Sprovieri *et al.*, “Five-year records of mercury wet deposition flux at GMOS sites in the Northern and Southern hemispheres,” *Atmos. Chem. Phys.*, vol. 17, no. 4, pp. 2689–2708, 2017.

[60] F. D’Amore, M. Bencardino, S. Cinnirella, F. Sprovieri, and N. Pirrone, “Data quality through a web-based QA/QC system: Implementation for atmospheric mercury data from the global mercury observation system,” *Environ. Sci. Process. Impacts*, vol. 17, no. 8, pp. 1482–1491, 2015.

[61] H. Selin, S. E. Keane, S. Wang, N. E. Selin, K. Davis, and D. Bally, “Linking science and policy to support the implementation of the Minamata Convention on Mercury,” *Ambio*, vol. 47, no. 2, pp. 198–215, 2018.

[62] R. J. C. Brown, N. Pirrone, C. Van Hoek, F. Sprovieri, R. Fernandez, and K. Toté, “Standardisation of a European measurement method for the determination of total gaseous mercury: Results of the field trial campaign and determination of a measurement uncertainty and working range,” *J. Environ. Monit.*, vol. 12, no. 3, pp. 689–695, 2010.

[63] A. Steffen *et al.*, “A synthesis of atmospheric mercury depletion event chemistry in the atmosphere and snow,” *Atmos. Chem. Phys.*, vol. 8, no. 6, pp. 1445–1482, 2008.

[64] M. S. Gustin, H. M. Amos, J. Huang, M. B. Miller, and K. Heidecorn, “Measuring and modeling mercury in the atmosphere: A critical review,” *Atmos. Chem. Phys.*, vol. 15, no. 10, pp. 5697–5713, 2015.

[65] Tekran, “Model 2537A Mercury Vapour Analyzer: User Manual,” no. September, 1999.

[66] S. C. Method, “Low Level Mercury Analysis - Gas Phase Calibration Background Information,” vol. 5726, pp. 3–4, 1985.

[67] M. S. Landis, R. K. Stevens, F. Schaedlich, and E. M. Prestbo, “Development and characterization of an annular denuder methodology for the measurement of divalent inorganic reactive gaseous mercury in ambient air,” *Environ. Sci.*

Technol., vol. 36, no. 13, pp. 3000–3009, 2002.

[68] J. Y. Lu, W. H. Schroeder, T. Berg, J. Munthe, D. Schneeberger, and F. Schaedlich, "A Device for Sampling and Determination of Total Particulate Mercury in Ambient Air," *Anal. Chem.*, vol. 70, no. 11, pp. 2403–2408, 1998.

[69] US-EPA, "Method 1631: Mercury in water by oxidation, purge and trap, and cold vapor atomic fluorescence spectrometry," *EPA 821-R-96-012. US EPA, Off. Water, Washington, DC*, no. August, pp. 1–46, 2002.

[70] R. E. J Munthe, F Sprovieri, M Horvat, "SOPs and QA/QC protocols regarding measurements of TGM, GEM, RGM, TPM and mercury in precipitation in cooperation with WP3, WP4 and WP5. GMOS deliverable 6.1, CNR-IIA, IVL." 2011.

[71] "GMOS Standard Operational Procedure Methods for the determination of TGM and GEM," pp. 1–22.

[72] GMOS, "GMOS Standard Operational Procedure Methods for the determination of speciated ambient Hg," pp. 1–22.

[73] GMOS, "GMOS Standard Operational Procedure Method for the determination of total mercury in precipitation," pp. 1–22.

[74] A. Steffen, T. Scherz, M. Olson, D. Gay, and P. Blanchard, "A comparison of data quality control protocols for atmospheric mercury speciation measurements," *J. Environ. Monit.*, vol. 14, no. 3, pp. 752–765, 2012.

[75] J. L. Campbell *et al.*, "Quantity is nothing without quality: Automated QA/QC for streaming environmental sensor data," *Bioscience*, vol. 63, no. 7, pp. 574–585, 2013.

[76] A. Tassone, S. Moretti, M. Martino, N. Pirrone, F. Sprovieri, and A. Naccarato, "Modification of the EPA method 1631E for the quantification of total mercury in natural waters," *MethodsX*, vol. 7, no. May, p. 100987, 2020.

[77] J. L. Parker and N. S. Bloom, "Preservation and storage techniques for low-level aqueous mercury speciation," *Sci. Total Environ.*, vol. 337, no. 1–3, pp. 253–263, 2005.

[78] K. Leopold, M. Foulkes, and P. Worsfold, "Methods for the determination and speciation of mercury in natural waters-A review," *Anal. Chim. Acta*, vol. 663, no. 2, pp. 127–138, 2010.

[79] UNEP, “Global Assessment of Laboratories Analyzing Mercury, First Round,” no. October, pp. 1–29, 2018.

[80] G. D. Draxler, R.R., Rolph, “HYSPLIT (Hybrid Single-Particle Lagrangian Integrated Trajectory),” no. NOAA Air Resour. Lab. Coll. Park. MD. 2003.

[81] M. Bencardino *et al.*, “Carbonaceous aerosols collected at the observatory of Monte Curcio in the Southern Mediterranean Basin,” *Atmosphere (Basel).*, vol. 10, no. 10, pp. 1–19, 2019.

[82] C. Perrino and F. Marcovecchio, “A new method for assessing the contribution of Primary Biological Atmospheric Particles to the mass concentration of the atmospheric aerosol,” *Environ. Int.*, vol. 87, pp. 108–115, 2016.

[83] C. Perrino, M. Catrambone, and A. Di Menno Di Bucchianico, “Gaseous ammonia from traffic emissions in the urban area of Rome,” *Adv. Air Pollut.*, vol. 13, no. 2002, pp. 601–609, 2003.

[84] M. Possanzini, G. Tagliacozzo, and A. Cecinato, “Ambient levels and sources of lower carbonyls at Montelibretti, Rome (Italy),” *Water. Air. Soil Pollut.*, vol. 183, no. 1–4, pp. 447–454, 2007.

[85] M. Gustin and D. Jaffe, “Reducing the uncertainty in measurement and understanding of mercury in the atmosphere,” *Environ. Sci. Technol.*, vol. 44, no. 7, pp. 2222–2227, 2010.

[86] D. S. McLagan *et al.*, “A High-Precision Passive Air Sampler for Gaseous Mercury,” *Environ. Sci. Technol. Lett.*, vol. 3, no. 1, pp. 24–29, 2016.

[87] J. Huang, S. N. Lyman, J. S. Hartman, and M. S. Gustin, “A review of passive sampling systems for ambient air mercury measurements,” *Environ. Sci. Process. Impacts*, vol. 16, no. 3, pp. 374–392, 2014.

[88] D. S. McLagan *et al.*, “Global evaluation and calibration of a passive air sampler for gaseous mercury,” *Atmos. Chem. Phys.*, pp. 5905–5919, 2018.

[89] D. S. McLagan, M. E. E. Mazur, C. P. J. Mitchell, and F. Wania, “Passive air sampling of gaseous elemental mercury: a critical review,” *Atmos. Chem. Phys.*, vol. 16, no. 5, pp. 3061–3076, 2016.

[90] A. Macagnano *et al.*, “Passive Sampling of Gaseous Elemental Mercury Based on a Composite TiO2NP/AuNP Layer,” *Nanomaterials*, vol. 8, no. 10, p. 798, 2018.

[91] I. Wängberg, U. Hageström, J. Sommar, and M. Ferm, “Development and Testing of a Passive Sampler for Measurement of Gaseous Mercury,” *Atmos. Chem. Phys.*, no. June, pp. 1–9, 2016.

[92] J. Munthe *et al.*, “Intercomparison of methods for sampling and analysis of atmospheric mercury species,” *Atmos. Environ.*, vol. 35, no. 17, pp. 3007–3017, 2001.

[93] W. J. Massman and USDA/Forest, “Molecular diffusivities of Hg vapor in air, O2 and N2 near STP and the kinematic viscosity and thermal diffusivity of air near STP,” *IEEE Micro*, vol. 31, no. 1, pp. 78–89, 1999.

[94] S. D. and R. C. T. . Pinheiro J, Bates D, DebRoy S, :“nlme: Linear and Nonlinear Mixed Effects Models. R package version 3.1-131, https://CRAN.R-project.org/package=nlme., R Packag. version 3.1-131, https//CRAN.R-project.org/package=nlme.,.” 2017.

[95] E. Paradis, J. Claude, and K. Strimmer, “APE: Analyses of Phylogenetics and Evolution in R language,” *Bioinformatics*, vol. 20, no. 2, pp. 289–290, Jan. 2004.

[96] K. Aspmo *et al.*, “Measurements of atmospheric mercury species during an international study of mercury depletion events at Ny-Ålesund, Svalbard, spring 2003. How reproducible are our present methods?,” in *Atmospheric Environment*, 2005, vol. 39, no. 39 SPEC. ISS., pp. 7607–7619.

[97] F. Slemr *et al.*, “Comparison of mercury concentrations measured at several sites in the Southern Hemisphere,” *Atmos. Chem. Phys.*, vol. 15, no. 6, pp. 3125–3133, 2015.

[98] C. Temme *et al.*, “Trend, seasonal and multivariate analysis study of total gaseous mercury data from the Canadian atmospheric mercury measurement network (CAMNet),” *Atmos. Environ.*, vol. 41, no. 26, pp. 5423–5441, 2007.

[99] A. R. Restrepo, S. J. Hayward, J. M. Armitage, and F. Wania, “Evaluating the PAS-SIM model using a passive air sampler calibration study for pesticides,” *Environ. Sci. Process. Impacts*, vol. 17, no. 7, pp. 1228–1237, 2015.

[100] D. S. McLagan, C. P. J. Mitchell, H. Huang, B. Abdul Hussain, Y. Duan Lei, and F. Wania, “The effects of meteorological parameters and diffusive barrier reuse on the sampling rate of a passive air sampler for gaseous mercury,” *Atmos. Meas. Tech.*, vol. 10, no. 10, pp. 3651–3660, 2017.